UAB
Universitat Autònoma de Barcelona

Shaped by light:
The interplay between light perception and acclimation responses in Chlamydomonas reinhardtii

Camila Sánchez Retuerta

Shaped by light:

The interplay between light perception and acclimation responses in *Chlamydomonas reinhardtii*

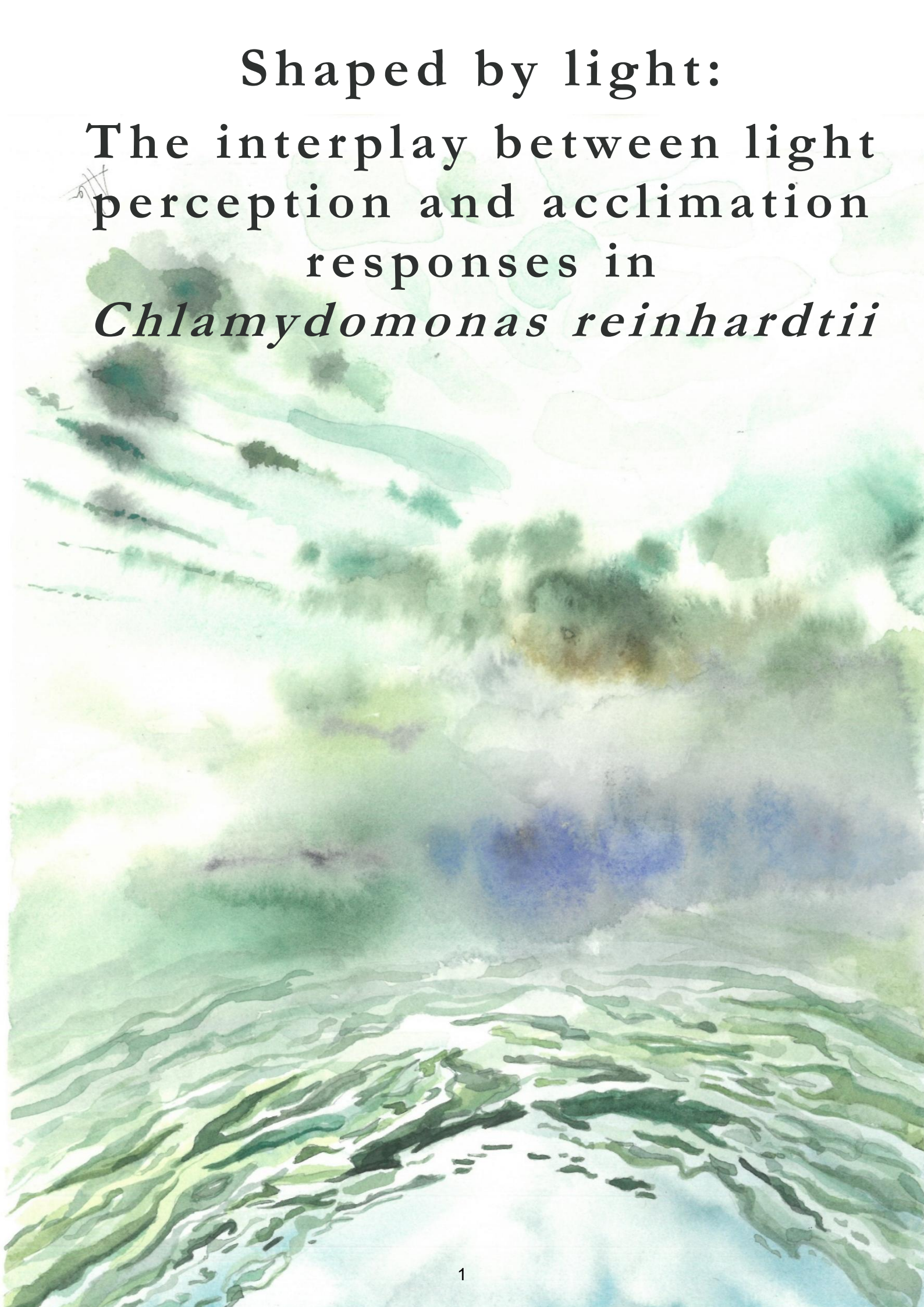

Acknowledgment of funding:
I was supported by a predoctoral contract *Ayudas para contratos predoctorales para la formación de doctores*, associated with the research project reference **PGC2018-099987-B-I00**.

Shaped by light:
The interplay between light perception and acclimation responses in *Chlamydomonas reinhardtii*

UNIVERSITAT AUTÒNOMA DE BARCELONA FACULTAT DE BIOCIÈNCIES

PhD in Plant Biology and Biotechnology

Dissertation presented by Camila Sánchez Retuerta for the PhD in

Plant Biology and Biotechnology at the Autonomous University of Barcelona (UAB).

The research was carried out at the Centre for Research in Agricultural Genomics (CRAG).

Thesis director

Dr. Elena Monte Collado

PhD candidate

Camila Sánchez Retuerta

Barcelona,

June 2025

ACKNOWLEDGEMENTS

La primera vez que pensé en ciencia tenía seis años, cuando me di cuenta de que ser gemela, no solo implicaba compartir un parecido físico, también un código genético. Des de aquí podría montarme la película más emotiva jamás dirigida y decir que fue ésa la razón que me empujó a hacer un doctorado. Y, ¿la verdad? -Fueron una cantidad de eventos casuales que me llevaron a donde estoy hoy. Aquí, sentada frente a mi ordenador, acabando de redactar esta tesis a contrarreloj, con todos los pros y contras habidos y por haber, mezclándose entre sí, intentando decantar esta balanza. Y mientras, yo, en un segundo plano, con un cigarro en la mano, pensando en cómo empezó todo y en el aumento sustancial de canas con las que lo acabo.

Y es que no vamos a romantizar absolutamente todo de estos cuatro años por el simple hecho de que se acerque el final y veamos las cosas con cierta perspectiva. No. Porque, realmente, ha habido desilusión, ansiedad, ganas de tirar la toalla, frustración, insomnio, lágrimas e incluso dolor. Sin embargo, el doctorado me ha enseñado eso, que no todas las etapas están llenas de las facilidades que nos gustarían y que todo conlleva un esfuerzo. Y, aun así, verdaderamente, la experiencia ha valido la pena.

Porque el doctorado ha sido cuatro años rodeada de las mismas paredes grises, verdes, naranjas y rojas, y de los mismos pasillos atestados de gente corriendo de un lado al otro para revelar un gel, para poner la PCR en el último momento y dejarla *overnight*, para bajar al seminario, para imprimir el *paper* del siguiente *Journal Club*, para huir del jefe, para buscar el café o incluso para hablar del último cotilleo en la fiesta de Navidad.

Y no sólo eso. El doctorado también ha sido cuatro años de aprender sobre ciencia, de preguntarse el por qué, de tomar decisiones y de celebrar los logros como si no hubiera un mañana porque, la verdad, son escasos. Cuatro años de *labmeetings* los lunes y domingos preparando el *Power Point*; de transformaciones de CRISPR, de licor de arroz, de *Chlamymeetings* interminables, de rotular y limpiar los Erlenmeyer, de hacer *screening* de millones de colonias y de repetir experimentos, una y otra vez. Cuatro años marcados por la luz: blanca, roja, azul; o por su ausencia: oscuridad. Luz intensa o tenue. De configurar el termómetro: a veintiuno o veintidós grados. Cuatro años de Chlamydomonas.

Cuatro años, doscientas ocho semanas, mil cuatrocientos sesenta y un días o treinta cinco mil horas de esa música reparadora. De música en vivo, reproducida en vinilo o en S*potify.* De ese *techno* que sacude el cuerpo o del *indie* que lo calma. Del séptimo arte, de infinitos créditos finales, de directores y directoras de cine que te muestran historias; de libros que te las cuentan. De ese contraste de emociones.

Cuatro años en esta estación de tren, el CRAG, donde la gente viene y va, pero también, los hay que se quedan. Cuatro años con personas que te alegran los días a base de putivueltas y humor negro, o de esa risa que, desde la primera planta, llena todos los huecos del edificio. Cuatro años sin recibir ese saludo al cruzármelo por el pasillo, o de encontrar a familia no solo por compartir el apellido. Cuatro años de su característica risa mezclada con lágrimas, de los matecitos con el termo *Pibe*, de camisetas de distintas ciudades, de *well well well*, de postres con sabor a Chile o de cafés con *Jacob*, de Chocotortas o de acento británico forzado, ¿*Right, mate*? Y de Vodka suavecín. De comentar *Fleabag* o de aprender sobre tintes de *Henna*. De descubrir Grecia Alemania o Cantabria. De argentinas con raíces catalanas y de italianas alocadas. De antiguos jefes que agarran del brazo y antiguas jefas que te enseñan a apreciar la ciencia. De laboratorios que se llenan y luego vacían, constantemente. De todas esas personas que, con su trabajo, te facilitan los días, y de todos esos caramelos demasiado azucarados que los endulzan cuando finalizan.

Cuatro años (más) de Ellas, de nuestros viajes, de nuestras risas, decepciones y alegrías. De bailes esporádicos, de peleas con la sombrilla y de esa naturalidad sobrehumana, valga la contradicción. De los planes culturales y palomitas. De todos los veinte de julio. De los reencuentros con sabor a Toña y de esos *Honest Green* con *Pokebowl* de salmón.

Cuatro años dan para muchas cosas, para ciencia o para todo aquello que no lo es, pero, al final, todas forman parte de una misma etapa que cierro hoy y que recordaré siempre. Así que Gracias.

Gracias al lucero del alba y a la estrella de la mañana, a las lecturas de Poliana, a las bragas navideñas y al trébol de cuatro hojas. A las alitas de pollo, a nuestros veranos alocados en el *Johnny's,* y a Ella, por vibrar conmigo en cada nota. Gracias por compartir el cariño y el estrés de un doctorado i a tú per acompanyar-la sempre.

Y gracias a Vosotros por darme la libertad de ser y hacer siempre lo que he querido, por inspirarme constantemente con vuestros conocimientos sobre ¿todo? O si más no, casi todo. Por abrirme la mente con desiertos interminables, volcanes y glaciares de otro mundo. Por compartir a *Bon Iver y* a *The Blaze.* Por vuestra originalidad y constante cariño. Por todo.

Y especialmente gracias a Ti, por acompañarme en esta experiencia y más. Por escucharme y ayudarme siempre. Por compartir la música, el humor, el amor por el cine y esas ganas constantes de viajar y descubrir cosas nuevas. Por todos nuestros enfados y locuras. Por esta conexión mágica e indescriptible que nos une.

Muchísimas Gracias. Nada de esto habría sido posible sin Vosotras.

TABLE OF CONTENTS

ABREVIATIONS

ΔpH - Proton Gradient **ΔpH** - Proton Gradient
1Chl* – Excited Chlorophyll
ATP – Adenosine Triphosphate
BPhy – Bacteriophytochrome
CA – Catalytic ATP-binding domain
Cas – CRISPR-associated protein
Cas9 – CRISPR-associated protein 9
Cas12a – CRISPR-associated protein 12a
CCM – CO_2 Concentrating Mechanism
CCM1 – Carbon-Concentrating Mechanism 1
Chl – Chlorophyll
ChR1 – Channelrhodopsin 1
ChR2 – Channelrhodopsin 2
CIA5 – Carbonic Anhydrase 5
CLiP – Chlamydomonas Library Project
COP – Cryptochrome Opsin (rhodopsin-related proteins)
COP1 – Constitutive Photomorphogenesis 1
Cpf1 – CRISPR from Prevotella and Francisella 1 (Cas12a)
CrCO – Chlamydomonas CONSTANS
CRC – Chlamydomonas Resource Center
CR-COP1 – Chlamydomonas reinhardtii COP1
CRISPR/Cas9 – Clustered Regularly Interspaced Short Palindromic Repeats / CRISPR-associated protein 9
CRY – Cryptochrome
CRY-DASH – Cryptochrome-DASH
Cyt b6f – Cytochrome b6f Complex
cw15 – Cell wall–deficient strain of *Chlamydomonas reinhardtii*
DDB1 – Damage-Specific DNA Binding Protein 1
DET1 – De-etiolated 1
DHp – Dimerization Histidine Phosphotransfer domain
DMSO – Dimethyl Sulfoxide
DSBs – Double-Strand Breaks
E3 – Ubiquitin Ligase
ETR – Electron Transport Rate
FAD – Flavin Adenine Dinucleotide
Fd – Ferredoxin
FMN – Flavin Mononucleotide
FNR – Ferredoxin–$NADP^+$ Reductase
gRNA – guide RNA
G1 – Gap 1 phase
G3P – Glyceraldehyde-3-Phosphate
HATPase_c – Histidine Kinase-like ATPase catalytic domain
HDR – Homology-Directed Repair
HEK – Human Embryonic Kidney
HIK – Histidine Kinase (general)
HIK1 – Histidine Kinase 1
HIK2 – Histidine Kinase 2
HisKA – Histidine Kinase A
HL – High Light
HKR – Histidine Kinase Rhodopsin

HR – Homologous Recombination
IFT – Intraflagellar Transport
IV – In Vitro
Jα – C-terminal α-helix in LOV domain
LHC – Light-Harvesting Complex
LHCI – Light-Harvesting Complex I
LHCII – Light-Harvesting Complex II
LHCSR – Light-Harvesting Complex Stress-Responsive
LHCSR1 – Light-Harvesting Complex Stress-Responsive 1
LHCSR3 – Light-Harvesting Complex Stress-Responsive 3
LL – Low Light
LOV – Light, Oxygen, Voltage domain
M – Mitosis phase
mt+ – Plus mating type
mt– – Minus mating type
$NADP^+$ – Nicotinamide Adenine Dinucleotide Phosphate
NADPH – Reduced Nicotinamide Adenine Dinucleotide Phosphate
NPQ – Non-Photochemical Quenching
OmpR – Outer membrane protein R family
PAS – Per-ARNT-Sim domain
PC – Plastocyanin
PHK – Photoreceptor Histidine Kinase
PHOT – Phototropin
pCRY – Plant-type Cryptochrome
PQ – Plastoquinone
PSBS – Photosystem II Subunit S
PSBS1 – Photosystem II Subunit S Homolog 1
PSBS2 – Photosystem II Subunit S Homolog 2
PSI – Photosystem I
PSII – Photosystem II
PSY1 – Phytoene Synthase 1
qE – Energy-Dependent Quenching
qI – Photoinhibitory Quenching
qT – State Transition-Dependent Quenching
qZ – Zeaxanthin-Dependent Quenching
REC – Receiver domain
RNAi – RNA interference
RNP – Ribonucleoprotein
ROS – Reactive Oxygen Species
RR – Response Regulator
Rubisco – Ribulose-1,5-bisphosphate carboxylase/oxygenase
S – Synthesis phase
sgRNA – Single Guide RNA
SID – Screening Indel
SPA1 – SUPPRESSOR OF PHYA-105 1
STT7 – Serine/Threonine Kinase 7
TAE – Tris-Acetate-EDTA buffer
TAP – Tris-Acetate-Phosphate medium
TE – Tris-EDTA buffer
TCS – Two-Component System

UV-B – Ultraviolet B Radiation
UVR8 – UV Resistance Locus 8
VDE – Violaxanthin De-Epoxidase
WT – Wild Type
ZFNs – Zinc-Finger Nucleases

SUMMARY

Photosynthetic organisms must continuously adjust to changing light environments to optimize energy capture while minimizing photodamage. This thesis examines how *Chlamydomonas reinhardtii*, a model unicellular alga, responds to variation in light intensity and photoperiod, while also focusing on strain-dependent differences in physiological light responses, such as photosynthetic efficiency, pigment composition, photoprotection, and growth. In parallel, it explores the role of candidate light-signaling genes and advances genome editing tools to facilitate functional genetic analysis.

A comparative analysis of four Chlamydomonas strains (CLiP, 4A+, CC-124, and CC-125) showed that under low light, differences were most evident in pigment content and growth, while photosynthetic performance remained stable. In high light, all responses were affected, with photoperiod significantly shaping photoprotective responses. Shorter light regimes enhanced NPQ and PSII stability, whereas longer ones or continuous exposure supported higher growth but led to increased photodamage. Strain-specific strategies emerged under these conditions: CLiP sustained high growth and photoprotection, while CC-124 favored growth at the cost of NPQ.

To investigate how specific signaling components contribute to these acclimation patterns, mutant lines in the light-responsive kinases HIK1 and HIK2 were examined. The *hik1 442* mutant exhibited elevated NPQ, and preliminary data showed strong upregulation of *LHCSR1*, *LHCSR3*, and *PSBS* under low blue light, suggesting that HIK1 modulates photoprotective gene expression. In contrast, the function of HIK2 remains unresolved. Only the *hik2 149* mutant in the CLiP background consistently exhibited a high-light–sensitive phenotype. Similar effects were absent or unstable in other genetic backgrounds, suggesting that the phenotype observed may involve additional genetic factors beyond HIK2 disruption. These findings raise the possibility that HIK2 may not be involved in photoprotection, and that its function may be related to other light signaling pathways.

In support of gene function analysis, a CRISPR-Cas9 protocol based on ribonucleoprotein electroporation was adapted for Chlamydomonas, and a complementary genotyping strategy was implemented to improve detection of small indels typically missed by standard screening.

Altogether, this work highlights the interplay between light conditions, genetic background, and signaling pathways in shaping acclimation responses in *Chlamydomonas reinhardtii*. Although based on a controlled laboratory system, the findings offer broader insight into how photosynthetic eukaryotes fine-tune their light acclimation strategies across diverse environmental regimes.

RESUMEN

Los organismos fotosintéticos deben ajustarse continuamente a los cambios en el ambiente para optimizar la captura de energía y minimizar el daño producidor por luz. Esta tesis examina cómo *Chlamydomonas reinhardtii*, un alga unicelular modelo, responde a variaciones en la intensidad de luz y fotoperiodo, centrándose también en las diferencias dependientes de la cepa en las respuestas fisiológicas a la luz, como la eficiencia fotosintética, la composición de pigmentos, la fotoprotección y el crecimiento. En paralelo, explora el papel de genes candidatos de señalización lumínica y desarrolla herramientas de edición génica para facilitar el análisis genético funcional.

El análisis comparativo de cuatro cepas de Chlamydomonas (CLiP, 4A+, CC-124 y CC-125) mostró que bajo luz tenue, las diferencias más evidentes se observaban en el contenido de pigmentos y el crecimiento, mientras que el rendimiento fotosintético se mantenía estable. Bajo luz intensa, todas las respuestas se vieron afectadas, y el fotoperiodo influyó significativamente en las respuestas fotoprotectoras. Los regímenes de luz más cortos potenciaron el NPQ y la estabilidad del PSII, mientras que los más largos o la exposición continua favorecieron un mayor crecimiento, pero también incrementaron el daño producidor por luz. Se observaron estrategias específicas de cada cepa: CLiP mantuvo un crecimiento y fotoprotección elevados, mientras que CC-124 priorizó el crecimiento a costa de un menor NPQ.

Para investigar cómo contribuyen componentes específicos de señalización a estos patrones de aclimatación, se analizaron líneas mutantes de las quinasas HIK1 y HIK2, sensibles a la luz. El mutante *hik1 442* mostró un NPQ elevado, y datos preliminares indicaron una fuerte sobreexpresión de *LHCSR1*, *LHCSR3* y *PSBS* bajo luz azul tenue, lo que sugiere que HIK1 modula la expresión génica fotoprotectora. En cambio, la función de HIK2 permanece sin resolver. Solo el mutante *hik2 149* en el fondo genético CLiP presentó consistentemente un fenotipo sensible a la luz intensa. Efectos similares no se observaron o fueron inestables en otros fondos genéticos, lo que sugiere que el fenotipo observado podría implicar factores genéticos adicionales más allá de la disrupción de HIK2. Estos resultados plantean la posibilidad de que HIK2 no esté implicado en la fotoprotección, y que su función esté relacionada con otras vías de señalización lumínica.

Como apoyo al análisis funcional de genes, se adaptó un protocolo de CRISPR-Cas9 basado en la electroporación de ribonucleoproteínas para Chlamydomonas, y se implementó una estrategia de genotipado complementaria para mejorar la detección de pequeñas inserciones o deleciones que suelen pasar desapercibidas con los métodos de cribado convencionales.

En conjunto, este trabajo resalta la interacción entre las condiciones lumínicas, el fondo genético y las rutas de señalización en la configuración de las respuestas de aclimatación en *Chlamydomonas reinhardtii*. Aunque se basa en un sistema de laboratorio controlado, los hallazgos ofrecen una visión más amplia de cómo los eucariotas fotosintéticos ajustan sus estrategias de aclimatación a la luz en diversos entornos.

RESUM

Els organismes fotosintètics han d'ajustar-se contínuament als canvis en les condicions de llum per optimitzar la captura d'energia i minimitzar el dany produit per la llum. Aquesta tesi examina com *Chlamydomonas reinhardtii*, una alga unicel·lular model, respon a variacions en la intensitat llumínica i en el fotoperíode, i també se centra en les diferències fisiològiques depenents de cada soca en la resposta a la llum, com ara l'eficiència fotosintètica, la composició de pigments, la fotoprotecció i el creixement. Paral·lelament, explora el paper de gens candidats en la senyalització lumínica i desenvolupa eines d'edició genètica per facilitar l'anàlisi funcional.

La anàlisi comparativa de quatre soques de Chlamydomonas (CLiP, 4A+, CC-124 i CC-125) va mostrar que sota llum feble, les diferències més destacades es trobaven en el contingut de pigments i el creixement, mentre que el rendiment fotosintètic es mantenia estable. En condicions de llum intensa, totes les respostes es van veure afectades, i el fotoperíode va influir de manera significativa en les respostes fotoprotectores. Els règims curts de llum van potenciar el NPQ i l'estabilitat del PSII, mentre que els més llargs o l'exposició contínua van afavorir un creixement més elevat, però també van augmentar el dany produit per llum. En aquestes condicions van aparèixer estratègies específiques segons la soca: CLiP va mantenir un alt creixement i fotoprotecció, mentre que CC-124 va prioritzar el creixement a costa d'una NPQ més baixa.

Per investigar com contribueixen certs components de senyalització a aquests patrons d'aclimatació, es van analitzar línies mutants de les quinases HIK1 i HIK2 sensibles a la llum. El mutant *hik1 442* mostrava un NPQ elevat, i dades preliminars van indicar una sobreexpressió clara de *LHCSR1*, *LHCSR3* i *PSBS* sota llum blava feble, suggerint que HIK1 modula l'expressió de gens fotoprotectors. En canvi, la funció de HIK2 continua sense estar clara. Només el mutant *hik2 149* amb fons CLiP va mostrar de manera consistent un fenotip sensible a la llum intensa. Efectes similars no es van observar, o van ser inestables, en altres fons genètics, suggerint que el fenotip observat podria implicar altres factors genètics més enllà de la disrupció de HIK2. Aquests resultats plantegen la possibilitat que HIK2 no estigui implicat en la fotoprotecció, i que la seva funció estigui relacionada amb altres vies de senyalització lumínica.

Per donar suport a l'anàlisi funcional de gens, es va adaptar un protocol de CRISPR-Cas9 basat en l'electroporació de ribonucleoproteïnes per a Chlamydomonas, i es va implementar una estratègia de genotipat complementària per millorar la detecció de petites insercions o delecions que sovint passen desapercebudes amb els mètodes de cribratge estàndard.

En conjunt, aquest treball posa en relleu la interacció entre les condicions de llum, el fons genètic i les vies de senyalització en la configuració de les respostes d'aclimatació en *Chlamydomonas reinhardtii*. Tot i basar-se en un sistema de laboratori controlat, els resultats obtingut ofereixen una visió més àmplia de com els eucariotes fotosintètics ajusten les seves estratègies d'adaptació lumínica en entorns ambientals diversos.

Chapter 1

Introduction to *Chlamydomonas reinhardtii*

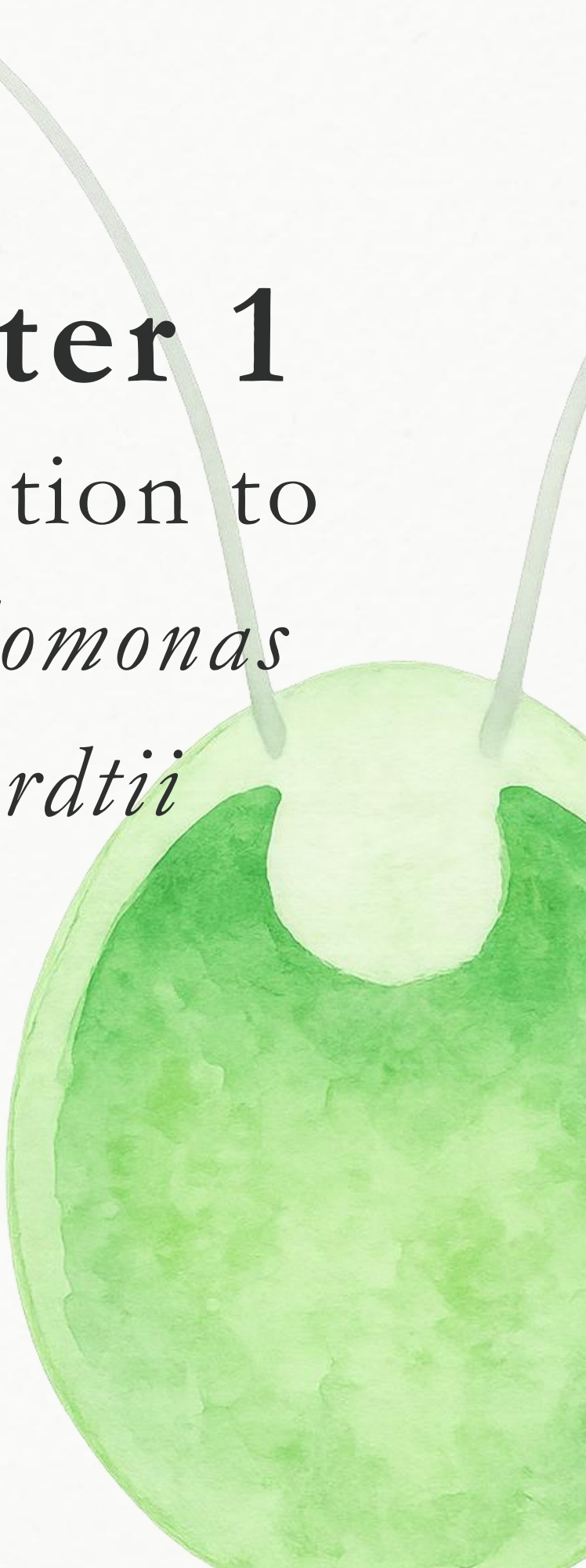

1.1 Chlamydomonas as a model organism

Chlamydomonas reinhardtii, a unicellular and biflagellate eukaryotic green microalga belonging to the chlorophyte lineage, was originally identified in Europe by Dangeard (1888). However, the widely used strains for research stem primarily from a single collection by G.M. Smith in the United States, isolated from the soil of a potato field in Amherst, Massachusetts, in 1945. (Harris, 2009)

Nowadays, distinct features make *Chlamydomonas reinhardtii* the current standard for algal research and a promising system to study fundamental processes. It has a short life cycle and grows fast and synchronously, doubling in number every 8 hours under optimal conditions (Harris, 2001). It is haploid during vegetative growth, which is particularly useful for genetic studies, since phenotypes can be immediately observed in loss-of-function mutants. However, under non-optimal conditions (nitrogen or light limitation) it can also reproduce sexually, triggering a zygote formation after gametes fusion. The maturation of the zygospore formed afterwards enhances adaptability to changing environments (de Carpentier et al., 2019)

Another advantage is that *C. reinhardtii* is metabolically flexible: cells can grow either autotrophically, heterotrophically or mixotrophically. Under autotrophic conditions, as it is well-known, this alga uses photosynthesis to fix carbon dioxide into organic compounds, relying solely on light as an energy source.

On the other hand, in heterotrophic growth, it relies on supplied organic carbon sources, acetate, to generate energy in the absence of light. This capability has allowed researchers to isolate light-sensitive photosynthesis mutants without compromising its survival and makes Chlamydomonas the organism of choice when studying photosynthesis. Furthermore, when growing mixotrophically, Chlamydomonas combines both methods, allowing the organism to perform photosynthesis and metabolize external carbon sources simultaneously, optimizing growth in environments where both light and organic nutrients are available. (Heifetz et al., 2000).

And unlike land plants, Chlamydomonas retains motile cilia (flagella), which are essential for its phototactic behavior and reorientation in response to light. These structures are directly involved in light perception and signaling, making them relevant for studying sensory responses in microalgae.

Sequencing technologies have enabled the complete sequencing of the *Chlamydomonas reinhardti*i nuclear, chloroplast, and mitochondrial genomes (Boynton et al., 1988). These datasets form the basis for functional genomics, genome editing, and synthetic biology.

Annotation of the three genomes has allowed the identification of coding regions, regulatory elements, and predicted gene functions. Most genetic tools developed to date target the nuclear and chloroplast genomes, where transformation and gene expression systems are well established.

Chloroplast genome transformation in *Chlamydomonas reinhardtii* was pioneered by Boynton et al. (1988) through particle bombardment, which introduces foreign DNA via homologous recombination. This method has enabled researchers to manipulate chloroplast genes for studying photosynthesis and advancing biotechnological applications, such as recombinant protein production. A similar approach has been adapted for mitochondrial genome transformation, improving our understanding of mitochondrial function and cellular respiration (Randolph-Anderson et al., 1993).

Transforming the nuclear genome has historically been more challenging than chloroplast transformation, though it has been extensively studied and improved over the years, mainly focusing on efficiency, stability, and expression levels. Early methods relied on glass bead-mediated transformation, where the cloning of native genes served as selectable markers to complement mutant phenotypes (Kindle, 1990). Over the years, electroporation has been optimized for both stable and transient transformations, making it an effective tool for studying gene expression and function without requiring prolonged cultivation (Shimogawara et al., 1998). However, a breakthrough was the development of codon optimization strategies and the use of strong endogenous promoters, which significantly boosted expression levels.

Gene-editing technologies (Fig. 1) have enabled precise modification of Chlamydomonas genomes. One of the first targeted approaches was Zinc-Finger Nucleases (ZFNs), which induce double-strand breaks (DSBs) at specific loci to trigger homologous recombination. Sizova et al. (2012) used ZFNs to disrupt the *COP3* gene, restoring aphVIII marker function. In contrast, CRISPR/Cas9 relies on a guide RNA for target recognition, simplifying design and allowing faster, more flexible editing across the genome.

In Chlamydomonas, however, early attempts to apply CRISPR/Cas9 were limited by low editing efficiency and cytotoxicity caused by constitutive Cas9 expression (Jiang et al., 2014). These limitations restricted its initial application in Chlamydomonas, even though the system was already well established in other models.

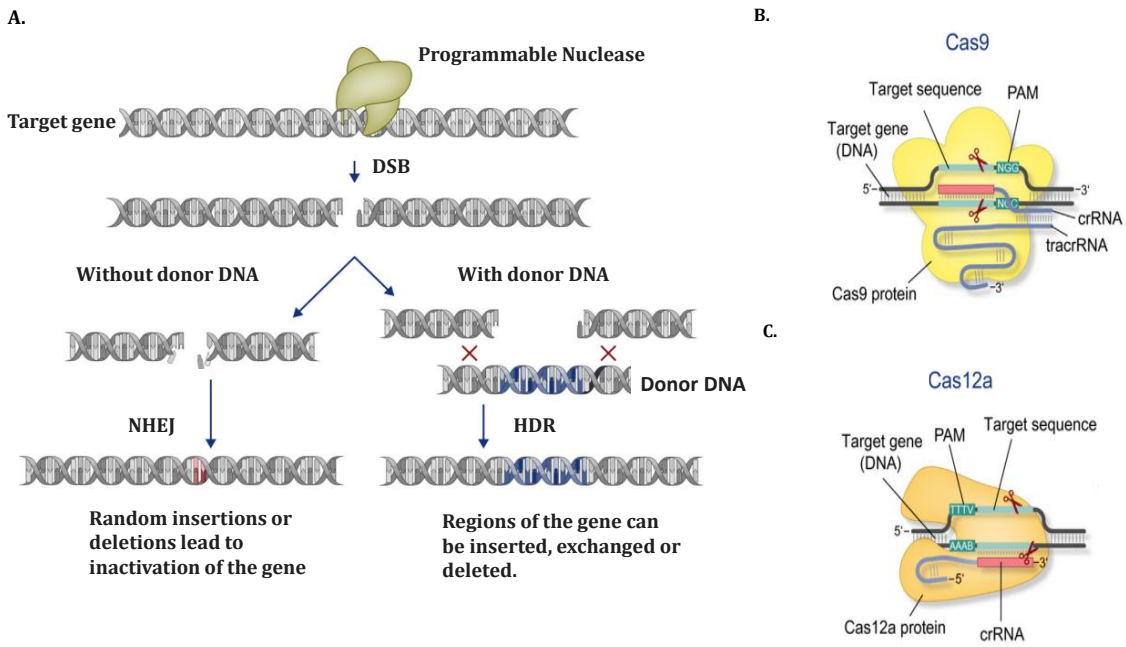

Fig. 1 Gene editing systems used in Chlamydomonas A. Programmable endonucleases create DSBs, which are then repaired by DNA repair mechanisms. Nonhomologous end-joining (NHEJ) results in random DNA changes, causing a dysfunctional gene. Alternatively, Homology-Directed Repair (HDR) uses donor DNA with homologous regions to guide precise repair, facilitating controlled insertions, deletions, or DNA exchanges. **B.** Function of Cas9 in CRISPR Cas gene editing system. The RNP complex is assembled from the Cas9 endonuclease, the crRNA, and the tracrRNA. The DNA is cleaved 3 bp away of the PAM (e.g., "NGG" for S. pyogenes), introducing a DSB with "blunt" ends. **C.** The Cas12a endonuclease binds to a single crRNA. DSBs with 45 bp overhangs are created 1721 bp away from the PAM (e.g., "TTTV" for Lachnospiraceae). Adapted from Kelterborn, et al., 2020).

Recent innovations, however, have improved CRISPR/Cas9 applications in Chlamydomonas. One successful strategy involves directly delivering pre-assembled Cas9-gRNA ribonucleoproteins (RNPs), eliminating the need for stable Cas9 expression in cells (Baek et al., 2016; Shin et al., 2016). Multiple gene co-targeting has also been achieved, allowing up to two genes to be modified simultaneously using separate CRISPR/Cas9 RNP complexes (Akella et al. 2021). Furthermore, Ferenczi et al. (2017) demonstrated that, by using another Cas version, Cas12a (Cpf1), within the RNP complex, allowed for precise homology-directed repair (HDR) of double-strand breaks (DSBs), achieving an efficiency of around 10%. However, this level of precision and efficiency was only achieved in the cell wall-deficient strain *cw15*. In contrast, Cas9-RNPs were shown to work across all tested wild-type strains, making Cas9 a more broadly applicable tool for genome editing in Chlamydomonas.

Additionally, gene-editing protocols for several Chlamydomonas strains have been optimized via Zinc-Finger Nucleases and CRISPR/Cas9 in the las few years for increasing efficiency (Greiner et al., 2017, Picariello et al., 2020).

RNA interference (RNAi) has also been explored as a gene repression strategy, particularly for essential genes where complete knockouts would be lethal. However, RNAi in Chlamydomonas has been hindered by instability and variable silencing efficiency (Yamasaki et al., 2008), highlighting the need for alternative approaches to gene modulation.

In addition, the creation of a comprehensive insertional mutant library (The Chlamydomonas Library Project (CLiP) and a resource for large-scale mutant phenotype screening have further implemented Chlamydomonas as a model reference.

The CLiP library provides a genome-wide collection of *Chlamydomonas reinhardtii* mutants for functional genomics and reverse genetics studies (Li et al., 2016; Li et al., 2019). It consists of over 60,000 mutants generated by random insertion of a paromomycin resistance cassette in the CC-4533 strain, each with a unique barcode for mapping. The library covers more than 80% of nuclear genes and has been widely used to study processes such as cell motility, photosynthesis, and stress responses.

In addition to the CLiP library, other tools are available for large-scale Chlamydomonas studies. The Chlamydomonas Resource Center (CRC) distributes thousands of strains, including mutants, plasmids, and cDNA libraries (Dent et al., 2015; Li et al., 2016). Phytozome provides access to the Chlamydomonas genome with tools for comparative genomics, gene family analysis, and gene structure visualization (Goodstein et al., 2012). ChlamyNET offers coexpression networks and predicted transcription factor binding sites, supporting gene function prediction and regulatory analysis (Romero-Campero et al., 2016).

1.2 Chlamydomonas cell structure and function

Chlamydomonas surface of the cell (Fig. 2) is covered with a wall that serves as a protective barrier and structural support. It also mediates environmental interactions and facilitates cellular communication. This cell wall is primarily composed of seven distinct layers with hydroxyproline-rich glycoproteins as major constituents, rather than the cellulose commonly found in higher plants. (Miller et al., 1974; Lee et al., 2007). Its multi-layered structure makes it both strong and flexible, allowing the cell to increase up to ten times in size during the light phase of its daily cycle (Cronmiller et al., 2019). Thus, *C.reinhardtii* cell wall is always in constant change throughout its life cycle (Harris, 1989): during nitrogen starvation, sexual gametes encounter each other and initiate a mating reaction, removing their cell walls to prepare for fusion and zygote formation. This

process, which exposes cells to their environment, requires immediate rebuilding of the cell wall to prevent cell lysis, showing the importance of this cell wall regeneration. This process has been studied and described to be governed by different signaling mechanisms. (Cronmiller et al., 2019).

From this cell wall, there are two emerging holes where the equal size flagella (cilium) extend. They allow two main functions: enabling the algae to swim toward or away from light sources (process known as phototaxis) and facilitating cell to cell recognition during mating process by releasing signals that promote gamete fusion. (Cronmiller, et al. 2019; Salomé and Merchant, 2019). The assembly of flagella occurs via intraflagellar transport (IFT), a key process in which molecular motors shuttle structural proteins from the cytoplasm to the flagellar tip, enabling flagellar growth and maintenance. This IFT mechanism was first discovered in *C. reinhardtii*, making it a model organism for studying cilia and flagella across species. (Cole, et al. 1998; Cronmiller, et al. 2019)

Just under the flagella are the basal bodies, which serve as the anchoring points from which the flagella extend. These basal bodies are connected by a complex network of fibers, linking them to each other, the intracellular microtubule cytoskeleton, and the nucleus (Marshall, 2024).

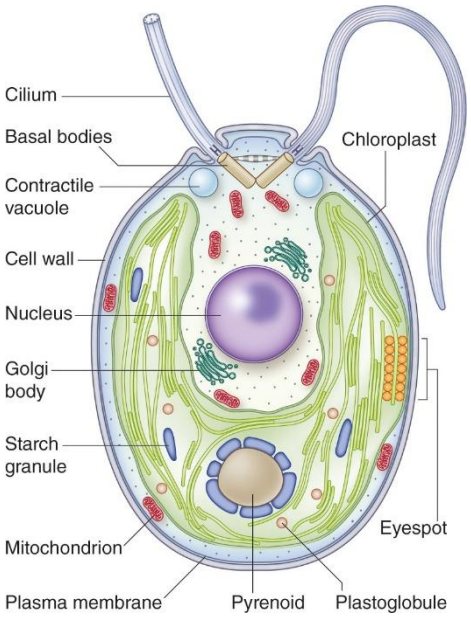

Fig 2. Structure of Chlamydomonas cells. Image retrieved from Sasso et al. (2018).

The nucleus is localized beneath the basal bodies, it emerges from an invagination of the chloroplast that covers the entire posterior half of the cell. (Cronmiller, et al. 2019; Marshall, 2024). This chloroplast is a large, cup-shaped structure that contains the photosynthetic machinery, including the thylakoid membranes, where the light-dependent reactions of photosynthesis occur (Engel et al., 2015). At the center of this chloroplast lies the pyrenoid, a key component of the CO_2 concentrating mechanism (CCM) of algae. It is a structure composed primarily of Rubisco (Mackinder et al., 2016).

Close to the cell equator, at the edge of the chloroplast, is the eyespot. This eyespot is a bright orange structure due to its rich content in carotenoid pigments. It plays a key role in light sensing, essential for phototaxis. It is localized within the chloroplast and directs light to a photoreceptor on the plasma membrane known as a retinal-binding rhodopsin homologue (chlamyopsin). This allows the cell to detect light direction and swim accordingly. Furthermore, while some studies based on mutants lacking an eyespot show they can still perceive light, their phototactic efficiency is reduced, indicating the importance of the eyespot in light-guided movement (Kröger and Hegemann, 1994).

The position of the eyespot creates asymmetry in the cell, influencing how its cis and trans flagella respond to light. During mitosis, the eyespot is rebuilt opposite the cleavage plane, ensuring proper alignment for phototactic responses. Both phototaxis and photophobia are distinct yet essential photoresponses that enable the organism to navigate its environment efficiently.

Additionally, phototaxis in *Chlamydomonas reinhardtii* is driven by calcium-induced changes in flagellar motion, enabling the organism to move toward or away from light. In contrast, the photophobic response is triggered by a calcium-dependent electric current, activated by the photoreceptor. Mutations affecting either the eyespot structure or the phototactic signaling pathway have been classified into six complementation groups, providing valuable insights into the molecular mechanisms governing light response in Chlamydomonas (Ueki, et al. 2016).

1.3 Chlamydomonas cell cycle

The life cycle of Chlamydomonas is one of the most well-understood algal life cycles and is frequently used as a textbook example. It comprises two main phases: the vegetative cycle (asexual reproduction) and the sexual cycle (sexual reproduction) (Fig. 3 and 4).

1.3.1 The vegetative cycle

During asexual reproduction (Fig. 3), a single Chlamydomonas parent cell divides through mitosis to produce genetically identical daughter cells. Interestingly, Chlamydomonas follows a modified cell cycle known as multiple fission. This type of cell cycle is characterized by an extended growth phase (G1), during which cells can increase in size by more than twofold. Under favorable conditions, Chlamydomonas cells can grow in volume by more than tenfold during a G1 phase lasting between 10 and 14 hours (Cross and Umen, 2015).

In the vegetative cycle, Chlamydomonas cells first lose their flagella, and the basal bodies migrate toward the nucleus. During prophase, these basal bodies move to opposite ends of the nucleus, initiating successive rounds of rapidly alternating S phases and mitoses (S/M). The chloroplast then divides, followed by cytokinesis, ultimately producing up to 32 daughter cells (2^n) from a single mother cell. The daughter cells, also called zoospores, then hatch from the mother cell and begin the cycle again (Cross and Umen, 2015).

The timing of cell division in Chlamydomonas is regulated by cell-size–dependent checkpoints during G1, including an irreversible "commitment" point. Under constant light, cells can divide every 8–10 hours. However, in typical diurnal cycles, cells grow during the light phase and divide during the dark, with up to four daughter cells released simultaneously through enzymatic rupture of the mother cell wall (Cross & Umen, 2015; Dupuis & Merchant, 2023).

Multiple fission is likely an adaptation of motile green algae which must resorb or remove their flagella prior to division, to use their basal bodies to coordinate mitosis and cytokinesis: the so-called flagellation constraint (Koufopanou, 1994).

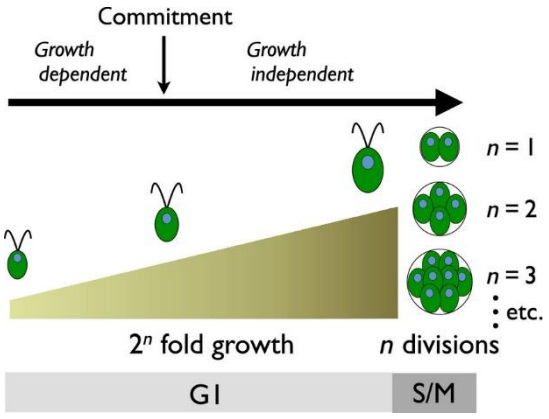

Fig 3. Chlamydomonas multiple-fission cell cycle schematic representation. This figure illustrates one complete cycle from left to right. During G1, daughter cells grow and can expand several times beyond their initial size. At the end of G1, a series of rapid, alternating S phases and mitoses (S/M) generates 2n daughter cells. The number of divisions (n) depends on the mother's cell size. G1 is divided into two phases, separated by the commitment point. Before commitment, cell-cycle progression depends on growth and reaching a minimum size. After commitment, progression no longer requires continued growth. Following S/M, daughter cells hatch and re-enter G1 to begin a new cycle. Image retrieved from Cross & Umen, 2015.

1.3.2 Sexual cycle

Chlamydomonas can also reproduce sexually through an isogamous cycle, meaning both gametes are morphologically identical. This process is triggered by nitrogen starvation, which causes haploid cells of opposite mating types (designated as 'plus' [mt+] and 'minus' [mt−]) to pair by connecting their flagella tips. Exposure to light, perceived by the blue light photoreceptor phototropin, commits nitrogen-starved cells to gametic differentiation, although this can be reversed in darkness (Huang & Beck, 2003).

Specifically, the sexual cycle consists of four main stages (Fig. 4): gametogenesis, zygote formation, zygote maturation (zygospore formation), and meiosis (zygospore germination). Gametogenesis is initiated by nitrogen depletion and light exposure. When gametes of opposite types meet, flagellar adhesion triggers activation, leading to cell fusion and zygote formation. The zygotes then mature into zygospores, which are dormant and protected by a thick cell wall.

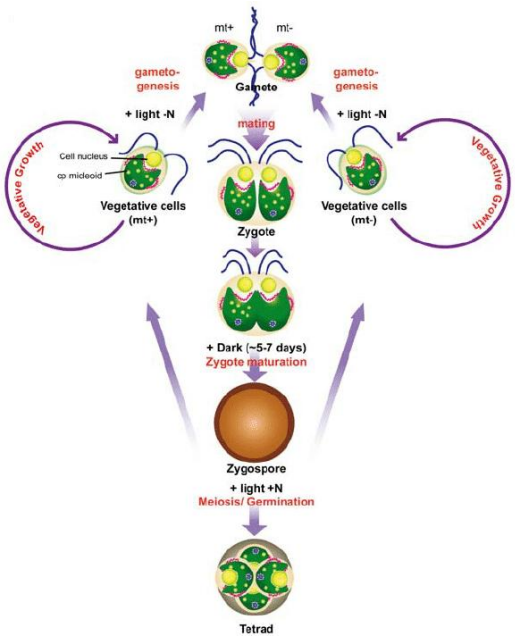

Fig 4. The sexual life cycle of *Chlamydomonas reinhardtii* consists of four key stages: gametogenesis, zygote formation, zygote maturation (zygospore formation), and meiosis (zygospore germination). Image retrieved from Y. Nishimura, 2010.

Once favorable environmental conditions occur, the zygospore germinates, producing 4 to 32 haploid cells of both mating types (mt+ and mt−), which develop new cell walls and flagella before being released as the zygospore wall breaks down (Dupuis and Merchant, 2023; Nishimura, 2010). During this process, chloroplast and mitochondrial DNA are inherited uniparentally from the mt+ and mt− parents, respectively.

1.4 Photosynthesis

Photosynthesis is a vital process that provides most of the energy supporting life on the planet. It is a process that converts solar energy into electrochemical energy and involves two main stages highly preserved through evolution: the light-dependent reactions (or the electron transport chain (ETR)) occurring in the thylakoid membranes, and the Calvin-Benson cycle, which takes place in the stroma of the chloroplast.

In *Chlamydomonas reinhardtii*, photosynthesis begins with the absorption of light by pigments such as chlorophylls (a and b), carotenoids, and xanthophylls (including lutein, zeaxanthin, violaxanthin, and neoxanthin) embedded in the thylakoid membranes. Chlorophylls absorb light primarily in the blue and red wavelengths, while carotenoids and xanthophylls assist in broadening the absorption spectrum and protecting against oxidative damage. The absorbed light energy is captured by Light-Harvesting Complexes (LHCs), which are protein-pigment complexes associated with both Photosystem II (PSII) and Photosystem I (PSI).

In PSII (Fig. 5), the energy excites electrons in chlorophyll molecules within the reaction center. These excited electrons are transferred through the electron transport chain and are eventually used to reduce NADP+ to NADPH in PSI (Johnson et al, 2013). To restore the loss of electrons, water molecules are split by PSII in a process known as photolysis, releasing oxygen (O_2) and protons (H^+). The electron transport process also creates a proton gradient (ΔpH) across the thylakoid membrane, which drives the synthesis of ATP via ATP synthase. Electron transport is mediated in the stroma by ferredoxin (Fd) and ferredoxin-$NADP^+$ reductase (FNR) and at the level of the thylakoid membrane by intersystem electron carriers (inter- PSII and PSI) plastoquinones, cytochrome b_6f complex, and plastocyanin (PC). (Johnson and Alric, 2013).

The excited electrons in PSI (Fig. 5) are re-excited by light absorbed by its chlorophyll a-rich antenna complex, and the resulting flow of electrons reduces NADP+ to NADPH (Asada, 2006).

Both ATP and NADPH are used in the Calvin cycle (Fig. 5), the light-independent phase of photosynthesis, for carbon fixation and synthesis of glucose precursors. This cycle is vital for converting inorganic carbon into organic compounds. It can be divided into three main stages: carbon fixation, reduction, and regeneration.

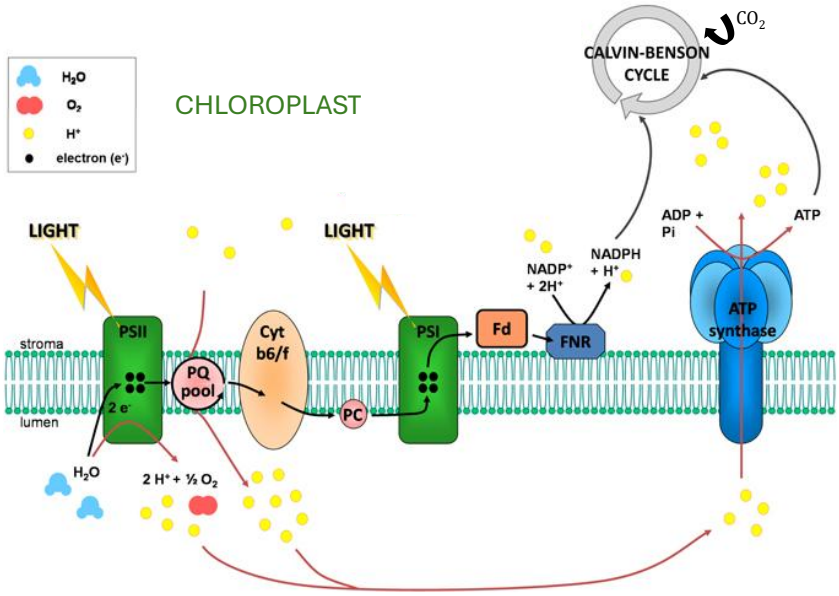

Fig 5. The Electron Transport Chain (ETR) and the light regulation of the Calvin-Benson cycle. In PSII, light splits water into oxygen, protons, and electrons, which reduce plastoquinone (PQ). These electrons move through Cytochrome b6f, reducing plastocyanin, and reach PSI, where another light reaction reduces ferredoxin (Fd), ultimately leading to NADPH formation via FNR. Meanwhile, Cytochrome b6f pumps protons into the thylakoid lumen, generating a proton gradient (ΔpH). ATP synthase uses this gradient to produce ATP. Both ATP and NADPH fuel the Calvin-Benson cycle, enabling carbon fixation into sugars (Adapted from Michelet et al. 2013).

It involves a series of twelve enzymatic reactions, which require the consumption of nine molecules of ATP and six molecules of NADPH. The cycle ultimately produces one molecule of the glucose precursor, glyceraldehyde-3-phosphate (G3P). G3P is crucial as it serves as a building block for the synthesis of sugars and other metabolic intermediates essential for the cell's energy and structural needs.

Thus, Photosystems I (PSI) and II (PSII) are integral to this process, facilitating charge separation and electron transport. However, although they share a common ancestor, PSI and PSII have evolved distinct roles, differing in the organization of their light-harvesting systems, pigment compositions, electron acceptors and donors (Minagawa & Tokutsu, 2015).

PSII is a large multisubunit pigment-protein complex that captures light energy to oxidize water and reduce plastoquinone, utilizing peripheral antennas composed of major trimeric and minor monomeric light-harvesting complex proteins (LHCII) proteins. In the green alga *C. reinhardtii*, there are four major LHCII proteins (types I–IV) with five, one, two and one isoform, respectively (LHCBM3, 4, 6, 8 and 9; LHCBM5; LHCBM2 and 7; LHCBM1) (Minagawa and Takahashi, 2004), and two minor LHCII proteins CP29 and CP26 that are encoded by LHCB4 and LHCB5, respectively (Minagawa, 2009). This is different from *Arabidpsis thaliana*, that has three majors trimeric LHCII proteins (types I–III) with

five, four and one isoform, respectively (LHCB1.1–1.5; LHCB2.1–2.4; LHCB3.1) and three minor LHCII proteins: CP29 and CP26 and CP24, encoded by LHCB4 LHCB5 and LHCB6, respectively (Teramoto et al., 2001).

The photosystem I (PSI) in *Chlamydomonas reinhardtii* is part of a large supercomplex formed with light-harvesting complex proteins (LHCI), comprising nearly 20 subunits. This complex absorbs light energy and drives electron flow from plastocyanin (Pc) to ferredoxin (Fd). Unlike cyanobacteria, which have dimeric or trimeric PSI cores, eukaryotic PSI cores, including those in *C. reinhardtii*, are monomeric and associate with LHCI proteins. In *C. reinhardtii*, nine LHCI proteins (LHCA1–9) form a double-layered LHCI belt that attaches to the PsaJ/F/G subunits under low light conditions. The composition of this LHCI belt is dynamic and adjusts to environmental factors, such as light and iron availability. This variability in LHCI proteins allows the organism to acclimate to environmental stressors like high or low light, temperature extremes, and nutrient shortages (Drop et al., 2011).

Furthermore, PSI's core complex, responsible for charge separation, is highly conserved across different photosynthetic organisms, indicating its evolutionary optimization for efficient oxygenic photosynthesis (Minagawa & Tokutsu, 2015). While the PSI core remains stable, its surrounding antenna system, including LHCI, is adaptable, facilitating the dynamic reorganization of photosystem supercomplexes in response to environmental changes. These adaptations include state transitions and switching between light-harvesting and energy-dissipating activities, essential for maintaining photosynthetic efficiency and protecting the system from photooxidative damage (Minagawa & Tokutsu, 2015). Thus, the ability of *C. reinhardtii* to modify its PSI–LHCI supercomplex in response to environmental cues is critical for its survival and performance.

Furthermore, The PSI antenna, which is enriched in chlorophyll a, absorbs light at longer wavelengths compared to PSII, which contains more chlorophyll b. This difference can cause an imbalance in the light-harvesting capacities of the two photosystems. To minimize this unequal distribution of light energy state transitions (qT) occur (Rochaix, 2014). There are two state transitions: State 1 and State 2 (Fig. 6).

In State 1, PSI is preferentially excited, leading to an increase in the light-harvesting capacity of PSI and a decrease in that of PSII to correct the excitation imbalance.

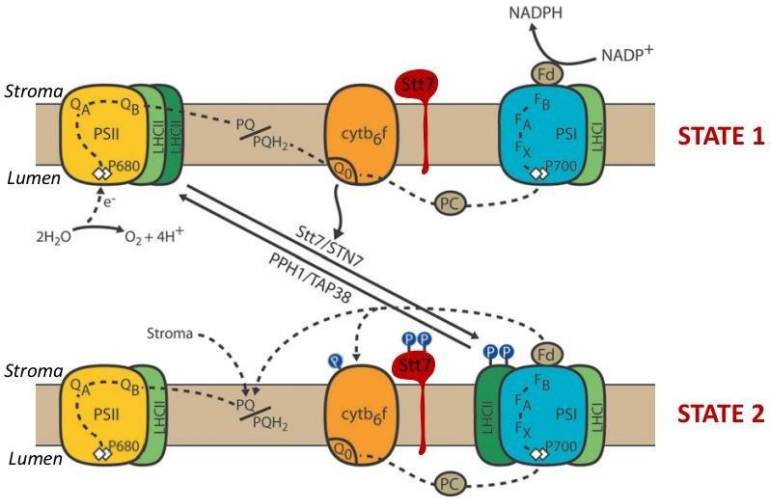

Fig 6. Model of state transitions in Chlamydomonas. State transitions occur through two redox-dependent states to balance excitation energy between photosystem I (PSI) and photosystem II (PSII). In State I, the excitation is balanced or favors PSI, and the PQ pool is oxidized, with Stt7 inactive and bound to the cyt b6f complex. When light conditions cause PSII to over-excite relative to PSI, the PQ pool becomes overreduced, activating Stt7, which is phosphorylated. This leads to the phosphorylation of PetO and LHCII proteins, causing LHCII to dissociate from PSII, migrate, and associate with PSI, resulting in State II. This adjustment helps reequilibrate excitation energy and the PQ pool's redox state, while Stt7 is later inactivated and reassociates with cyt b6f Adaptet from (Rochaix 2011).

During this state, the stroma of the chloroplast and the plastoquinone (PQ) pool are oxidized. As a result, LHCIIs are primarily bound to PSII, facilitating this adjustment (Minagawa, 2009).

State 2 occurs when light conditions shift to favor PSII. In this situation, the plastoquinone pool becomes reduced by electrons coming from PSII to PSI, and PQ binds the Q_o site of the cytochrome b_6f complex (Cyt *bf*). This reduction activates STT7 serine/threonine kinase, which phosphorylates LHCII major and minor proteins. This, in turn, causes LHCII to dissociate from PSII and migrate to PSI, optimizing energy distribution between the two photosystems (Lemeille et al., 2009).

In *C. reinhardtii*, up to 80% of LHCII antennae can migrate, a greater proportion than in plants. Phosphorylation is crucial for this migration, but not all phosphorylated proteins dissociate from PSII, and some remain associated with PSII while others form aggregates in the thylakoid membrane (Ünlü et al., 2014), potentially contributing to quenching.

State transitions are associated with photoprotection, particularly under high light conditions, by reducing photo-oxidative damage, likely through a decrease in hydrogen peroxide (H_2O_2) production (Allorent et al., 2013). They are also linked to changes in growth conditions, such as carbon availability (Iwai et al., 2007). Furthermore, state transitions are believed to work together with other photoprotective mechanisms, such as

qE (non-photochemical quenching), to prevent the photosystems from damage (Allorent et al., 2013), although the precise interaction between these processes is still not fully understood.

1.5 Photoprotection in Chlamydomonas (revisar si tengo que espaciar uno)

Chlamydomonas reinhardtii faces light stress in fluctuating environments, requiring mechanisms to avoid or repair damage from excess light. Thus, although light is essential for photosynthesis, excessive absorption can lead to the formation of reactive oxygen species (ROS), causing photo-oxidative damage and photoinhibition which can eventually lead to cell death.

To cope with this light stress, *C. reinhardtii* employs a range of strategies which can be short- or long-term responses. Short-term responses include phototaxis to move away from harmful light levels, dynamic regulation of light-harvesting antenna size and electron transport adjustment to balance light absorption, and non-photochemical quenching (NPQ) to dissipate excess energy as heat. Over time, the cell activates repair mechanisms, such as photosystem II turnover to maintain photosynthetic capacity, adjusts gene expression for acclimation and accumulates antioxidants to eliminate reactive oxygen species (ROS) in the chloroplast (Erickson et al., 2015) (Fig. 7).

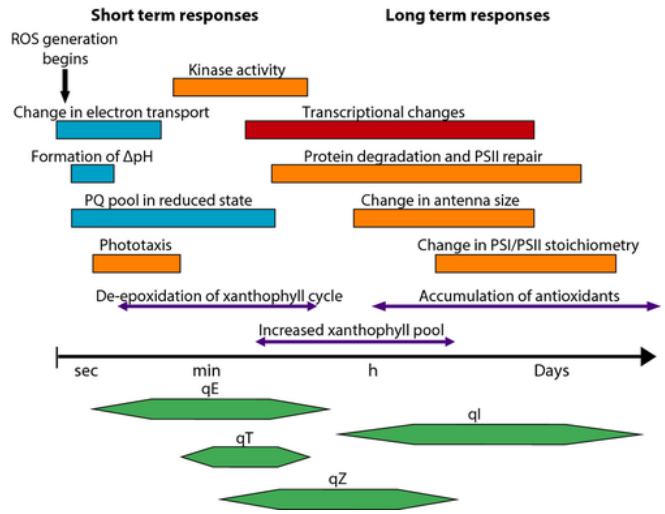

Fig 7. Relative time scales of high light responses. Changes related to chloroplast energetic states and ROS occur within seconds to minutes (blue). Changes involving protein activity(orange) and transcriptional responses (red) take place in the time scale of minutes, hours, or even days. Changes in pigment composition and antioxidant accumulation occur across a wide range of time scales (purple arrows). Non-photochemical quenching processes (qE, qZ, qT, and qI) are shown at the bottom (Retrieved from Erickson et al. 2015)

1.5.1 NPQ

When light absorption surpasses the cell's ability to use energy, photoprotective mechanisms activate to quench excess excited chlorophyll (1Chl*) and release the energy as harmless heat. These processes, collectively known as non-photochemical quenching (NPQ), are indicated by a reduction in chlorophyll fluorescence from PSII.

NPQ has both immediate responses to rapid changes in light and longer-term adaptations that help the cell adjust to prolonged exposure to high light. It involves four mechanisms: energy-dependent quenching (qE), a short-term response to excess light; state transition-dependent quenching (qT) that helps balance light absorption between photosystems; zeaxanthin-dependent quenching (qZ) which involves pigments that help dissipate excess energy and photoinhibitory quenching (qI), which protects against damage to photosystems (Erickson et al., 2015) (Fig. 7).

1.5.2 qE: A Rapid Photoprotective Mechanism

The fastest and most rapidly reversible component of NPQ, called the energy-dependent quenching (qE), operates on a timescale of seconds to minutes. This mechanism has been extensively studied across plants and green algae highlighting evolutionary differences over millions of years of separation (Peers et al., 2009).

The activation of qE relies on a proton gradient (ΔpH) generation across thylakoid membranes, which is triggered by enhanced photosynthetic electron transport upon high light (HL) exposure. In plants, the acidic pH in the thylakoid lumen triggers two critical processes: protonation of the lumenal domain of PSII subunit S (PSBS), leading to quenching in light-harvesting complex II (LHCII) proteins, and activation of the violaxanthin de-epoxidase (VDE) enzyme, which converts violaxanthin into antheraxanthin and zeaxanthin. Mutants lacking VDE demonstrate severely impaired NPQ (Niyogi et al., 1998). Thus, both PSBS and zeaxanthin are necessary for full induction of qE in plants.

In the green algae *Chlamydomonas reinhardtii,* the ΔpH is equally crucial for qE, but the mechanism differs from that in plants. Instead of PSBS as a main actor, Chlamydomonas relies on stress-responsive Light-Harvesting Complex (LHC) proteins (LHCSRs), which serve dual roles as pH sensors and quenching sites. In addition, Chlamydomonas primarily depends on lutein instead of zeaxanthin for its qE mechanism (Bonente et al., 2011; Peers et al., 2009).

Thus, three key proteins—LHCSR3, LHCSR1, and PSBS—play central roles in this qE activation mechanism. LHCSRs are membrane-bound proteins capable of binding pigments such as chlorophylls and xanthophylls. In Chlamydomonas, LHCSR1 and LHCSR3 are encoded by three genes: *LHCSR1*, *LHCSR3*.1, and *LHCSR3.2*, all located on the same chromosome. *LHCSR3.1* and *LHCSR3.2* encode identical proteins, while *LHCSR1* encodes LHCRS1 protein that differs from LHCSR3 mostly at the C-terminus.

Structurally, LHCSR3 binds 7–8 chlorophylls, with higher affinity for Chl a than Chl b, and 2–3 carotenoids (one lutein and one violaxanthin or zeaxanthin), with lutein forming a radical cation for rapid quenching. Its activation is pH-dependent, occurring under acidic conditions at specific pH-sensing residues (Bonente et al., 2011). Furthermore, LHCSR3 interacts with LHCII and PSII-LHCII super complexes by binding to specific subunits and it is hypothesized to interact with LHCBM1, another light-harvesting protein, as LHCBM1-deficient mutants exhibit impaired qE (Bonente et al., 2011). LHCSR1 also participates in the pH-dependent LHCII quenching.

LHCSR3 is indispensable for qE induction, as mutants lacking both *LHCSR3.1* and *LHCSR3.2* (*npq4*) show impaired qE capacity, heightened sensitivity to high light and reduced fitness. *LHCSR1* plays a supplementary role, compensating for *LHCSR3* under certain conditions, such as mixotrophic growth or overexpression scenarios. However, double mutants lacking both *LHCSR3* and *LHCSR1* (*npq4lhcsr1*) are completely unable to perform qE, leading to significant photodamage and decreased growth rates under HL and fluctuating light conditions (Peers et al., 2009; Allorent et al., 2016; ; Ruiz-Sola et al., 2021).

The expression of *LHCSR* genes is regulated by environmental cues, including high light (HL), UV-B, and blue light (Fig. 8). These responses are mediated by photoreceptors, such as UVR8 UV-B and phototropin blue light photoreceptors (Allorent et al., 2016; Petroutsos et al., 2016). Under LL conditions, Chlamydomonas cells are known to show limited qE capacity due to *LHCSR* lack of expression (Peers et al., 2009). However, photoautotrophic cells growing in day/night cycles have relatively high qE capacity, which has been associated with *LHCSR* accumulation (Nawrocki, Liu, & Croce, 2020). And even at very LL intensities, UV-B and blue light strongly increase *LHCSR* mRNA levels within an hour (Redekop et al., 2022).

In parallel to LHCSR proteins, PSBS plays a role in photoprotection, which is another member of the LHC superfamily encoded by two PSBS homolog genes (*PSBS1* and *PSBS2*). While PSBS is widely studied in plants, its function in Chlamydomonas remains unclear. Unlike LHCSRs, PSBS lacks pigment-binding capabilities but responds to ΔpH by

protonating exposed residues to trigger quenching (Fan et al., 2015). *PSBS* shows increased expression during transitions from darkness to low light (LL) or from LL to high light (HL) (Strenkert et al., 2019). Recent studies have shown that little low UV-B illumination induces *PSBS* expression at similar levels to those observed under HL (Redekop et al., 2022).

Expression of *LHCSR1* and *LHCSR3* in Chlamydomonas, however, differ significantly based on light conditions. *LHCSR1* is predominantly expressed in response to UV-B exposure, whereas *LHCSR3* is strongly induced under high light (HL) conditions, including white, blue, and red light (Allorent et al., 2016; Tilbrook et al., 2016). UV-B exposure influences the activity of the COP1/SPA1 E3 ligase complex, leading to the accumulation of the transcription factor Chlamydomonas CONSTANS (CrCO), which activates *LHCSR* genes (Gabilly et al., 2019) (Fig. 8). The induction of these *LHCSR* genes has been similarly observed in *phot* mutants lacking the blue-light photoreceptor phototropin (Aihara et al., 2019).

PSBS is also regulated via COP1/SPA1-mediated signaling (Gabilly et al., 2019). Under HL conditions, its protein accumulation is transient, contributing to the qE activation (Allorent et al., 2016) (Fig. 8). Interestingly, when cells are grown under diurnal light cycles, PSBS protein levels remain elevated throughout the day (Nawrocki, Liu, & Croce, 2020).

In addition to COP1/SPA1, another E3 ubiquitin ligase complex, CUL4-DDB1DET1, plays a regulatory role in *LHCSR* expression. DET1 and DDB1 are two downstream components of PHOT which are involved in qE quenching and in the induction of photoprotective genes including *LHCSR1/3* and *PSBS* under high-light conditions. Minagawa's group proposed that high-light conditions enhance qE gene expression due to the inactivation of the E3 ligase complex CUL4–DDB1DET1 through the PHOT signal (Fig. 8). Furthermore, CUL4-DDB1DET1complex has been suggested to enhance the activity of COP1/SPA1, further fine-tuning the response to HL conditions (Aihara et al., 2019).

Additionally, in Aihara et al., 2019 it was demonstrated that high-light signaling regulates photoprotective gene expression through multiple distinct pathways. As said, one pathway is mediated by PHOT, due to the absence in the *phot* mutant suppresses high-light-induced gene expression. However, the presence of high *PSB1/2* and *LHCSR1/3* transcript levels in both dark and high-light conditions in *det1 phot* mutants suggests additional regulatory mechanisms involving DET1 (Fig. 8).

Indeed, they observed that while *LHCSR1* and *PSBS1/2* are expressed even in the absence of photosynthesis, *LHCSR3* is only expressed when photosynthesis is active.

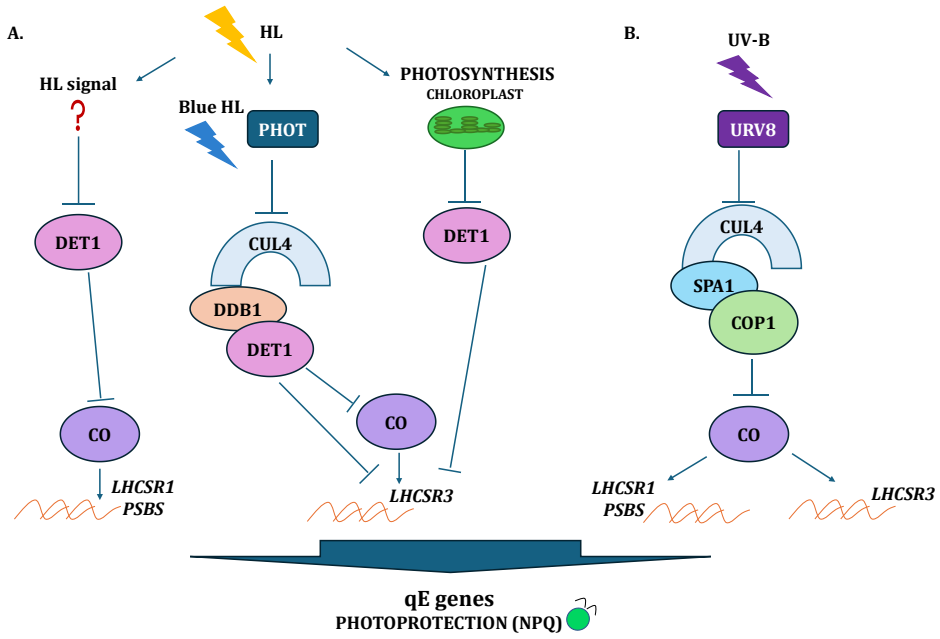

Figure 8. Proposed models for the regulation of *LHCSR1*, *LHCSR3*, and *PSBS* expression in C. reinhardtii under high light and UV-B stress. A. High light triggers expression of *LHCSR1*, *LHCSR3*, and *PSBS* through the potential involvement of the E3 ligase complex CUL4-DDB1DET1, along with other DET1-dependent signaling pathways. **B.** UV-B induces the expression of *LHCSR1*, *LHCSR3*, and *PSBS* via an SPA1/COP1-associated E3 ligase complex. Further details on these signaling cascades are provided in the main text (Adapted from Lu et al. 2022)

This led them to conclude that DET1 regulates two distinct high-light signaling pathways: one that functions regardless of photosynthesis (for *LHCSR1* and *PSBS1/2*) and another that requires active photosynthesis (for *LHCSR3)* (Fig. 8).

Notably, the accumulation of *LHCSR3*, but not *LHCSR1* or *PSBS*, in *crco* and *crco spa1-1* mutants suggests a high-light-dependent but SPA1/CrCO-independent pathway. Since *phot* and *crco* mutants show similar phenotypes, PHOT may function as a photoreceptor in this pathway. Additionally, this SPA1/CrCO-independent pathway might be regulated similarly to the chloroplast-DET1-dependent high-light signaling pathway (Aihara et al., 2019) (Fig. 8).

Interestingly, *LHCSR* expression can also be triggered by non-light stressors like low CO_2 or nutrient deprivation. CIA5 (also CCM1), a transcription factor regulating carbon-concentrating mechanisms, upregulates *LHCSR3* even in darkness and stabilizes LHCSR1 protein, though it has a minimal impact on *PSBS* expression (Ruiz-Sola et al., 2021).

Furthermore, the thylakoid calcium-sensing receptor (CAS) integrates light and calcium signals to induce *LHCSR3* expression during HL exposure (Petroutsos et al., 2011).

These distinct yet interconnected mechanisms underscore the complexity of photoprotection in Chlamydomonas and the evolutionary divergence of qE regulation between algae and plants.

1.6 Light as an environmental cue: sensory photoreceptors

Light plays a dual role in plants and algae, providing both energy and information that influence various processes, such as growth, development, orientation, adaptation, and stress responses, making it a critical environmental factor.

In plants, light-induced responses are mediated by various photoreceptors, including those sensitive to UV, blue, and red/far-red light (Fig. 9).

In Chlamydomonas, at least 18 sensory photoreceptors have been identified, spanning the light spectrum from UVB to infrared, enabling the regulation of numerous electrical and biochemical processes (Fig. 10).

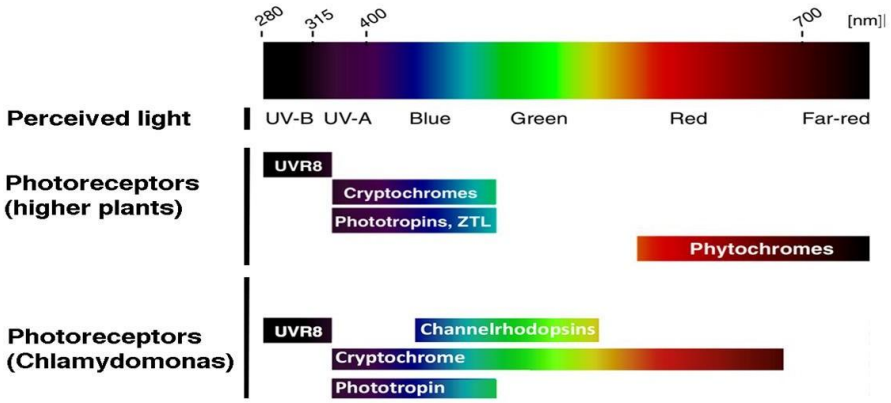

Figure 9. Photoreceptor families in higher plants and *Chlamydomonas reinhardtii.* In both land plants and *Chlamydomonas reinhardtii*, UVR8 detects UV-B light, while Cryptochromes and Phototropins sense blue light. Unlike plants, Chlamydomonas also contains rhodopsins. Land plants use phytochromes to perceive red light, but Chlamydomonas lacks these and instead relies on an animal-type Cryptochrome (CRY), which senses red, yellow, and blue light in its reduced form. Adapted from Heijde & Ulm, 2012.

Some of these photoreceptors are more universal, such as the blue-light-sensitive phototropin (PHOT) and the UV-B light-sensitive UVR8. Additionally, Chlamydomonas possesses two opsin-related photoreceptors, two channelrhodopsins (absent in plants), four cryptochromes, and eight rhodopsin-like proteins that respond to yellow and green

light (Hegemann, 2008). However, Chlamydomonas appears to lack phytochromes, the photoreceptors responsible for detecting red and far-red light, despite its ability to synthesize the bilin chromophore, phycocyanobilin (Hegemann, 2008) (Fig. 9 and 10).

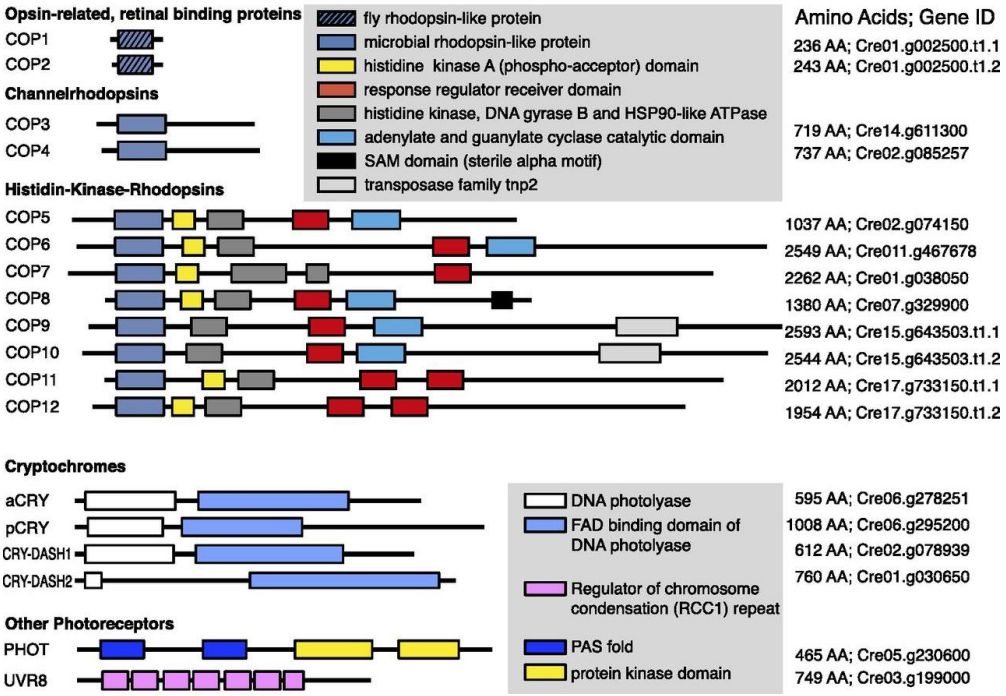

Fig 10. Sensory photoreceptors and domain structures in Chlamydomonas *reinhardtii*. Image retrieved from Greiner et al., 2017

1.6.1 Rhodopsins

Rhodopsins consist of a retinal chromophore and an opsin apoprotein. Based on sequence similarity, opsins are classified into two groups. Type-I rhodopsins (archaeal or microbial type) are found in various organisms, including archaea, bacteria, and fungi, but not in land plants or animals. Type-II rhodopsins are exclusive to animals. Despite their similar molecular structure, these two groups differ in amino acid sequences, chromophore configuration, and photochemical properties (Ernst et al. 2014).

In Chlamydomonas, two animal-type rhodopsins, COP1 and COP2, are located in the eyespot, playing a role in phototaxis (Deininger et al. 1995). This alga also contains two bacterial-type rhodopsins, the so called channelrhodopsin ChR1 and ChR2 (previously named as chlamyopsins, COP3 and COP4). They are encoded by *COP3* and *COP4,* respectively, serve as light-gated ion channels and play key roles in phototaxis and photophobic responses (Berthold et al. 2008). Specifically, these channelrhodopsins facilitate photoreceptor currents in the eyespot and drive flagellar photocurrents, leading to calcium flux changes across the membrane. This calcium flux initiates a cascade of

electrical signals, depolarizing the cell and ultimately regulating flagellar beating (Holland et al., 1997)

Notably, CrCHR2 has been expressed in HEK cells, confirming its functionality outside Chlamydomonas (Nagel et al., 2002). This result enabled the development of optogenetics, where CHRs are used to control cell activity with light (Boyden et al., 2005; Hegemann, 2008).

In addition, Chlamydomonas possesses eight microbial-type rhodopsins with histidine kinase and response regulator domains (COP5-COP12), forming the histidine kinase rhodopsin (HKR) subfamily, though their functions remain unidentified (Luck et al., 2012).

1.6.2 Blue-light photoreceptors

In Chlamydomonas and higher plants, two photoreceptors that respond to blue light, cryptochromes and phototropins, have been characterized at the molecular level. Specifically, in *C. reinhardtii*, a single phototropin (CrPHOT) has been identified (Huang & Beck, 2003).

Cryptochromes

Cryptochromes represent a group of diverse sensory photoreceptors present in all kingdoms of life. Together with the UV-light-dependent DNA repair enzymes, the photolyases, they constitute the cryptochrome/photolyase family.

The *Chlamydomonas reinhardtii* genome encodes four distinct cryptochromes (Beel et al., 2012; Kottke et al., 2017). One animal-type aCRY (previously named: Chlamydomonas photolyase homolog-1, CPH1) one plant-type pCRY (previously named PLH) and two CRY-DASH-like proteins, CRY-DASH1 and CRY-DASH2 (Beel et al., 2012).

The animal-like cryptochrome (aCRY) in *Chlamydomonas reinhardtii* plays a crucial role in regulating the expression of several genes in response not only to blue but also to yellow and red light. These genes code for proteins involved in chlorophyll and carotenoid biosynthesis, light-harvesting complexes, nitrogen metabolism, cell cycle control, and the circadian clock (Beel et al., 2012, Oldemeyer et al., 2016). aCRY can control both the transcript levels and the sexual cycle of the alga in a positive (germination) and negative manner (mating ability) (Müller et al., 2017, Franz et al., 2018). Furthermore, aCRY exhibits photolyase activity, catalyzing the repair of UV-DNA lesions (Franz et al., 2018). Its red-light absorption responses were studied in detail with a focus on an unusually long-

lived tyrosyl radical which may contribute to its photoreceptor functions (Oldemeyer et al., 2016)

The plant-type cryptochrome pCRY in *Chlamydomonas reinhardtii* is rapidly degraded when exposed to light (Reisdorph and Small, 2004) and has shown to be involved in the circadian clock and in the algal sexual cycle (Müller et al., 2017). The flavin cofactor within pCRY primarily absorbs UV-A/blue light, forming a neutral radical upon illumination in vitro. Recent research has highlighted pCRY's involvement in regulating ROC75, a key component of the central circadian clock. pCRY accumulates in darkness and is degraded by light, modulating *ROC75* expression to prevent over-accumulation. This process is vital for the activation of LHCSR3 through PHOT-mediated signaling (Kamrani et al., 2018).

In addition to pCRY and aCRY, the *C. reinhardtii* genome also encodes two CRY-DASH-like proteins, CRY-DASH1 and CRY-DASH2 (Beel et al., 2012). While research on these CRY-DASH proteins is still ongoing, their precise functions remain to be fully characterized. However, it is known that CRY-DASH1 is localized in the chloroplast and utilizes light as a signal to regulate algal photoautotrophic growth and modulate the photosynthetic machinery (A, Rredhi et al., 2021).

Phototropin

Phototropin (PHOT) in *Chlamydomonas reinhardtii* plays a critical role in regulating different light-dependent processes essential for the organism's survival and reproduction. Unlike *Arabidopsis*, which has two phototropins, PHOT1 and PHOT2, Chlamydomonas contains a single phototropin, CrPHOT. However, the three different PHOT domains (two blue-light-sensitive domains, LOV1 and LOV2 (Light Oxygen and Voltage) at the N-terminal, as well as a C-terminal serine-threonine kinase) are well conserved across species (Christie et al., 1998; Christie, 2007) (Fig 11. A).

The LOV domains, which are members of the Per-ARNT-Sim (PAS) domain superfamily, act as light sensors and participate in an independent photocycle. In the dark, the protein is in an inactive state, with a noncovalent bond between the LOVs domains and the FMN chromophore with an absorption maximum at 447 nm (LOV1-447) (Fig. 11 B).

Upon exposure to blue light, the protein becomes active, forming a covalent adduct between the FMN and a conserved cysteine residue within each LOV domain. This adduct exhibits an absorption maximum of around 390 nm (LOV-390). (Alexandre et al., 2009; Kay et al., 2003) (Fig. 11 B).

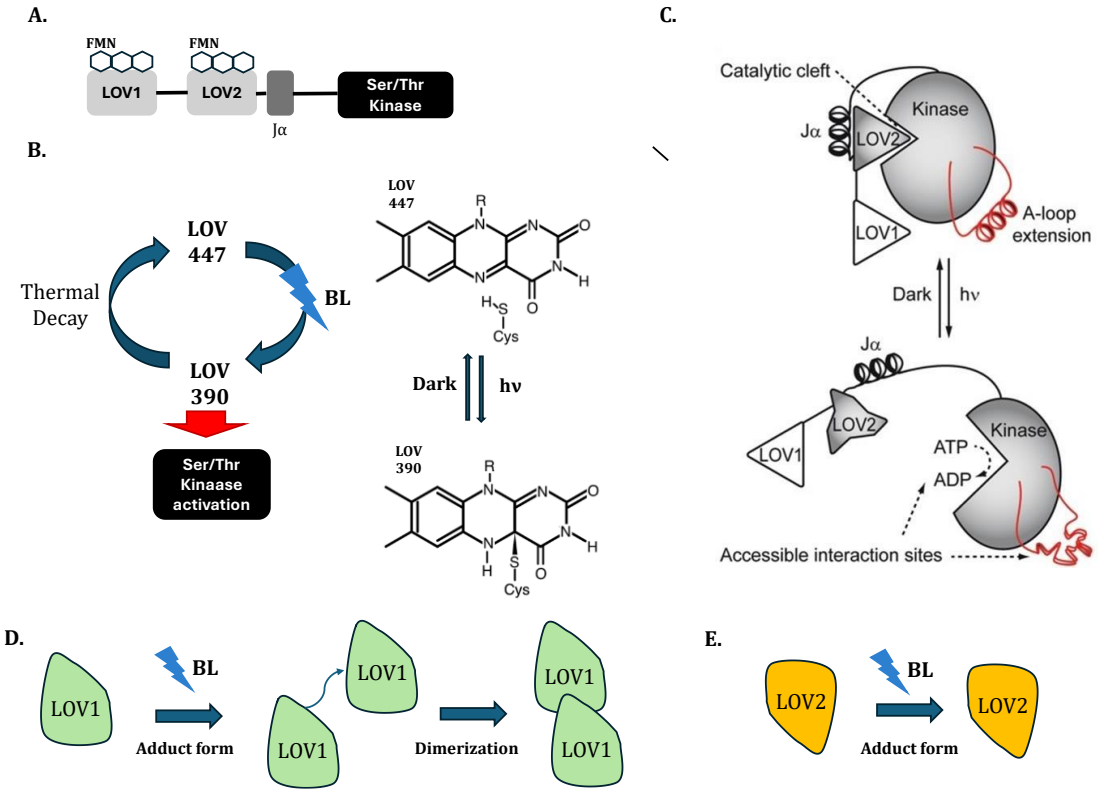

Fig 11. A. Illustration showing the structural organization of phototropin (Phot) in *C. reinhardtii* with its LOV1 and LOV2 domains and their corresponding FMN chromophores, the Jα helix and the Ser/Thr kinase domain. B. Schematic drawing of the LOV photocycle and chemical structures of the dark (inactive) state (LOV-447) and the light (active) state (LOV-390) where the flavin-cysteine adduct is formed (Adapted from K Okajima, 2016) C. Activation mechanism of CrPHOT: in darkness, LOV2 inhibits the kinase in CrPHOT. Blue light triggers dissociation of the Jα helix, causing structural changes that activate the kinase. The activation loop also undergoes conformational changes, creating a second interaction site. (Retrieved from Pfeifer et al. 2010). D and E Proposed reaction schemes of Cr LOV1 and Cr LOV2 (Adapted from Nakasone et a. 2018)

This reaction, occurring in microseconds, triggers small conformational changes in the protein, activating its serine-threonine kinase domain by autophosphorylation (K. Okajima, 2012) (Fig X. A and B). This kinase activation is central to the CrPHOT role in signal transduction.

Like in *Arabidopsis*, the LOV2 domain is crucial in regulating the kinase activity and is sufficient for this activation by itself (Matsuoka and Tokutomi, 2005; Nakasone et al., 2018). Upon photoexcitation, under blue light, LOV2 undergoes a well-characterized photochemical cycle involving the formation of a cysteinyl adduct with the chromophore flavin mononucleotide (FMN). This is accompanied by structural changes that can involve slight alterations in the protein backbone, particularly at the Jα helix, whose detachment from LOV2, relieves the kinase inhibition happening at dark (Harper, Neil, and Gardner 2003) (Pfeifer et al. 2010), and leads to autophosphorylation of the kinase domain along with exposure of new interaction sites (Onodera et al. 2005). The activation loop, which

can serve as a second interaction site for protein- protein interaction, also goes through conformational changes at CrPHOT, an observation which has been disputed for AtPHOTs (Takakado et al. 2017) (Fig. 11 C).

The photoreaction of LOV2 affects the overall light sensitivity of the phototropin, and although it is primarily responsible for transducing the light signal, it can also interact indirectly with LOV1. Furthermore, it has been recently described that LOV2, in the dark state, predominantly exists as a monomer and it does not dimerize in the absence of light, which contrasts with the behavior of LOV1 (Fig 11. D). This characteristic allows it to function distinctly within the photoreceptor system.

Conversely, while LOV1 primarily modulates PHOT photosensitivity in *Arabidopsis* (Matsuoka and Tokutomi, 2005), this regulatory role of LOV1 is less pronounced in Chlamydomonas, though its exact role remains less clear. It is known that LOV1 does not independently activate the kinase domain like LOV2, however, the presence of LOV1 significantly alters the recovery dynamics of LOV2, suggesting that LOV1 can enhance light sensitivity by modifying how quickly LOV2 returns to its base state after activation. Specifically, the recovery rate of LOV2 is reduced in the presence of LOV1, which may lead to prolonged signaling in response to light.

Interestingly, recent studies have shed some light on LOV1 role. Apparently, in the dark state, LOV1 exists in dynamic equilibrium between monomeric and dimeric forms. The primary photochemical reaction associated with LOV1 is its dimerization upon light exposure (Nakasone et al., 2018) (Fig 11. E). In this process, monomers come together to form dimers, while dimers can also dissociate back into the monomer form depending on the light stimulus.

Therefore, the monomeric state of LOV2 in the dark allows for flexible interactions and independent signaling in photoreception, enhancing the plant's ability to respond quickly to light stimuli. Unlike LOV1, which dimerizes, LOV2's structure facilitates distinct regulatory mechanisms essential for its function. Conversely, in LOV1, this dynamic equilibrium between its monomeric and dimeric forms allows for versatile signal modulation in response to light. Upon light exposure, monomers dimerize, enhancing signaling activity, while dimers can dissociate back to monomers, enabling quick recovery and adaptation to changing light conditions. This cycling mechanism conserves resources and enables organisms to efficiently respond to their environment. This functional diversity between LOV1 and LOV2 contributes to the overall efficiency of photoregulation in *Chlamydomonas reinhardtii*.

Like in *Arabidopsis,* LOV2 plays a key role in regulating the kinase activity (Matsuoka and Tokutomi, 2005; Nakasone et al., 2018) although the exact mechanism of kinase activation remains to be fully elucidated. Conversely, while LOV1 primarily modulates PHOT photosensitivity in *Arabidopsis* (Matsuoka and Tokutomi, 2005), this regulatory role of LOV1 is less pronounced in Chlamydomonas, where its function seems to be more focused on structural changes and dimerization (Nakasone et al., 2018).

In Chlamydomonas, CrPHOT plays a crucial role in regulating gametogenesis, mating ability, and zygote germination. Studies have shown that strains with reduced phototropin levels exhibit significant impairments in these key life cycle stages, highlighting CrPHOT's essential function in controlling the alga's life cycle in response to light (Huang and Beck, 2003).

CrPHOT is found in both the eyespot and flagella, which highlights its key role in cellular signaling and environmental cues. Phototropin trafficking is driven by intraflagellar transport (IFT), a motor-based, bidirectional protein transport system in cilia and flagella. IFT is essential for ciliogenesis, and defects in this process can lead to ciliopathies, disorders caused by mutations disrupting cilia function (Huang & Beck, 2003; Huang, Kunkel, and Beck, 2004). While IFT's involvement in phototropin trafficking is recognized (Beauclair et al., 2015), the detailed mechanisms of this interaction are still not fully understood.

Additionally, CrPHOT regulates phototaxis by modulating the abundance of Channelrhodopsins (CrCHR1 and CrCHR2), which are critical for light sensing and movement toward or away from light (Trippens et al., 2012).

As previously explained, CrPHOT also plays a role in photoprotection, regulating LHCSR3 protein, which is known to help dissipate excess light energy in photosystem II through non-photochemical quenching (NPQ). The process is regulated by proteins such as COP1 and the CUL4-DDB1DET1 E3 ligase complex, which also influence the induction of *LHCSR1* and *LHCSR3* genes under blue high light (Petroutsos et al., 2016; Aihara et al., 2019).

1.6.3 UVR8

The UV-B acclimation response is controlled by the UV-B-sensing photoreceptor UV RESISTANCE LOCUS 8 (UVR8), which plays a key role in the cellular response to UV-B exposure.

In *Chlamydomonas reinhardtii*, UVR8 shares sequence and structural similarity to *Arabidopsis thaliana* UVR8, particularly has the conserved tryptophan residues key for UV-B photoreception. It monomerizes upon UV-B exposure, and interacts with the E3 ubiquitin ligase complex, specifically the CONSTITUTIVELY PHOTOMORPHOGENIC1 (Cr-COP1). As a result, gene expression is altered, triggering accumulation of genes involved in photosynthesis and photoprotection, in particular *ELIP1, 4,* and *5*, as well as specific members of the light-harvesting complex (LHC) superfamily that contribute to qE, specifically *PSBS*1, *PSBS*2, *LHCSR1* and *LHCSR3* (Tilbrook et al., 2016, Allorent et al, 2016).

Furthermore, it is known that *LHCSR3.1* and *LHCSR3.2* are regulated by both blue (PHOT) (Petroutsos et al., 2016; Aihara et al., 2019) and UV-B light (UVR8) (Allorent et al, 2016) photoreceptors, suggesting an interplay between UVR8/PHOT signaling pathways that regulate LHCSR3 expression (Allorent & Petroutsos, 2017; Petroutsos, 2017).

Together, these features make *Chlamydomonas reinhardtii* a versatile and consistent model for studying a wide range of biological processes, including photosynthesis, motility, metabolism, and stress responses. Its combination of fast growth, metabolic flexibility, and established genetic tools (together with resources such as the CLiP mutant library and well-characterized transformation protocols) have made it a reference system for algal biology. Altogether, Chlamydomonas offers a unique opportunity to investigate how single-celled eukaryotes integrate environmental cues, especially light, with gene regulation, signal transduction, and dynamic cellular responses.

OBJECTIVES

This thesis is based on three main objectives:

1- **To characterize how light intensity and photoperiod shape the physiological responses of different *Chlamydomonas reinhardtii* laboratory strains,** primarily focusing on pigment content, growth, cell morphology, photosynthetic efficiency, and non-photochemical quenching (NPQ).

2- **To characterize the role of the histidine kinase proteins HIK1 and HIK2 in blue light signaling**, by generating and analyzing mutant lines, and quantifying NPQ dynamics, photosystem II efficiency, and the expression of qE-related genes.

3- **To develop a PCR-based screening method capable of detecting both large insertions and small indels in CRISPR-Cas9-edited mutants**

Chapter 2

Physiological Acclimation to Photoperiod and Light Intensity in *Chlamydomonas reinhardtii* Strains

1. INTRODUCTION

1.1 Background and Variation in Common Chlamydomonas Strains

The modern history of *Chlamydomonas reinhardtii* as a model organism began in 1945, when Gilbert M. Smith isolated a single diploid zygospore from a potato field near Amherst, Massachusetts. This zygospore gave rise to haploid MT+ and MT– progeny that formed the foundation for what are now referred to as laboratory strains. These strains were propagated and diversified over the following decades, giving rise to three major sublines identified in the 1950s: the Sager, Cambridge, and Ebersold/Levine lineages (Harris, 2009).

Over time, repeated crosses and sharing between laboratories reduced the traceability of each strain and complicated efforts to clearly define their differences. Many strains traditionally considered "wild type" have accumulated spontaneous mutations or been selectively bred for traits favorable to laboratory growth, resulting in notable genotypic and phenotypic divergence (Gallaher et al., 2015). Whole-genome resequencing has revealed a mosaic of sequence variation within laboratory strains and highlighted the absence of a universally accepted Chlamydomonas reference strain (Flowers et al., 2015; Gallaher et al., 2015).

The Ebersold/Levine subline, which many commonly used strains come from, carries two unlinked mutations in NIT1 and NIT2, making it unable to use nitrate as a nitrogen source. These mutations are found in two of the most widely used laboratory strains: CC-124 (MT– , agg1–) and CC-125 (MT+, AGG1+), which are both direct descendants of the original 137c line (Harris, 2009). While they're often assumed to be very similar, these two strains differ in several traits, including phototactic aggregation, how they respond to blue light, and photoreceptor activity. For instance, CC-124 is particularly sensitive to blue light (440 nm) in circadian phase-resetting assays, likely due to cryptochrome signaling (Gallaher et al., 2015).

Genome studies (Craig et al., 2023) have shown that structural changes, like the insertion of mobile elements, vary between laboratory strains and can affect gene expression and how stable transgenes are. These differences can influence transgene stability, stress responses, and phenotypic reproducibility across laboratories.

Beyond these classical strains, additional derivatives have been developed to address specific research needs. For instance, 4A+ (CC-4051), a mating type plus strain, originated in Jean-David Rochaix's lab as a fast-growing acetate-utilizing derivative of the 137c lineage. Like CC-124 and CC-125, it carries nit1 and nit2 mutations, but it was selected for

enhanced growth in the dark, making it well-suited for studies under heterotrophic or mixotrophic conditions.

More recently, researchers have developed new strains to help with large-scale functional studies. The CC-5325 strain (also listed as CC-4533 or CMJ030) was developed as the background for the Chlamydomonas Library Project (CLiP) mutant library. It resulted from a cross between 4A– (cell wall-intact) and D66+ (cell wall-deficient), chosen for beneficial traits such as efficient transformation, reliable cryopreservation, reduced clumping in culture, and consistent growth under both autotrophic and heterotrophic conditions (Dent et al., 2005).

CC-5325 grows faster than many other strains when using acetate in the dark, but it shows lower photosynthetic efficiency and higher sensitivity to heat compared to strains like CC-1690 (also referred to as *21gr*). Notably, although previously thought to lack a cell wall (as cw15 derivatives do), it appears to retain a thin, intact cell wall (Zhang et al., 2022). Additionally, CC-5325 shows deficient circadian rhythms in phototactic behavior, indicating that even in "wild-type" genetic backgrounds, there can be hidden physiological divergence.

Despite the label "wild type," these laboratory strains differ significantly from true environmental isolates, such as CC-2931 or CC-2935. Wild isolates exhibit greater sequence divergence, structural rearrangements, and phenotypic variability under environmental stress (Flowers et al., 2015). Such natural variation is being increasingly studied to understand intraspecific diversity, ecological fitness, and evolutionary adaptation.

Furthermore, the choice of strain background influences not only physiological traits but also experimental tractability. For example, strains lacking cell walls (e.g., cw15, D66) exhibit higher transformation efficiencies but altered stress responses and cell cycle regulation (Neupert et al., 2009). These characteristics directly influence the usefulness of strains for mutant libraries and transgenic studies.

As a result of independent subculturing, storage, or handling practices, many strains now exist in slightly different versions across stock centers. Since freezing and repeated handling over time can introduce small changes, it is now recommended to verify the genomic sequence of the strain before starting important experiments, to prevent unexpected effects on the results.

This diversity and divergence between laboratory versions have important consequences for research. Unlike *Arabidopsis thaliana*, which benefits from the well characterized

Columbia ecotype as a universal reference, Chlamydomonas research relies on a mix of related but genetically different laboratory strains. While some exhibit conserved traits, others vary significantly, especially under stress or in specific physiological pathways. Comparative studies have begun to uncover this intraspecific variation, such as differential triacylglycerol accumulation, circadian responses, and growth phenotypes (Siaut et al., 2011).

Understanding the history, genome, and main traits of each strain is essential, not only to ensure reproducibility, but also to correctly interpret mutant phenotypes and make meaningful comparisons between strains. As new genomic and trait-analysis tools continue to improve, knowing the specific features of each strain will remain key to making the most of Chlamydomonas as a model organism.

1.2 Light as an Environmental Cue and Stress Signal

Photosynthetic organisms are profoundly influenced by light throughout their life cycle. In natural environments, they are exposed to fluctuating light conditions caused by daily light-dark cycles, seasonal changes, and geographic or atmospheric factors. To adapt to these rhythms, they have evolved mechanisms to synchronize key biological processes with external light patterns.

Unicellular algae, in particular, can coordinate critical developmental and physiological processes based on photoperiodic signals. For example*, Ostreococcus tauri* shows a daily pattern of starch synthesis, with peak levels at the end of a 12-hour light cycle (Sorokina et al., 2011). In *Dunaliella salina*, cell volume and glycerol production follow similar daily rhythms (Xu et al., 2016). In *Chlamydomonas reinhardtii*, processes like cell cycle progression, starch biosynthesis, chloroplast activity, and lipid accumulation are all influenced by light-dark cycles (Serrano-Bueno et al., 2017).

Photoperiod refers to the duration of light exposure within a 24-hour cycle, while light intensity describes the strength of the light received. Both play key roles in both natural and industrial settings. These factors directly influence photosynthesis, growth, and the biochemical composition of the cells. While extended light exposure can boost productivity, too much light can lead to photoinhibition and reduced efficiency (Baroli & Melis, 1998; Mulders et al., 2014). Understanding how to balance light and dark periods and adjust light intensity is therefore essential for optimizing algal growth and biomass yields.

In this context, light is not only a growth signal but also a potential source of stress. Many of the physiological processes it regulates are influenced by the circadian clock, which helps algae anticipate daily fluctuations in light availability (Matsuo and Ishiura, 2011). Because these responses can vary between genotypes, studying how Chlamydomonas strains react to photoperiod and light intensity is key to understanding their physiological diversity. A central aspect of this response involves the function and regulation of chlorophyll fluorescence, a non-invasive indicator of photosynthetic performance and photoprotection. The following section introduces the biophysical principles underlying chlorophyll fluorescence and explains how these measurements can be used to assess strain-specific differences in light responses.

1.2.1 Chlorophyll Fluorescence

Chlorophyll, the green pigment essential for photosynthesis, exists primarily in two forms: chlorophyll a and chlorophyll b. These pigments absorb light mainly in the blue and red regions of the spectrum and are part of large pigment-protein complexes that include photosystems I and II (PSI and PSII) and light-harvesting complexes (LHCs). Together, these complexes capture and funnel light energy to the reaction centers, where photochemical conversion occurs (see also Introduction, Section 1.4).

In low-light environments, photosynthetic organisms enhance light-harvesting efficiency by increasing the number of chlorophyll a and b molecules in LHCs associated with PSI and PSII (Friedland et al., 2019). In *Chlamydomonas reinhardtii*, chlorophyll a is the primary pigment involved in light absorption, residing in both PSII and PSI reaction centers where it drives electron excitation. Chlorophyll b acts as an accessory pigment, transferring absorbed energy to chlorophyll a within the LHCs, thereby broadening the spectral range of light absorption (Melis et al., 1996). Carotenoids, such as lutein and zeaxanthin, also contribute to light capture and transfer energy to chlorophyll a (Lohr, 2023).

Upon light absorption, chlorophyll can undergo three competing processes (Fig. 1): (1) photochemistry, in which energy is used to drive photosynthesis; (2) heat dissipation, which protects the photosynthetic machinery; and (3) fluorescence, where excess energy is re-emitted as light. Chlorophyll fluorescence analysis relies on these processes, particularly fluorescence, to assess the efficiency and status of PSII.

The technique involves exposing dark-adapted cells to a series of controlled light treatments, including actinic light (which drives photosynthesis) and saturating pulses (which close PSII reaction centers). In darkness, when PSII centers are fully open and non-photochemical quenching (NPQ) is inactive, a weak measuring light determines the minimum fluorescence yield (Fo). A subsequent saturating pulse yields the maximum fluorescence (Fm). The variable fluorescence (Fv = Fm – Fo) and the Fv/Fm ratio ((Fm – Fo)/Fm) reflect the maximum quantum efficiency of PSII. In healthy higher plants, Fv/Fm is typically ~0.83; in Chlamydomonas, values can be slightly lower or more variable, often ranging from 0.65 to 0.75 under optimal conditions (Bonente et al., 2011).

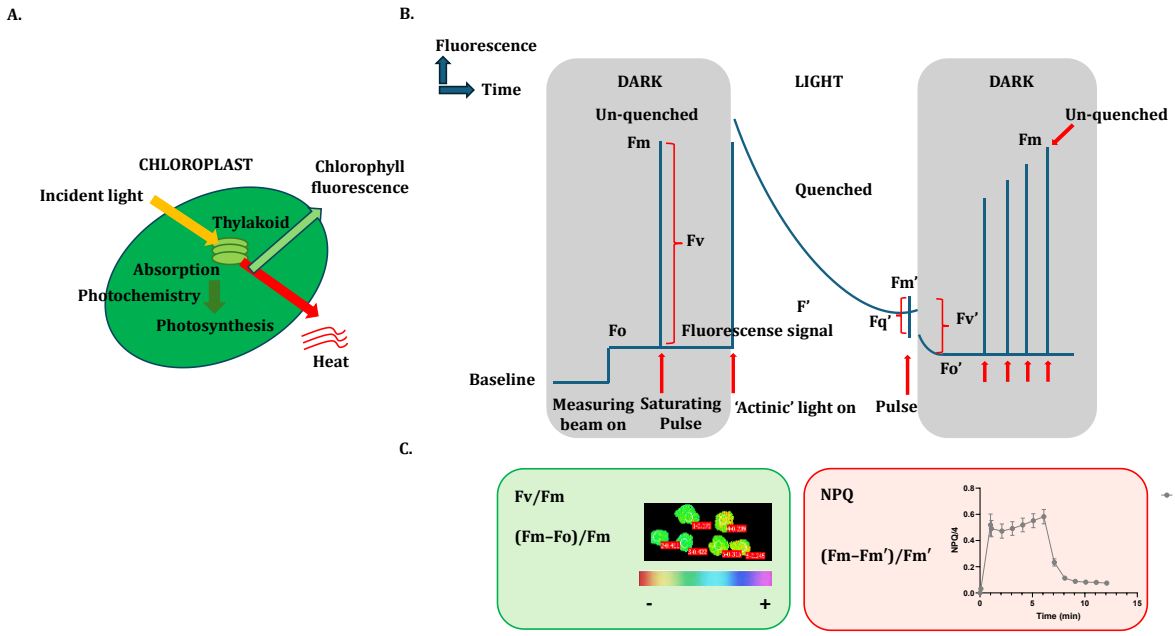

Fig. 1 A. Events occurring with the hitting light: the energy absorbed by chlorophyll within the light-harvesting complex can be dissipated via photochemistry (to drive photosynthesis), by heat (non-photochemical quenching), or as fluorescence. B. Minimal level of chlorophyll fluorescence, referred to as Fo in a dark-adapted state, and the corresponding light-adapted minimal fluorescence level, Fo′, which is recorded immediately after turning off the actinic light. Also represented the Fm, the maximum fluorescence level when a saturating pulse of light is applied to a dark-adapted sample, and the variable fluorescence (Fv), with its light-adapted counterpart being Fv′. If sufficiently strong actinic light is applied, fluorescence initially rises but is subsequently quenched due to increasing interactions with photochemical and non-photochemical processes. The steady-state fluorescence level under actinic light is denoted as F′. By applying a saturating pulse during actinic illumination, a transient closure of all PSII centers occurs, allowing the measurement of maximum fluorescence in the light-adapted state, denoted as Fm′. The fluorescence quenched by photochemical processes in the light-adapted state is represented by Fq′. C. Most common parameters used to assess the efficiency and photoprotective mechanisms of PSII with their corresponding formulas. Fv/Fm gives a robust indicator of the maximum quantum yield of PSII chemistry and NPQ (non-photochemical quenching) estimates the rate constant for heat loss from PSII. Also represented the NPQ curve showing how non-photochemical quenching changes over time. Image adapted from Murchie et al., 2013.

As light intensity increases, photosynthesis saturates, but excess absorbed light persists. Without protective mechanisms, this can lead to the formation of reactive oxygen species (ROS) and photooxidative damage to PSII, PSI, and other cellular components (Niyogi, 1998). To mitigate this, *C. reinhardtii* utilizes NPQ, especially its energy-dependent component (qE), to convert surplus excitation energy into heat. High NPQ values, calculated as (Fm – Fm′)/Fm′ (where Fm′ is the maximum fluorescence under light), indicate robust photoprotective capacity. Carotenoids like zeaxanthin play a crucial role in this process by dissipating excess energy and limiting ROS production (Lohr, 2023).

Although the importance of light as a regulatory signal in *Chlamydomonas reinhardtii* is well established, the specific mechanisms by which it modulates photosynthetic efficiency and photoprotective responses remain only partially understood. In particular, the extent to which these processes differ among widely used laboratory strains has not been systematically characterized. Filling this gap is essential for both fundamental research and the development of optimized cultivation protocols in applied contexts.

This chapter investigates how changes in light intensity and photoperiod shape physiological and photoprotective responses in four commonly used *C. reinhardtii* strains, CLiP, 4A+, CC-124, and CC-125, revealing distinct phenotypic profiles and strain-specific requirements that are critical to consider in experimental design and biotechnological applications.

2. MATERIALS AND METHODS

2.1 Biological material and pre-culture conditions

Chlamydomonas strains CC-5325 (also called CMJ030, identical to CC-4533, mt–, CLiP library background) 4A+, CC124, and CC125 were obtained from the Chlamydomonas Resource Center (CRC) (University of Minnesota).

The biological material used to develop the following study was taken from individual Tris-acetate-phosphate medium (TAP) solid media plates with homemade trace elements (Kropat et al., 2011) (Composition available **Supplementary information: Media preparation**) containing each strain. These plates were refreshed using the sowing handle a week before starting the pre-cultures TAP solid media. To inoculate the pre-cultures, some of the biological material was harvested from the agar plates and added, in aseptic conditions, to a 100mL flask containing 40ml of liquid TAP for mixotrophic growth. Cultures were left in a chamber (ARALAB 1200) at 21°C and 30µmol m-2 s-1 of LED light

intensity under continuous illumination for 3 days. Dilution was done by adding new fresh TAP liquid media, which was subsequently transferred to 12/12 dark/light cycles' chamber (ARALAB 600) in order to synchronize the cells for 3 more days.

2.2 Culture conditions and experiment set-up

Cultures were counted manually and kept in minimal media (HSM) (Composition available in **Supplementary information 1: Media preparation**) for autotrophic growth to a concentration of 0.5 million cells/ml by using the following method. A 200 µL sample was transferred to a 1.5 mL tube, and 20 µL of 0.25% (v/v) iodine/ethanol solution was added to immobilize the cells. A 10 µL volume of the immobilized cell suspension was loaded onto a hemocytometer, and after allowing 20 seconds for the cells to settle into a single focal plane, cell counting was performed using the Leica DMLM optical microscope (Leica Microsystems). Cells were counted either across all 25 quadrants of the hemocytometer grid or within the 5 diagonal quadrants, with the resulting number multiplied by 5 if only 5 quadrants were counted. Cell concentration, expressed in millions of cells per milliliter, was calculated by dividing the total count by 100. At least three counts per sample were performed to ensure accuracy. Successively, each culture was placed in an incubation chamber (ARALAB 600) with the corresponding photoperiod in low light (50 µmols of photons m^{-2} s^{-1}) for five days; then measurements were performed. After these five days, 5 mL of HSM medium was added to each culture to avoid substrate deficiencies. Then, cultures were kept in low light 50µmols of photons m^{-2} s^{-1}) (ARALAB 600) or transferred to high light (250 µmols of photons m^{-2} s^{-1}) (ARALAB HL) for five more days and again measurements were taken. At least 3 biological replicates were done for each strain (CLiP, 4a+, cc124 and cc125), light regime (SD, 12/12, LD and CL) and intensity (LL, HL). The temperatures were maintained constant in all conditions at 22°C and aseptic conditions were ensured during all manipulations.

Light Spectrum	Percentage present (%)
PFD-UV (350~400nm)	0.01
PFD-B (400~500nm)	15.92
PFD-G (500~600nm)	46.57
PFD-R (600~700nm)	34.78
PFD-FR (700~800nm)	2.72

Table 1. Irradiance spectrum of white light used

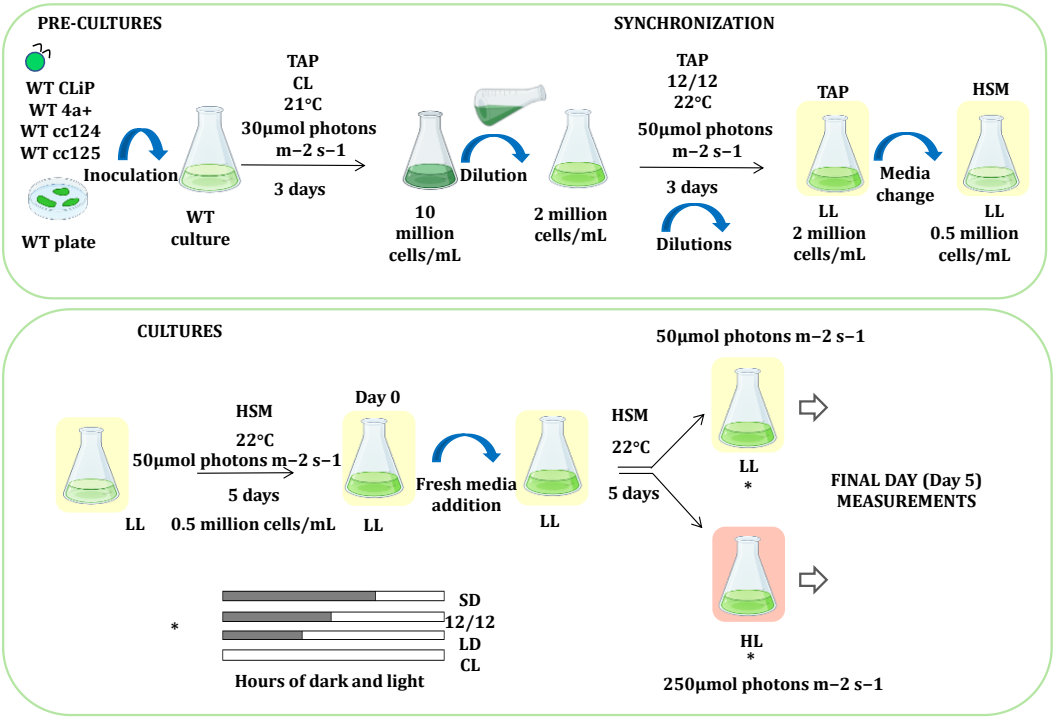

Figure 2. Schematic representation of the experimental set-up. The first panel shows the pre-culture conditions and synchronization of Chlamydomonas strains, while the second panel illustrates the culture conditions, light regimes, and intensities used in the experiment.

2.3 Cell quantification

Cell quantification during the experiments was monitored using two methods. The first method involved turbidity measurements. Triplicates of 100 µL from each culture were loaded into a 96-well transparent, flat-bottom plate, and 50 µL of Tween 20 suspension in HSM medium at a 0.67% (v/v) concentration was added to each well. HSM medium alone in triplicates served as the blank. After shaking, absorbance at 730 nm (A730) was measured for all wells using the SpectraMax® spectrophotometer. The final A730 value for each sample was determined by calculating the mean absorbance of the technical replicates and subtracting the mean blank value. The second method involved manual cell counting as explained in 2.2. At least three counts per sample were performed to ensure accuracy.

2.4 Measurements of photosynthetic parameters

2.4.1 Pigment extraction and quantification

a) Pigment extraction

Pigment extraction from *Chlamydomonas reinhardtii* cells was performed using an adapted version of Strand's lab protocol – UPSC, March 2022 for *Arabidopsis thaliana*. Duplicates of 1000 µL for each sample were taken and poured into a 1.5mL microcentrifuge tube. Centrifugation was carried out at room temperature for 8 min at 13000 rpm. Supernatants were then discarded. Afterwards, 200 µL of methanol were added to each sample and vortexed until the green pellet was resuspended obtaining a homogenic green color. Microcentrifuge tubes for the same sample (200µL each) were put together into one (obtaining a total volume of 400 µL) and then centrifuged at 4C° until the pellet looked completely white, approximately 10 minutes. The 96 multi-well plate was then filled by adding 100 µL of sample into each well. Three technical replicates were made for each sample. For this experiment, three different biological replicates were carried out for each WT and conditions (light intensity and regime).

b) Pigment quantification: chlorophylls and carotenoids

The quantifications for chloroophyll (total, a and b) and carotenoids were extracted from modified protocols provided in literature (Warren, 2008) (Lichtenthaler & Buschmann, 2001). The spectrophotometer (SpectraMax® Plus 384 Microplate Reader spectrophotometer (Molecular Devices, LLC)) was set at four different wavelengths: 470, 652, 665, and 750 nm. The 750nm wavelength is to correct any errors in the reading. The equations used to get the proper quantification in µg/mL for each wavelength were the following ones:

$$Corrected\ A652\ c = \frac{(A652 - A750)}{0.58}$$

$$Corrected\ A665\ c = \frac{(A665 - A750)}{0.58}$$

$$Corrected\ A470\ c = \frac{(A470 - A750)}{0.58}$$

$$Chl\ A(ug/mL)\ = -6{,}5079 * A652\ c\ +\ 16{,}2127 * A665\ c$$

$$ChlB(ug/mL)\ =\ 32{,}1228 *\ A652\ c\ -\ 13{,}8255 *\ A665\ c$$

$$Carotenoids\ \left(\frac{ug}{mL}\right) = \frac{(1000 * A470\ c\ -\ 1{,}63 * ChlA\ -\ 104{,}96 * ChlB}{221}$$

After completing the calculations, the results were divided by the number of cells.

$$Chl\frac{a}{b}ratio = \frac{ChlA}{Chl\ B}$$

$$\frac{Car}{Chl}ratio = \frac{Car}{Chl}$$

For chlorophyll a to chlorophyll b (Chl a/b) and the Carotenoid to Chlorophyll (Car/Chl) ratios, the formulas are expressed above.

2.4.2 Fluorescence-based measurements

CC-5325 (WT-CLiP), 4a+, cc124 and cc125 cultures grown at 22°C in PBRs were used for all fluorescence-based photosynthetic measurements, which were determined with a pulse-modulated amplitude fluorimeter (MAXI-IMAGING-PAM, HeinzWaltz GmbH, Germany). Prior to this, Chlamydomonas cells were kept in the dark to ensure that their photosynthetic apparatus was in a relaxed state, which is crucial for accurate and reproducible measurements. This dark adaptation allows the cells to recover from any previous exposure to light, ensuring the photosystems are in their basal energy state. Cultures were kept in the dark for 20 minutes before measurements. Triplicates of 200µL at the same cell concentration were spotted to a squared cut micro-glass fiber filter paper put on a black plastic holder in complete dark conditions. Samples were covered with aluminum foil to ensure complete darkness before taking them to the PAM fluorometer for measurements. The samples' setup was adjusted to the PAM image and chlorophyll fluorescence measurements were taken.

Chlorophyll fluorescence was recorded during 5.5min under 460 µmol m^{-2} s^{-1} of actinic white light followed by finishing with 5.5min of measurements of fluorescence relaxation in the dark. Measurements were taken every 30 and 60 interval seconds. A saturating pulse of white light was applied for determination of Fm (the maximal fluorescence yield in dark-adapted state) or Fm' (maximal fluorescence in any light-adapted state). NPQ was calculated as (*F*m—*F*m′)/*F*m′. PSII efficiency (Fv/Fm ratio) was calculated as (Fv/Fm =

(Fm-Fo/ Fm) where Fo and Fm are minimal and maximal chlorophyll fluorescence in dark-adapted algal cells. The difference between Fm and Fo gives the variable fluorescence (Fv), and Fv/Fm is defined as the quotient between Fv and Fm.

2.5 Cell Area Measurements

Cell area was used as a proxy for cell size, assuming generally round to ellipsoidal cell shape. Morphological measurements were obtained using a Leica DM6 upright brightfield microscope equipped with a digital camera and imaging software. For each sample, a 200 µL aliquot was taken from the culture and transferred to a previously labeled 1.5 mL microcentrifuge tube. Before imaging, the general condition of the cells was assessed, and they were subsequently immobilized using iodine solution. Images were acquired at 40× magnification, capturing at least 25 individual cells per biological replicate.

Image analysis was performed using ImageJ software (National Institutes of Health, USA). A consistent scale was set for all images based on the microscope calibration at 40×. Each cell was manually outlined using the freehand selection tool to ensure accurate boundary definition. Cells that were aggregated, overlapping, or visibly dividing were excluded from the analysis to maintain measurement consistency. Cell area was measured using the "Analyze > Measure" function, and values were expressed in square micrometres (μm^2).

2.6 Growth analysis

The specific growth rate (µ), which reflects the exponential increase in cell number over time, was calculated using the following formula:

$$\mu = \frac{\ln(Nf) - \ln(N_0)}{t}$$

where:

1. N_0 is the cell density at day 0, which was 0.5 million cells for all strains
2. Nf is the cell density at day 10 (final day)
3. "t" is the duration of the growth period (5 days)
4. µ is expressed in day^{-1}.

2.7 Statistical analysis

For individual analyses under LL and HL conditions, a one-way ANOVA was conducted to evaluate differences among the four *Chlamydomonas reinhardtii* strains (CLiP, 4a+, CC-124, and CC-125) using SPSS Statistics (IBM SPSS Statistics, version 26). ANOVA was selected because it enables comparison of mean values across multiple groups and determines whether strain identity significantly affects the measured variable. To verify that the assumptions for ANOVA were satisfied, data normality was tested using the Shapiro–Wilk test in GraphPad Prism (version 9). This test assesses whether the distribution of values within each group approximates a normal distribution, which is a key assumption for valid parametric inference. When these assumptions were met, post-hoc pairwise comparisons were carried out using Tukey's Honest Significant Difference (HSD) test in SPSS. Tukey's test corrects for multiple comparisons and offers a consistent approach to identifying significant differences between all pairs of strains. A p-value < 0.05 was considered statistically significant. Data is presented as mean ± standard error of the mean (SEM), unless otherwise stated.

To compare responses between LL and HL conditions within each strain and light regime, unpaired two-tailed t-tests with Welch's correction were performed using GraphPad Prism (version 9). This version of the t-test accounts for unequal variances between groups, providing a more robust comparison when standard deviations differ. Results are presented as mean ± standard deviation (SD), unless otherwise noted. Statistical significance was defined as $p < 0.05$. Significance is indicated in figures as: $p < 0.05$ (*), $p < 0.01$ (**), $p < 0.001$ (***), $p < 0.0001$ (****); ns= not significant.

3. RESULTS

3.1 Set up of the experiment

Thus, the aim of this chapter is to understand how *Chlamydomonas reinhardtii* wild-type (WT) strains adjust their responses to varying light conditions. To this end, we set up an experiment with four different WT strains, CLiP, 4A+, CC-124, and CC-125, that were grown under four light regimes: short days (SD), 12-hour light/dark cycles (12/12), long days (LD), and continuous light (CL). These strains were exposed to two light intensities, low light (LL) (50 µmols of photons m^{-2} s^{-1})) and high light (HL) (250 µmols of photons m^{-2} s^{-1})). This experimental setup provides a comprehensive view of how light intensity and photoperiod influence the algae's ability to perform photosynthesis and adapt to changing environmental conditions, while also offering insights into how these Chlamydomonas strains differ or behave similarly.

As described in the Methods and shown in Figure 2, the Chlamydomonas WT strains were grown in LL conditions for 5 days. Following this, they were transferred to HL conditions or kept in LL for an additional 5 days, with measurements taken at the end of the exposure. This process was repeated for each light regime (SD, 12/12, LD, and CL).

3.2 Growth dynamics in *Chlamydomonas reinhardtii* are enhanced by extended light exposure and CL, while revealing strain-specific responses under HL

We first started to evaluate how light regime and intensity influenced growth. For this purpose, we monitored cell density in all *Chlamydomonas reinhardtii* strains (CLiP, 4A+, CC-124, and CC-125) over a 10-day period. From these measurements, we calculated the specific growth rate (μ) (Fig. 3), which serves as an integrative indicator of how efficiently each strain responds to different environmental conditions.

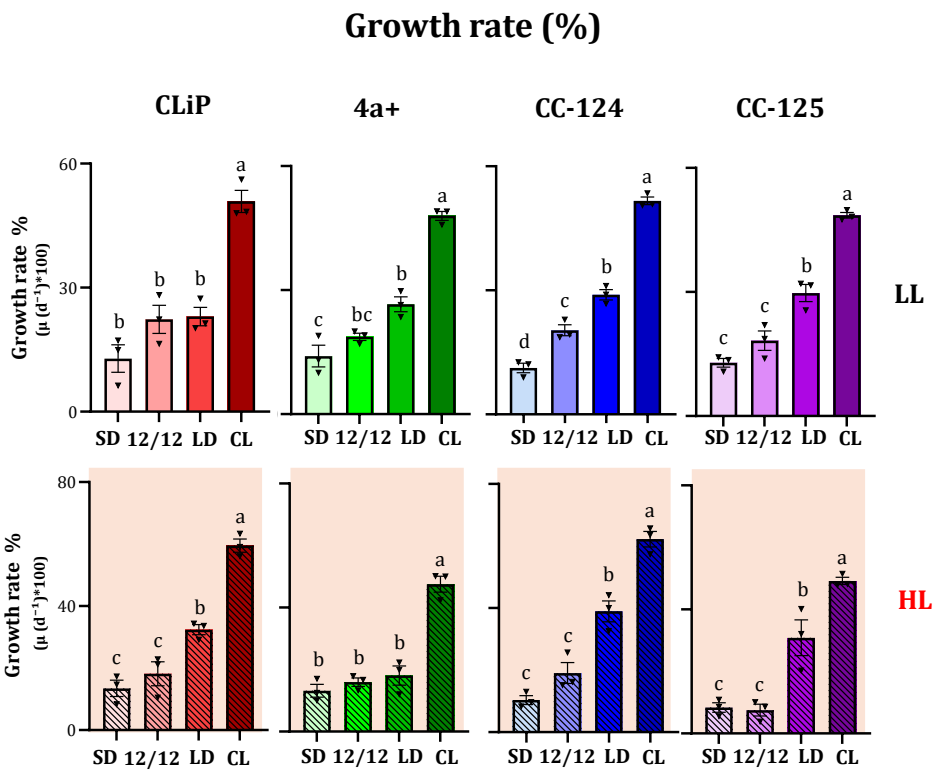

Figure 3. Growth rate of *Chlamydomonas reinhardtii* strains under different light regimes and intensities (LL and HL). Bar graphs show growth rates (μ, d^{-1}) expressed as percentages (%) calculated from day 0 to day 5 for each strain and light condition: **A.** LL **B.** HL. CliP (red), 4a+ (green), CC-124 (blue) and CC-125 (purple). Data represent mean ± SEM from three biological replicates shown as small triangles. Different lowercase letters above the bars indicate statistically significant differences within each individual graph ($p < 0.05$, one-way ANOVA followed by Tukey's post hoc test). Photoperiod conditions are shown from paler to darker colors: SD (short day), 12/12 (12 h light/12 h dark), LD (long day), and CL (continuous light). LL: low light (50μmol photons m^{-2} s^{-1}). HL: high light (250μmol photons m^{-2} s^{-1}).

Overall, longer photoperiods and CL significantly increased growth rates under both LL and HL conditions (Fig. 3). In LL, however, responses were relatively consistent across strains, with no major differences observed (Table 2).

Under HL, the same trend as LL was observed. However, strain-specific differences became more pronounced, particularly in LD and CL regimes. In LD, CC-124 exhibited the highest growth rate among all strains, while in CL, both CC-124 and CLiP outperformed 4A+ and CC-125, which showed significantly lower values (Fig. 3B). These differences show that, although prolonged light exposure generally enhances growth, some strains, especially CC-124, are better suited to maintaining high growth rates under continuous or extended high-light conditions.

Low Light				
Light regime	**Strain**	**Million cells (Day 0; N_0)**	**Million cells (Day 5; Nf)**	**Growth rate (μ (d^{-1}))**
SD	CLiP	0,70 ± 0,02	1,37 ± 0,39	0,13 ± 0,06^{a}
	4a+	0,67 ± 0,02	1,38 ± 0,36	0,14 ± 0,05^{a}
	cc124	0,72 ± 0,05	1,25 ± 0,05	0,11 ± 0,02^{a}
	cc125	0,70 ± 0,06	1,32 ± 0,09	0,13 ± 0,03^{a}
12_12	CLiP	0,72 ± 0,05	2,24 ± 0,52	0,22 ± 0,06^{a}
	4a+	0,65 ± 0,03	1,65 ± 0,19	0,19 ± 0,02^{a}
	cc124	0,69 ± 0,05	1, 92 ± 0,28	0,20 ± 0,02^{a}
	cc125	0,74 ± 0,05	1,83 ± 0,24	0,18 ± 0,04^{a}
LD	CLiP	0,73 ± 0,02	2,33 ± 0,44	0,23 ± 0,04^{a}
	4a+	0,74 ± 0,03	2,81 ± 0,45	0,27 ± 0,03^{a}
	cc124	0,73 ± 0,05	3,12 ± 0,43	0,29 ± 0,02^{a}
	cc125	0,72 ± 0,02	3,19 ± 0,47	0,30 ± 0,04^{a}
CL	CLiP	0,73 ± 0,03	6,27 ± 1,32	0,51 ± 0,04^{a}
	4a+	0,63 ± 0,03	4,64 ± 0,47	0,48 ± 0,02^{a}
	cc124	0,72 ± 0,02	6,35 ± 0,33	0,52 ± 0,02^{a}
	cc125	0,68 ± 0,05	5,14 ± 0,55	0,49 ± 0,01^{a}

High Light				
Light regime	**Strain**	**Million cells (Day 0; N_0)**	**Million cells (Day 5; Nf)**	**Growth rate (μ (d^{-1}))**
SD	CLiP	0,70 ± 0,02	1,40 ± 0,33	0,13 ± 0,05^{a}
	4a+	0,67 ± 0,02	1,31 ± 0,21	0,13 ± 0,04^{a}
	cc124	0,72 ± 0,05	1,21 ± 0,22	0,10± 0,02^{a}
	cc125	0,70 ± 0,06	1,06 ± 0,16	0,08 ± 0,03^{a}
12_12	CLiP	0,72 ± 0,05	1,85 ± 0,59	0,18 ± 0,07^{a}
	4a+	0,65 ± 0,03	1,15 ± 0,36	0,16 ± 0,02^{a}
	cc124	0,69 ± 0,05	1,81 ± 0,40	0,19 ± 0,06^{a}
	cc125	0,74 ± 0,05	1,07± 0,11	0,08 ± 0,03^{a}
LD	CLiP	0,73 ± 0,02	3,71 ± 0,54	**0,32 ± 0,03^{ab}**
	4a+	0,74 ± 0,03	1,86 ± 0,43	**0,18 ± 0,05^{b}**
	cc124	0,73 ± 0,05	5,21 ± 1,72	**0,39 ± 0,06^{a}**
	cc125	0,72 ± 0,02	3,66 ± 1,79	**0,30 ± 0,10^{ab}**
CL	CLiP	0,73 ± 0,03	9,60 ± 1,41	**0,60 ± 0,04^{a}**
	4a+	0,63 ± 0,03	4,57 ± 0,80	**0,48 ± 0,04^{b}**
	cc124	0,72 ± 0,02	10, 91 ± 2,14	**0,62 ± 0,04^{a}**
	cc125	0,68 ± 0,05	5,33 ± 0,73	**0,49 ± 0,02^{b}**

Table 2. Growth rate of *Chlamydomonas reinhardtii strains* after 5 days of growth under low light (LL) and high light (HL) conditions across different light regimes. Mean initial and final cell densities (N_0 and Nf, in million cells mL^{-1}) and growth rates (μ, d^{-1}) ± standard deviation (SD) are shown. Statistically significant differences between LL and HL within the same light regime and strain are indicated in bold. Comparisons were performed using one-way ANOVA followed by Tukey's post hoc test (n = 3 to 5 replicates). Different lowercase letters denote statistically significant differences ($p < 0.05$). LL: low light (50µmol photons m^{-2} s^{-1}). HL: high light (250µmol photons m^{-2} s^{-1}).

All strains exhibited increased growth under CL at both light intensities. However, CLiP maintained stable growth across all cycling light regimes (SD, 12/12, and LD) under LL. Similarly, 4A+ displayed a comparable pattern under HL, indicating resilience to changes in day length in both cases (Fig. 3).

Altogether, these findings emphasize the importance of both photoperiod and strain background in shaping growth responses, particularly under HL, where light stress amplifies physiological differences between strains.

3.3 Photoperiod affects cell size in a strain-dependent way while HL irradiance triggers differences in morphological aspects, especially in longer light periods

We next measured cell size and morphology. Cell size provides a rapid proxy for biomass, as larger cells generally contain more cellular material. Combined with cell morphology, this helps reveal how environmental and genetic factors influence physiology and light acclimation in *Chlamydomonas reinhardtii*.

Under LL, cell size wass relatively stable across light regimes in CLiP and 4A+, but CC-124 and CC-125 show noticeable photoperiod-dependent variation (Fig. 4A). In CC-124, cell size increased under 12/12 and LD, but then dropped under CL, suggesting a sensitivity to prolonged photoperiods even at low intensity. CC-125 shows a similar trend, though less pronounced

Under HL, cell size dynamics varied across strains and photoperiods. In 4A+, cell size decreased significantly with increasing photoperiod, reaching its lowest values under CL. For CC-124 and CC-125, there was a similar trend of decreasing cell size from SD to CL, but these differences were not statistically significant, indicating that while a reduction is visually evident, it may not be robust or consistent across replicates. This suggests that 4A+ is more sensitive to the duration of light exposure under HL, potentially adjusting growth or cell division timing in response to photoperiod stress (Fig. 4B).

In contrast, CLiP maintained remarkably consistent cell size across all photoperiods under HL, and also across both LL and HL overall. This indicates a high degree of morphological stability. This pattern sets CLiP apart from the other strains, highlighting its photoperiod- and intensity-independent cell size consistency, which could be a valuable trait for further physiological or genetic investigation. (Fig. 4B)

In addition, morphological studies revealed further findings (Fig. 5 and 6). Under LL condition, the cells appeared generally healthy, with a regular round shape and compact, uniformly pigmented chloroplasts across all regimes (Fig. 5). In the SD and 12/12, cells showed well-organized internal structures, with chloroplasts appearing as smooth cup-shaped bodies with uniform yellow-green coloration. Some cells displayed a central lighter area suggestive of a visible pyrenoid, and small, dispersed yellow granules likely represent moderate starch accumulation. The eyespot was occasionally visible as a reddish or orange dot near the cell periphery. In contrast, in the LD and CL columns, chloroplasts were still compact and dense, but contained more numerous yellow inclusions, interpreted as starch granules, without a clearly distinguishable central pyrenoid.

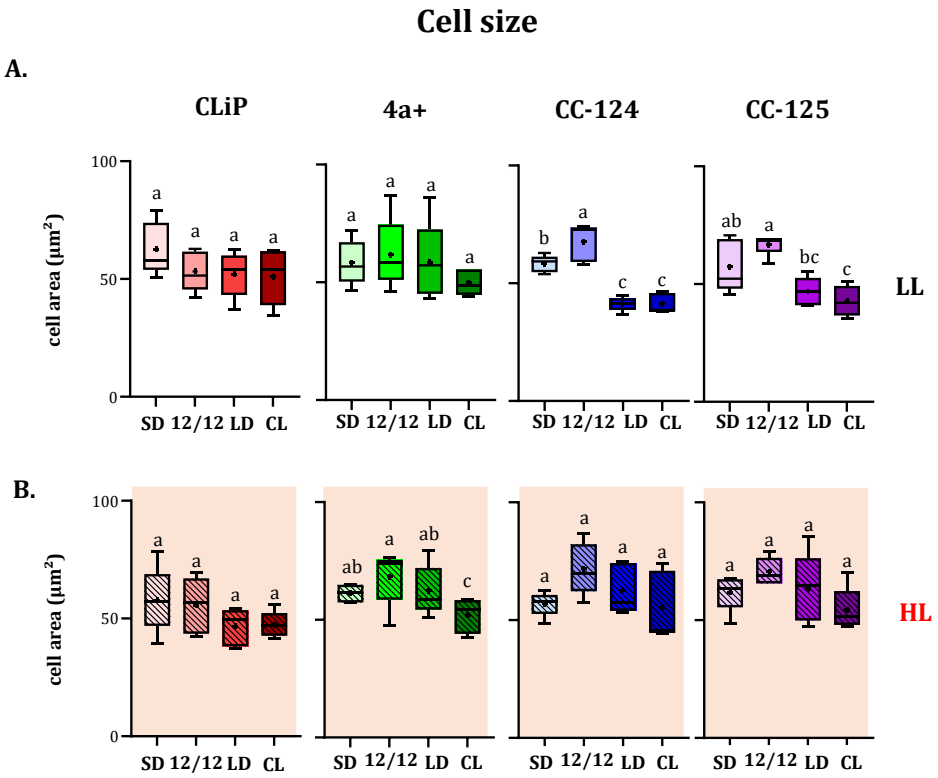

Figure 4. *Chlamydomonas reinhardtii* cell size (area) under different light regimes and intensities (LL and HL). Each boxplot shows the distribution of cell size values (n ≥ 25 per group), for each strain and light condition: A. LL B. HL, with the horizontal line indicating the median, the whiskers marking the minimum and maximum values, and the "x" representing the mean. CliP (red), 4a+ (green), CC-124 (blue) and CC-125 (purple). Different lowercase letters above the bars indicate statistically significant differences within each individual graph ($p < 0.05$, one-way ANOVA followed by Tukey's post hoc test). Photoperiod conditions are shown from paler to darker colors: SD (short day), 12/12 (12 h light/12 h dark), LD (long day), and CL (continuous light); LL: low light (50µmol photons m^{-2} s^{-1}). HL: high light (250µmol photons m^{-2} s^{-1}).

However, the pigmentation remained smooth and uniformly distributed, suggesting that the internal chloroplast structure is still well maintained. However, cells in CL presented and ellipsoidal shape rather than being completely round. The eyespot was rarely visible in these light regimes, and although a few cells appeared to be dividing, no external halos or signs of HL stress were present. Overall, the cells maintained an organized appearance across all regimes, with slightly increased starch accumulation and reduced eyespot visibility under prolonged photoperiods, but without strong indicators of structural damage.

On the other hand, under HL, *Chlamydomonas reinhardtii* cells displayed marked morphological differences across the four light regimes (Fig. 6).

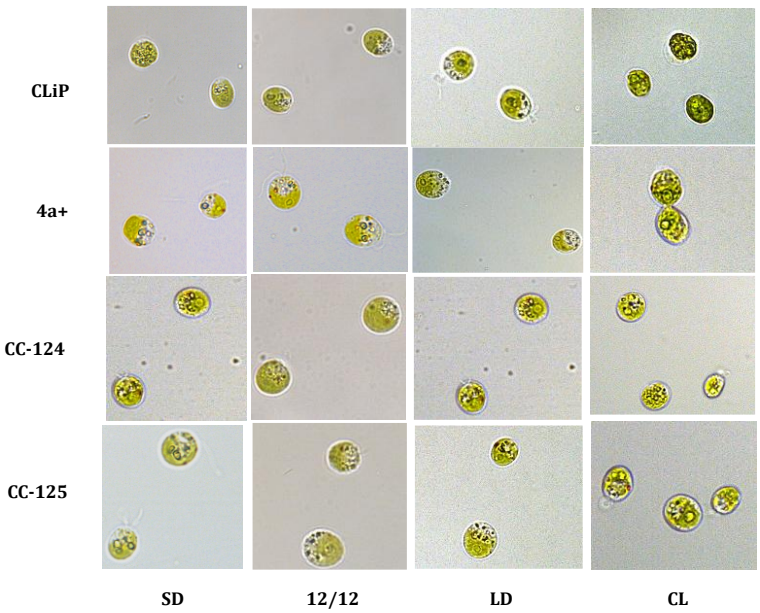

Figure 5. Representative micrographs of *Chlamydomonas reinhardtii* cells grown under LL. Four photoperiods were used: short day (SD), 12/12, long day (LD) and continuous light CL) and four strain (CLiP, 4a+, CC-124 and CC-125). Images were acquired using brightfield microscopy. LL: Low Light (50µmol photons m^{-2} s^{-1}).

In SD and 12/12, cells generally showed a regular morphology, with more visible internal structures, resembling those of LL conditions. However, while the chloroplast appeared as a cup-shaped structure occupying much of the cell, the color of the cells was more yellow-green. In addition, in several cells, a lighter or denser central region was visible, likely the pyrenoid. Surrounding this area, small yellow granules were also seen, probably starch grains, but overall, their abundance was moderate. The compact chloroplast structure, visible pyrenoid, and low starch accumulation suggest a metabolically balanced state, with efficient photosynthesis and carbon utilization, rather than stress-induced storage or structural disruption (Fig. 6).

Conversely, LD and CL showed cells with signs of stress. Many cells contained numerous bright yellow inclusions, indicative of starch overaccumulation, which suggests photodamage or overstimulation by light. The internal structure appeared less organized, with a not clearly visible pyrenoid. The eyespot was absent, which could be due to changes in orientation, but its consistent absence in the different strains suggests a potential functional alteration or degradation under prolonged or continuous light exposure. Notably, several cells in the continuous light condition exhibited a clear, well-defined halo around the cell, likely corresponding to a thickened cell wall or extracellular matrix (ECM), a known stress response in HL environments (Fig. 6).

Thus, under LL Chlamydomonas cells generally maintained an organized morphology across all light regimes. Under prolonged photoperiods, however, there was a slight increase in starch accumulation and a reduction in eyespot visibility. No major structural damage was observed across conditions. On the other hand, under HL, extended

photoperiods (LD and CL) were associated with disrupted chloroplast organization, increased starch content, extracellular matrix (ECM) formation, and diminished visibility of the eyespot.

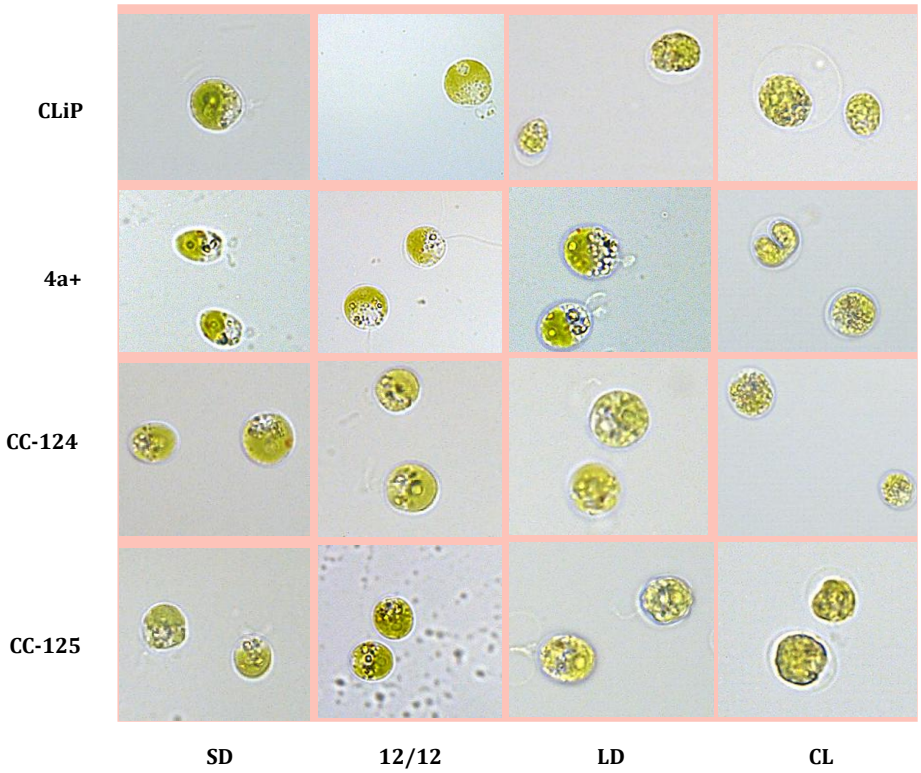

Figure 6. Representative micrographs of *Chlamydomonas reinhardtii* cells grown under HL. Four photoperiods were used: short day (SD), 12/12, long day (LD) and continuous light CL) and four strain (CLiP, 4a+, CC-124 and CC-125). Images were acquired using brightfield microscopy. HL: high light (250µmol photons m^{-2} s^{-1}).

3.4 Enhanced photosynthetic performance in shorter light regimes under HL conditions and strain-specific behavior under CL

Then, the Fv/Fm ratio was measured, which is a widely used proxy for PSII efficiency and photophysiological health.

Under LL conditions, no significant differences in Fv/Fm were observed across photoperiods or under CL for most strains. The only exception was WT-CLiP, which showed a clear decrease in Fv/Fm under CL, indicating impaired PSII performance in the absence of a dark period (Fig. 7A). No significant differences between strains were found under SD, 12/12, or LD conditions. Although CLiP tended to show lower values than the other strains under CL, these differences were not statistically significant ($p > 0.05$), likely due to high variability among biological replicates (**Supplementary information: Table. 1**).

Under HL conditions, photoperiod had a stronger influence on PSII performance. Across all strains, Fv/Fm values were consistently higher in light-dark cycles (SD, 12/12, LD) than under CL, reflecting enhanced photoprotection when a recovery period was available (Fig. 7B). CLiP and CC-125 showed particularly elevated Fv/Fm ratios under SD and 12/12 compared to LD, suggesting better performance under reduced daily light exposure. In contrast, 4A+ and CC-124 maintained relatively stable values across all three light-dark regimes.

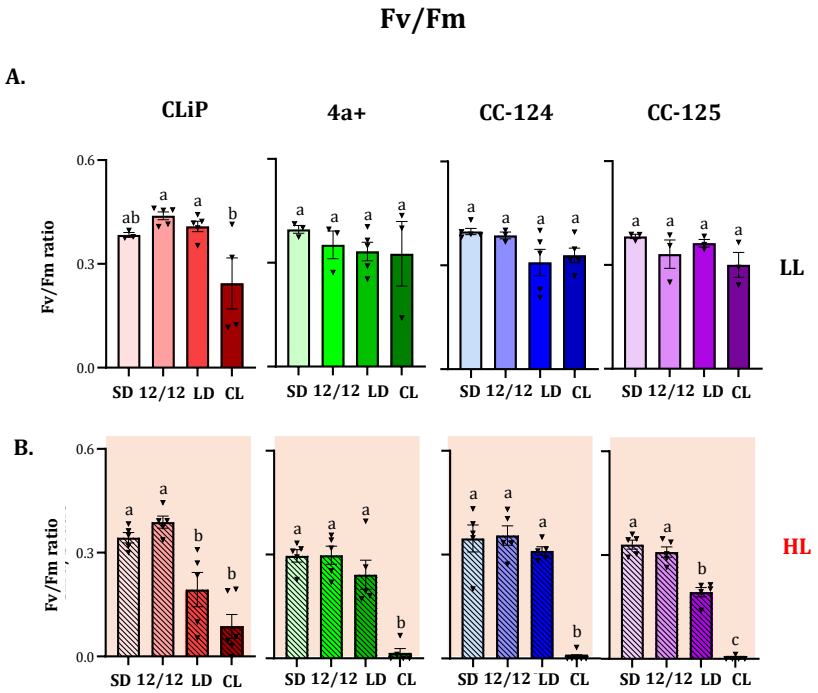

Figure 7. Fv/Fm ratio of *Chlamydomonas reinhardtii* strains under different light regimes and intensities (LL and HL). Bar graphs show chlorophyll content (µg/mL / cell number x10^6) for each strain and light condition: **A.** LL **B.** HL. CliP (red), 4a+ (green), CC-124 (blue) and CC-125 (purple). Data represent mean ± SEM from three to five biological replicates shown as small triangles. Different lowercase letters above the bars indicate statistically significant differences within each individual graph ($p < 0.05$, one-way ANOVA followed by Tukey's post hoc test). Photoperiod conditions are shown from paler to darker colors: SD (short day), 12/12 (12 h light/12 h dark), LD (long day), and CL (continuous light); LL: low light (50µmol photons m^{-2} s^{-1}); HL: high light (250µmol photons m^{-2} s^{-1}).

Differences between strains under SD and 12/12 were not statistically significant ($p > 0.05$) **(Supplementary information: Table. 2)**. Under LD, both CLiP and CC-125 showed a tendency toward reduced Fv/Fm, though variability between replicates prevented these differences from reaching significance.

In continuous HL, however, strain-specific effects became more pronounced. CLiP exhibited significantly higher Fv/Fm values than both CC-124 and CC-125 (*p = 0.035* and *p = 0.038*, respectively) (**Supplementary information: Table. 3**). Thus, although all

strains were affected by this sustained light exposure, CLiP showed the least negative impact on their PSII function.

These results mainly reveal the importance of cycling regimes to cope to HL stress, as well as differences in photophysiological resilience among strains when exposed to prolonged stress.

3.5 Photoperiod-Driven Variations in Total Chlorophyll Content across Chlamydomonas Strains

To further explore the impact of photoperiod on wild-type Chlamydomonas strains, we quantified total pigment content, focusing on chlorophylls and carotenoids due to their essential roles in light absorption, energy transfer, and overall photosynthetic efficiency.

Total chlorophyll (ChlT), the sum of chlorophyll a and b, provides a global measure of the photosynthetic pigment pool and reflects the algae's light-harvesting capacity under different lighting conditions. This parameter was used to assess overall pigment abundance across strains, with individual chlorophyll types addressed in a separate section.

Under LL, total chlorophyll content tended to decrease with increasing photoperiod duration (Fig. 8A). This trend was especially evident under LD, where ChlT levels dropped across most strains. Interestingly, in CL, all strains displayed higher ChlT values compared to LD, with the exception of CC-124, which maintained similar levels. Additionally, CLiP showed the highest chlorophyll content in 12/12 light regime, which was statistically significant compared to CC-125 ($p = 0.018$) (**Supplementary information: Table. 2**).

Under HL, the pattern was similar: shorter photoperiods (SD) supported higher chlorophyll content, while LD led to a marked reduction (Fig, 8B). CLiP showed the highest values under SD and significantly exceeded 4A+, CC-124, and CC-125 ($p = 0.003$, $p = 0.012$, and $p = 0.012$, respectively). Conversely, under LD, 4A+ exhibited the highest ChlT levels among all strains, with significant differences observed when compared to CLiP ($p = 0.006$), CC-124 ($p = 0.001$), and CC-125 ($p = 0.014$) (**Supplementary information: Table. 2**).

These results suggest that pigment accumulation in Chlamydomonas is not only photoperiod-dependent but also strongly influenced by strain background, with CLiP and 4A+ showing distinct chlorophyll allocation strategies under SD and LD, respectively.

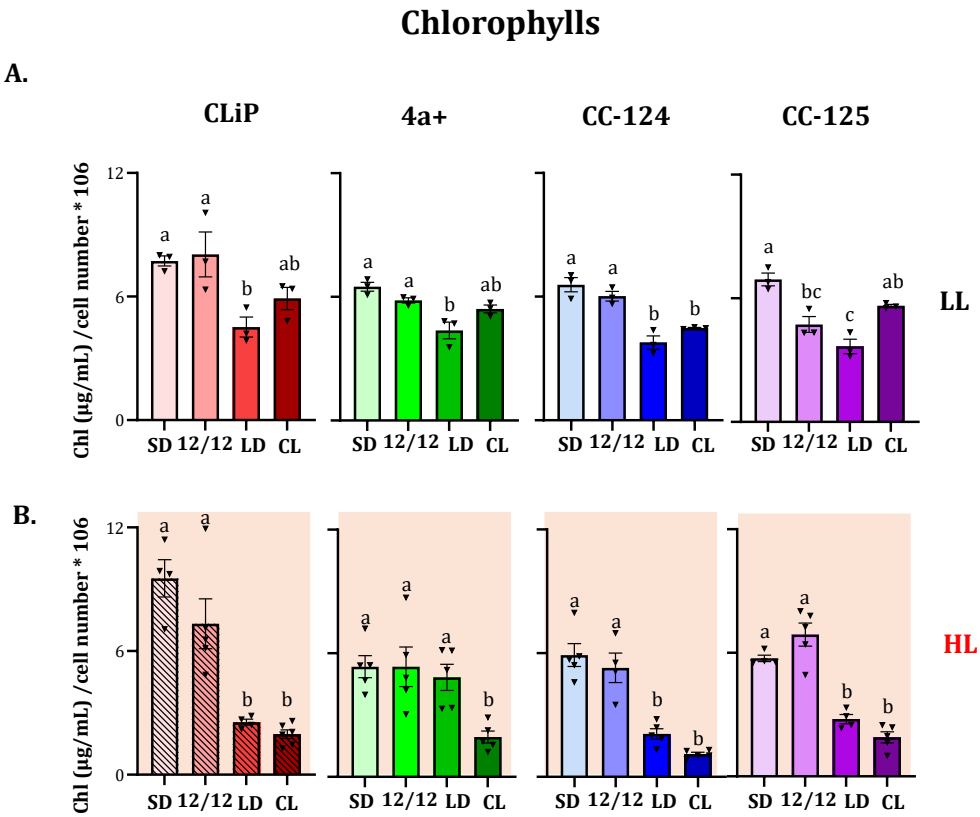

Figure 8. Total chlorophyll content of *Chlamydomonas reinhardtii* strains under different light regimes and intensities (LL and HL). Bar graphs show total chlorophyll content (µg/mL / cell number x10^6) for each strain and light condition: **A.** LL **B.** HL. CliP (red), 4a+ (green), CC-124 (blue) and CC-125 (purple). Data represent mean ± SEM from three to five biological replicates shown as small triangles. Different lowercase letters above the bars indicate statistically significant differences within each individual graph ($p < 0.05$, one-way ANOVA followed by Tukey's post hoc test). Photoperiod conditions are shown from paler to darker colors: SD (short day), 12/12 (12 h light/12 h dark), LD (long day), and CL (continuous light); LL: low light (50µmol photons m^{-2} s^{-1}); HL: high light (250µmol photons m^{-2} s^{-1}).

3.6 Shorter photoperiods enhance carotenoid content, while longer light periods and CL promote carotenoid degradation in HL

Carotenoids play a dual role in Chlamydomonas physiology: they protect against photooxidative damage by dissipating excess excitation energy and also contribute to light harvesting by absorbing in the blue-green region of the spectrum. By analysing carotenoid levels in parallel with chlorophylls, we gained a more complete view of each strain's light-harvesting efficiency and photoprotective capacity across photoperiods and light intensities.

Under LL conditions, carotenoid levels showed distinct strain-specific patterns (Fig. 9A). CLiP and 4A+ maintained relatively stable carotenoid content across all photoperiods and

CL. In contrast, CC-124 and CC-125 were more sensitive to photoperiod changes. CC-124 showed a gradual reduction in carotenoids with photoperiod length increase, which continued under CL. CC-125, however, exhibited its highest carotenoid levels in SD and CL, while showing marked reductions in 12/12 and LD.

CC-124 showed the highest carotenoid content under SD conditions with statistically significant differences compared to CLiP (*p = 0.008*), while CLiP the highest content in 12/12, which was statistically significant compared to CC-125 in 12/12 (*p = 0.026*) (**Supplementary information: Table. 3**).

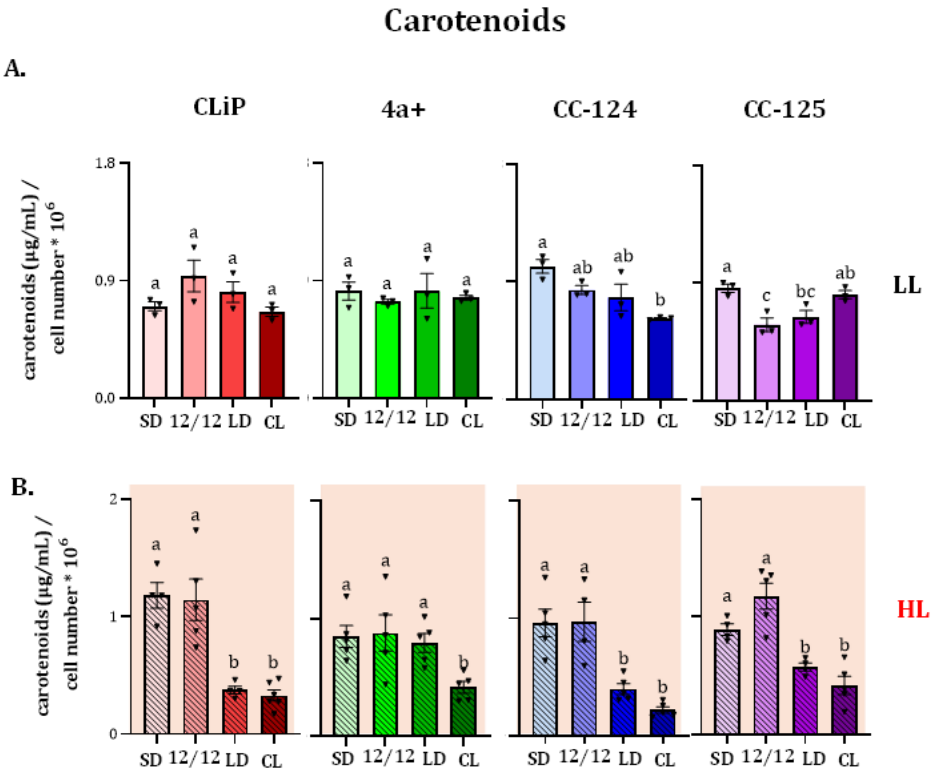

Figure 9 Total carotenoid content of *Chlamydomonas reinhardtii* strains under different light regimes and intensities (LL and HL). Bar graphs show total carotenoid content (µg/mL / cell number x10^6) for each strain and light condition: **A.** LL **B.** HL. CliP (red), 4a+ (green), CC-124 (blue) and CC-125 (purple). Data represent mean ± SEM from three to five biological replicates shown as small triangles. Different lowercase letters above the bars indicate statistically significant differences within each individual graph ($p < 0.05$, one-way ANOVA followed by Tukey's post hoc test). Photoperiod conditions are shown from paler to darker colors: SD (short day), 12/12 (12 h light/12 h dark), LD (long day), and CL (continuous light); LL: low light (50µmol photons m^{-2} s^{-1}); HL: high light (250µmol photons m^{-2} s^{-1}).

Under HL, the trend observed for chlorophylls was mirrored in carotenoids: shorter photoperiods (SD, 12/12) were associated with higher carotenoid content, while LD and CL triggered substantial reductions across all strains (Fig. 9B). Notably, 4A+ showed the highest carotenoid levels in LD HL, significantly surpassing CLiP and CC-124 (*p = 0.001* for

both comparisons), though the difference with CC-125 did not reach statistical significance (*p = 0.059*) (**Supplementary information: Table. 3**).

Overall, these results suggest that shorter photoperiods support both chlorophyll and carotenoid accumulation under HL, while longer or CL exposure may lead to pigment degradation. Strain-specific differences in carotenoid content under HL also indicate varying photoprotective strategies, with CLiP and 4A+ showing distinct responses depending on photoperiod length.

3.7 Strain-Specific Adjustments in Chlamydomonas antenna size across photoperiods under both LL and HL

We used the chlorophyll a/b ratio as a proxy for the relative size of the light-harvesting antenna, since a higher proportion of chlorophyll b reflects a larger LHC complex. In parallel, the carotenoid-to-chlorophyll (Car/Chl) ratio was used to evaluate how pigments involved in photoprotection are adjusted across photoperiods under LL and HL conditions.

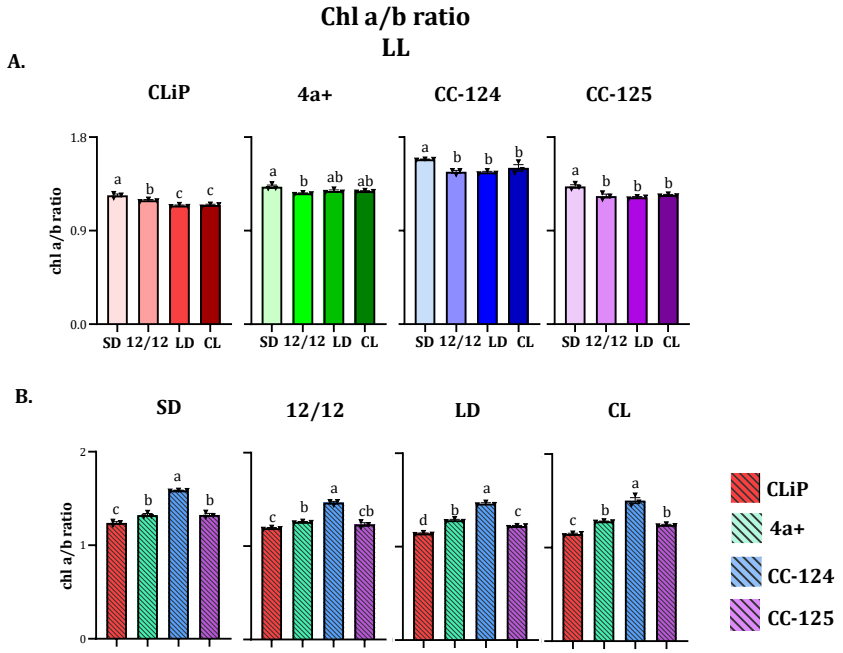

Figure 10. Chlorophyll a to b (Chl a/b) ratio in *Chlamydomonas reinhardtii* strains under different light regimes in LL conditions. **A.** Bar graphs represent the Chl a/b ratio for each strain, individually, across light regimes. Light regimes are represented from paler to darker colors: SD (short day), 12/12 (12 h light/12 h dark), LD (long day), and CL (continuous light), and within each color-coded strain group (CLiP in red, 4a+ in green, CC-124 in blue, and CC-125 in purple). **B.** Bar graphs show the Car/Chl ratio represented by photoperiod; CliP (red), 4a+ (green), CC-124 (blue) and CC-125 (purple). Data indicate mean ± SEM from three to five biological replicates shown as small triangles. Different lowercase letters above the bars indicate statistically significant differences within each individual graph ($p < 0.05$, one-way ANOVA followed by Tukey's post hoc test). LL: Low Light (50µmol photons m^{-2} s^{-1}).

Under LL conditions, the chlorophyll a/b ratio was highest under SD across all strains (Fig. 10), indicating a general trend toward reduced antenna size in response to shorter daily light exposure. However, notable differences emerged in how each strain adjusted to increasing photoperiod length. While CC-124, CC-125, and 4A+ maintained relatively stable Chl a/b values under 12/12, LD, and CL, CLiP showed a gradual decline with greater light exposure, reaching its minimum under continuous light.

Across all photoperiods, CC-124 consistently exhibited the highest Chl a/b ratio. In contrast, CLiP maintained the lowest values, while 4A+ and CC-125 displayed intermediate responses. (Fig. 10).

Under HL conditions, a similar general pattern was observed: shorter photoperiods (SD and 12/12) were typically associated with higher Chl a/b ratios, whereas LD and CL led to reduced values (Fig. 11). Yet, strain-specific behaviors were again evident. CC-125 remained largely unaffected by photoperiod, maintaining stable ratios across all conditions.

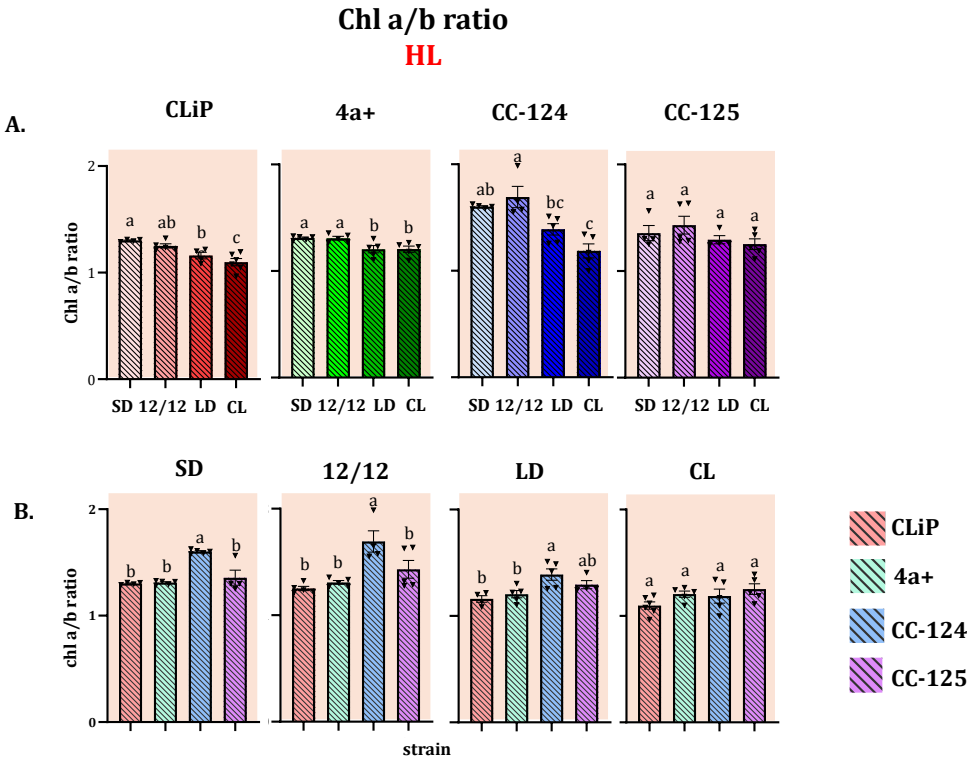

Figure 11. Chlorophyll a to b (Chl a/b) ratio in *Chlamydomonas reinhardtii* strains under different light regimes in HL conditions. A. Bar graphs represent the Chl a/b ratio for each strain, individually, across light regimes. Light regimes are represented from paler to darker colors: SD (short day), 12/12 (12 h light/12 h dark), LD (long day), and CL (continuous light), and within each color-coded strain group (CLiP in red, 4a+ in green, CC-124 in blue, and CC-125 in purple). B. Bar graphs show the Car/Chl ratio represented by photoperiod; CliP (red), 4a+ (green), CC-124 (blue) and CC-125 (purple). Data indicate mean ± SEM from three to five biological replicates shown as small triangles. Different lowercase letters above the bars indicate statistically significant differences within each individual graph ($p < 0.05$, one-way ANOVA followed by Tukey's post hoc test). HL: High Light (250µmol photons m^{-2} s^{-1}).

In contrast, 4A+ showed elevated Chl a/b values under SD and 12/12, but these dropped under LD and CL. Both CLiP and CC-124 appeared more responsive to photoperiod variation, with a gradual decrease in the Chl a/b ratio as the light period lengthened. The most marked reduction occurred under CL, particularly in CC-124.

Consistent with the LL results, CC-124 maintained the highest Chl a/b ratio across all photoperiods under HL. Meanwhile, CLiP, 4A+, and CC-125 showed comparable values under these conditions. Notably, no statistically significant differences between strains were detected under CL in HL (Fig. 11B).

3.8 Strain-specific pigment adjustments are enhanced under LL compared to HL, while photoperiod sensitivity differs across strains.

By assessing the Car/Chl ratio, we gained more information about pigment allocation strategies across photoperiods and light intensities, as this parameter reflects the balance between light-harvesting and photoprotective pigments.

Under LL, the Car/Chl ratio remained relatively stable across SD, 12/12, and CL for all strains except CLiP, which showed a significantly lower ratio under SD (Fig. 12A). These steady values likely resulted from proportional decreases in both chlorophyll and carotenoid content. In contrast, under LD, the Car/Chl ratio increased in most strains, primarily due to a more pronounced reduction in chlorophylls. This increase was statistically significant for CLiP and 4A+, but not for CC-124 or CC-125, likely due to greater variability between replicates (Fig 12A).

Among the strains, CLiP consistently exhibited the lowest Car/Chl ratios in SD, 12/12, and CL, while CC-124 displayed the highest, especially under SD. The lower ratios observed in CLiP were largely driven by its relatively elevated chlorophyll content, despite also accumulating high levels of carotenoids. In CL, CLiP maintained the lowest ratio, while 4A+, CC-124, and CC-125 showed similar values (Fig 12B).

Under LD, differences between strains diminished, as all displayed comparable Car/Chl values (Fig 12B). This observation likely reflected a common reduction in carotenoid levels across strains, whereas chlorophyll concentrations remained largely unchanged.

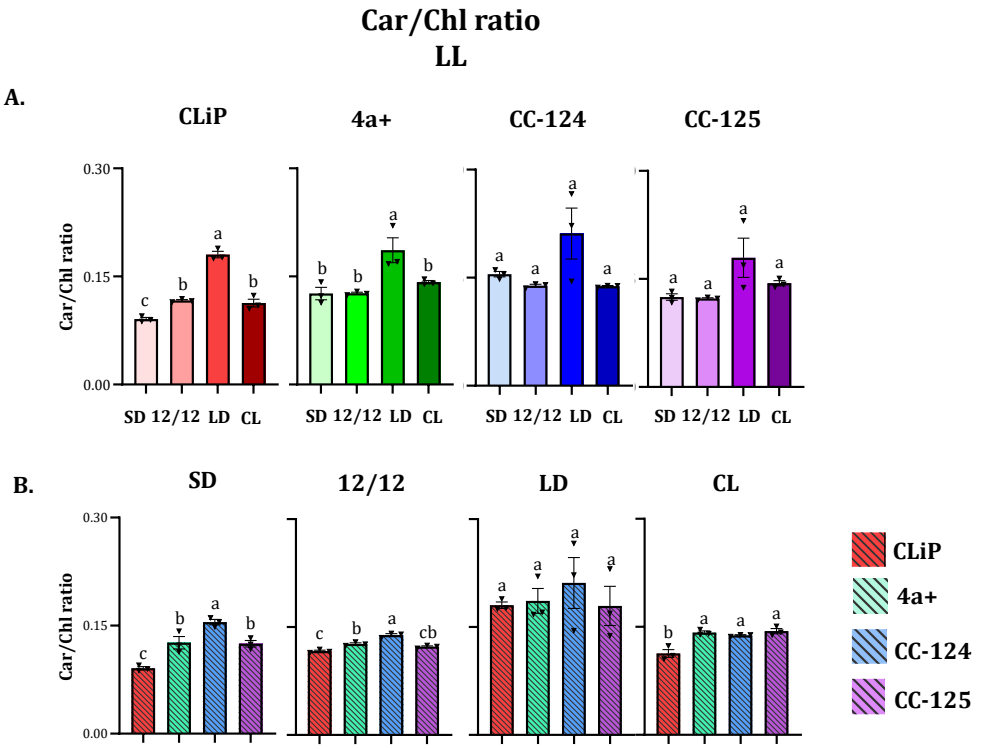

Figure 12. Carotenoid to chlorophyll (Car/Chl) ratio in *Chlamydomonas reinhardtii* strains under different light regimes in LL conditions. A. Bar graphs represent the Car/Chl ratio for each strain, individually, across light regimes. Light regimes are represented from paler to darker colors: SD (short day), 12/12 (12 h light/12 h dark), LD (long day), and CL (continuous light), and within each color-coded strain group (CLiP in red, 4a+ in green, CC-124 in blue, and CC-125 in purple). **B.** Bar graphs show the Car/Chl ratio represented by photoperiod; CliP (red), 4a+ (green), CC-124 (blue) and CC-125 (purple). Data indicate mean ± SEM from three to five biological replicates shown as small triangles. Different lowercase letters above the bars indicate statistically significant differences within each individual graph ($p < 0.05$, one-way ANOVA followed by Tukey's post hoc test). LL: Low Light (50µmol photons m^{-2} s^{-1}).

Under HL conditions, CLiP and CC-124 displayed stable Car/Chl ratios across light regimes, although values were higher in CC-124 (Fig. 13A). In contrast, the elevated ratio in 4A+ under CL was mainly driven by a marked decrease in both carotenoids and chlorophylls relative to other regimes. For CC-125, a gradual increase in the Car/Chl ratio across photoperiods and CL reflected a slower reduction in carotenoids compared to chlorophylls.

Moreover, 12/12 and CL produced similar Car/Chl ratios among most strains, whereas SD and LD revealed clear differences. In SD, 4A+, CC-124, and CC-125 showed comparable values, while for CLiP remained consistently lower. . Under LD, CLiP showed the lowest Car/Chl ratio, whereas CC-124 exhibited the highest, underscoring differences in pigment regulation under extended light exposure (Fig, 13B). Conversely, under LD, CLiP exhibited the lowest ratio, whereas CC-124 reached the highest, underscoring divergent pigment regulation under extended light exposure (Fig. 13B).

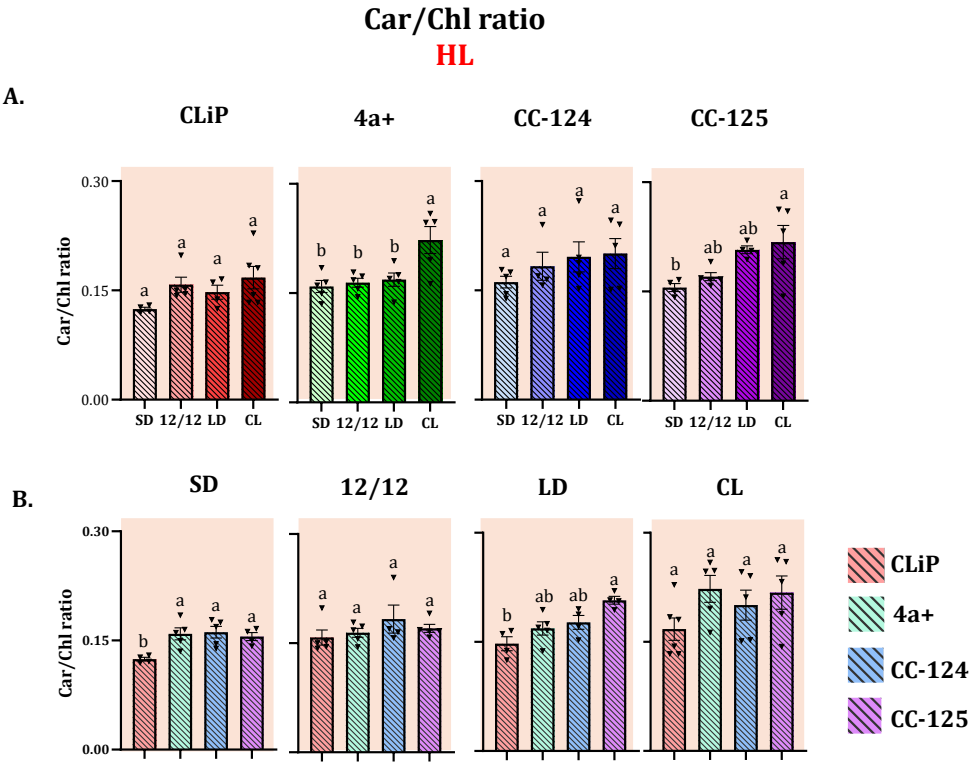

Figure 13. Carotenoid to chlorophyll (Car/Chl) ratio in *Chlamydomonas reinhardtii* strains under different light regimes in HL conditions. A. Bar graphs represent the Car/Chl ratio for each strain, individually, across light regimes. Light regimes are represented from paler to darker colors: SD (short day), 12/12 (12 h light/12 h dark), LD (long day), and CL (continuous light), and within each color-coded strain group (CLiP in red, 4a+ in green, CC-124 in blue, and CC-125 in purple). B. Bar graphs show the Car/Chl ratio represented by photoperiod; CliP (red), 4a+ (green), CC-124 (blue) and CC-125 (purple). Data indicate mean ± SEM from three to five biological replicates shown as small triangles. Different lowercase letters above the bars indicate statistically significant differences within each individual graph ($p < 0.05$, one-way ANOVA followed by Tukey's post hoc test). HL: High Light (250µmol photons m^{-2} s^{-1}).

Altogether, ratios remained stable under LL across photoperiods, except for LD. Conversely, HL conditions generally promoted an increase in longer light regimes. Furthermore, strain-specific differences point to different strategies in pigment balance.

3.9 Strain-specific differences in NPQ kinetics across photoperiods and CL under light stress in Chlamydomonas

While Fv/Fm values provide insights into the overall health and efficiency of PSII, pigment content reflects the light-absorbing capacity of the cells. However, in HL conditions, understanding NPQ allows us to assess how well the algae protect themselves from photooxidative damage under varying light conditions, which is crucial for photosynthetic efficiency and stress response. Measuring NPQ helps us understand how effectively Chlamydomonas strains regulate energy dissipation when exposed to excess light.

Thus, under HL conditions, where this photoprotective mechanism takes place, the highest NPQ values were obtained in shorter light regimes (SD and 12/12) for all strains, except for CC-124, which not only showed similar and low NPQ values in all dark-to-light regimes studied, but a significant decrease in CL (Fig. 14).

Furthermore, NPQ kinetics differed between strains and light regimes. CLiP consistently exhibited the highest NPQ induction across all regimes, with values peaking around 0.7–0.8 in SD and 12/12 conditions, followed by the typical gradual dark-relaxation; while 4a+ showed similar dynamics but reached slightly lower values (~0.6). In contrast, CC-125 and, especially, CC-124, displayed lower NPQ responses overall, particularly under continuous light (CL), where NPQ values remained below 0.3 (Fig. 14).

Under SD and 12/12, all strains exhibited a rapid NPQ induction within the first 2–3 minutes, with CLiP maintaining the highest levels and CC-124 the lowest, even though the high variability observed (Fig. 14).

In LD, CLiP again maintained the strongest response, while CC-124 NPQ values were considerably lower and showed minimal decline during the dark period. In CL, differences between strains were even more pronounced: CLiP sustained higher NPQ throughout the light period (~0.5), whereas the other strains showed low, relatively flat NPQ profiles, especially CC-124 and CC-125, which showed minimal induction or relaxation (Fig. 14).

These patterns suggest that CLiP has a more robust NPQ induction and relaxation capacity under HL, likely reflecting enhanced photoprotective mechanisms.

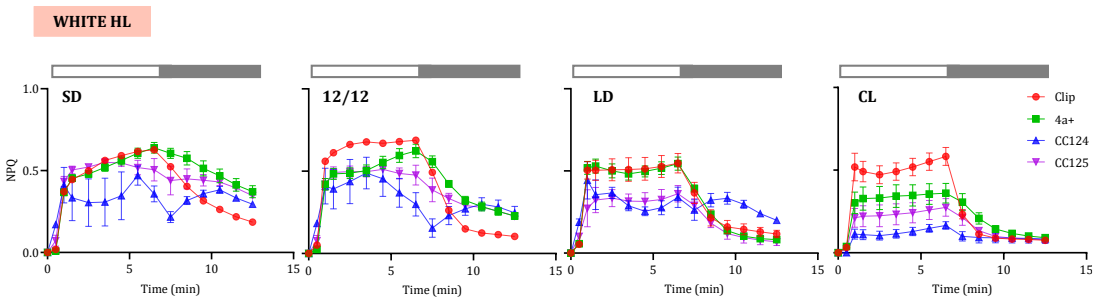

Fig 14. NPQ kinetics of Chlamydomonas WT-CLiP, 4a+ CC-124 and CC-125 under different light regimes and HL conditions. Bars on top: white = light period, black = dark period. WT-CLiP (red), 4a+ (green), CC-124 (blue), CC-125 (purple). Data are means ± SEM from five independent biological replicates (n = 5). SD: short day; 12/12: 12 h dark/12 h light; LD: long day; CL: continuous light. Measurements were performed after 5 days of HL (High Light) exposure (250µmol photons m^{-2} s^{-1}).

3.10 Exposure to HL resulted in differential effects on growth, photosynthetic performance, and pigment composition across *Chlamydomonas reinhardtii* strains.

In the preceding results, each *Chlamydomonas reinhardtii* strain was analyzed under LL and HL separately. Here, we bring these findings together in a direct comparison across light intensities and photoperiods, focusing on PSII efficiency (Fv/Fm), growth and cell size, and pigment-related indicators (Car/Chl and Chl a/b ratios), which serve as established markers of photoprotection and antenna remodeling in light-stressed *Chlamydomonas* (Tables 3–5).

Interestingly, cell area and growth were mostly unchanged in all WT strains (Table 3).

Among the strains, CLiP exhibited the most pronounced changes under HL. Fv/Fm values declined in all photoperiods with light-dark cycles (SD, 12/12, and LD), and although this reduction did not reach statistical significance in CL due to high variability, a clear tendency toward lower values was evident. Across all HL regimes, CLiP also showed an increase in the Car/Chl ratio, consistent with enhanced carotenoid accumulation. A significant rise in the Chl a/b ratio was detected under SD and 12/12, indicating antenna size reduction in shorter photoperiods. However, growth was only significantly enhanced under HL in LD, as reflected in a higher specific growth rate.

By contrast, CC-124 displayed fewer changes and responded primarily under CL in HL. Under this condition, Fv/Fm declined, growth rate increased, and Car/Chl ratios rose. Notably, a decrease in the Chl a/b ratio under CL suggested an increase in antenna size, pointing to an alternative acclimation strategy that differs from the more typical reduction observed in other strains.

4a+ showed a consistent increase in the Car/Chl ratio across all light regimes under HL, indicating enhanced photoprotection. However, significant changes in the Chl a/b ratio were limited to the 12/12 regime, and no substantial effects on growth were observed. Fv/Fm values tended to decrease under HL, but only reached statistical significance in SD and CL.

Growth rate		Low Light	High Light	
Strain	Light regime	Growth rate (μ (d^{-1}))	Growth rate (μ (d^{-1}))	Significance LL vs HL
CLiP	SD	0,13 ± 0,06	0,13 ± 0,05	ns
	1212	0,22 ± 0,06	0,18 ± 0,07	ns
	LD	0,23 ± 0,04	0,32 ± 0,03	*
	CL	0,51 ± 0,04	0,60 ± 0,04	ns
4a+	SD	0,14 ± 0,05	0,13 ± 0,04	ns
	1212	0,19 ± 0,02	0,16 ± 0,02	ns
	LD	0,27 ± 0,03	0,18 ± 0,05	ns
	CL	0,48 ± 0,02	0,48 ± 0,04	ns
CC-124	SD	0,11 ± 0,02	0,10± 0,02	ns
	1212	0,20 ± 0,02	0,19 ± 0,06	ns
	LD	0,29 ± 0,02	0,39 ± 0,06	ns
	CL	0,52 ± 0,02	0,62 ± 0,04	*
CC-125	SD	0,13 ± 0,02	0,08 ± 0,03	ns
	1212	0,18 ± 0,04	0,08 ± 0,03	*
	LD	0,30 ± 0,04	0,30 ± 0,10	ns
	CL	0,49 ± 0,01	0,49 ± 0,02	ns

Cell size		Low Light	High Light	
Strain	Light regime	Cell area (μm^2)	Cell area (μm^2)	Significance LL vs HL
CLiP	SD	62,70 ± 11,26	57,72 ± 13,88	ns
	1212	53,18 ± 8,52	55,62 ± 11,96	ns
	LD	53,05 ± 8,52	46,63 ± 7,88	ns
	CL	51,08 ± 11,44	47,40 ± 5,46	ns
4a+	SD	58,28 ± 9,48	61,21 ± 3,73	ns
	1212	61,18 ± 15,16	68,38 ± 11,92	ns
	LD	58,48 ± 16,78	62,27 ± 10,77	ns
	CL	49,79 ± 5,41	51,87 ± 7,44	ns
CC-124	SD	58,26 ± 3,58	56,96± 5,29	ns
	1212	67,69 ± 7,93	71,78 ± 11,06	ns
	LD	41,25 ± 3,01	62,73 ± 10,61	**
	CL	41,37 ± 4,16	55,34 ± 14,47	ns
CC-125	SD	57,34 ± 11,10	61,85 ± 7,69	ns
	1212	66,77 ± 4,43	70,61 ± 5,84	ns
	LD	46,84 ± 6,11	63,38 ± 14,88	ns
	CL	41,76 ± 6,49	54,41 ± 9,21	ns

Table 3. Growth rate (μ d^{-1}) and cell size (μm^2) of *Chlamydomonas reinhardtii* strains under low light (LL) and high light (HL) conditions across different light regimes. Mean values ± standard deviation (SD) are shown. Statistical significance between LL and HL within each condition was assessed using unpaired t-tests with Welch's correction. Asterisks indicate significant differences: $p < 0.05$ (*), $p < 0.01$ (**), $p < 0.001$ (***), $p < 0.0001$ (****). LL: low light (50µmol photons m^{-2} s^{-1}). HL: high light (250µmol photons m^{-2} s^{-1}).

Lastly, CC-125 exhibited reduced Fv/Fm values in all HL conditions except 12/12, where levels remained comparable to LL. Increases in the Car/Chl ratio were observed across all photoperiods, though the rise in LD did not reach significance. No significant differences were detected in the Chl a/b ratio, and growth rates were largely unaffected by HL exposure, except for a slight decrease noted under 12/12.

Altogether, these comparisons show that HL exposure generally reduced PSII efficiency, increases in the Car/Chl ratio (indicating enhanced photoprotection), and changes in the Chl a/b ratio (reflecting antenna remodeling) in most strains, while growth and cell size remained more stable. At the same time, the magnitude and direction of these responses varied between strains, with CLiP displaying the strongest shifts and others such as CC-124 and CC-125 showing more moderate or condition-specific acclimation patterns. These integrative results highlight both common and divergent strategies among *Chlamydomonas* strains and provide the basis for the following Discussion, where we interpret how light intensity and photoperiod interact to shape acclimation responses.

Chl a/b ratio		Low Light	High Light	
Strain	Light regime	Chl a/b (mean ± SD)	Chl a/b (mean ± SD)	Significance LL vs HL
CLiP	SD	1,24 ± 0,02	1,30 ± 0,01	*
	12/12	1,19 ± 0,01	1,25 ± 0,04	*
	LD	1,14 ± 0,01	1,16 ± 0,06	ns
	CL	1,15 ± 0,01	1,10 ± 0,08	ns
4a+	SD	1,32 ± 0,03	1,31 ± 0,02	ns
	12/12	1,26 ± 0,01	1,31 ± 0,04	*
	LD	1,28 ± 0,02	1,20 ± 0,08	ns
	CL	1,28 ± 0,01	1,21 ± 0,07	ns
CC-124	SD	1,59 ± 0,01	1,60 ± 0,02	ns
	12/12	1,47 ± 0,02	1,69 ± 0,20	ns
	LD	1,46 ± 0,02	1,39 ± 0,12	ns
	CL	1,50 ± 0,05	1,19 ± 0,15	**
CC-125	SD	1,32 ± 0,03	1,36 ± 0,14	ns
	12/12	1,23 ± 0,03	1,43 ± 0,19	ns
	LD	1,22 ± 0,01	1,29 ± 0,08	ns
	CL	1,24 ± 0,01	1,25 ± 0,11	ns

Car/Chl ratio		Low Light	High Light	
Strain	Light regime	Car/Chl (mean ± SD)	Car/Chl (mean ± SD)	Significance LL vs HL
CLiP	SD	0,09 ± 0,00	0,12 ± 0,00	***
	12/12	0,12 ± 0,00	0,16 ± 0,02	*
	LD	0,18 ± 0,01	0,15 ± 0,02	*
	CL	0,11 ± 0,01	0,17 ± 0,04	*
4a+	SD	0,13 ± 0,01	0,16 ± 0,02	*
	12/12	0,13 ± 0,00	0,16 ± 0,01	**
	LD	0,19 ± 0,03	0,17 ± 0,02	ns
	CL	0,14 ± 0,00	0,22 ± 0,04	*
CC-124	SD	0,15 ± 0,01	0,16 ± 0,02	ns
	12/12	0,14 ± 0,00	0,18 ± 0,04	ns
	LD	0,21 ± 0,06	0,20 ± 0,05	ns
	CL	0,14 ± 0,00	0,20 ± 0,05	*
CC-125	SD	0,12 ± 0,01	0,16 ± 0,01	**
	12/12	0,12 ± 0,00	0,17 ± 0,01	***
	LD	0,18 ± 0,05	0,21 ± 0,01	ns
	CL	0,14 ± 0,01	0,22 ± 0,05	*

Table 4. Chl/ab and Car/Chl ratios of *Chlamydomonas reinhardtii* strains under low light (LL) and high light (HL) conditions across different light regimes. Mean values ± standard deviation (SD) are shown. Statistical significance between LL and HL within each condition was assessed using unpaired t-tests with Welch's correction. Asterisks indicate significant differences: $p < 0.05$ (*), $p < 0.01$ (**), $p < 0.001$ (***), $p < 0.0001$ (****). LL: low light (50µmol photons m^{-2} s^{-1}). HL: high light (250µmol photons m^{-2} s^{-1}).

Fv/Fm ratio		Low Light	High Light	
Strain	Light regime	Fv/Fm (mean ± SD)	Fv/Fm (mean ± S)	Significance LL vs HL
CLiP	SD	0,38 ± 0,01	0,34 ± 0,03	*
	12/12	0,44 ± 0,03	0,39 ± 0,04	*
	LD	0,41 ± 0,03	0,19 ± 0,11	*
	CL	0,19 ± 0,17	0,09 ± 0,08	ns
4a+	SD	0,40 ± 0,02	0,30 ± 0,04	**
	12/12	0,35 ± 0,07	0,30 ± 0,06	ns
	LD	0,33 ± 0,06	0,24 ± 0,09	ns
	CL	0,33 ± 0,16	0,02 ± 0,03	*
cc124	SD	0,40 ± 0,02	0,35 ± 0,09	ns
	12/12	0,39 ± 0,02	0,36 ± 0,06	ns
	LD	0,31 ± 0,09	0,31 ± 0,03	ns
	CL	0,33 ± 0,05	0,00 ± 0,00	****
cc125	SD	0,38 ± 0,01	0,33 ± 0,03	*
	12/12	0,33 ± 0,07	0,31 ± 0,03	ns
	LD	0,36 ± 0,02	0,19 ± 0,03	****
	CL	0,30 ± 0,06	0,00 ± 0,01	*

Table 5. Photosynthetic efficiency (Fv/Fm) of *Chlamydomonas reinhardtii* strains under low light (LL) and high light (HL) conditions across different light regimes. Mean values ± standard deviation (SD) are shown. Statistical significance between LL and HL within each condition was assessed using unpaired t-tests with Welch's correction. Asterisks indicate significant differences: $p < 0.05$ (*), $p < 0.01$ (**), $p < 0.001$ (***), $p < 0.0001$ (****). LL: low light (50µmol photons m^{-2} s^{-1}). HL: high light (250µmol photons m^{-2} s^{-1}).

4. DISCUSSION

4.1 Light intensity and photoperiod as key environmental drivers

Light intensity and photoperiod are key environmental variables that regulate photosynthesis, growth, pigment composition, and photoprotection in *Chlamydomonas reinhardtii*. Most laboratory studies, however, examine these factors in isolation, limiting our understanding of how algae respond to different light regimes. Natural environments expose cells to fluctuating light levels and periodic darkness, which can profoundly influence acclimation strategies. Here, we examined how intensity and photoperiod interact

to shape physiological responses in four wild-type Chlamydomonas strains, focusing on traits relevant to light utilization, stress mitigation, and growth.

While the effects of light intensity on photosynthesis and photoprotection are well documented (Niyogi, 2000; Peers et al., 2009), and some studies have addressed temporal regulation under diurnal conditions (Strenkert et al., 2019), few works have considered their combined impact across different strains (Treves et al., 2017). Our results demonstrate that while some responses are conserved, others are clearly strain-specific. This highlights the importance of avoiding overgeneralizations, as physiological and photoprotective traits can differ substantially between strains. Understanding these differences is essential for designing robust experiments and for interpreting results in a broader context, particularly when aiming to apply laboratory findings to natural or biotechnological settings.

4.2 Growth responses and morphological changes

We began by examining growth and cell size, as these traits offer a first look at how cells cope with different light regimes and are directly relevant for both ecological function and biotechnological applications.

The most striking observation is that, overall, longer photoperiods lead to smaller cell sizes, with no substantial differences between LL and HL conditions. This points to photoperiod duration as the dominant factor shaping Chlamydomonas morphology. Notably, the largest cells are found under the 12/12 light/dark regime, where cell division is synchronized across the population. Early studies showed that in *Chlamydomonas reinhardtii*, cell cycle progression is light-driven, but division is subjected to the dark phase, making 12/12 ideal for temporally separating biomass accumulation and mitosis (Spudich & Sager, 1980). This reflects a well-established coupling between cell growth and cell division, whereby cells grow to a critical size during the light phase before committing mitosis in the dark. Under prolonged or CL, this temporal coordination seems to be disrupted, leading to more frequent divisions and, consequently, smaller cells.

At the same time, growth rates increase with photoperiod duration, peaking under CL, yet remain similar between LL and HL within each regime. This pattern further supports the idea that it is the length of light exposure, not its intensity, that governs both cell growth and division timing. These dynamics align with the multiple-fission cycle of Chlamydomonas, where rapid growth under extended light accelerates commitment to division, producing more, but smaller daughter cells (Heldt et al., 2020). Thus, longer photoperiods trigger proliferation at the expense of cell size, reflecting a physiological

trade-off between growth rate and biomass accumulation. In this context, the usually tight connection between growth and division becomes uncoupled, as faster growth under extended light does not produce larger cells but instead results in further division cycles, ultimately yielding smaller daughters.

Interestingly, the fact that similar growth rates emerged under such contrasting light conditions made us question whether cells were genuinely unaffected, or whether HL was triggering physiological stress that growth rates alone couldn't reveal. This prompted us to explore how the morphology of the cells was affected.

Our findings are consistent with previous reports describing structural adaptations to light stress. In LL conditions across all photoperiods, cells displayed compact chloroplasts, visible eyespots, moderate starch levels, and no evidence of extracellular matrix (ECM) formation, reflecting a balanced physiological state. However, under HL conditions, especially during LD and CL, cells exhibited signs of light-stress, including disrupted chloroplast organization, significant starch accumulation, diminished eyespot visibility, and ECM formation, consistent with known stress-induced phenotypes (Erickson et al., 2015; Minagawa & Tokutsu, 2015). Notably, starch accumulation has been documented as a hallmark response to excessive light exposure or carbon fixation stress in Chlamydomonas (Koo et al., 2017; Erickson et al., 2015), while disassembly or visibility loss of eyespot components correlates with impaired phototactic function under stress (Ueki et al., 2025). The observed ECM or halo formation in prolonged HL aligns with previous reports describing cell wall reinforcement and extracellular polysaccharide secretion as part of *Chlamydomonas reinhardtii*'s protective response to high irradiance (Erickson et al., 2015). Accordingly, our results suggest that sustained HL and extended photoperiods shift cellular priorities from efficient light harvesting toward protective strategies, such as starch storage and structural reinforcement.

4.3 Photosynthetic efficiency and photoprotective responses

First, it is important to note that the Fv/Fm values observed in LL HSM cultures (~0.4) were lower than the ~0.6–0.7 range usually reported for LL-acclimated Chlamydomonas reinhardtii (Bonente et al., 2011). Long-term photoautotrophic growth under low light can create a stressful environment; dense cultures in minimal medium frequently experience CO_2 limitation, which suppresses photosynthetic efficiency, and extended CO_2 deprivation has been shown to induce PSII downregulation and degradation of photosynthetic complexes (Grechanik et al., 2022). Because these conditions were consistent across all

strains and treatments, the comparative trends we describe remain robust, even if the absolute values are reduced.

On the other hand, the decline in Fv/Fm under high light, particularly in longer photoperiods, suggests that extended light exposure exacerbates PSII photodamage in *Chlamydomonas reinhardtii*. In contrast, stable Fv/Fm values under low light across most photoperiods indicate limited stress and better photosynthetic performance. The parallel trend observed in NPQ, higher under short photoperiods and reduced under prolonged exposure, further supports the idea that dark intervals play a protective role by facilitating PSII recovery and enabling effective energy dissipation. These findings highlight the importance of light–dark cycles in modulating photoprotection and photoinhibition, consistent with prior observations in other photosynthetic organisms (Nawrocki et al., 2019).

4.4 Pigment content and regulation

To evaluate how light acclimation influences pigment systems, we next investigated the total pigment content and pigment ratios. Chlorophyll levels were higher in SD compared to LD under LL, consistent with findings in land plants such as *Arabidopsis thaliana* and *Atrichum undulatum* (Becker et al., 2006; Cvetić, 2009).

In our experiments, chlorophyll content was higher under CL than under other photoperiods such as LD. *C. reinhardtii* can synthesize chlorophyll in both light and dark phases, although under a 12/12 cycle this mainly occurs during the light period (Harris, 1989). Based on our results, continuous illumination likely enables uninterrupted pigment synthesis, while in LD or 12/12 it is limited by day length. The higher levels observed in SD, despite shorter exposure, suggest an adaptive adjustment. This may involve circadian control or structural remodeling of the chloroplast to improve light capture. Carotenoid content, in contrast, remained unchanged under low light intensity, consistent with a baseline role in light harvesting.

Under HL, both chlorophyll and carotenoid contents increased in shorter photoperiods but declined under LD and CL. Chlorophyll degradation in HL has been reported before and linked to changes in the expression of Chl-binding proteins (Bonente et al., 2012; Erikson et al., 2015). In contrast, the carotenoid decline observed during prolonged HL in LD and CL opposes the commonly reported carotenoid accumulation under HL (Bonente et al., 2012). This suggests that extended exposure to high irradiance may impair carotenoid biosynthesis.

In LL, Chl a/b ratios were higher under SD, indicating reduced antenna size (Kirst et al., 2012) compared to longer photoperiods. This result is unexpected, since low irradiance typically promotes antenna expansion to improve photon capture (Negi et al., 2020). In our case, although total chlorophyll content increased in SD, the relative proportion of Chl b was lower, suggesting that pigment accumulation did not translate into antenna enlargement. One possible explanation is that the short light window limits the time available for LHC remodeling, preventing full antenna expansion despite elevated chlorophyll levels. Alternatively, circadian regulation of chlorophyll biosynthesis may favor Chl a accumulation during SD, leading to smaller functional antennae. Thus, in our experiments, photoperiod duration appears to override irradiance as the main determinant of antenna size.

CC-124 displayed the highest ratio while CLiP consistently had the lowest Chl a/b ratios across all light regimes. This strategy seems to be beneficial in shorter light regimes, but under CL, larger antennae may lead to an over absorption, possibly explaining CLiP's Fv/Fm drop. In turn, Car/Chl ratios remained stable under LL, consistent with no high demand of carotenoids in non-stress conditions.

A similar trend was also observed in HL, meaning shorter photoperiods allowed for higher ratios and thereby reduced antenna. Interestingly, Chl a/b ratios were generally stable under HL relative to LL. Thus, although total chlorophyll content per cell decreases under HL, the functional antenna size remains largely unchanged across light intensities, suggesting that cells rely more on pigment adjustment and photoprotective responses than on structural remodeling of the light-harvesting complex (Spät, Kropat, Malasarn, & Merchant, 2011). This contrasts with strategies observed in other algae, such as *Chlorella vulgaris* and *Chlorella sorokiniana,* where high light typically triggers a reduction in antenna size to limit excitation pressure on photosystem II. By reducing antenna size, these algae lower excess light absorption, decrease the risk of photoinhibition, and improve light-use efficiency under high irradiance (Shin et al., 2016; Cazzaniga et al., 2014). These contrasting strategies highlight specific acclimation mechanisms between species. On the other hand, Car/Chl ratios rose under HL compared to LL, and in some strains, such as 4A+ and CC-125, increased even more under LD and CL compared to other photoperiods, consistent with stress-induced carotenoid accumulation (Bonente et al., 2012).

4.5 Broader implications and applications

Our results reveal distinct cellular strategies depending on light regime. Under LL, cells prioritize light harvesting: chlorophyll levels rise, antennae expand, and longer

photoperiods support higher growth. Under HL, the focus shifts to protection: chlorophyll declines, carotenoids increase, and NPQ is activated.

The effect of photoperiod also depends on light intensity: longer exposure promotes growth in LL but exacerbates stress in HL unless protective responses are in place. In contrast, short photoperiods support more stable physiological performance under both intensities, though at the cost of reduced growth. Moreover, under HL, cells exposed to shorter photoperiods retain a healthier morphology, whereas extended regimes seem to be associated with stress-related alterations. This underscores the need to consider light intensity and duration as interacting factors rather than independent variables.

Beyond general trends, strain-specific responses revealed distinct physiological strategies. CLiP stood out for its resilience under HL, maintaining good growth rates, PSII performance and strong NPQ even when carotenoid content declined, suggesting the involvement of alternative photoprotective pathways, such as LhcSR3-mediated quenching (Bonente et al., 2011). Its efficient NPQ recovery during dark phases highlights the benefit of diurnal cycles for stress mitigation. In contrast, CC-124 appeared to trade off stress resilience for growth, with low NPQ capacity and signs of photodamage under continuous HL. CC-125 and 4A+ adopted more moderate or intermediate strategies, showing pigment adjustments and some photoprotection, but remained vulnerable under prolonged HL. These patterns show how even laboratory-maintained lineages harbour functional diversity, likely shaped by genetic background, mating type, or historical selection pressures.

Our findings also suggest that dark periods support PSII recovery and sustained physiological function, and that diurnal cycles may enhance long-term performance under stress. From an applied perspective, optimizing both light intensity and photoperiod could improve the balance between productivity and protection. More broadly, our results highlight the diversity of acclimation strategies among Chlamydomonas strains and underscore the importance of incorporating multiple backgrounds and varied light conditions that capture the environmental complexity these organisms face.

5. CONCLUSIONS

1. Growth and cell size are shaped by photoperiod rather than intensity in most of the strains, allowing for higher rates but smaller cells in longer light periods and CL. However, CLiP seems to maintain similar cell sizes across photoperiods and intensities, while higher growth rates in increased day lengths.

2. Cell morphology reveals no big differences across photoperiod and strains in LL, while HL reveals light-stress signs, especially in longer light periods and in CL.
3. PSII integrity is promoted in LL independently of photoperiod, though shorter photoperiods allow for a better photosynthetic performance in HL. CL triggers greater sensitivity for CLiP in LL but greater resilience in HL.
4. Pigment composition is light intensity and photoperiod shaped: in LL chlorophylls are enhanced in shorter photoperiods while carotenoids remain mostly stable, suggesting a baseline light-harvesting role. Under HL, chlorophyll and carotenoid contents increase in short photoperiods while decrease in long photoperiods and CL, indicating pigment degradation in extended day lengths.
5. SD allows for the highest Chl a/b ratio in LL, with most of the strains showing minor changes in this ratio in the rest of the light regimes, except for CLiP which seems to be more photoperiod-shaped. Under HL, Chl a/b ratios increase in shorter photoperiods indicating a reduction in antenna size. In addition, CLiP generally shows the largest antenna and CC-124 the smallest, pointing to strain-specific adjustments.
6. Chl a/b ratios are higher in SD but show minor changes modulated by photoperiod under LL, reflecting antenna size adjustments, with CLiP showing the largest antenna and CC-124 the smallest. Under HL, Chl a/b ratios increase in shorter photoperiods indicating a reduction in antenna size, while CC-124 shows an atypical decrease under HL + CL.
7. Car/Chl ratios are mostly stable in LL, with some increases in LD due to chlorophyll reduction rather than carotenoid accumulation. High light, in turn, promotes an increase in Car/Chl ratios in a photoperiod-dependent manner, mainly due to chlorophyll degradation. Strain-specific pigment balance becomes apparent.
8. NPQ is highly induced in short HL photoperiods and reduced under CL, with CLiP showing the best NPQ kinetics across conditions.
9. Strain-specific responses reveal distinct trade-offs: CLiP combines high photoprotection with sustained growth, whereas CC-124 prioritizes proliferation at the expense of photosynthetic integrity under light stress. 4a+ and CC-125 show intermediate responses. ´
10. Other inter-strain differences observed appear to rely more on pigment adjustment strategies than on morphological traits.
11. Overall growth, pigment composition and adjustment are regulated by photoperiod under LL, while photosynthetic efficiency remains stable. In HL, typical light-stress responses appear and seem to be shaped by photoperiod, with shorter ones revealing overall better performance.

12. These findings show that photoperiod modulates light acclimation more than intensity alone and highlight the importance of considering strain background in *Chlamydomonas reinhardtii* research.

Chapter 3

Unravelling the role of the novel Chlamydomonas photoreceptors HIK1 and HIK2

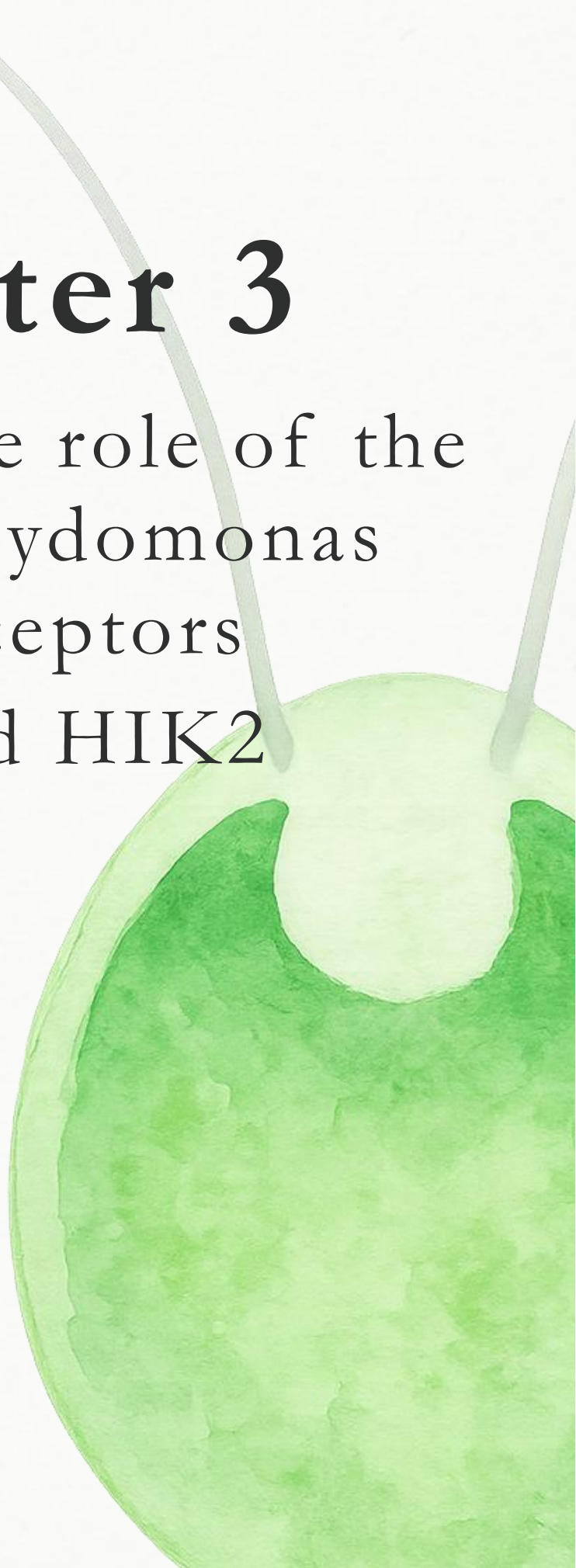

1. INTRODUCTION

1.1 Two-Component Signaling System

Two-component systems (TCS) are fundamental signaling mechanisms that enable organisms to sense and respond to environmental cues. Each system typically consists of two protein domains: a sensor histidine kinase (HK) and a response regulator (RR). Upon phosphorylation, these components work together to convert external signals into specific cellular responses (Appleby et al., 1996).

Prokaryotic and eukaryotic two-component systems (TCS) involving histidine kinases (HK) exhibit key differences in structure, complexity, and functionality. Prokaryotic TCS are generally simpler, consisting of a direct phosphorylation pathway from the histidine kinase to a response regulator (RR), allowing bacteria to efficiently respond to a wide range of environmental stimuli. In contrast, eukaryotic TCS often involve more complex, multi-step phosphorelay pathways, which can introduce additional layers of regulation and control (Fig. 1) (Galperin et al., 2010; Alvarez et al., 2016; Papon et al., 2019).

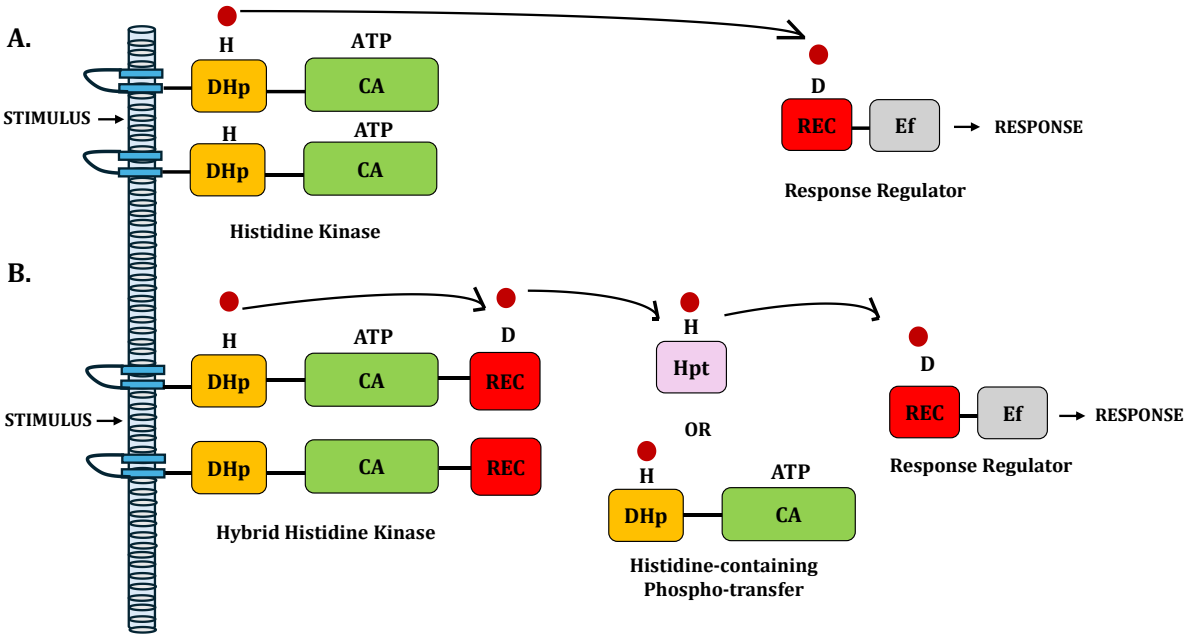

Fig. 1 Two-component system (TCS) A. In prokaryotes, a typical pathway begins with a histidine kinase (HK) sensing a stimulus through its extracytoplasmic domains (DHp, CA), leading to autophosphorylation at a conserved histidine (H) residue using ATP. The phosphoryl group (dark red circle) is then transferred to a conserved aspartate (D) in a response regulator (RR), triggering a downstream response. B. In eukaryotes, a more complex multi-step phosphorelay occurs, often involving a hybrid HK that contains an additional aspartate domain. The phosphorelay progresses through sequential phosphorylation events: first steps are equal to prokaryotes; however, the phosphoryl group is then transferred to a histidine-containing phosphotransfer protein (either Hpt, pale violet or pseudo-HK), and finally to an RR (Figure adapted from Papon et al., 2019).

In eukaryotes, the classic HK structure (which is a hybrid histidine kinase HHK), usually membrane-bound but also located in cytoplasmic regions, consists of distinct domains (Fig 2) (Appleby et al. 1996). The N-terminal region, known as the "sensing domain," is key for detecting various environmental cues, such as light, temperature, or nutrient fluctuations. From these sensing domains, the PAS (Per-ARNT-Sim) family domain is particularly common and highly conserved, serving as a key sensing element (Möglich et al, 2009).

The central HK structure includes the transmitter domain, composed of the dimerization histidine phosphotransfer (DHp) domain (usually a Histidine Kinase A (HisKA)) and the histidine kinase-like ATPase catalytic (HATPase_c) subdomains. The HisKA domain contains an H-box, which typically has a phosphorylatable histidine, and an X-box. The HATPase_c subdomain is characterized by four conserved regions: the N-, G1-, F-, and G2-boxes (Möglich et al., 2009) (Fig. 2). Together, these subdomains enable autophosphorylation of the kinase on a conserved histidine residue within the HK, which propagates the signal. This phosphorylation event is powered by ATP binding in the ATP-binding domain, which provides the necessary energy for the reaction.

Furthermore, in contrast to prokaryotic HKs, the HK C-terminal region in eukaryotes contains a receiver domain (REC) as part of the RR. This domain includes a conserved DDK motif with a phosphorylatable aspartate residue (Appleby et al. 1996) (Fig 1, 2).

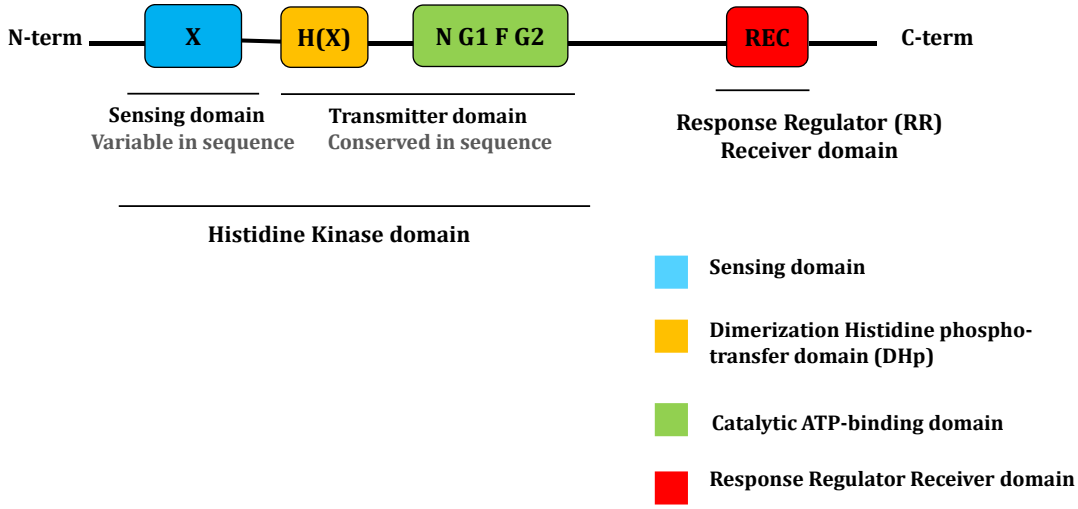

Fig 2. Histidine kinases (HKs): variable and conserved domains. The N-terminal region, known as the sensing domain (X, blue), is variable. The central transmitter region is more conserved and includes two key domains: the dimerization histidine phosphotransfer (DHp, yellow) domain (usually a His kinase A, (HisKA)), which contains the phosphorylatable H-box and X-box, and the catalytic (CA) ATP-binding domain, which features conserved sequence motifs (N-, G1-, F-, and G2-boxes, green). Finally, the C-terminal is a response regulator (REC, red) domain, which contains a phosphorylatable aspartate residue (Figure adapted from Papon et al., 2019).

When phosphorylated, this aspartate induces a conformational shift that activates the RR, initiating downstream responses, often through regulation of gene expression or interactions with other proteins. A linker region connects the receiver and output domains, facilitating the necessary structural changes for activation.

Response regulators (RRs) output domains play a crucial role in determining their functional diversity. These domains allow RRs to regulate various cellular processes, and they can be broadly categorized into four types: DNA-binding domains, enzymatic domains, protein-binding domains, and unknown function domains. Many bacterial RRs contain DNA-binding domains, such as the Winged Helix (OmpR/PhoB family), Helix-turn-helix (NarL/FixJ family), and the LytTR domain, which enable them to act as transcriptional regulators. Other RRs possess enzymatic domains like Methylesterases (CheB family), Adenylate Cyclases, and Diguanylate Cyclases (GGDEF domain), which are directly involved in signal transduction and secondary messenger regulation. Additionally, some RRs, such as PhyR, engage in protein-protein interactions, regulating processes like stress responses. A subset of RRs, including CheY, consists solely of the REC domain, which is involved in phosphorelay and processes like chemotaxis (Galperin et al., 2010).

HKs regulate essential processes across species. In plants, HKs control gametophyte development, growth, stress responses (drought, salt, stomatal closure), light perception, and phytohormone signaling (cytokinin, ethylene) (Osakabe et al., 2013). In fungi, they contribute to stress adaptation (osmolarity, oxidative stress), red-light perception, morphogenesis, and virulence (Hérivaux et al., 2016). In the green microalga *Ostreococcus tauri,* a LOV-HK was also found, whose expression is induced by blue light and is under circadian control (Djouani-Tahri et al., 2011).

Overall, TCSs constitute a highly adaptable signaling strategy that has been conserved throughout evolution. While prokaryotic systems are typically linear and efficient, eukaryotic TCSs often involve more elaborate phosphorelays and regulatory domains, allowing for additional layers of control. In photosynthetic eukaryotes such as *Chlamydomonas reinhardtii,* although TCS components are less well characterized than in land plants or fungi, several putative histidine kinases have been identified, including light-sensitive histidine kinase rhodopsins (HKRs) implicated in photoperception and signal transduction (Luck et al., 2012). Due to its photoautotrophic lifestyle and sensitivity to environmental changes, Chlamydomonas is likely to use TCS-like elements to adjust gene expression and regulate its physiological responses. Studying these signaling components in Chlamydomonas could

provide insights into how unicellular green algae perceive and integrate external cues, and how TCS pathways have diversified across eukaryotes.

1.2 Photoreceptor Histidine Kinases

Photoreceptor histidine kinases (PHKs) are a subset of HKs specialized in sensing light across the near-ultraviolet to near-infrared spectral range. Using light-absorbing chromophores, PHKs initiate signal transduction upon light exposure. Unlike typical HKs, which respond to a variety of environmental cues such as temperature, osmolarity, or chemical gradients, PHKs specifically modulate their kinase activity in response to light. However, like other HKs, PHKs involve autophosphorylation and the subsequent phosphorylation of response regulators in their signaling process. (Möglich et al, 2019)

PHKs often contain unique light-sensitive sensor domains, such as light-oxygen-voltage (LOV) domains, bacteriophytochrome (BPhy) domains, and microbial rhodopsins, which are finely tuned for light detection (Vreede et al., 2003).

1.3 LOV structure and signalling

Light–oxygen–voltage (LOV) domains are specialized members of the Per–ARNT–Sim (PAS) domain superfamily, and their structure is integral to their function in light signal transduction. LOV photosensors share a conserved architecture consisting of a five-stranded antiparallel β-sheet flanked by two α-helices (Eα and Fα) that enclose a flavin chromophore—either flavin mononucleotide (FMN) or flavin adenine dinucleotide (FAD) (Möglich et al., 2009; Herrou et al., 2011). The flavin, typically in its oxidized quinone state, is buried within a hydrophobic pocket formed by these structural elements, enabling efficient absorption of light in the UV-A to blue range (Möglich et al., 2009).

In addition to this core structure, the functional LOV domains contain N-terminal and C-terminal extensions identified as A'α and Jα. These extensions are predominantly α-helical and are crucial as they interact with the β-sheet, influencing the overall conformation and signaling capabilities of the LOV proteins (Möglich et al., 2009; Berntsson et al., 2017). The A'α and Jα helices engage in critical interactions that are essential for the reversible conformational changes that occur upon light activation.

Upon light absorption, the LOV domain experiences significant conformational changes that

facilitate signal transduction. The first step involves the formation of a covalent adduct between the flavin chromophore (FMN) and a conserved cysteine residue within each LOV domain, which stabilizes the signaling state. This conserved cysteine is located on the Eα helix of the central core in a conserved GXNCRFLQ motif. This bond formation triggers a cascade of structural alterations which include the detachment of the Jα helix from the core. This process is crucial as it initiates the interaction with downstream effector modules, particularly in histidine kinases, enabling the transduction of light signals into biochemical responses (Möglich, 2009).

LOV receptors play a pivotal role in various cellular functions, including phototaxis, regulation of gene expression, and developmental processes, by integrating environmental light signals (Herrou et al., 2011). The ability to convert light into a biochemical signal is a critical evolutionary adaptation that enables organisms to respond dynamically to their environment. Moreover, the efficiency and specificity of light signal transduction are influenced by the unique structural features of different LOV proteins, which vary across species and functional contexts. This diversity highlights the versatility of LOV domains as light sensors and underscores their potential for engineering light-responsive systems in synthetic biology and biotechnology.

Although *Chlamydomonas reinhardtii* is widely used to study light perception, not all photoreceptors have been identified or functionally characterized. Several families have been reported, including cryptochromes, rhodopsins, and the well-characterized LOV-domain phototropin CrPHOT (Greiner et al., 2017). CrPHOT has been extensively studied and is known to regulate multiple light-dependent processes (Huang & Beck, 2003; Huang, Kunkel and Beck, 2004; Trippens et al., 2012; Petroutsos et al., 2016; Aihara et al., 2019). Apart from CrPHOT, only a few other LOV-domain proteins have been identified in Chlamydomonas, and their roles remain unknown. In contrast, in *Arabidopsis thaliana*, all major photoreceptor types have been described in detail, including five phytochromes (phyA–phyE), two cryptochromes (cry1, cry2), two phototropins (phot1, phot2), and the UV-B receptor UVR8, each associated with specific developmental and physiological functions (Christie et al., 2015; Wang and Lin, 2021).

In the laboratory, we identified two previously uncharacterized LOV-domain proteins, HIK1 and HIK2. This chapter investigates their potential role in light signaling, with the aim of gaining further insight into light perception and photoadaptation in Chlamydomonas and contributing to current understanding of LOV-based signaling mechanisms.

2. METHODOLOGY

2.1 Biological material and culture maintenance

Chlamydomonas strains CC-5325 (also called CMJ030, identical to CC-4533, mt−, CLiP library background) *hik1 442*, *hik2 038, hik2 149 hik2 408* and *hik2 506* used for these chapters were obtained from the Chlamydomonas Library (CLiP) Center (CRC) (University of Minnesota).

The biological material for this study was obtained from individual TAP solid media plates (see **Supplementary Information 1: Media preparation**) (Kropat et al., 2011). Each plate contained a single strain and was stored in a growth chamber (ARALAB 1200) under controlled conditions (21 °C, 30 μmol m^{-2} s^{-1} LED light). One week before starting each experiment, the cultures were re-streaked onto fresh TAP–agar plates using a sowing handle.

2.2 Genomic DNA extraction

DNA extraction was performed following a rapid method suggested by CLiP mutant library. Cells were first picked with a sterile sowing handle and released in a 1.5 ml Eppendorf tube containing 30μl of EDTA 10mM pH8 (NaOH) buffer. After vortex, the mixture showed a green color. This mixture was then heated to 100ºC during five minutes and then kept on ice for five more minutes. Mixture was vortexed again and centrifuged for 5minutes at 13000rpm to spin down cell debris. This supernatant was then released to a new Eppendorf which was the extracted genomic DNA (1μl was used for the PCRs).

2.3 PCR and electrophoresis gels

PCR reactions were prepared in a total volume of 10 μL using NZYTaq II 2× Green Master Mix. Each reaction contained 5 μL of the enzyme buffer, 0.5 μL of DMSO, 1 μL of template DNA, 0.6 μL of each primer (see Table 1), and 2.3 μL of nuclease-free water. Amplification was carried out for 40 cycles, each consisting of: denaturation at 95 °C for 30 s, annealing at the primer-specific optimal temperature for 30 s, and extension at 72 °C for 1 min. PCR products were resolved by electrophoresis on a 1% agarose gel containing one or two drops of ethidium bromide (depending on gel size). Gels were run at 120 V for at least 15 min and visualized under UV light using a gel imaging system.

Primer name	Sequence	Gene
EM13	GCACCAATCATGTCAAGCCT	5' end binding the CIB1 cassette and facing outwards towardsthe genome
EM14	GACGTTACAGCACACCCTTG	3' end binding the CIB1 cassette and facing outwards towardsthe genome
EMP1520	GGTCCGGAGGGTGCTGACTC	Fw primer for CRISPR-Cas9 mutant screening
EMP1509	AGTGTGCTCACCAAAGATCGCAT	Rev primer for CRISPR-Cas9 mutant screening
EMP1624	CTTCAATCCCACCACCATCA	*HIK1* mutant 442 genotyping
EMP1625	CTCACCACACCTCACTACATAC	*HIK1* mutant 442 genotyping
EMP1626	CCGGGCGCAAATTCAATAAC	*HIK2* mutant 038 149 genotyping
EMP1627	CTCATGTTGGCCAGGAACT	*HIK2* mutant 038 149 genotyping
EMP1628	GCTCTTCCTTGGACATGCT	*HIK2* mutant 408 genotyping
EMP1629	CTTGAGCACCACCTTCTGATT	*HIK2* mutant 408 genotyping
EMP1630	GGTGAGGAGTCTGCAAAGAA	*HIK2* mutant 506 genotyping
EMP1631	GAATGCACTCGTTGGGAATG	*HIK2* mutant 506 genotyping
EMP1661	GTTTGGATCGTCGGTGGAG	Specific primer for *hik2 038* and *149* cDNA

Table 1. Primers used for tDNA mutants' genotyping, CRISPR-Cas9 screening and specific cDNA synthesis

2.4 PCR clean up and sequencing of the mutants

PCR amplification was carried out using gDNA and strain-specific primers that targeted the expected band for each case, in a total reaction volume of 40 µL prepared according to the concentrations described in **section 2.3.** An aliquot of 5 µL was run on a 1% agarose gel to confirm the presence of the expected amplicon. The remaining reaction was purified using the NZYGelpure kit and eluted in 40 µL of elution buffer. The purified product was then cloned into the pNZY28 vector using the NZY-A PCR Cloning Kit, which enables direct cloning of PCR products with 3′-A overhangs. The cloning mixture was sent to Macrogen, Inc., where sequencing was performed using a universal primer (T7 promoter primer: 5′-TAATACGACTCACTATAGGG-3′). Sequencing analysis was conducted using the Sequence Alignment Tool (VectorBuilder) and Benchling.

2.5 Culture conditions to determine gene expression levels

All pre-cultures were grown in TAP medium under continuous low white light (50 µmol photons m^{-2} s^{-1}) for 4 days at 22 °C. Cultures were then diluted to a density of 2×10^6 cells mL^{-1} and transferred to a 12 h dark / 12 h light photoperiod at the same light intensity and temperature for an additional 3 days to ensure synchronization. After successive dilutions, cultures were adjusted to 1×10^6 cells mL^{-1} and transferred to HSM medium under continuous light. Minimal medium was used to promote autotrophic growth, relying exclusively on light as the energy source.

Samples were collected for RNA extraction and cDNA synthesis. qPCR results were normalized to the housekeeping gene *GBLP* and expression levels were compared to those of the WT–CLiP strain (see following sections for details). All experiments were performed with three biological replicates. For determination of *HIK1* and *HIK2* transcript levels in the mutant lines, samples were collected on day 3. For *LHCSR1* and *LHCSR3*, *PSBS1*, *CO* and *SPA1* expressions samples were collected on days 4 and 8.

For all cell density determination, cultures were counted manually as follows: 200 µL sample were transferred to a 1.5 mL tube, and 20 µL of 0.25% (v/v) iodine/ethanol solutions were added to immobilize the cells. A 10 µL volume of the immobilized cell suspension was loaded onto a hemocytometer, and after allowing 20 seconds for the cells to settle into a single focal plane, cell counting was performed using the Leica DMLM optical microscope (Leica Microsystems). Cells were counted either across all 25 quadrants of the hemocytometer grid or within the 5 diagonal quadrants, with the resulting number multiplied by 5 if only 5 quadrants were counted. Cell concentration, expressed in millions of cells per milliliter, was calculated by dividing the total count by 100. At least three counts per sample were performed to ensure accuracy.

2.6 RNA extraction

RNA extraction was carried out using the Maxwell® RSC Plant RNA Kit (Promega) and automated with the Maxwell® RSC Instrument. This system utilizes prefilled reagent cartridges and paramagnetic particles to facilitate nucleic acid purification through different cartridge wells.

For each extraction, 10–20 million cells were collected by centrifuging cultures at 4000 rpm for 5 minutes. The resulting pellet was resuspended in 400 µl of Homogenization Solution and directly frozen in liquid nitrogen for later processing. Prior to extraction, Maxwell® RSC Cartridges were loaded into the instrument tray. A 5 µl aliquot of DNase I solution (prepared by dissolving the lyophilized enzyme in 275 µl of nuclease-free water and adding 5 µl of Blue Dye) was added to well #4, while plungers were placed in well #8, and elution tubes containing 30 µl of nuclease-free water were positioned in the designated tray slots. Before loading, frozen samples were thawed on ice, mixed with 200 µl of lysis buffer by vortexing, and incubated for 10 minutes at room temperature. The lysate was then transferred to well #1 of the cartridges. After extraction, the eluted RNA samples were centrifuged to remove

any residual magnetic beads and stored at -20°C.

2.7 cDNA synthesis

For cDNA synthesis, the Thermo Scientific™ RevertAid™ First Strand cDNA Synthesis Kit was used. First, removal of genomic DNA from RNA was performed. For that, 1000 ng of RNA, 1 µl of 10X Reaction Buffer with MgCl2, 1 µl of DNase I RNase-free and Nuclease-free Water were added to a RNase-free tube in 10 µl total volume reaction. The mixture was then incubated at 37 °C for 30 min. 1 µL 50 mM EDTA was added and incubated at 65 °C for 10 min. The prepared RNA was then used as a template for reverse transcriptase.

1000ng of the template RNA, 1 µl of Oligo (dT) primer and Nuclease-free Water were added to a final 12 µL total volume. The optional step for GC-rich RNA templates was performed. For that, the mixture was incubated at 65 °C for 5 min, chilled on ice, spun down, and placed again on ice. Then, the following components in the indicated order were added to the previous 12 µL total volume mixture: 4 µL of 5X Reaction Buffer, 1 µL of RiboLock RNase Inhibitor (20U/ µL) 2 µL of 10 mM dNTP Mix and 1 µL of RevertAid M-MuLV RT (200 U/ µL) to a total volume of 20 µL. The 20 µL total volume mix was then mixed gently, centrifuged briefly and incubated for 60 min at 42 °C. The reaction was terminated by heating at 70 °C for 5 min. The reverse transcription reaction product can then be directly used in PCR applications or stored at -20 °C for less than one week. For longer storage, -70 °C is recommended.

2.8 qPCR

qPCR reactions were performed using the LightCycler® 480 RT-PCR System with PowerUp SYBR™ Green Master Mix as the fluorescence dye. The qPCR setup involved a previous cDNA dilution step. The cDNA (from 1000 ng of RNA) obtained using the Thermo Scientific™ RevertAid™ First Strand cDNA Synthesis Kit, was 1:2 diluted and 1 µl was used. Thus, each qPCR well contained 1 µl of the final cDNA dilution, 5 µl of the fluorescence dye, 0.6 µl of each primer (listed in Table 2), and 2.8 µl of water, reaching a total volume of 10 µl. All samples were run in three technical replicates.

Primer name	Sequence	Gene
EMP1262	CAGTTACGGTTTAGGCCGGT	*HIK1* 3' UTR
EMP1263	CAACGACCACATCCAATGCC	*HIK1* 3' UTR
EMP1266	AGAGAGGGAATGGCTGGGAG	*HIK2* 3' UTR

EMP1267	GCGAGGAAACACACTCGGTA	*HIK2* 3' UTR
EMP1270	CAAGTACACCATTGGCGAGC	*GBLP* (housekeeping gene)
EMP1271	CTTGCAGTTGGTCAGGTTCC	*GBLP* (housekeeping gene)
EMP1272	CACAACACCTTGATGCGAGATG	*LHCSR3*
EMP1273	CCGTGTCTTGTCAGTCCCTG	*LHCSR3*
EMP1276	GAGTCTGAGATCACCCACGG	*LHCSR1*
EMP1277	CCGATCTGCTGGAAGTGGTA	*LHCSR1*
EMP1278	TAAACCGTGTATTGGAACTCCG	*PSBS*
EMP1279	CTCTGCACGCGGCGTGTT	*PSBS*
EMP1465	TGTGGTCCATACAGCACGAG	*SPA1*
EMP1466	AGGAAGATGCGGTAGTTGGC	*SPA1*
EMP1459	CGCAGCATGTATTGGATGCC	*CO*
EMP1460	GACTCGTCACTCGACCAACT	CO

Table 2. Primers used for qPCR

The qPCR program consisted of two main phases: an amplification phase with 40 cycles of denaturation at high temperature followed by annealing and extension at 60°C (polymerase working temperature) and a melting curve analysis to determine product specificity. Once the reaction was completed, the software calculated Ct values, representing the cycle number at which fluorescence surpassed background levels, corresponding to transcript abundance.

Relative gene expression was determined using the ΔΔCt method, which is a widely used approach in qPCR for determining relative gene expression by normalizing to a reference gene and comparing to a control sample. First, Ct values are obtained, and the ΔCt is calculated by subtracting the reference gene Ct from the target gene Ct to account for RNA input differences. The housekeeping (reference) gene G protein subunit-like protein (GBLP) was chosen due to its stable mRNA levels across various conditions (Schloss 1990, Im et al. 1996). Then, the ΔΔCt is determined by subtracting the ΔCt of the control sample from the ΔCt of the experimental sample. Finally, the relative expression (Fold Change) is calculated using FC = 2^(-ΔΔCt), where values greater than 1 indicate upregulation and values less than 1 indicate downregulation.

2.9 Culture conditions for the white/blue light experiments for HIK1 and HIK2

CC-5325 (WT-CLiP), *hik1 442*, *hik2 038 149 408* and *506* mutant pre-cultures were grown in TAP medium under continuous low white light (50 µmol photons m^{-2} s^{-1}) for 3 days at 22 °C. Cultures were then diluted to a density of 2 × 10^6 cells/ml and transferred to 12/12 h dark–light cycles under the same light intensity and temperature for an additional 3 days to achieve proper synchronization. After successive dilutions, cultures were resuspended in HSM

medium (**Supplementary information: Table. 1**) at a density of 0.5 × 10^6 cells/ml and transferred to either continuous blue or white light conditions at 22 °C.

For *hik1* 442 mutant light was set at either 50 or 250µmol photons m^{-2} s^{-1}. The experiment consisted of fluorescence-based measurements over eight consecutive days. On the other hand, for *hik2 (038 149 498* and *506)* mutants, light intensity was set at 250µmol photons m^{-2} s^{-1}, and the experiment consisted of fluorescence-based measurements after 3 days of HL exposure.

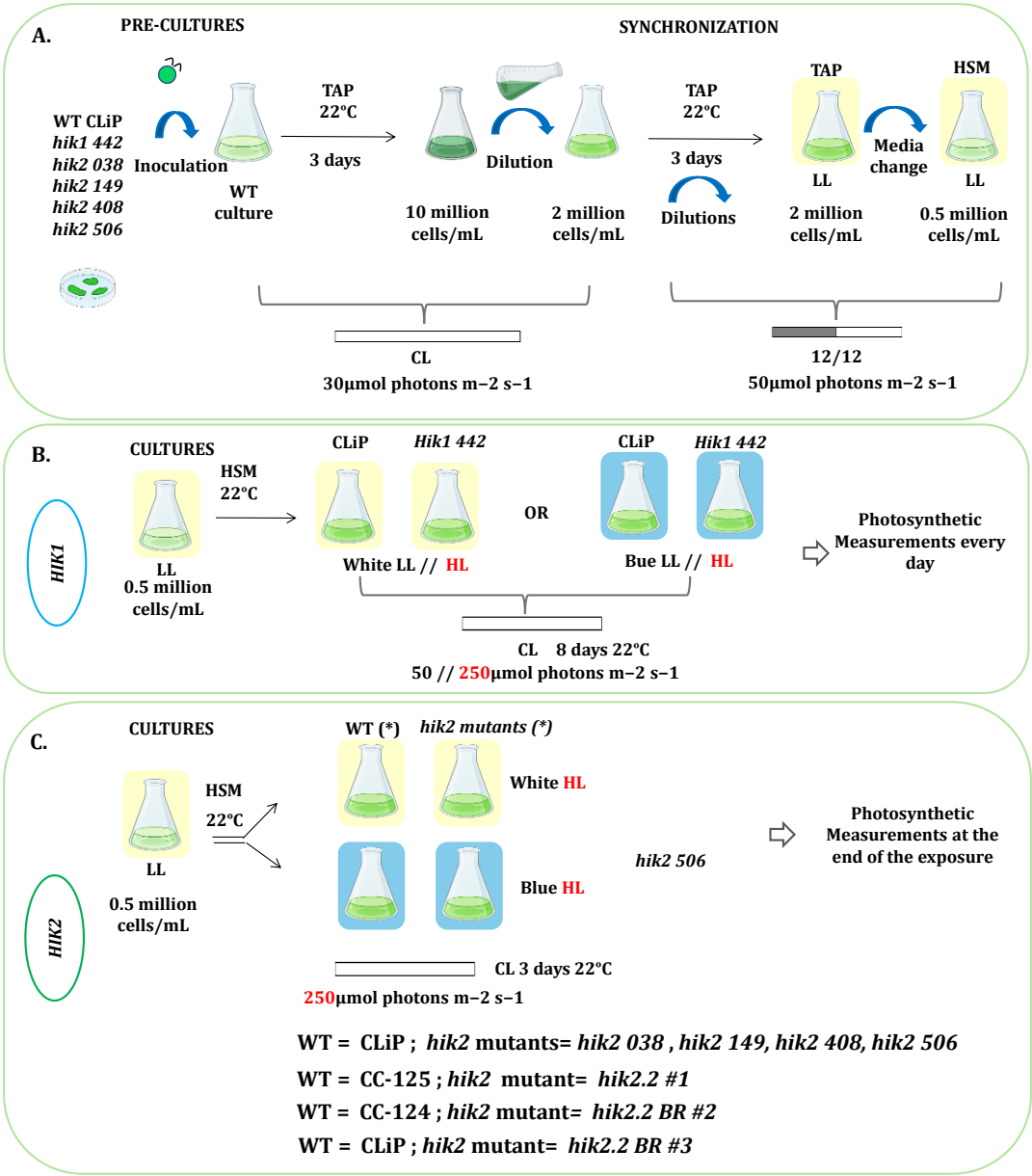

Fig. 3. Schematic representation of the experimental setup for *HIK1* and *HIK2* assays. (A) Pre-culture synchronization and final culture conditions, common to all experiments. (B) Specific setup for *HIK1* mutants. (C) Specific setup for *HIK2* mutants.

2.10 Fluorescence-based measurements

CC-5325 (WT-CLiP) and *hik1 442* mutant cultures were used for all fluorescence-based photosynthetic measurements, which were determined with a pulse-modulated amplitude fluorimeter (MAXI-IMAGING-PAM, HeinzWaltz GmbH, Germany). Prior to this, Chlamydomonas cells were kept in the dark to ensure that their photosynthetic apparatus was in a relaxed state, which is crucial for accurate and reproducible measurements. This dark adaptation allows the cells to recover from any previous exposure to light, ensuring the photosystems are in their basal energy state. Cultures were kept in the dark for 20 minutes before measurements. Triplicates of 200µL were spotted to a squared cut micro-glass fiber filter paper put on a black plastic holder in complete dark conditions. Samples were covered with aluminum foil to ensure complete darkness before taking them to the PAM fluorometer for measurements. The samples' setup was adjusted to the PAM image and chlorophyll fluorescence measurements were taken.

Chlorophyll fluorescence was recorded during 5.5min under 460 µmol photons m^{-2} s^{-1} of actinic white light followed by finishing with 5.5min of measurements of fluorescence relaxation in the dark. Measurements were taken every 30 and 60 interval seconds. A saturating pulse of white light was applied for determination of Fm (the maximal fluorescence yield in dark-adapted state) or Fm' (maximal fluorescence in any light-adapted state). NPQ was calculated as (Fm—Fm′)/Fm′. PSII efficiency (Fv/Fm) was calculated as (Fv/Fm = (Fm-Fo/ Fm) where Fo and Fm are minimal and maximal chlorophyll fluorescence in dark-adapted algal cells. The difference between Fm and Fo gives the variable fluorescence (Fv), and Fv/Fm is defined as the quotient between Fv and Fm.

2.11 CRISPR/Cas9-mediated gene editing

CRISPR/Cas9-mediated knockout lines were generated to disrupt the *HIK2* gene in *Chlamydomonas reinhardtii*. A Cas9 ribonucleoprotein (RNP) complex targeting the third exon of *HIK2* was assembled using a synthetic guide RNA with the sequence TTTTAACTGGTCCGCCTACG (called gRNA 2.2), adjacent to the PAM site CGG. The RNP complex was delivered by electroporation using the NEPA21 electroporator, together with the plasmid pSL18, which carries the *aphVIII* gene conferring paromomycin resistance, which enables selection of transformed cells. Genome editing outcomes were assessed through a PCR-based screening assay designed to detect mutations at the target site. The primers used for screening are shown in Table 1.

A detailed protocol, including RNP preparation, electroporation conditions, and the screening assay, is provided in Chapter 4: "A quick and optimized CRISPR-Cas9 protocol to obtain insertional and small indel mutants in *Chlamydomonas reinhardtii"*.

2.12 **Statistical analysis**

Statistical analyses were performed using nd GraphPad Prism (version 9) to compare differences between each mutant and their corresponding WTs. Unpaired two-tailed t-tests assuming equal variances were used. Results are shown as mean ± SD, and differences were considered significant at $p < 0.05$. Significance is indicated in figures as: $p < 0.05$ (**), $p < 0.01$ (**), $p < 0.001$ (***), $p < 0.0001$ (****); ns= not significant.

3. RESULTS

3.1 LOV sensing domains in HIK1 and HIK2

Through a bioinformatic search in the *Chlamydomonas reinhardtii* genome database, two histidine kinases were identified, HIK1 (*Cre02.g079750*) and HIK2 (*Cre13.g571200*), both of which possess the domains required for a two-component system (TCS) as shown in Fig. 2.

Analysis of conserved domains revealed that the N-terminal sensor PAS domain of these proteins belongs to the LOV type. Using the LOV domain from *C. reinhardtii* phototropin (CrPhot) as a reference, we characterized them. While CrPhot contains two N-terminal LOV domains (LOV1 and LOV2) and a C-terminal serine/threonine kinase domain, HIK1 and HIK2 each possess a single N-terminal LOV domain, followed by a histidine kinase (HisKA) + HATPase domain and a C-terminal response regulator (REC) domain (Fig. 4A).

Sequence alignment was also performed and results revealed that HIK1 and HIK2 present the GXNCRFLQ motif needed to sense blue light, which is also present in Chlamydomonas Phot (*CrPhot: Cre03.g199000*). (Fig 4B).

A.

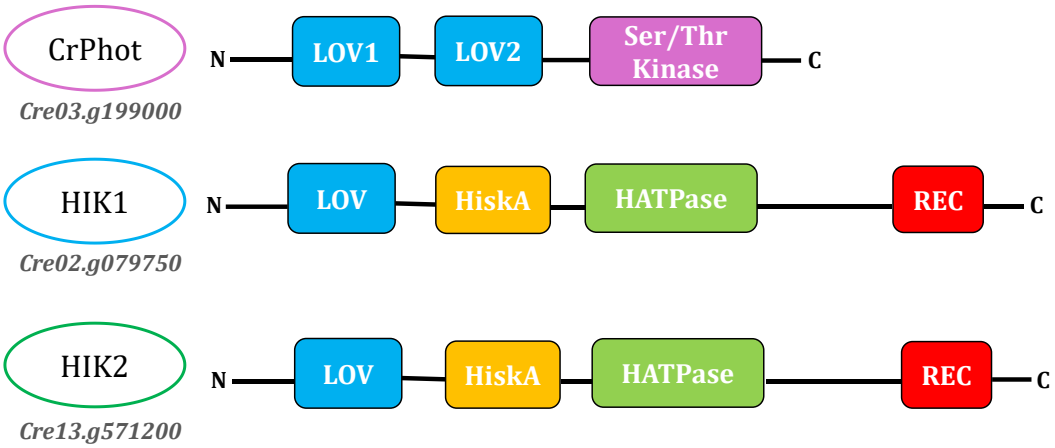

B.

```
CrPhot    IQQNFCISDPTLPDCPIVFASDAFLELTGYSREEVLGRNCRFLQGAGTDRGTVDQIRAAI
HIK1      LQEGITIADCSLPDMPLIYANAGFVRTTGYSAAYVLGKNCRFLQGEGTDSQPVLDLKKAI
HIK2      VREGITISDPSLPDNPIVYTNQAFLAMTGYSREEVLGRNCRFLQGPDTDPGSVAAIREAL
                                             *  ******
```

Fig 4. A. Identification of different types of LOV domain containing proteins in *Chlamydomonas reinhardtii*: LOV serine/threonine kinase (CrPhot) and LOV histidine kinases (HIK1 and HIK2). **B.** Protein sequence alignment showing the conserved motif GXNCRFLQ in HIK1 and HIK2 as in CrPhot, needed for blue light sensing.

3.2 HIK1

3.2.1 Molecular characterization of *HIK1* CLiP mutant line

a) CLiP *HIK1* mutant ordering and genotyping

Next, to study the function of these two putative novel photoreceptors, HIK1 and HIK2, different mutant lines, together with CC-4533 (here referred as WT-CLiP) which is the background strain used to generate this mutant collection. This chapter, however, is going to be focused on HIK1.

As previously mentioned, this CLiP library comprises Chlamydomonas mutants generated by random insertion of T-DNA cassettes (*CIB1* cassette) through electroporation, leading to gene disruptions. To determine insertion sites and categorize mutant lines, researchers use a mapping system called ChlamySeq, which amplifies and sequences the regions flanking the

T-DNA cassette ends, yielding about 20 base pairs of adjacent genomic sequences. This sequence data allows researchers to precisely identify the insertion sites, helping them catalog mutants based on which specific genes have been disrupted. Furthermore, the specific orientation (sense or antisense) of this CIB cassette can also be identified (Fig. 5).

By checking in the CLiP library, we found one mutant line for *HIK1* (Cre02.g079750). However, due to the percentage of confidence (less than 80%), we decided to only order the line that was next named *hik1 442* (95% of percentage of confidence). This insertion is supposed to be localized in the CDS (coding sequence), specifically in the 15th exon of *HIK1*, at the end of the CDS (Fig 6A).

To verify that this insertion was indeed located in the gene of interest and in a specific orientation, two PCR strategies were followed: WT-Band PCR and tDNA-Band PCR.

For the WT-Band PCR, a primer pair was designed to target the flanking regions on the 5' and 3' sides of a specific insertion site within the gDNA (genomic DNA), referred to as flanking primers (FP) (Fig. 5). In a wild-type (WT) scenario, meaning no insertion, this would produce a band of the expected size. In mutants with a tDNA insertion, however, the insertion distance would be too large for amplification to occur.

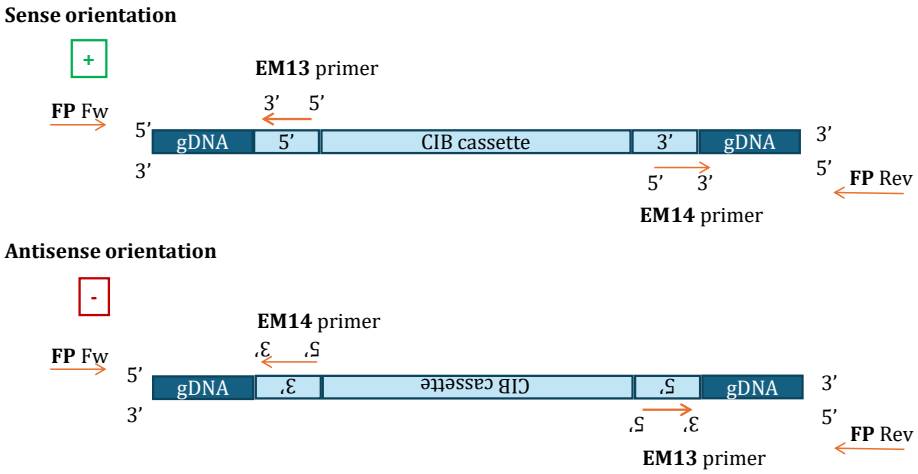

Fig. 5
tDNA cassette (CIB) and orientation within the gDNA. Schematic representation of a gDNA with the insertion of the tDNA cassette (CIB) from the CLiP mutant library with the corresponding primers for the genotyping: the primers localized in the gDNA, which are flanking the tDNA insertion (FP Fw and FP Rev), as well as the primers within the tDNA (CIB) cassette facing outwards towardsthe genome (EM13 and EM14). Also represented the sense (+) and antisense (-) orientation of the tDNA (CIB) cassete in respect to the gDNA.

For the T-DNA-Band PCR, one primer binds to one end of the tDNA cassette (EM13 at the 5' end or EM14 at the 3' end, as shown in Table 1), and the other primer is localized in the

genomic region adjacent to the insertion (Fig. 5). Amplification occurs only if the T-DNA end is inserted in the specific orientation at that insertion site.

To perform all these PCRs, primers were specifically designed to genotype the predicted *HIK1* mutant line (*hik1 442*). These primers are described in Table 1. Primers EMP 1624 and EMP 1625 were used for the WT-band PCR, localized within the *HIK1* gDNA (Fig. 6B).

To detect the T-DNA band, given the possibility of sense or antisense orientation, four primer combinations were tested: EMP1624+EM13 and EMP1625+EM14 for the sense orientation and EMP1624+EM14 and EMP1625+EM13 for the antisense shown in (Fig. 6B).

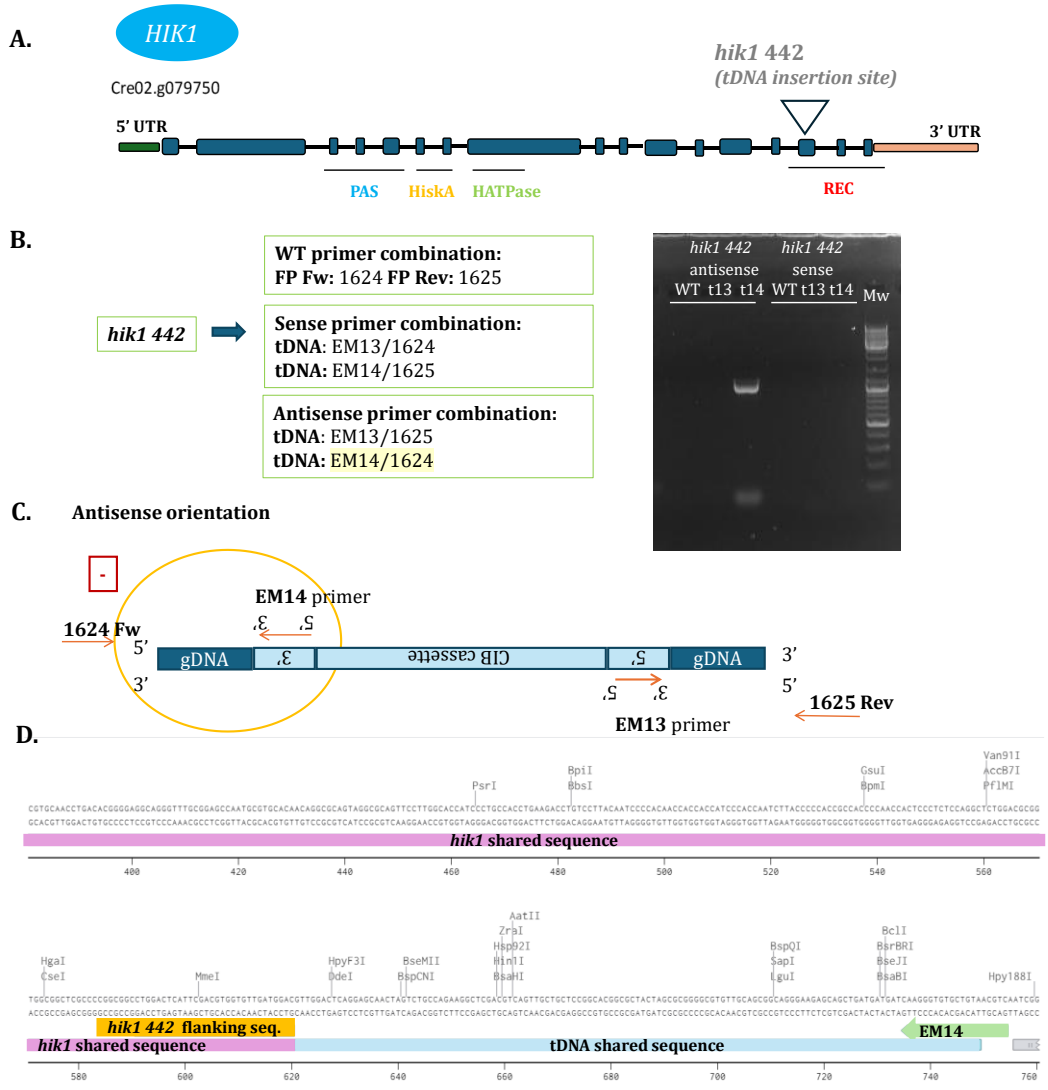

Fig 6. Genotyping and sequencing of *hik1 442 mutant*. A. Schematic representation of the *HIK1* gDNA with the tDNA (CIB) insertion of *hik1 442* mutant B. Primer combination for genotyping and PCR showing the EM14+EMP1624 combination amplification. C. Primer combination and orientation of the CIB cassette in the *hik1 442* mutant line. D. Sequencing of the *hik1 442* mutant line showing that the exact position of the insertion, positioned in the indicated locus, within the 15th exon.

The WT-band PCR showed no amplification for *hik1 442*, as expected. For the T-DNA band PCR, primer combinations for sense orientation showed no amplification. However, in the antisense orientation only EMP1624+EM14 yielded amplification but not EMP1625+EM13. These results confirm that *hik1 442* has a partial insertion in the antisense orientation, as shown in Fig. 6B.

Following the genotyping and to investigate the exact position of the cassette insertion, the genomic region from the mutant was amplified from the gDNA using the 1624 primer (localized at the end of exon 13th) until M14 position, which is localized at the 3' of the cassette. It was then purified and cloned in a pnzy28 vector for sequencing, using T7 promoter universal primer. The sequencing results showcased that the exact position of the insertion was positioned in the indicated locus, within the 15th exon right after 9687bp, where the flanking region of the tDNA cassette is supposed to be localized. Antisense orientation was also confirmed (Fig. 6C).

b) Molecular characterization: *hik1 442* transcript levels

Next, *HIK1* transcript levels were measured in the WT (WT-CliP) and *hik1 442* mutant line by qPCR to assess the effect of the T-DNA insertion. A primer pair targeting the 3′ UTR was designed to evaluate whether a full-length transcript is produced in the mutant line (Table 2). This region was chosen because it allows us to infer transcript integrity downstream of the insertion site.

Cultures were performed as described in Methods. On day 3, samples were collected, RNA was extracted from the cells and cDNA was synthesized. The qPCR results were normalized using *GBLB* as the housekeeping gene, and expression levels were compared to those of the WT-CliP.

The 3′ UTR primers revealed reduced *HIK1* transcript levels in the *hik1 442 line*, suggesting that no full-length transcript is produced, although partial transcription cannot be ruled out. (Fig. 7).

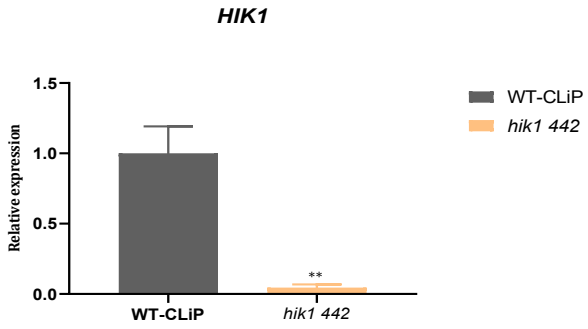

Fig 7. *HIK1* expression levels in *hik1 442* mutant. Expression levels of *HIK1* in WT-CLiP and *hik1 442* using 3' end primer combination. The data represent means ± SD from three independent biological replicates (n = 3). Statistical significance was determined using Student's t-test: $P < 0.05$ compared to the control WT-CLiP. The expression of *HIK1* gene was normalized with the expression of *GBLP*.

3.2.2 Higher NPQ induction in blue LL in *hik1 442 mutant*

Since HIK2 contains a LOV domain, and they are known to be involved in blue-light sensing, we conducted an experiment under both blue and white HL conditions to compare the responses.

WT-CliP and *hik1 442* cultures were as described in **Methods Section 2.9** and transferred to continuous blue or white light LL 50µmol photons m^{-2} s^{-1}) and HL (250µmol photons m^{-2} s^{-1}) at 22ºC to begin the experiment, which consisted in photosynthetic measurements (Fv/Fm and NPQ) over eight consecutive days (Fig. 3, in Methods).

We first characterized the photosynthetic performance of *hik1 442* mutant and WT-CLiP. The intrinsic quantum yield of photosystem II (Fv/Fm) was similar to those of the WT-CLiP under white LL across all days of measurements.

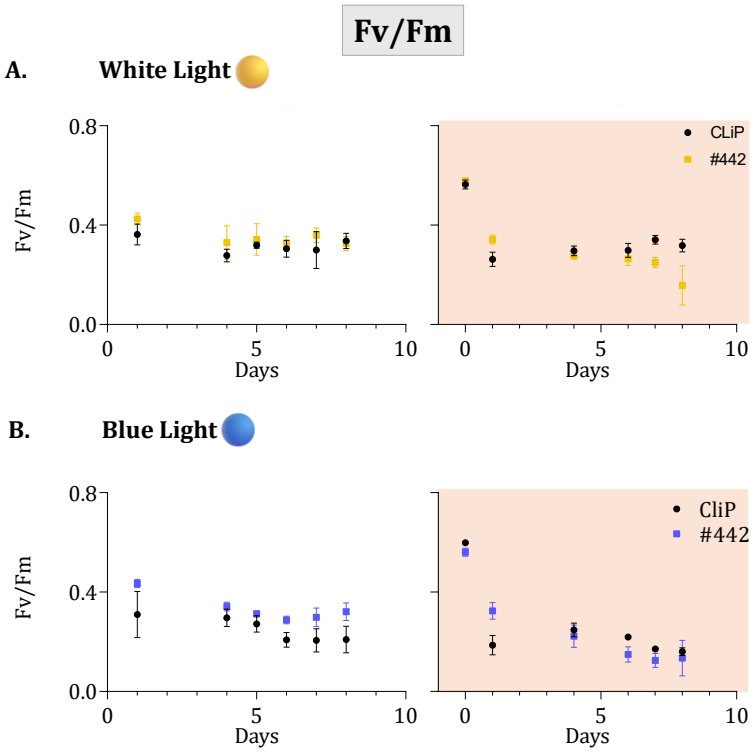

Fig 8. Photosynthetic efficiency (Fv/Fm) in *Chlamydomonas reinhardtii* WT-CLiP and *hik1 442* mutant under white and blue LL and HL intensities over 8 days. WT-CLiP (dark line), *hik1 442* (blue line). The data represent means ± SEM from three independent biological replicates (n = 3). Upper panel White Light (Right LL, Left HL) Lower panel Blue Light (Right LL, Left HL). Low light (50µmol photons m^{-2} s^{-1}). High Light (250µmol photons m^{-2} s^{-1}).

However, under blue LL, Fv/Fm values were slightly higher in the mutant compared to the WT during Days 6, 7 and 8. Conversely, under HL, Fv/Fm values in *hik1 442* were slightly higher or similar compared to those of the WT-CLiP under white and blue high light during the first days of measurements. However, these values decrease below those of the WT during the final days of exposure (Day 6-7-8) (Fig. 8). However, any of the changes observed under LL or HL showed any statistical significance.

As outlined in the Introduction (see section 1.5, 'Photoprotection in Chlamydomonas'), *C. reinhardtii*'s qE capacity, along with the induction of *LHCSR1*, *LHCSR3*, and *PSBS* transcription, is activated by high light, whereas low light results in minimal qE and weak NPQ induction (Fig. 9).

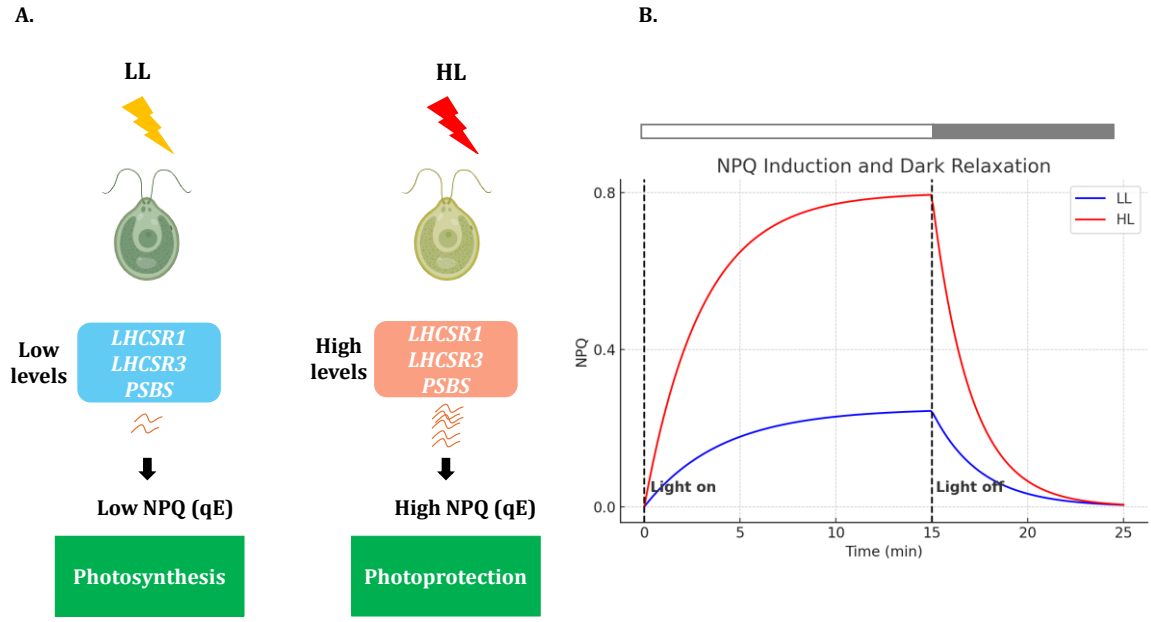

Fig 9. Schematic representation showing Photoprotection in *Chlamydomonas reinhardtii.* A. LL triggers low *LHCSR* an *PSBS* expression, together with low qE capacity, whereas HL triggers *LHCSR* an *PSBS* induction and strong qE. B. Expected NPQ kinetics in LL (blue line) and HL (red line).

We therefore compared NPQ kinetics under white and blue light at both LL and HL, revealing several key differences.

Under white LL conditions, NPQ induction was comparable between WT–CLiP and *hik1 442* across most measurement days. From days 4 to 8, however, *hik1 442* exhibited slightly higher NPQ values during the initial minutes of the measurements, with the difference reaching statistical significance on day 7. Furthermore, in both WT and mutant line, NPQ levels relaxed rapidly upon transition to darkness (Fig. 10).

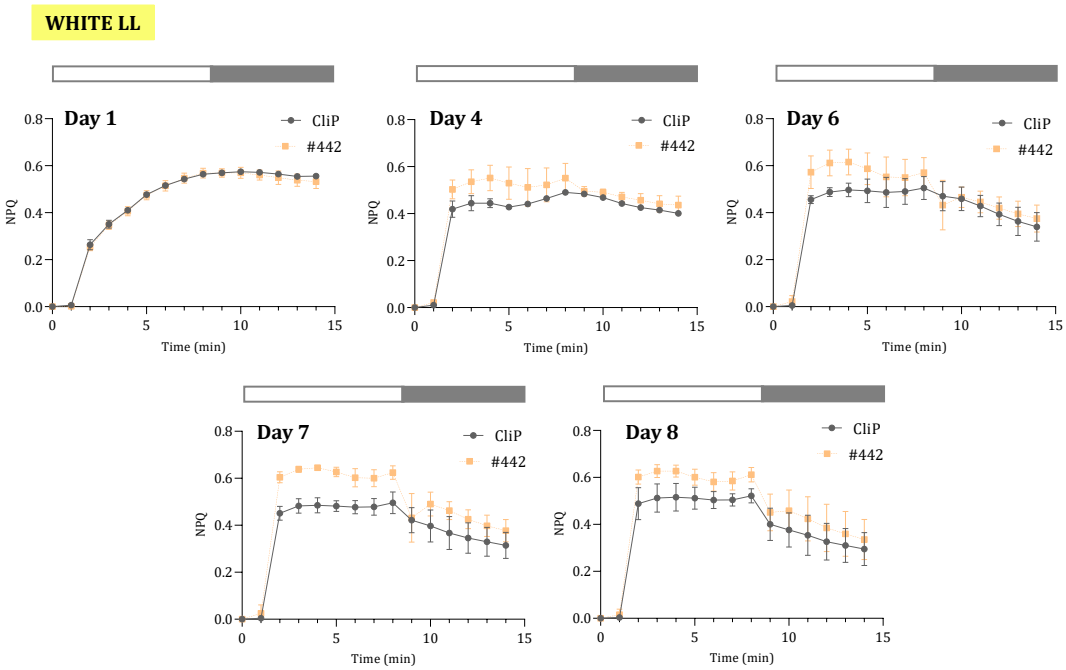

Fig 10. NPQ kinetics of Chlamydomonas WT-CLiP and *hik1 442* during white LL treatment. Bars on top, white bar (light on) and black bar (dark). WT-CLiP (dark line), *hik1 442* (yellow line). The data represent mean ± SEM from three independent biological replicates (n = 3). LL= Low light (50µmol photons m^{-2} s^{-1}).

Conversely, under blue LL, *hik1 442* mutant showed a rapid increase in the level of NPQ from the dark-adapted state. Second, *hik1 442* mutant showed a higher NPQ value than that of the WT cells, however, this higher NPQ induction appeared in prolonged blue LL exposure, (starting on Day 5) which was especially evident at day 8, suggesting that the mutation leads to a constitutively enhanced NPQ response under prolonged non stress conditions (LL). Third, the high NPQ levels observed in the mutant relaxed quickly upon a dark transition, which differed from the almost null dark-relaxation observed in WT-CLiP (Fig. 11).

Under high light, NPQ dynamics were similar between WT and *hik1 442* across all days, with the only noticeable difference being a transient increase in NPQ in *hik1 442* on Day 1 under blue HL (Fig. 13). From Day 4 onwards, both strains showed comparable NPQ induction and relaxation patterns under both white and blue HL (Figs. 12 and 13)."

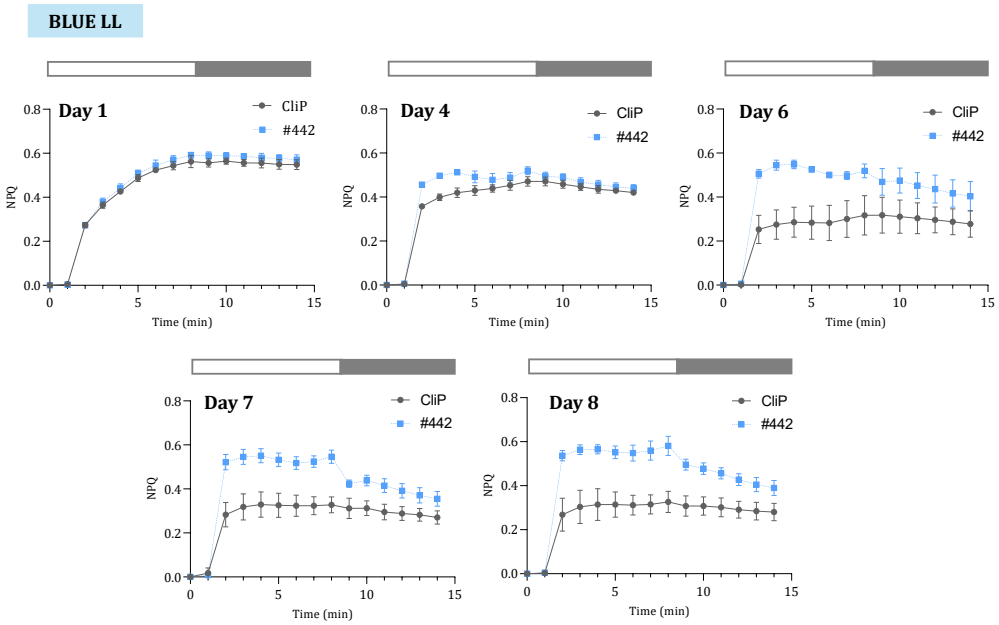

Fig 11. NPQ kinetics of Chlamydomonas WT-CLiP and *hik1 442* during blue LL treatment. Bars on top, white bar (light on) and black bar (dark). WT-CLiP (dark line), *hik1 442* (blue line). The data represent mean ± SEM from three independent biological replicates (n = 3). LL= Low light (50µmol photons m^{-2} s^{-1}).

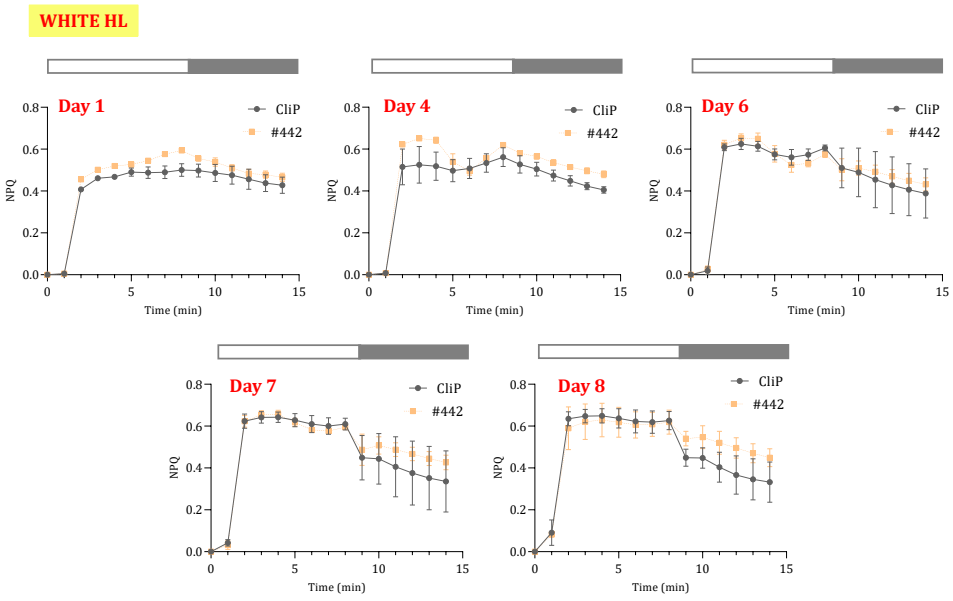

Fig 12. NPQ kinetics of Chlamydomonas WT-CLiP and *hik1 442* during white HL treatment. Bars on top, white bar (light on) and black bar (dark). WT-CLiP (dark line), *hik1 442* (yellow line). The data represent mean ± SEM from three independent biological replicates (n = 3). HL= High Light (250µmol photons m^{-2} s^{-1}).

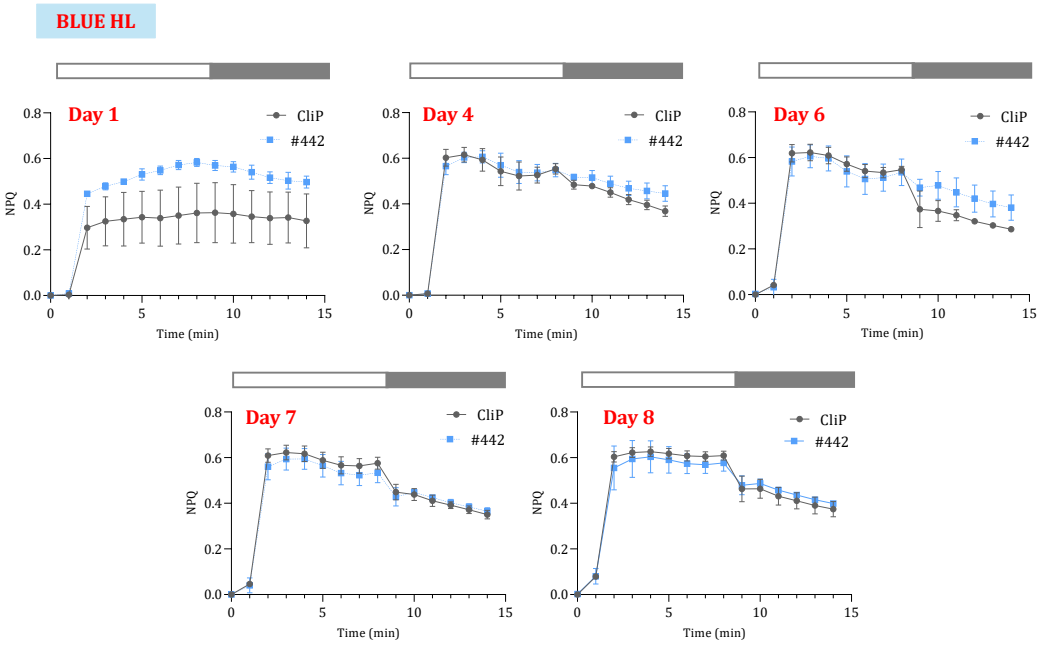

Fig 13. NPQ kinetics of Chlamydomonas WT-CLiP and *hik1 442* during blue HL treatment. Bars on top, white bar (light on) and black bar (dark). WT-CLiP (dark line), *hik1 442* (blue line). The data represent mean ± SEM from three independent biological replicates (n = 3). HL= High Light (250µmol photons m^{-2} s^{-1}).

3.2.2 Preliminary results show higher *LHCSR*, *PSBS* expression while lower *SPA1* levels in *hik1 442* mutant

Thus, due to the higher NPQ induction observed in *hik1 442* mutant under blue LL, we next examined qE effectors expression, *LHCSR1*, *LHCSR3* and *PSBS* under these specific conditions, as they are key components of the NPQ induction mechanism.

Cultures were performed as described in Methods. Then, on day 4 and 8, samples were collected, RNA was extracted, and cDNA was synthesized. The qPCR results were normalized using *GBLB* as the housekeeping gene, and expression levels were compared to those of the WT-CliP.

Preliminary results (n=1) showed higher expression of *LHCSR1,3* genes in *hik1 442* mutant compared to WT-CLiP on Day 4, while similar levels of these genes are observed on Day 8 between them. On the other hand, *PSBS* levels remained similar to those of the WT-CLiP on Day 4 but were highly increased on Day 8 (Fig. 14).

Because the qE effectors were elevated in *hik1 442*, we assessed whether upstream regulators in this pathway were affected. In *Chlamydomonas*, SPA1 functions in photoprotection through

the COP1–SPA complex, which modulates the activity of the transcription factor CrCO. CrCO in turn induces *LHCSR* and *PSBS* expressions in response to high, UV, and blue light (Aihara et al., 2019; Gabilly et al., 2019). HIK1 contains a CheY-like phosphotransfer domain, a hallmark of two-component signaling systems in which a sensor histidine kinase phosphorylates a response regulator, and the N-terminus of SPA1 includes a CheY-like response regulator domain, suggesting potential functional interaction between the two proteins. We therefore measured *SPA1* and *CO* transcript levels in *hik1 442* and WT to assess whether HIK1 disruption affects the expression of these genes.

Interestingly, *SPA1* transcripts were reduced to about half of WT-CLiP values, whereas *CrCO* levels were unchanged (Fig. 14).

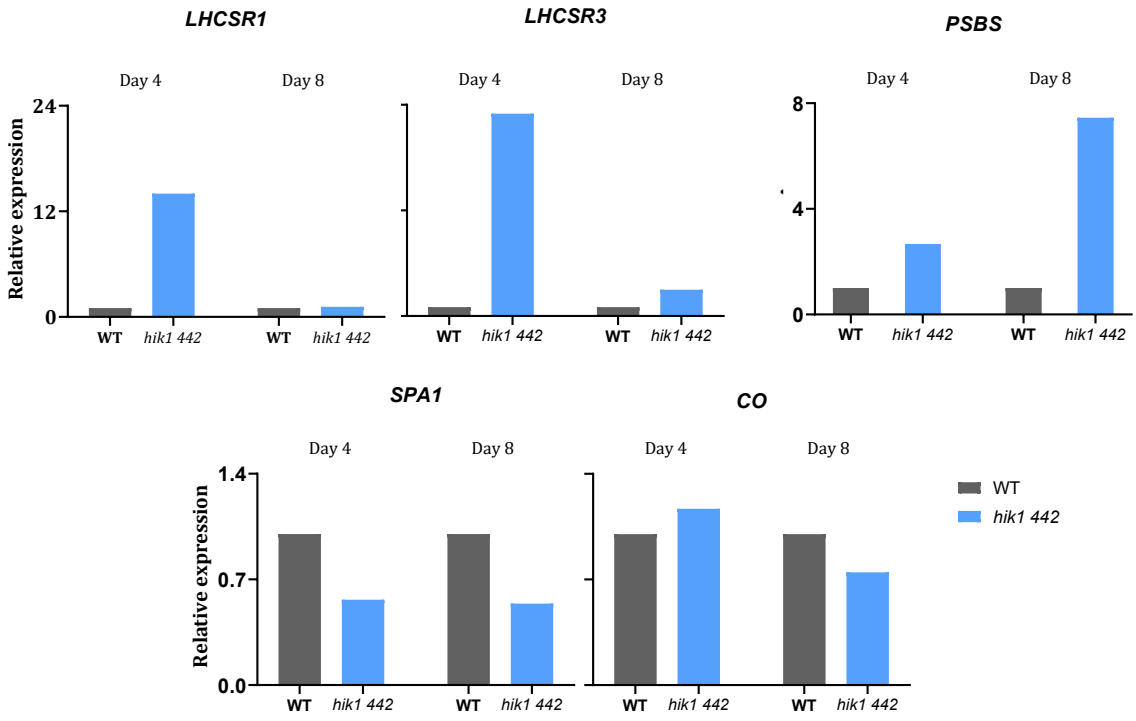

Fig 14. Relative gene expression of *LHCSR1*, *LHCSR3*, *PSBS*, *SPA1*, and *CO* in *Chlamydomonas reinhardtii* WT-CLiP and *hik1 442* mutant under LL blue light at day 4 and day 8. Relative expression of *LHCSR1*, *LHCRSR3*, *PSBS*, *SPA1* and *CO* in WT-CLiP and *hik1 442* at day 4 and 8 under blue LL (50µmol photons/m²/s). Preliminary result. Bars represented is the mean of three technical replicates from a single biological replicate (n=1). No statistical analysis was performed.

3.3. HIK2

3.3.1 Molecular characterization of *HIK2* CLiP mutant lines

a) CLiP *HIK2* mutant ordering and genotyping

By consulting the CLiP library, we identified four mutant lines for *HIK2* (*Cre13.g571200*). The insertions in *hik2 038* and *hik2 149* are predicted to be located within intron 4, overlapping the PAS domain. In contrast, the insertion in *hik2 408* is predicted to lie within intron 9, and in *hik2 506* within exon 9. Both are positioned downstream of the PAS, HisKA, and HATPase domains, and just upstream of the REC domain (Table 3, Fig. 15A).

Gene ID	Gene name	Mutant strain	Mutant name	Orientation	Insertion junction feature
Cre13.g571200	*HIK2*	LMJ.RY0402.108038	*hik2 038*	Antisense	Intron
Cre13.g571200	*HIK2*	LMJ.RY0402.119149	*hik2 149*	Sense/antisense	Intron
Cre13.g571200	*HIK2*	LMJ.RY0402.144408	*hik2 408*	Sense	Intron
Cre13.g571200	*HIK2*	LMJ.RY0402.245506	*hik2 506*	Sense	CDS

Table 3. CLiP insertional mutants of *HIK2* analyzed in this study. Table summarizing the gene ID, mutant strain identifier, mutant name, insertion orientation, and insertion junction feature for four *HIK2* mutant lines obtained from the CLiP library. All insertions are located within intronic or coding regions of *HIK2* (*Cre13.g571200*), with orientations and junction positions varying between lines.

To verify that these insertions were indeed located in the gene of interest and in a specific orientation, two PCR strategies were followed: WT-Band PCR and tDNA-Band PCR, as described previously in HIK1 section.

For the *HIK2* mutant lines (*hik2 038* and *hik2 149*), which have nearly identical insertion sites within an intron, the same primer pair (EMP 1626 and EMP 1627) was used for the WT-band PCR. As expected, no amplification was observed (Fig. 15C).

For the *hik2 038* T-DNA band PCR, with the insertion in antisense orientation, primer combinations EMP1626+EM14 and EMP1627+EM13 were used (Fig. 15C). A complete insertion was confirmed, as these antisense-oriented primers yielded amplification at both ends (Fig. 15C).

In contrast, for the *hik2 149* T-DNA band PCR, where both sense and antisense insertion orientations were possible, an unusual band pattern was shown. Four primer combinations

were tested: EMP1626+EM13 and EMP1627+EM14 for the sense orientation, and EMP1626+EM14 and EMP1627+EM13 for the antisense orientation. Of these, only EMP1626+EM14 and EMP1627+EM14 showed amplification indicating that, while a complete insertion is absent, at least one band is present in each orientation (Fig. 15C). This confirmed *hik2 149* as a mutant as well, however, further characterization was needed.

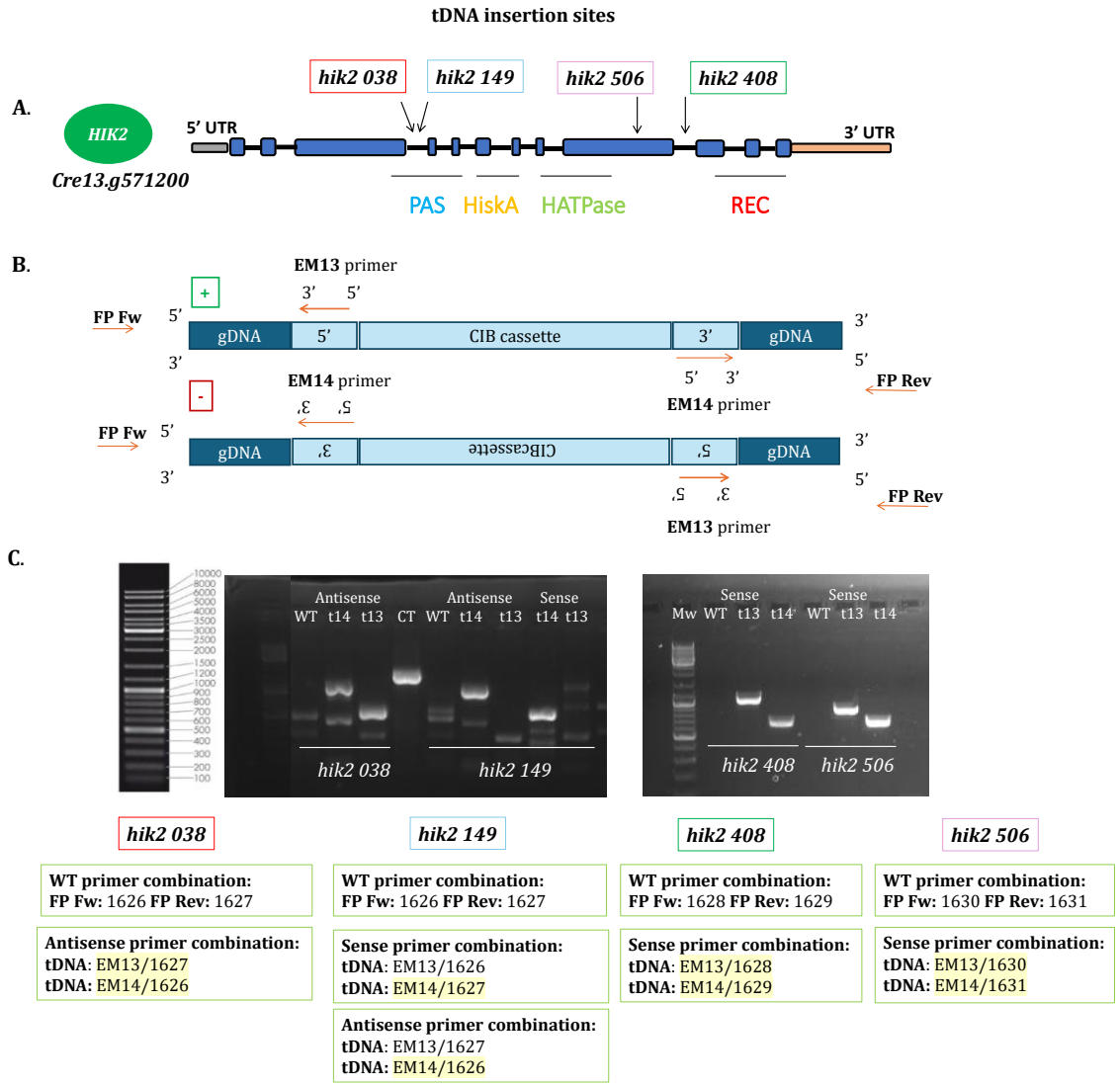

Fig 15. Genotyping and *HIK2* tDNA mutants. **A.** Schematic representation of the *HIK2* gDNA with the tDNA (CIB) insertions of *hik2 038*, *hik2 149*, *hik2 408* and *hik2 506* mutants. **B.** Options for the primer combinations for the sense and antisense orientation of the CIB cassette **C.** Primer combination used for the PCR (highlighted in yellow) and PCR gel showing the corresponding amplifications.

Following the genotyping and to investigate the exact position of the cassette insertions, the genomic region from the *hik2 038* and *hik2 149* mutants were amplified using the EMP1626

primer (localized at the end of the 3rd exon) until M14 position, which is localized at the 3' of the cassette. They were then purified and cloned in a pnzy28 vector for sequencing, using T7 promoter universal primer. The sequencing results showcased that the exact position of both *hik2 038* and *hik149* insertions were exactly positioned in the indicated locus, within the 4th intron right after 5221bp for *hik2 149* and 5245bp for *hik2 038*, where the flanking regions of the tDNA's cassette are supposed to be localized (Fig. 16). The distance between both insertions is 24bp. Antisense orientation was also confirmed in both mutants.

CCGGGCGCAAATTCAATAACGGCCGCACAAGCAGAGCGGGCGCTGGCGGCGGCACTTCACTCCATGGTCCCGCAGGCCGCCGCCGC
GGCCGCGGCCGCCGCCGCCGCTGCGGGAGCGCCGGCCCTGGTCGGCCCAACAACGGTGACGTCAGCTGCCGCCGCAGCCGCCGCCGC
GGCCGCCGCCTGCGGCTTTGGCGGCGGCCCTGCGGGCCTGCGTGACTTTGCGCTGGACTGTGTTCGTGAAGGCATCACGATCTCGG
ACCCCTCGCTGCCCGACAACCCCATTGTGTACACCAACCAGGCCTTCCTGGCCATGACCGGCTACAGCCGCGAGGAGGTGCTGGGC
CGCAACTGCCGCTTCCTGCAGGTGCGGTTGGGCGGCGGCGTGTATATATGTGTGTGGGGGGGGGGGGGTTGCATTCATGATTAGT
TAAGGGGGGGCGCTGGCATAGGGGGAGCGTGGTTCGGGGCAGTGGCGGTGGCGCAGTGGCGGTGGGTTGGGGTACCGCAGTTGTG
TGGGTCGGGGGGGACGGGCACGCGTGTCTAGGGTGGTGAGGTGAGCTGGCAGTGCGGTTGCGGTTAGGCAGCAGTCACGAGAGGG
GCGAGGCCGGGGCAGGCAAGGAGGCGGGCACGACGTGAGCGAGGGCTACAGCGCGGGTAGGGAGGGGCTCCAGGGCCAGGGTTAT
ACCTATCGACTCTCAAACGCCTGCCTTGCATCGCCCCTCGTCCTTGCTGCTGCCCCGCCGCAGGGTCCCGACACTGACCCGGGCTCG
GTGGCCGCCATACGTGAGGCGCTGTCGCAGCGCCGCGGCGCCACCGTGCGCCTAGTCAACTACACCAAACAGGTGGGCAGCGCGGG
CTGAGGACGGGGTCAACGATGTCACACCAGCGCGCATGCTTACACGAATGCATACACTCGCACAGTGCACGGGGAGCTGTCTTTGG
CCTTGCCCTTGAGGCTGCTCGACATTGCTGTGACACGTGTTAAAGAGCACAAGGAA(*hik2149_tDNA*)AACGTTGCGCAAAGACA
CGTGTGT(*hik2038_tDNA*)ACACATGTTCGTCCTTTTCTGCTTGTCTTCACGCGCACCCACCCACCTACTTGAACGCGATTGCAGG
GCTGCCGCTTTGTGAACGAACTGCGGCTGGCGCCAGTGCGGGAGCCGGGCAGCGGGCGTGTGATCGCCATCGTGGGCGTACAGAAT
GACGTCACAGAGCTG

Fig 16. Schematic representation of the sequencing results indicating the localization of *hik2 038 and hik2 149* tDNA insertions. *HIK2* gDNA fraction with the exons (blue highlighted) and introns (white, not highlighted) where the tDNA mutants are localized (4th intron): blue color for *hik2 149* and red color for *hik2 038.* Highlighted in green the EMP1626 primer used to amplify the fragments.

For the *hik2 408* mutant line, localized in an intron, primers EMP 1628 and EMP 1629 were used for the WT-band PCR. The WT-band PCR showed no amplification (Fig. 15C).

To detect the T-DNA band, given the sense orientation, primer combinations EMP1628+EM13 and EMP1629+EM14 were tested, as shown in Figure 15C. These primer combinations yielded amplification at both ends, indicating a complete insertion.

Finally, for *hik2 506* mutant line, localized in an exon, primers EMP 1630 and EMP 1631 were used for the WT-band PCR. As expected, no amplification was observed.

To detect the T-DNA band in the sense orientation, primer combinations EMP1630+EM13 and EMP1631+EM14 were tested, as shown in Figure 15C. These primer combinations yielded amplification at both ends, indicating a complete insertion.

In conclusion, all *HIK2* mutant lines showed a tDNA insertion which was complete for *hik2 038*, *hik2 408* and *hik2 506* and partial (or strange pattern) for *hik2 149.* Unluckily, the sequencing

of *hik 408* and *hik2 506* never succeeded, so we couldn't define the exact position of the tDNA cassette.

b) Molecular characterization: transcript levels of the four distinct *hik2* mutant lines (*038*, *149*, *408*, and *506*).

Next, *HIK2* transcript levels were measured in the WT (WT-CliP) and *hik2* mutant lines by qPCR to assess the effect of the T-DNA insertion.

Cultures were again performed as described in Methods. On day 3, samples were collected, RNA was extracted from the cells and cDNA was synthesized. The qPCR results were normalized using *GBLB* as the housekeeping gene, and expression levels were compared to those of the WT-CliP.

The 3′ UTR primers revealed *hik2 149*, *hik2 408* and *hik2 506* showed *HIK2* disrupted expression, indicating, at least, that no full transcript was originated. However, *hik2 038* showed similar *HIK2* mRNA levels to that of the WT (Fig. 17).

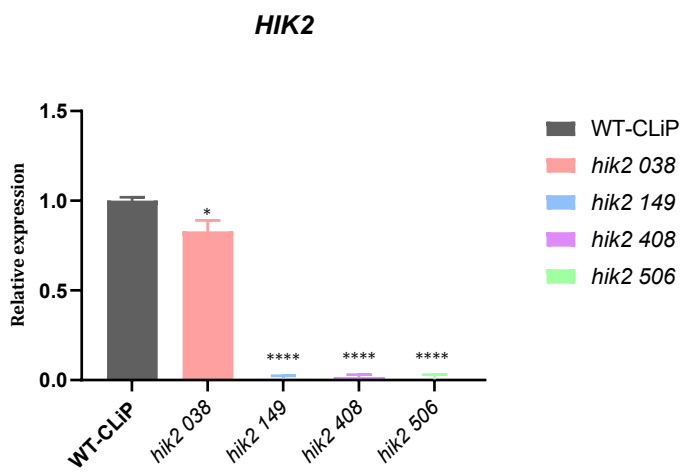

Fig 17. *HIK2* expression levels in *hik2* mutants. Expression levels of *HIK2* in WT-CLiP and *hik2 038, 149, 408* and *506* mutants using 3' end primer combination. Statistical significance was determined using Student's t-test: $P < 0.05$ compared to the control WT-CLiP. The expression of all the genes were normalized with the expression of *GBLP*.

3.3.2 Null NPQ induction and cell death for *hik2 149* mutant

To assess the functional consequences of different *HIK2* insertions, we evaluated the phenotype of the four mutant lines (*hik2 038, hik2 149*, *hik2 408*, and *hik2 506*) under HL conditions due to previous characterization in the laboratory showed a bleaching phenotype in *hik2 149* after 3 days of white HL exposure, as seen in Fig 18C.

Cultures were performed as described in Methods. Then, they were transferred to continuous HL (250µmol photons/m^2/s) at 22ºC to begin the experiment, which consists in photosynthetic measurements (Fv/Fm and NPQ) after 3 days of HL exposure.

The reproduction of this experiment confirmed the bleaching phenotype for *hik2 149* mutant line, which became visibly transparent in HSM media, indicating a high light sensitivity (Fig. 18C). In contrast, *hik2 038*, *hik2 408*, and *hik2 506* retained normal growth under the same conditions.

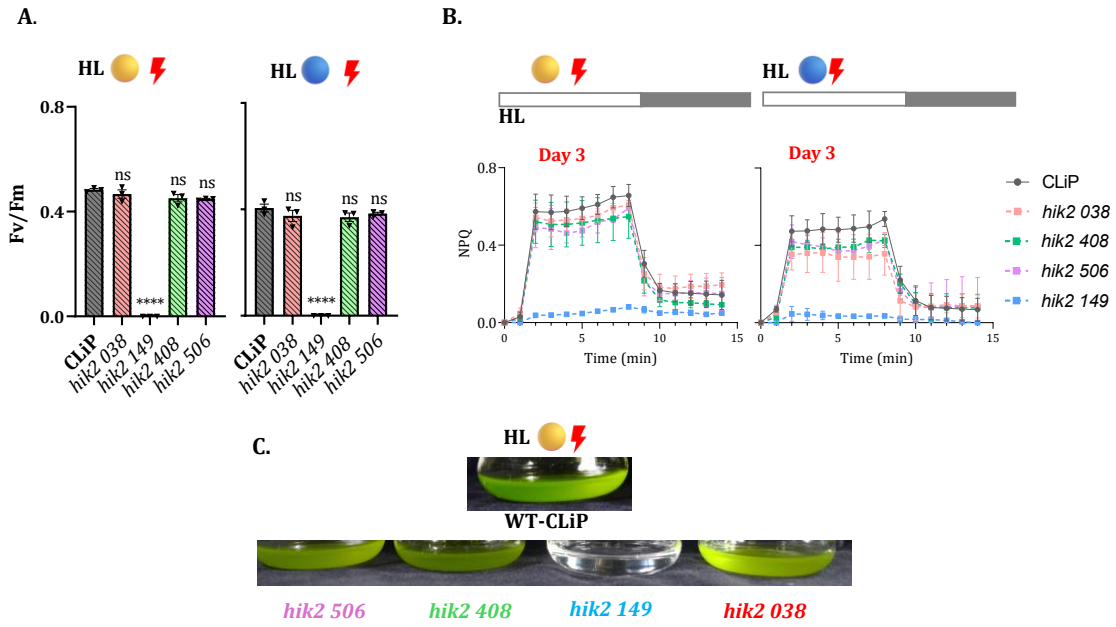

Figure 18. Phenotypic analysis of *HIK2* CLiP mutants HL conditions. A. Fv/Fm ratio and **B.** NPQ kinetics of the WT-CLiP and four *hik2* mutant lines on Day 3 of HL treatment, under white HL (yellow) and blue HL (blue). **B.** Images of HSM cultures from WT-CLiP and *hik2* mutant lines after 3 days of white HL treatment. WT-CLiP is shown above, with the four mutants displayed below. The data represent means ± SEM from three independent biological replicates (n = 3). HL= High Light (250µmol photons m^{-2} s^{-1}). Statistical significance was determined using Student's t-test: $P < 0.05$ compared to the control WT-CLiP.

Due to this starting point, we wanted to deep further, thus, photosynthetic measurements were assessed and supported these previous observations. In *hik2 149*, NPQ induction was completely absent after HL treatment, and Fv/Fm values were almost zero (Fig. 18A and B) under both blue and white light. In the other three mutant lines, however, both NPQ and Fv/Fm remained comparable to WT, indicating preserved photoprotection and photosystem II function.

Together, these results demonstrate that only the *hik2 149* mutant displays a high light–sensitive phenotype, characterized by severe impairment in both photoprotective capacity

and photosynthetic efficiency, whereas other *HIK2* insertion lines do not show detectable defects under the same conditions.

3.3.3 Differential transcript processing in *hik2 149* in dark

Although both *hik2 149* and *hik2 038* lines have the tDNA inserted at the same genomic location, and PCR and sequencing confirmed correct insertion in both cases, only *hik2 149* displayed the high light–sensitive phenotype. Furthermore, we examined *HIK2* transcription in *hik2 038* and *hik2 149* using oligo(dT) primers targeting the 3' UTR. This showed similar expression levels in *hik2 038* compared to WT, but impaired expression in *hik2 149*. Thus, to explore why this difference occurs, we investigated transcript processing in both lines.

To this purpose, reverse transcription was performed using a gene-specific primer (EMP1661) located near the insertion site; specifically in the 9th exon, 1,2kb away from the exon junction surrounding *hik2 038* and *hik2 149*. The resulting cDNA served as a template for PCR amplification with primers flanking the insertion (EMP1626 and EMP1627), enabling the detection of transcripts spanning the insertion site under both light and dark conditions (Fig. 19). These points were selected as *HIK2* expression has been described to be induced at the end of the dark period in a 12/12 dark-to-ligh regime (Strenkert et al., 2019).

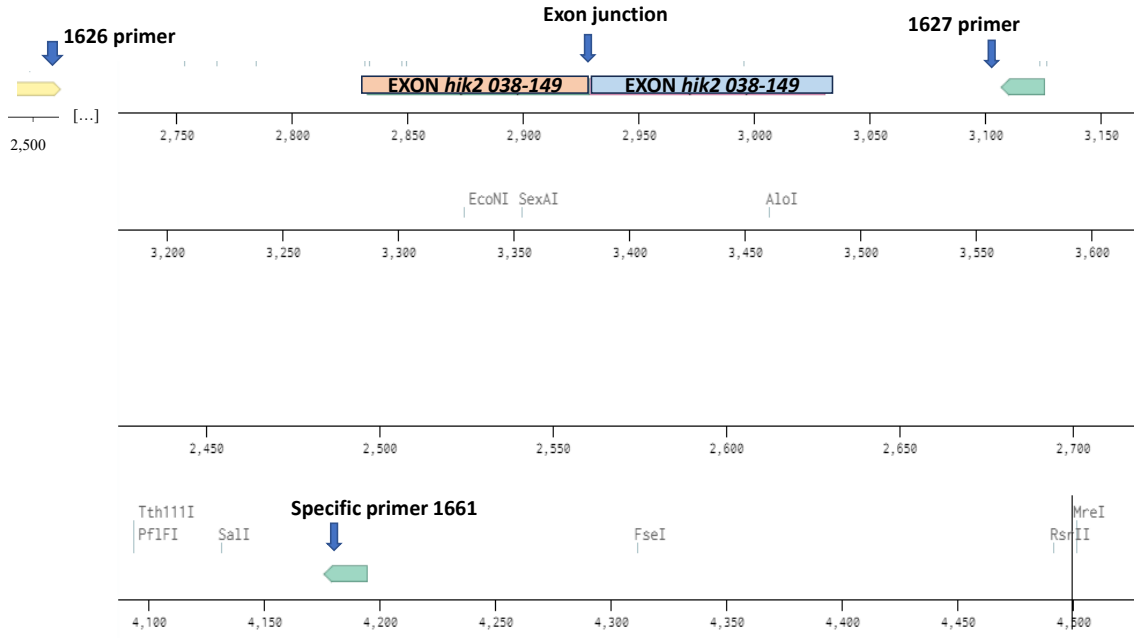

Figure 19. Schematic representation of the *HIK2* coding sequence (CDS) showing the positions of the specific primer EMP1661 (used for cDNA synthesis across the *hik2-038* and *hik2-149* insertion sites), and the flanking primers EMP1626 and EMP1627 used to amplify cDNA spanning the two t-DNA insertions. The exon junction corresponding to the insertion sites is indicated.

In *hik2 149*, we observed a shorter *HIK2* transcript in the dark compared to WT-CLiP, while under light conditions, no band amplification was obtained. In contrast, no differences in transcript size were detected for *hik2 038* under either condition, suggesting that the T-DNA may have been spliced out, resulting in a cDNA of wild-type size. Analysis of this specific cDNA by qPCR confirmed that, again transcript levels in *hik2 038* were similar to WT levels, while *hik2 149* showed disrupted expression patterns (Fig. 20C and D).

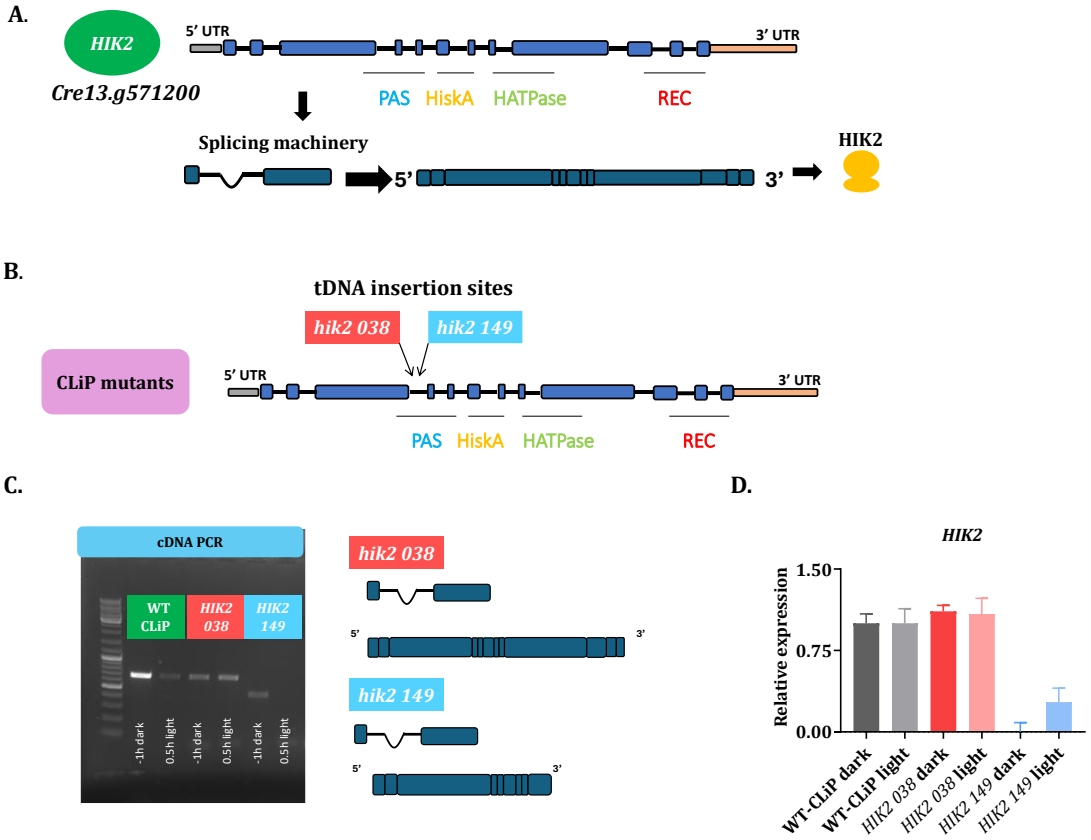

Figure 20. Structural and expression analysis of *HIK2* and CLiP *hik2 038* and *149* mutants. A. Gene model of *HIK2* (*Cre13.g571200*) showing predicted domains (PAS, HisKA, HATPase, REC) and splicing from pre-mRNA to mature transcript and final protein formation. **B.** Schematic representation showing the position of t-DNA insertions in the *hik2 038* and *hik2 149* CLiP mutants. **C.** RT-PCR analysis of *HIK2* cDNA using flanking primers in WT-CLiP and *hik2 038* and *149* mutant lines under dark and high light conditions (250µmol photons/m²/s), alongside schematics of the expected transcript structure. **D.** Relative expression levels of *HIK2* measured by qPCR in WT-CLiP and *hik2 038* and *149* mutant lines under dark and

Thus, the likely splicing out of the t-DNA in *hik2 038* allows for near-normal *HIK2* expression, whereas *hik2 149* shows disrupted transcript structure and reduced expression, particularly under dark conditions. Given the similar insertion sites of these two mutants, this difference may indicate additional regulatory effects, such as altered splicing efficiency or condition-specific transcriptional control, beyond the direct impact of the T-DNA insertion.

3.3.4 CRISPR Cas9 mutants' generation and screening

Given that a clear phenotype was observed in only one of the CLiP T-DNA insertion lines for *HIK2*, we used the CRISPR-Cas9 system established in our laboratory to produce a complete disruption of *HIK2* by generating three independent *hik2* knockout lines (*hik2.2 #1*, *hik2.2 BR #2*, and *hik2.2 BR #3*). The guide RNA was designed to target the third exon of *HIK2*, upstream of all functional domains, and Cas9-RNPs were co-transformed with the psL18 vector carrying a paromomycin resistance cassette, enabling selection of successful transformants

The mutants called *hik2.2 #1* was generated in collaboration with Heggeman laboratory in CC-125 background (mutant obtained by Dr. Mariano de Silvio). The two other mutants (*hik2.2 BR #2* and *hik2.2 BR #3*) were obtained in the laboratory: one in CLiP and the other in CC-124 WT backgrounds, respectively.

All colonies were screened as described in (Methods section 2.2 and 2.3) using the primer combination EMP1520 (GGTCCGGAGGGTGCTGACTC) and EMP1509 (AGTGTGCTCACCAAAGATCGCAT). For a the *hik2.2 #1* mutant the band yielded 660bp, as for the different mutants obtained in the laboratory, they yielded 2.5Kb for *hik2.2 BR #2* and 3kb *hik2.2 BR #3*, as seen in Figure 21.

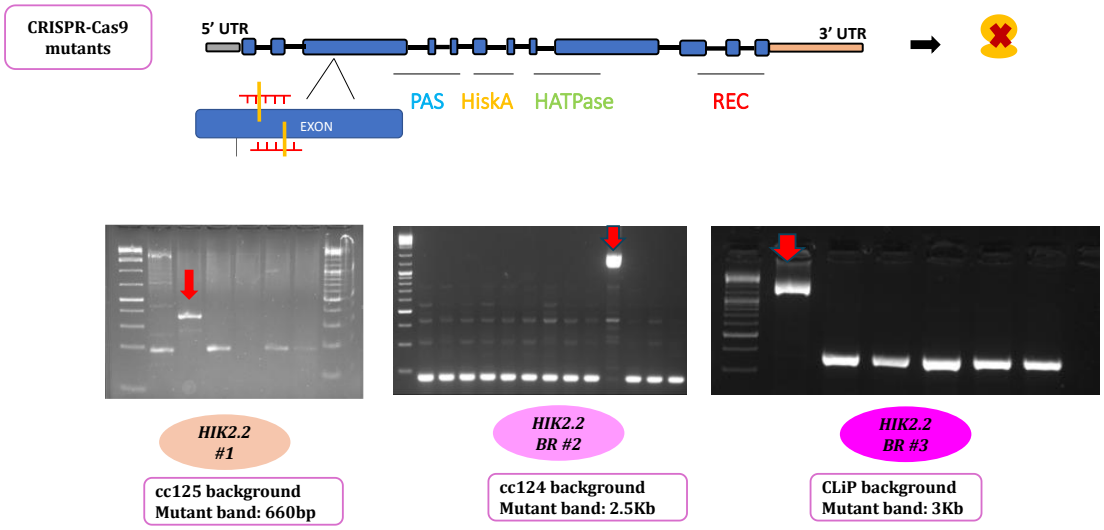

Fig 21. Schematic representation of the CRISPR-Cas9 design (in the third exon) and screening of the *hik2* transformants showing the band size for each mutant obtained: 660bp, 2.5Kb and 3Kb for each respective mutants: *hik2.2 #1*, *hik2.2 BR #1* and *hik2.2 BR #2*.

Following the initial screening, the sequencing of the CRISPR-Cas9 mutants was performed to verify the nature of the genomic edits introduced by the gRNA. In the case of the *hik2.2 #1* mutant, the gRNA induced a precise cut upstream of a thiamine, resulting in a 17 bp deletion and the insertion of a 103 bp fragment from the paromomycin resistance cassette. This alteration introduced a premature stop codon (TAA), effectively truncating the protein (Fig.

22).

Thus, screening was successful for *hik2.2 #1*. However, repeated sequencing attempts failed for both *hik2.2 BR #2* and *#3*, likely due to the presence of a large insertion that interfered with read-through.

***Hik2.2 #1* mutant sequencing**

"GGGCCGATGGCTCCGCCGTCGCGAGCGGCCTCTGCAGCGGTCCGGAGGGTGCTGACTCCGCGCACGCCTCCTCCGC
CTCCAACGCCATCGACTAAGAGTCCGAGCAGAAGAAGAACGGTGTAGACGCGGTGCTGTACGCCTCCTCCGCCTCG
AAGGCCATCGACTAAGAGTCCGAGCAGAAGAAGAACGGTTATACGCGGTGCTGTCGGGCGCGCGCTCCGTGGAGCG
GGAGCTGGACG"

gRNA: TTTTAACTGGTCCGCCXTACGCGG

deleted nucleotides: GTTTTAACTGGTCCGCC 17bp

inserted nucleotides:
ACTAAGAGTCCGAGCAGAAGAAGAACGGTGTAGACGCGGTGCTGTACGCCTCCTCCGCCTCGAAGGCCATCGACTA
AGAGTCCGAGCAGAAGAAGAACGGTTA 103 bp

TAA STOP codon

Fig 22. *hik2.2 #1* mutant sequencing fragment showing the sequence of the gRNA (TTTTAACTGGTCCGCCXTACGCGG) with the PAM sequence highlighted in blue, as well as the precise cut of the Cas9 ("X" in blue). Deleted nucleotides are shown in red color (17bp) while the inserted in green (103bp). Highlighted in yellow color is the sequence generating a premature STOP codon.

3.3.5 Low NPQ induction and cell death for *hik2.2 #1* mutant under white and blue HL

To see whether these mutants reproduced the phenotype observed in *hik2* 149, we conducted an experiment under white and blue light (250µmol photons m^{-2} s^{-1})).

Upon HL exposure, only *hik2.2 #1* showed a clear bleaching phenotype, becoming visibly white in HSM media, indicative of high light sensitivity. However, it didn't resemble 100% the phenotype observed in *hik2 149*, which turned completely transparent (Fig. 23C).

Further photosynthetic measurements supported these observations. In *hik2.2 #1*, NPQ induction was completely absent after HL treatment, and Fv/Fm values were significantly reduced relative to WT. This phenotype was consistently observed in three independent biological replicates performed initially. However, when additional replicates were carried out several months later, the phenotype was no longer detectable, leaving us uncertain about

its stability and whether it can be unequivocally attributed to the *HIK2* disruption (Fig. 23A and B).

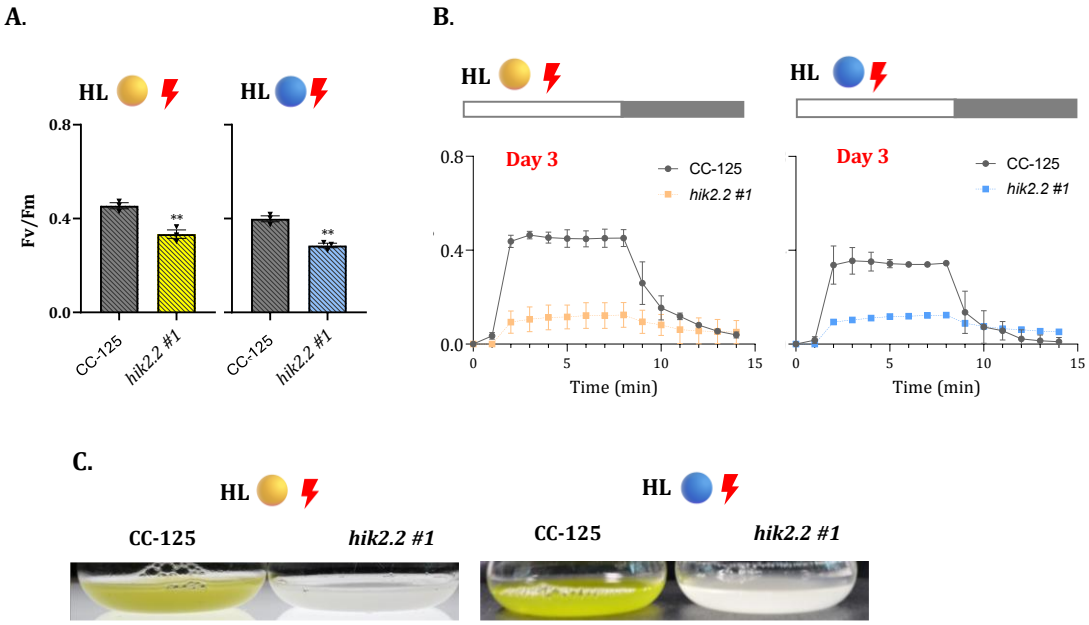

Figure 23. Phenotypic analysis of *hik2.2 #1* mutant in white and blue HL. **A.** Fv/Fm ratio **B.** NPQ kinetics of the CC-125 (WT) and *hik2.2 #1* mutant line on Day 3 of HL treatment, under white HL (yellow) and blue HL (blue).**B.** Images of HSM cultures from CC-125 and *hik2.2 #1* mutant line after 3 days of white (left) and blue (right) HL treatment. The data represent means ± SEM from three independent biological replicates (n = 3). HL, high light (250µmol photons/m²/s) for 3 d. Statistical significance was determined using Student's t-test: $P < 0.05$ compared to the control WT- CC-125.

3.3.6 No HL-sensitive phenotype observed for *hik2.2 BR #1* and #3 mutants under HL

Due to the loss of the high-light–sensitive phenotype in *hik2.2 #1*, the additional mutant lines *hik2.2 BR #1* and *BR #3* were generated to assess phenotype reproducibility. However, as shown in Fig. 24, neither *hik2.2 BR #1* nor *BR #3* exhibited a high-light–sensitive phenotype. Both lines showed normal growth under white and blue HL, with NPQ and Fv/Fm values comparable to WT, indicating intact photoprotection and PSII function. These results leave the role of HIK2 in high-light acclimation unresolved.

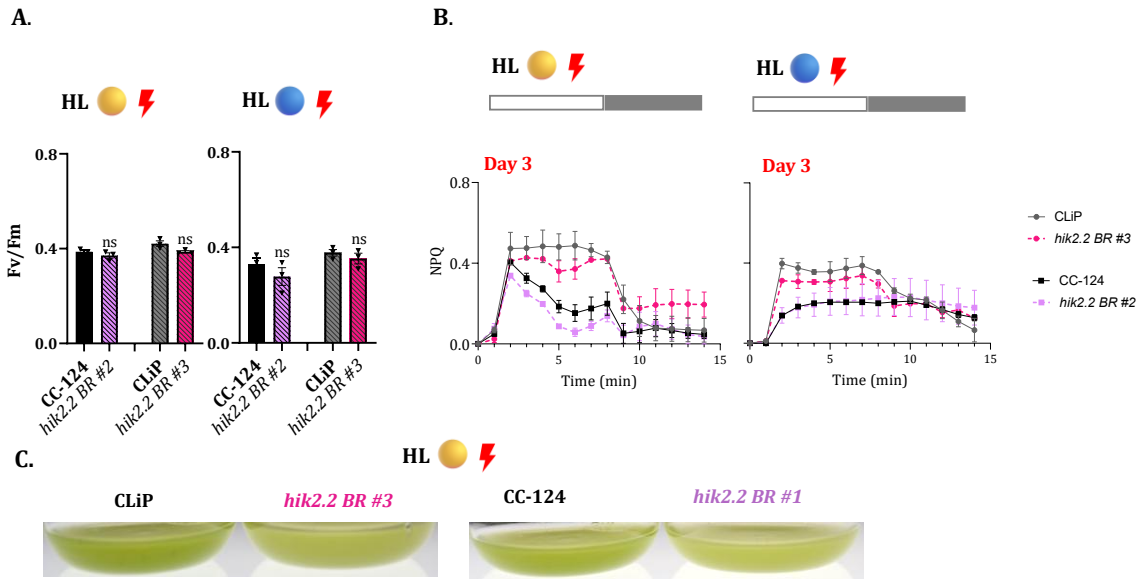

Figure 24. Phenotypic analysis of *hik2.2 #1* mutant in white and blue HL. A. Fv/Fm ratio **B.** NPQ kinetics of CLiP, CC-124 (WTs) and *hik2.2 BR #2 hik2.2 BR #3* mutant lines on Day 3 of HL treatment, under white HL (yellow) and blue HL (blue). **B.** Images of HSM cultures from CLiP, CC-124 (WTs) and *hik2.2 BR #2 hik2.2 BR #3* mutant lines after 3 days of white HL treatment. The data represent means ± SEM from three independent biological replicates (n = 3). HL, high light (250 µmol photons/m²/s) for 3 d. Statistical significance was determined using Student's t-test: $P < 0.05$ compared to the control WT CC-124.

4. DISCUSSION

Histidine kinases (HIKs) are versatile environmental sensors conserved across bacteria and lower eukaryotes, including algae. In *Chlamydomonas reinhardtii* and related green algae, they combine sensory, catalytic, and signaling domains, allowing them to link environmental cues (especially light), to phosphorylation-based cellular responses. Still, their physiological roles in algae remain largely unknown.

A key example comes from *Ostreococcus tauri*, where a LOV-domain histidine kinase functions as a blue-light photoreceptor required for circadian clock entrainment (Djouani-Tahri et al., 2011). In *C. reinhardtii*, several histidine kinase rhodopsins (HKRs) have been biochemically characterized. For instance, HKR1 responds to both UV-A and blue light (Luck et al., 2012). It localizes to the eyespot and cilia and has been implicated in phototaxis and photophobic responses, though its downstream effectors remain unclear. Comparative genome analyses indicate that modular HIKs, including but not limited to rhodopsin-type HIKs, are broadly conserved among green algae, supporting their general role in transducing environmental signals, particularly light (Beel et al., 2012).

In this study, we characterized two novel photoreceptor HIKs: *Cre02.g079750* and *Cre13.g571200*, which we refer to as *HIK1* and *HIK2*, respectively. Our findings suggest a role

for HIK1 in photoprotection, while the function of HIK2 remains unclear.

HIK1

Strenkert et al. (2019) conducted a comprehensive multi-omics analysis of *C. reinhardtii* across a diurnal cycle, revealing dynamic transcriptional responses to light. Notably, *HIK1* (*Cre02.g079750*) was strongly induced one hour after lights-on during the dark-to-light transition, following a temporal expression pattern similar to early light-responsive genes such as *LHCSR1*, *LHCSR3.1*, and *PSBS*, all known to mediate photoprotective energy dissipation. This led us to hypothesize that *HIK1* may contribute to photoprotection during the onset of illumination.

Although HIK1 is known to be upregulated in a 12:12 light–dark cycle (Strenkert et al., 2019), the enhanced NPQ phenotype in the *hik1 442* mutant was observed under continuous low blue light. Further investigation under diurnal conditions is warranted, as these regulatory pathways are not necessarily mutually exclusive.

However, before considering regulatory roles of HIK1, the molecular nature of the *hik1 442* line must be clarified. The T-DNA insertion lies near the 3′ end, raising the possibility that most of the protein could still be expressed and act in a dominant-negative manner. However, transcript analyses revealed normal initiation (5′UTR primers) but strongly reduced signals at the 3′ end, indicating premature termination or degradation of incomplete transcripts. This suggests that stable near full-length truncated proteins are less likely, and the phenotype is more consistent with loss of function. Still, definitive direct assessment of protein accumulation, complementation, and independent mutant lines will be required to fully resolve this point.

Given that the *hik1 442* phenotype most likely reflects loss of HIK1 function, the unusual activation of photoprotective genes under LL, instead of HL, suggests that the mutant may misinterpret LL as HL due to defects in light-sensing pathways.

In addition, our preliminary data (n=1) show that in continuous low blue light, *hik2 442* mutants transiently upregulate *LHCSR1* and *LHCSR3* at Day 4, returning to WT levels by Day 8. In contrast, *PSBS* is induced only at Day 8, suggesting distinct regulatory dynamics. Further confirmation of this pattern (n=3) would also justify examining protein levels to assess whether transcript changes correspond to functional differences in photoprotection.

A similar phenotype was reported, where the *spa1-1* mutant displayed enhanced NPQ and *qE* gene expression under LL. In *spa1-1*, each *qE* gene reached LL expression levels comparable to WT under HL. This phenotype depends on CrCO, placing SPA1 upstream of CrCO in a

ubiquitin ligase complex that represses photoprotective genes in low light (Gabilly et al., 2019). Our findings suggest that HIK1 might also participate in this regulatory pathway.

Interestingly, other studies have described NPQ activation in the absence of HL, such as in *det1phot* mutants, where *LHCSR* expression in darkness reached levels comparable to those of WT under HL (Aihara et al., 2019). Together, these observations suggest that HIK1 may function as part of a light-responsive pathway regulating photoprotective mechanisms.

The reduction in *SPA1* transcript levels observed in *hik1 442* suggests that HIK1 signaling may influence the COP1–SPA complex. Given the CheY-like phosphotransfer domain in HIK1 and the CheY-like response regulator domain in SPA1, a two-component signaling–type interaction is plausible and could, directly or indirectly, modulate SPA1 activity, thereby affecting downstream CrCO-mediated transcription of photoprotective genes. Although these data are preliminary (n = 1) and require confirmation (n = 3), future work should assess whether the decrease in *SPA1* mRNA is mirrored at the protein level and whether HIK1 physically or functionally interacts with COP1–SPA components. Such experiments will be essential to determine whether the NPQ phenotype of *hik1 442* is mediated via this pathway.

In contrast, *CrCO* transcript levels were unchanged in *hik1-442*. Under low-light conditions, SPA1 promotes ubiquitination and degradation of CrCO, reducing qE activation and expression of *LHCSR* and *PSBS*. Our findings therefore raise the possibility that HIK1 affects SPA1 without altering *CrCO* transcript abundance, although confirmation with additional replicates (n = 3) is needed, and post-transcriptional or post-translational effects on CrCO cannot be excluded.

Finally, the elevated *LHCSR* and *PSBS* transcript levels in *hik1-442* (if confirmed) may also involve SPA1-independent regulation. While SPA1 is a known transcriptional regulator of these genes, Gabilly et al. (2019) identified a light-dependent, SPA1-independent post-transcriptional mechanism that modulates LHCSR3 and PSBS protein accumulation. This suggests that, in addition to SPA1-dependent transcriptional control, other regulatory layers could contribute to the observed phenotype.

Thus, while previous work has expanded our understanding of *qE* regulation, our data adds a new regulatory layer that remains unresolved. Further analysis will require testing whether the phenotype is consistent across independent *hik1* mutant lines. Until recently, no additional insertions were available in the CLiP library, and alternative approaches (e.g., CRISPR/Cas9, RNAi) have not succeeded. Complementation assays and double/triple mutants (e.g., *hik1spa1, hik1spa1co*) will be necessary to define HIK1's role more clearly.

HIK2 and the HL-sensitive phenotype in *hik2 149*

On the other hand, the *hik2 149* mutant of *Chlamydomonas reinhardtii* displays a consistent high-light–sensitive phenotype, including bleaching, growth inhibition, and photophysiological impairment. This observation initially suggested a possible role for the putative sensor kinase HIK2 in light stress responses. However, this phenotype was not reproduced in any other *HIK2*-disrupted lines: neither additional CLiP insertion mutants nor three independent CRISPR/Cas9 knockouts exhibited a similar response.

Among the CRISPR lines, only *hik2.2 #1* in the CC-125 background showed HL sensitivity. Although the phenotype was consistently reproduced in three independent biological replicates performed initially, it was not observed in additional experiments conducted several months later. This raises uncertainty about the stability of the phenotype and whether it can be unequivocally attributed to the *HIK2* disruption or instead, reflects secondary effects or compensatory changes that emerged over time. A possible way to clarify this would be to measure *HIK2* transcript abundance at time points when the phenotype is present and when it disappears, to determine whether the recovery is linked to changes in *HIK2* expression or to unrelated compensatory processes. While such analyses were beyond the scope of the present study, they represent an important direction for future work.

These inconsistencies imply that the phenotype observed in *hik2 149* may not result directly from *HIK2* disruption. Instead, it may reflect background mutations, transformation-induced stress, or instability within the mutant population.

Such variability is well documented in *Chlamydomonas* genetics. Insertional and genome-editing approaches often introduce additional mutations or chromosomal rearrangements that complicate phenotype interpretation. For instance, only 52% of photosynthesis-deficient mutants generated by glass bead transformation were found to co-segregate their phenotype with the resistance marker, indicating that unrelated background mutations frequently contribute to observed phenotypes (Dent et al., 2005). Moreover, mutant populations may undergo recovery or adaptation through transcriptional reprogramming, epigenetic changes, or selection of more tolerant subpopulations, especially under stress conditions (Morgan et al., 2014; Ngan et al., 2015; Strenkert et al., 2019). These considerations underscore the importance of validating gene-function relationships using multiple independent alleles and genetic complementation (Jinkerson & Jonikas, 2015; Shin et al., 2016).

Importantly, the T-DNA in *hik2 149* disrupts *HIK2* within the PAS domain, located closer to the 5′ region of the gene. This position would normally be expected to cause premature termination and loss of the kinase domain, consistent with a loss-of-function. However, the

fact that *hik2 149* is the only mutant line to display a clear HL-sensitive phenotype, it suggests that the phenotype may not arise solely from loss of *HIK2* function. Instead, it could reflect insertion-specific consequences such as disruption of nearby elements, or production of a truncated PAS fragment with partial activity. To distinguish between these possibilities, it will be essential to determine whether truncated products accumulate and interact with signaling partners, and to test whether complementation with full-length *HIK2* or expression of the truncated form in wild type can reproduce the phenotype.

Despite uncertainties surrounding the *hik2 149* phenotype, HIK2 may still contribute to regulatory signaling. PAS domains are commonly found in proteins that sense light, redox state, or oxygen (Möglich et al., 2009), and in *Chlamydomonas*, they occur in photoreceptors involved in integrating environmental cues (Beel et al., 2012). In *Arabidopsis*, PAS-domain proteins such as ZEITLUPE (ZTL) and FKF1 function in circadian regulation (Somers et al., 2000; Imaizumi et al., 2003). HIK2 may therefore be involved in light sensing, redox signaling, or diurnal control.

Given HIK2's domain architecture, future studies should test its potential roles in redox signaling, circadian timing, or metabolic regulation under fluctuating conditions. This could include monitoring *HIK2* expression and protein levels during environmental shifts (e.g., light/dark cycles or redox changes) and identifying interaction partners via co-immunoprecipitation or tagged constructs. In addition, *hik2 hik1* double mutants have been generated and warrant further analysis, as HIK2 may act in the same pathway as HIK1 or exhibit functional redundancy. Testing whether the two genes regulate overlapping targets or converge on shared signaling components will be essential.

Altogether, these approaches are needed to distinguish the specific consequences of the *hik2 149* insertion from the actual physiological role of HIK2. Combining targeted genetic experiments with transcriptomic, proteomic, and interaction-based methods will be key to understanding whether HIK2 contributes to general stress integration or to more specific regulatory pathways in *Chlamydomonas*.

5. CONCLUSIONS

1. Two novel histidine kinases in *Chlamydomonas reinhardtii,* HIK1 and HIK2, were identified. Both HIK1 and HIK2 possess conserved LOV motifs (GXNCRFLQ), characteristic of blue-light photoreceptors, supporting their putative function as LOV-HKs.

HIK1

2. The *hik1 442* mutant carries a T-DNA insertion in the 15th exon of *HIK1* in antisense orientation, leading to reduced transcript levels and likely disruption of full-length expression.
3. Under blue LL, the *hik1 442* mutant exhibits enhanced NPQ induction relative to the WT-CLiP, particularly after prolonged exposure, while Fv/Fm values remain only slightly higher.
4. Under white LL, NPQ induction and Fv/Fm values were similar between *hik1 442* and WT-CLiP.
5. Preliminary expression analyses show transient upregulation of *LHCSR1* and *LHCSR3* at Day 4 and increased *PSBS* expression at Day 8 in *hik1 442* under blue LL.
6. Differences in the timing of *LHCSR* and *PSBS* expression suggest that qE effectors are regulated through distinct, gene-specific signaling mechanisms.
7. Preliminary expression analyses show *SPA1* transcript levels are reduced in *hik1 442,* while *CrCO* expression remains unchanged. Further investigations are needed to unravel the possible role of HIK1 in this pathway
8. This atypical enhancement of NPQ induction and qE gene upregulation in prolonged blue LL suggests misregulation of photoprotection and a response that mimics high-light conditions, indicating that HIK1 normally acts to suppress qE activation under non-stress conditions.
9. Together, these results propose HIK1 as a novel component of light signaling in Chlamydomonas, influencing NPQ capacity and photoprotection under blue LL.

HIK2

1. The HL-sensitive phenotype is unique to *hik2 149* and wasn't observed in other independently generated *HIK2*-disrupted strains, including three additional CLiP insertional mutants and three CRISPR/Cas9 knockout lines.
2. The PAS domain of HIK2 is truncated in *hik2 149*, but it remains unclear whether this specific truncation exerts dominant-negative effects or whether the altered protein (if originated) is expressed and stable.
3. The disappearance of the HL-sensitive phenotype in *hik2.2 #1* (CRISPR line in the CC-125 background) suggests plasticity within mutant populations, potentially driven by selection, adaptation, or epigenetic reprogramming.

4. The lack of consistent correlation between *HIK2* disruption and HL sensitivity suggests that loss of *HIK2* function is not responsible for the phenotype observed in *hik2 149*.
5. Although its function remains unresolved, the presence of a PAS domain in HIK2 suggests potential involvement in environmental signal transduction, and future studies should explore roles in light, redox, or other signaling pathways.
6. Characterization of *hik1hik2* double mutant may help clarify whether these genes operate within a shared signaling pathway or exhibit functional redundancy.

Chapter 4

A quick-to-implement and optimized CRISPR-Cas9 protocol to obtain insertional and small indel mutants in *Chlamydomonas reinhardtii*

This chapter corresponds to a publication in *MethodsX: "A quick-to-implement and optimized CRISPR-Cas9 protocol to obtain insertional and small indel mutants in Chlamydomonas reinhardtii"* (https://doi.org/10.1016/j.mex.2025.103416).

My contribution to this article was the development of the indel screening strategy presented. It provides a streamlined approach for detecting small insertions and deletions through PCR and gel electrophoresis (Fig. 1, Fig. 2, and Fig. 5).

Article title

A quick-to-implement and optimized CRISPR-Cas9 protocol to obtain insertional and small indel mutants in *Chlamydomonas reinhardtii*

Authors

Mariano A. De Silvio[a,1], Camila Sánchez-Retuerta[a,1], M. Águila Ruiz-Sola[a,b,c], Olga Baidukova[d], Elena Monte[a,e,*]

[a] Centre for Research in Agricultural Genomics (CRAG) CSIC-IRTA-UAB-UB, Campus UAB, Bellaterra, 08193 Barcelona, Spain
[b] Instituto de Bioquímica Vegetal y Fotosíntesis, Universidad de Sevilla-CSIC, Av. Américo Vespucio, 49, 41092, Sevilla, Spain
[c] Departamento de Bioquímica Vegetal y Biología Molecular, Universidad de Sevilla, Sevilla, Spain
[d] Institute of Biology, Experimental Biophysics, Humboldt University of Berlin, Berlin, Germany
[e] Consejo Superior de Investigaciones Científicas (CSIC), 08028 Barcelona, Spain

[*] Corresponding author.
E-mail address: elena.monte@cragenomica.es
[1] These authors contributed equally to this work.

Keywords

CRISPR-Cas9 protocol; Chlamydomonas; microalgae; indel detection, knockout mutants; simple and quick

Related research article

None.

Abstract

Chlamydomonas reinhardtii is a leading model organism in algal research, widely used to study photosynthesis, chloroplast and cilia biology, and more recently, metabolism, light signaling, the cell cycle, and algal biotechnology. Its sequenced genome has significantly accelerated research in the field, while improved genome-editing tools are key to advancing reverse genetics and genetic engineering. Building on previous advances, we present a streamlined and efficient CRISPR-Cas9 protocol for generating knockout mutants in Chlamydomonas via non-homologous end joining (NHEJ), using only commercially available reagents. Additionally, we introduce a cost-effective, PCR-based screening method capable of detecting mutants with large insertions as well as short indels -as small as one base pair- thereby enhancing overall CRISPR efficiency.

- This protocol is easy to setup and can be fully executed using commercially available reagents.
- This protocol allows for quick implementation and generation of mutants: 5 weeks from design to sequencing of candidate mutants.
- This protocol describes a novel PCR-based strategy to identify mutants containing short indels. Screening is designed to identify large insertion mutants and the often overlooked small indel mutants.

Specifications table

This table provides general information on your protocol.

Subject area	Biochemistry, Genetics and Molecular Biology
More specific subject area	CRISPR Cas9 mediated Genome Editing
Name of your protocol	Quick-to-implement and optimized protocol for the generation of CRISPR-Cas9 knockout mutants that allows detection of short indels in a cell-wall featuring *Chlamydomonas reinhardtii* strain
Reagents/tools	Although provided, reagents and tools listed in this box can be purchased from any supplier. 1. MATERIALS TAP-agar refreshed 1-week-old Chlamydomonas cells (CC-124 - cell wall containing, Chlamydomonas Resource Center) 10 mM EDTA pH 8 Primers PCR Master Mix Kit (NZYTaq II 2x Green Master Mix - NZYTaq II DNA polymerase, NZYtech) GeneRuler DNA Ladder Mix (Thermo Fisher) Dimethylsulfoxid (DMSO) Nuclease Free Water TAE 1X Agarose Electrophoresis loading buffer (6X Loading Dye, Thermo Fisher) PCR clean-up kit (NZYGelpure, NZYtech) crRNA (Alt-R™ CRISPR-Cas9 crRNA - 2 nmol, IDT) tracrRNA (Alt-R® CRISPR-Cas9 tracrRNA - 5 nmol, IDT) *Streptococcus pyogenes* Cas9 (Alt-R™ S.p. Cas9 Nuclease V3, IDT) CRISPR buffers (Nuclease Free Duplex Buffer; IDTE pH 7.5 (1X TE Solution), IDT) Buffer O (Thermo Fisher) {can also be homemade prepared following manufacturers specifications} MAX Efficiency™ Transformation Reagent for Algae (Thermo Fisher) {can be replaced with autolysin solution as shown by Picariello et al. [12]} Sterilized 1 M Sucrose 2 mL, 1.5 mL and 200 µL sterile tubes 2 mm gap electroporation cuvette 24-well plates TAP liquid medium TAP agar plates with paromomycin (10 µg mL^{-1}) Linearized resistance-carrying vector (pSL18 vector, *pAPHVIII* cassette) Parafilm Hemocytometer Iodine (0.25% w/v in EtOH) 50 mL tubes Aluminum foil Razor blades Square 120x120 mm Petri dishes Round 60x60 mm Petri dishes Paromomycin sulfate (Merck) 2. LABORATORY EQUIPMENT Thermoblock Thermoshaker Thermocycler Centrifuges for 1.5, 2 and 50 mL tubes Electrophoresis equipment Transilluminator Growth Chamber (with programmable light-dark cycles) Electroporator (NEPA21 from NEPAGENE or other) Laminar flow hoods Water bath (with cooling system) Spectrophotometer (Nanodrop or other) Rotary Shaker Optical microscope 3. OPTIONAL Vacuum Concentrator Cell Counter TOPO-TA cloning kit for Sequencing (Thermo Fisher)

Experimental design	Cell wall featuring Chlamydomonas cells, grown in synchronizing conditions, were electroporated with pre-assembled Cas9-gRNA ribonucleotides (RNPs) and a linearized resistance-carrying vector. Electrophoresis screening for mutants allowed detection of both large insertions and small indels.
Trial registration	N/A
Ethics	N/A
Value of the Protocol	• **Easy to reproduce**. Our protocol can be fully executed using commercially available reagents. • **Quick implementation and generation of mutants**. From CRIPSR design to sequencing of candidate mutants this protocol can be completed in 5 weeks. • **Detection of mutants containing short indels**. Electrophoresis screening was designed to identify both large insertion mutants and often overlooked small indel mutants, increasing overall CRISPR efficiency.

Background

In Chlamydomonas, a fundamental requirement in both basic and applied research is the ability to inactivate specific genes. To address this, several techniques have been developed in recent years, with CRISPR-Cas9 emerging as the most widely used tool. However, its robustness and efficiency remain limited [1,2]. The principle of the Cas9 gene-editing technique is straightforward: a Cas9 endonuclease binds to a guide RNA (gRNA), which is designed to target a specific genomic site, forming a ribonucleoprotein complex (RNP). These RNPs are pre-assembled *in vitro* and subsequently introduced into cells via electroporation. Guided by the gRNA, Cas9 induces a double-strand break (DSB) at the target site, which is then repaired by the cell's intrinsic repair machinery [3-5]. This repair process can lead to mutations at the target site. In Chlamydomonas, DSBs are typically repaired via non-homologous end joining (NHEJ), a process that can result in short insertions or deletions (indels) or in large insertions in the presence of exogenous DNA (such as a resistance cassette) [4]. Alternatively, Chlamydomonas can repair DSBs through homologous recombination (HR) if DNA fragments with homology regions flanking the cut site are provided [6], or through single-strand templated repair (SSTR) in the presence of single-stranded oligodeoxynucleotides (ssODNs) [7-9].

Recent CRISPR protocols for *Chlamydomonas* have primarily focused on taking advantage of the HR mechanism, as it enables precise gene modifications such as creating custom knockout mutations, introducing resistance markers or other tailored cassettes, performing single-base substitutions, or adding tags [10-14], or the SSTR for scar-less gene editing with a transgene-free approach [7-9]. While these advanced modifications are highly desirable, they involve time-consuming procedures including cloning optimizations and the often costly purchase of custom cassettes for HR or ssODNs for SSTR. Despite these efforts, the overall efficiency of these approaches remains lower compared to non-homologous end joining (NHEJ)-based mutagenesis [9-11]. Higher efficiencies have been reported when HR is employed to disrupt a gene using a resistance marker cassette [12,14]. This strategy, however, has two key limitations: (1) the resistance marker cannot be crossed out, and (2) it does not allow for certain types of gene editing such as single base substitutions [11]. Given its simplicity, cost-effectiveness, and higher efficiency, NHEJ remains the preferred strategy for generating knockout mutants.

Another common challenge in performing CRISPR in Chlamydomonas is the screening for mutants with unknown or subtle phenotypes. Typically, this is done by amplifying a short section of the target gene that includes the Cas9 cut site and analyzing it via electrophoresis. The goal is to identify larger amplicons compared to the wild type, indicative of an insertion [11-13]. However, this method often overlooks mutants with small indels, leading to their misclassification as false negatives.

Here, we present a streamlined and efficient CRISPR-Cas9 protocol for generating knockout mutants in Chlamydomonas. This approach eliminates the need for complex additional procedures and can be fully carried out using standard laboratory equipment and commercially available reagents. Additionally, we introduce a cost-effective screening strategy capable of detecting mutants with short indels, thereby enhancing overall CRISPR efficiency.

Description of protocol

The following is a quick and simple protocol for the generation of Chlamydomonas knockout mutants in any gene of interest (*GOI*) using CRISPR-Cas9, followed by a PCR-based screening strategy that allows detection of large insertional mutants as well as short indels.

The protocol was established and optimized using the *PHYTOENE SYNTHASE 1 (PSY1)* gene as a target. *psy1* knockout mutants are known to have severely impaired carotenoid biosynthesis, which is essential for chlorophyll stabilization [16]. As a result, *psy1* mutants exhibit a distinct pale coloration. During our initial PCR screens for large insertions, we observed that some pale colonies did not show the expected PCR bands, suggesting they might carry small indels in *PSY1* that were undetectable with the original method. This realization prompted us to optimize the protocol and develop a PCR-based approach to detect small indels. Importantly, this protocol enables detection of both large insertional and small indel mutations in any *GOI*, regardless of whether the mutation produces a visible phenotype. While the *psy1* phenotype facilitated the development of the method, a visible phenotype is not required for broader application.

CRISPR-Cas9 ribonucleoproteins (RNPs) are composed of a Cas9 nuclease and a guide RNA (gRNA): the latter is an RNA duplex composed of a complementary base pairing CRISPR RNA (crRNA), which is custom designed to target the *GOI*, and a transactivating CRISPR RNA (tracrRNA), a constant sequence that forms a secondary structure and serves as a scaffold recognized by the Cas9. Here, gRNA design refers to the specific design of crRNAs (as the tracrRNA is constant in all gRNA). The gRNA is designed immediately upstream of an NGG sequence, called protospacer adjacent motif (PAM), which is required by the SpCas9 (from *Streptococcus pyogenes*) for DNA recognition.

The entire protocol takes about 5 weeks from the design (Step 1) to mutant detection (Step 5). A general overview of the method is presented in the Graphical Abstract, while the CRISPR design process (Steps 1-3) is schematically summarized in Fig. 4.

Step 1 – gRNA and primer design

Time of execution: one day.

1.1 Design of custom single guide RNA (gRNA) for your *GOI*.

Use CRISPR-P 2.0 (http://crispr.hzau.edu.cn/CRISPR2/) [17] to choose the most suitable gRNA in the region of your *GOI* where you would like to have your mutation. Use the following settings: -choose NGG as PAM sequence, 20 as guide length, and "Chlamydomonas v5.5" as target genome. Copy and paste the *GOI* sequence, and leave default values for the rest of the options; select the gRNA with the highest on-score (>0.5, if possible) and with low off-score levels for the identified off-targets.

Note 1.1.1. To generate knockout mutants, we recommend to have the Cas9 target site localized in the first exon of the coding sequence (CDS) and as close to the start codon as possible, to minimize the possibility of generating functional truncated proteins.

Note 1.1.2. when ordering gRNA from IDT, make sure these do not include the NGG sequence at the 3', as indicated by the company.

Note 1.1.3. We recommended to design and test two different gRNA to maximize the options of generating mutations, given that different gRNA might display different efficiencies.

Note 1.1.4. After the design, we do not recommended purchasing the gRNA until successfully completing the primer tests (Step 2).

1.2 Design of primers.

The protocol uses a total of 6 different primers (see Graphical Abstract and Fig. 1-4):

(a) Four Screening (S) primers to be used in the mutant screen:

a.1-Two S primers to screen for Indels (id): Indel primer wild-type reverse (SIDrv), with the same sequence as the gRNA, and Indel primer mutated reverse (SIDrv*), with 3 mismatches at the 3'-

end. SIDrv is designed to detect the presence of mutations at the Cas9 cleavage site (if these are present it won't produce amplification), while SIDrv* serves as a negative control, to check that mismatches caused by the introduction of short indels at this *locus* do not result in PCR amplification (see Primer test).
a.2-Two S primers to screen for large (L) insertions: SL forward (fw) and SL reverse (rv), which combined should give a 100-500 bp amplicon flanking the Cas9 cleavage site.
(b) Two *in vitro* (I.V.) test primers (I.V.fw and I.V.rv), which combined should give a 600-800 bp amplicon asymmetrically flanking the Cas9 cleavage site (Fig. 3). Cas9 cleavage in the *in vitro* test of the resulting amplicon will give two different sized bands.
Note 1.2. Depending on the Cas9 site and the overall design and strategy, one of the SL and I.V. primers can have the same sequence.

We use Primer-BLAST (https://www.ncbi.nlm.nih.gov/tools/primer-blast/) [18] to design SL and I.V. primers, with the following parameters:
- optimal primer melting temperature 63 ºC (min 60 ºC and max 66 ºC),
- optimal primer size of 23 bp (min 22 and max 24 bp);
- choose primer pairs with the least number of unspecific amplifications (<3) and with at least a G or a C in the two last bases at 3'.
Oligo Cal can be used to check primer self-complementation (http://biotools.nubic.northwestern.edu/OligoCalc.html) [19].

For *PSY1*, the designed gRNA had a 0.78 on-score and maximum off-score of 0.23 (Fig. 1). The gRNA and the indel primer sequences are shown in Fig. 1. SLfw and SLrv primer pair was designed to give an amplicon of 429 bp. I.V.fw and I.V.rv (which was the same as SLrv) primer pair was designed to give an amplicon of 769 bp (Fig. 1).

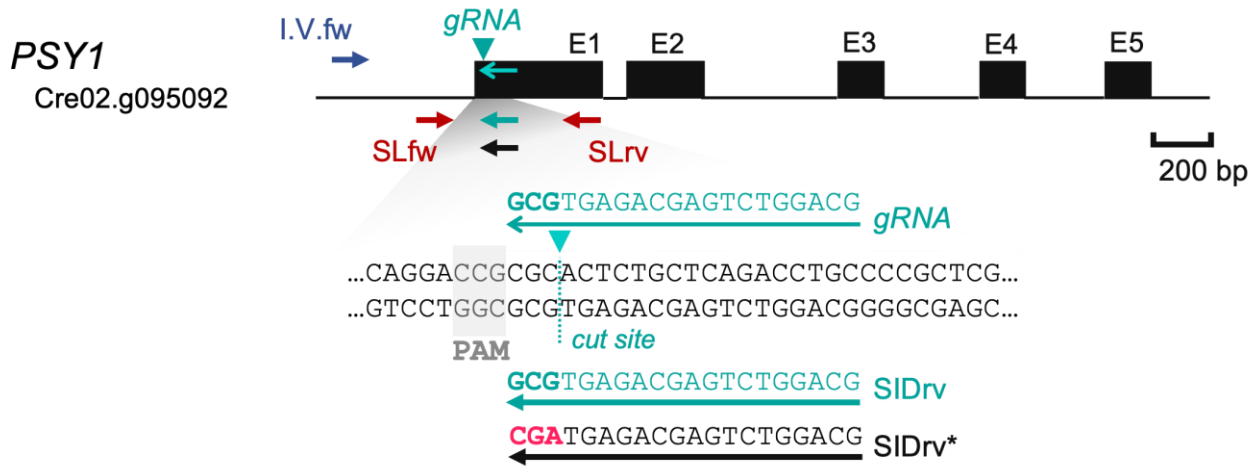

Fig. 1. CRISPR-Cas9 design to target *PSY1* gene. Scaled representation of the *PSY1* gene is shown with its five exons (black boxes, E1-5). A gRNA was designed in the beginning of the first exon of this gene: the sequence is shown below (light blue), with the predicted cut site by the Cas9 (triangle) and the PAM region (grey). In this example, 4 screening primers were designed, two for the screening of large insertions (SLfw and SLrv, red) and two for the screening of short indels (SID). SID primers are both reverse primers which are paired with SLfw to detect short indels by PCR: SIDrv (light blue) features the same sequence as the gRNA, while SIDrv* (black) features the 3 bases at 3' changed (light red), and serves as a negative control, to check that mismatches caused by the introduction of short indels at this *locus* do not result in PCR amplification. For the *in vitro* test a single forward primer was designed (I.V.fw, blue), and SLrv was employed as reverse primer for this test.

Step 2: Primer test

Time of execution: one week.

2.1 Obtain a crude gDNA extract. Scrape Chlamydomonas cells (approximately the size of a lentil) from a recently refreshed plate (1-3 weeks) using a sterile toothpick and transfer to a 1.5 mL tube. Resuspend cells in 30-50 µL of 10 mM EDTA pH 8 with vigorous vortexing until the suspension is homogenous. Heat suspension at 100ºC for 5 min, and transfer to ice for 5 min. Centrifuge at max speed for 3 min, and collect the supernatant into a new 1.5 mL tube: this is your crude gDNA extract.

Note 2.1. The use of 10 mM EDTA as buffer for gDNA crude extracts is standard [10,12,20], but failed PCR amplifications could be caused by EDTA chelating effects on Mg. In this case, alternative buffers can be used for gDNA extraction (see Troubleshooting).

2.2 Primer test: Perform a PCR using the designed primer pairs choosing the most suitable annealing temperature (T_m) according to the primer pair specifications (typically 3–5°C lower than the lowest T_m of the primers). Both the content of a single 10 µL PCR reaction and the PCR cycling conditions are indicated in Table 1. Perform an electrophoresis run of PCR reactions on a 1% agarose gel: the optimum T_m temperature should give the expected band without unspecific amplification.

Note 2.2. In case of failed PCRs (no amplification or unspecific amplification) see Troubleshooting.

2.3 Screening Indel primer test. Perform a PCR combining the SLfw primer with either the SIDrv or the SIDrv* primer. If your indel primers are suitable for detecting short indels, the PCR performed using SLfw+SIDrv should amplify a band, whereas the PCR performed using SLfw+SIDrv* should not amplify anything.

2.4 Screening Large insertions primer test. Perform a PCR using the SLfw+SLrv primer combination.

2.5 *In vitro* primer test. Perform a PCR using the I.V.fw+I.V.rv primer combination.

Note 2.5. Once successfully confirmed, proceed with purchasing gRNAs and with Step 3. If test PCRs give unspecific bands, even after correcting with troubleshooting adjustments, repeat using different primer sequences. If the indel primer test is unsuccessful, even after correcting with troubleshooting adjustments, repeat from Step 1.1 using a different gRNAs sequence.

For *PSY1*, 64 ºC Tm was employed for all PCRs in the protocol (Fig. 2A-C). Primer pair SLfw+SLrv gave a unique band of the expected size (Fig. 2A). PCR with indel test combination SLfw+SIDrv showed the presence of the expected size amplicon (Fig. 2B), whereas the indel test combination SLfw+SIDrv* did not amplify (Fig. 2C). These results indicated that the designed indel primers were suitable for detecting small base mismatches resulting from the presence of short indels in the gRNA target site. Primer pair I.V.fw+I.V.rv gave a unique band of the expected size (Fig. 2D).

Step 3: Cas9 *in vitro* cleavage test

Time of execution: two days (one day to prepare and purify PCR amplicons and one day to perform the in vitro digestion and electrophoresis run of the digested fragments).
This step is recommended to test functionality of Cas9 and a given gRNA when used for the first time. PSY1 can be used as a positive control.

3.1 Prepare PCR amplicons for *in vitro* digestion. For each gRNA prepare a 60 µL PCR using *in vitro* test primers (I.V.fw+I.V.rv) and scaling up the reagents of Table 1. Purify the PCR product with a PCR cleanup kit and elute in nuclease free H_2O. Measure DNA concentration. For the *in vitro* test, a total of 750 ng of amplicon is required, in a concentration of minimum 75 ng/µL (lower concentrations can be concentrated using a vacuum concentrator).

3.2 Assemble CRISPR-Cas9 RNPs. Prepare RNPs following the procedure explained in “Assembly of the CRISPR-Cas9 machinery” (*in vitro* test).

Table 1
Single PCR reaction in 10 µL volume. For the annealing step, choose the most suitable T_m according to the primer pair specifications (typically 3–5°C lower than the lowest T_m of the primers): the optimal T_m should yield the highest amount of amplicon without unspecific amplification.

Single PCR reaction in 10 µL volume

Reagent		Volume
NZYTaq II Green Master Mix	2X	5 µL
DMSO	-	1 µL
Primer Fw	10 µM	0.6 µL
Primer Rv	10 µM	0.6 µL
gDNA crude extract	-	1 µL
Nuclease free water	-	1.8 µL
TOTAL		10 µL

Cycling conditions

Step	Temperature	Time	
Initial Denaturation	95 ºC	3 min	
Denaturation	95 ºC	30 s	X40 cycles
Annealing	X	30 s	
Extension	72 ºC	1 min	
Final Extension	72 ºC	5 min	
Store	4 ºC	∞	

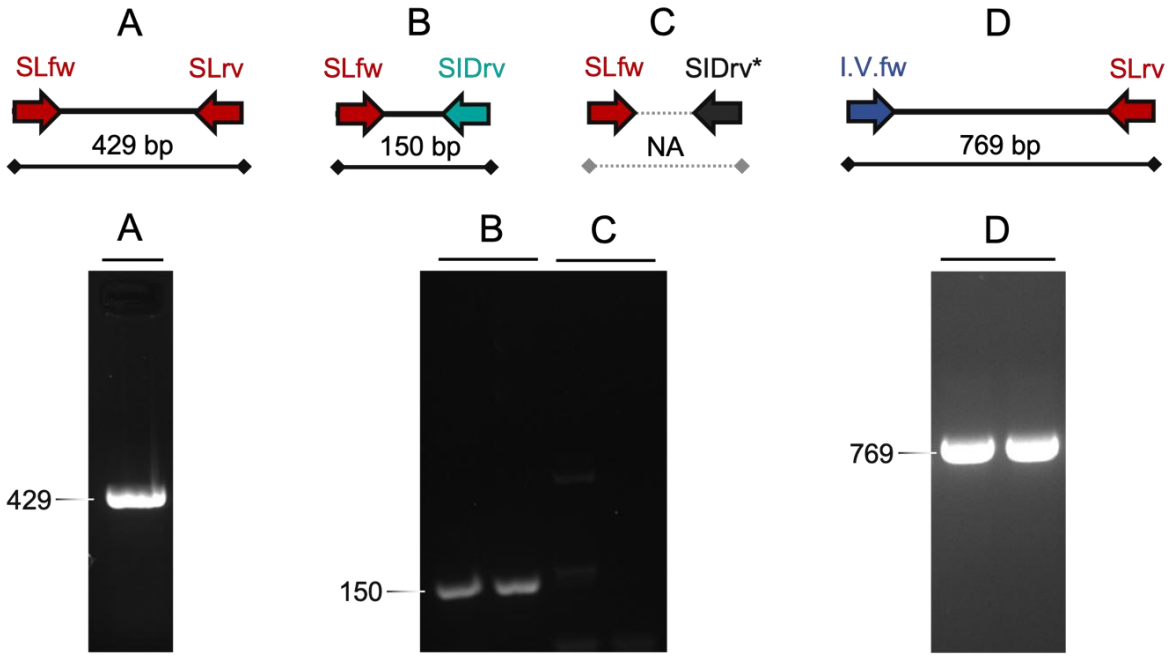

Fig. 2. PCR test of all the designed primers for *PSY1*. All PCR reactions were performed at 64 ºC and yielded bands with the length indicated on top or no band (NA), as expected. A) PCR for the screening of large insertions (SLfw+SLrv), B) PCR for the screening of short indels (SLfw+SIDrv), C) negative control of short indels screening (SLfw+SIDrv*), D) in vitro test PCR (I.V.fw+SLrv). Two technical replicates are shown for each amplicon. Uncropped electrophoresis gel images including the DNA ladder are provided in Supplemental Fig. 1.

3.3 Digest amplicons with the assembled RNPs. Combine RNPs with the purified amplicons and Buffer O (Thermofisher) and follow the reaction procedure specified in Table 2.

3.4 Clean digested amplicons and visualize bands. Purify the PCR product with a PCR cleanup kit and elute in 20 µL of Elution Buffer or nuclease free water. Combine this volume with 6X Loading Dye (Thermo Fisher). Perform an electrophoresis run of 20 µL of this mix on a 1% agarose gel: 2 bands corresponding to the digested fragments from the original amplicon and with the expected length should be observed. It is likely that original undigested amplicon will also be visible. The higher the amount of digested fragments compared to the original undigested amplicon the more efficient the digestion *in vitro*.

Note 3.4. A PCR clean up step is necessary to ensure that Cas9 is released from DNA and will not interfere with gel visualization of the DNA.

Table 2

in vitro digestion reaction. See "Assembly of the CRISPR-Cas9 machinery" to obtain RNPs.

in vitro digestion		
Reagent		***in vitro* test**
RNPs	2.75 µM	3.4 µL
Purified amplicon	75 ng μL^{-1}	10 µL
Buffer O	10X	1.5 µL
Nuclease free water	-	0.6 µL
TOTAL	-	15 µL

***Reaction condition**: 37 ºC for 60 min, 98 ºC for 5 min and store at 4ºC*

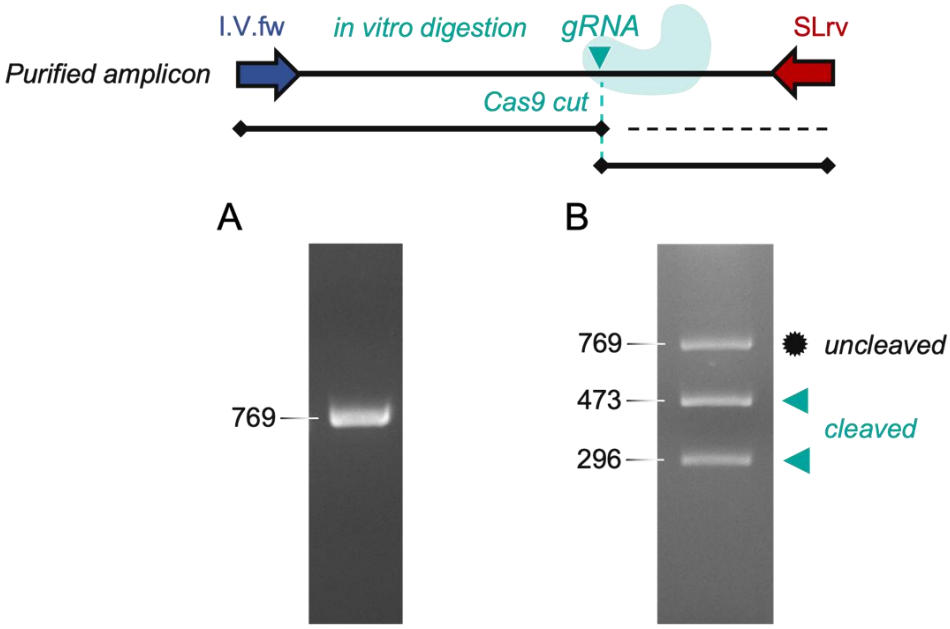

Fig. 3. *In vitro* test of CRISPR machinery designed to target *PSY1*. PCR was performed as indicated in Fig. 1 (I.V.fw+SLrv) and yielded amplicons of 769 bp; these were afterwards purified (left electrophoresis gel). *In vitro* digestion gave the two expected fragments of 473 and 296 bp (cleaved, right electrophoresis gel). The additional largest band corresponds to rests of the original undigested (uncleaved) amplicons. Uncropped electrophoresis gel images including the DNA ladder are provided in Supplemental Fig. 2.

To test the functionality of our designed gRNA to target *PSY1*, first an amplicon of 769 bp was generated using primers I.V.fw+SLrv and cleaned up (Fig. 3A). After *in vitro* digestion the expected digested fragments were obtained (fragments of 473 and 296 bp) (Fig. 3B, cleaved). A higher size band corresponding to the original undigested amplicon was also observed (Fig. 3B, uncleaved).

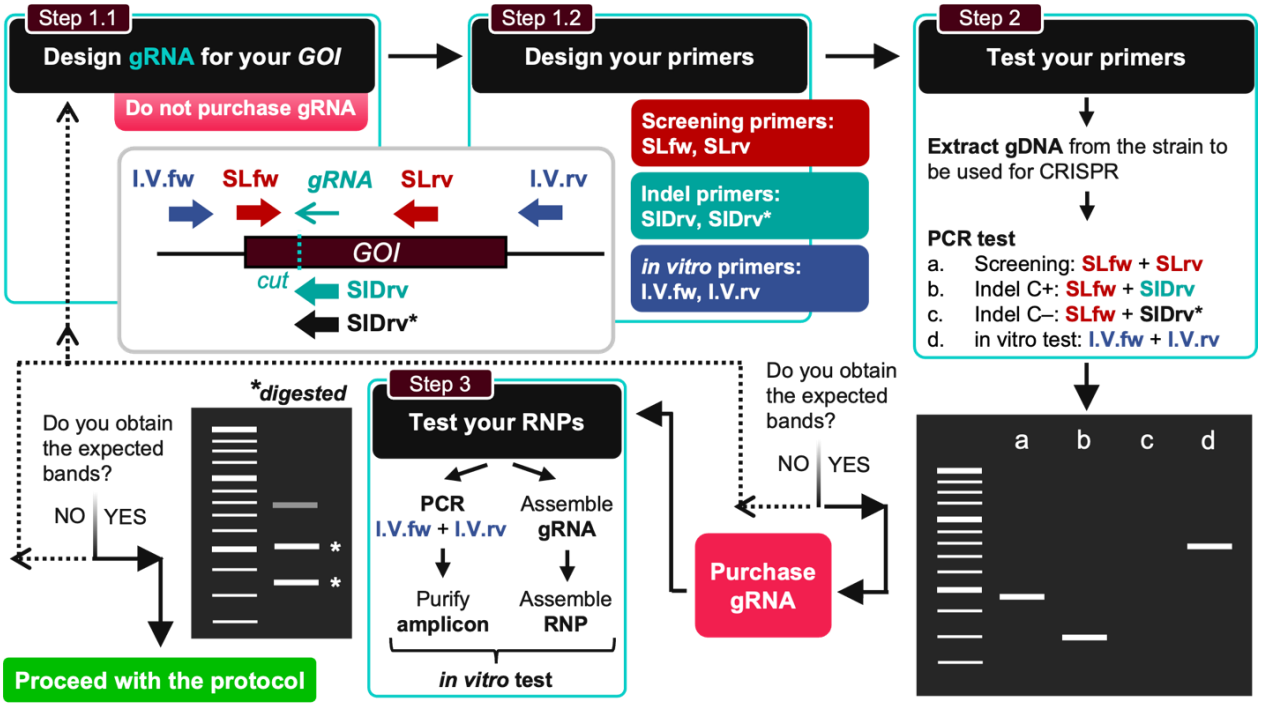

Fig. 4. General overview of the CRISPR design (Step 1-3). Step 1.1. Design gRNA(s) for your gene of interest (*GOI*), but do not purchase gRNA(s) before successfully testing all primers. Step 1.2 Design all the primers required for this protocol, which will depend on the target site of the chosen gRNA(s): screening primers (SLfw, SLrv), indel primers (SIDrv, SIDrv*) and *in vitro* primers (I.V.fw, I.V.rv). Step 2. Test the designed primers (Step 2), by performing 4 different PCRs with gDNA from the strain to be used for CRISPR (follow indications in Table 1). If PCRs give the expected bands then purchase the designed gRNA(s); if not, go back to Step 1.1 and design new gRNA(s). Step 3. Test your RNPs (*in vitro* test): for this purpose, perform a PCR using I.V. primers and purify the resulting amplicon; also, assemble RNPs as indicated in "Assembly of the CRISPR-Cas9 machinery" following iv (*in vitro* test) reagent proportions; finally, *in vitro* digest the purified amplicon with the assembled RNPs, purify the reaction and perform an electrophoresis run. *PSY1*, as described here, can be used as positive control in Step 3.

Prior to transformation

Time of execution: five days (time needed to grow Chlamydomonas cells in synchronizing conditions).

- Grow Chlamydomonas cells in synchronizing conditions. Inoculate a tris-acetate phosphate (TAP) liquid culture with scraped cells from an agar plate of the strain you wish to transform, and grow in alternating light and dark conditions (12:12), under 22-23ºC in white light (~50 µmol m^{-2} s^{-1}) for at least 5 days and under mild shaking (150 rpm). Dilute culture on day 3 so that cells are in logarithmic growth phase at day 5 (2-4 x 10^6 mL^{-1}). Keep track of the cell concentration of your culture, preferably by cell counting, using a cell counter or manually: take a 200 µL sample, add 20 µL of iodine (0.25% w/v in EtOH) to immobilize cells, load 10 µL of sample in an hemocytometer and count cells with the help of an optical microscope.
- Prepare linearized *pAPHVIII*-containing plasmid. Digest a *pAPHVIII* (paromomycin resistance)-containing plasmid using a restriction enzyme that performs a single cut outside of the paromomycin cassette. Ensure successful digestion by running an aliquot on a 1% agarose gel. Inactivate restriction enzyme at 80 ºC for 10 min, and keep it in sterile conditions. For each transformation, a total of 2 µg of linearized plasmid at a concentration of 200 ng μL^{-1} is required.

- Prepare TAP-agar + paromomycin plates. Combine melted TAP-agar with filter-sterilized paromomycin sulphate (for a final concentration of 10 µg mL^{-1}) and spread into square Petri dishes (120x120 mm) with approximately 100 mL selection medium each.

The *pAPHVIII* containing plasmid pSL18 (Chlamydomonas Resource Center) was employed to generate *psy1* mutants. This was linearized using EcoRV (Thermo Fisher) which performs a single cut in this plasmid. The digestion reaction was carried out following manufacturer's instructions.

Step 4: Transformation

Time of execution: 2 days (one day for electroporation and one day for recovery and plating).
Important. The following steps (except the last one) should be done during the same day. All steps should be performed under sterile conditions.

4.1 Cell preparation and heat shock. Determine the concentration of cells growing at logarithmic growth phase. Calculate the amount of cells that you will need to perform the planned transformations, and transfer the necessary volume of culture into a 50 mL tube. Perform a mild centrifugation (6 min at 2500 rpm). Resuspend in the appropriate amount of MAX Efficiency™ Transformation Reagent for Algae (Thermo Fisher, ME) plus sterilized 1 M sucrose (for a final concentration of 40 mM) to obtain a suspension of $2x10^8$ cells mL^{-1}, and transfer cells into a 1.5 mL sterile tube. Apply heat shock using a thermoshaker at 40 ºC for 30 min with mild shaking (350 rpm). Let the cells recover for 30 min at RT (22-25 ºC), always with mild shaking.
Note 4.1.1. See Troubleshooting (h) for best time to harvest cells during the day cycle.
Note 4.2.2. Autolysin solution can be used instead of ME as shown by Picariello et al. [12].

4.2 Assemble CRISPR-Cas9 RNPs. Prepare RNPs following the procedure explained in "Assembly of the CRISPR-Cas9 machinery" (transformation). Keep RNPs on ice.

4.3 Transform by electroporation. Combine 120 µL of heat-shocked cells (at $2x10^8$ cells mL^{-1}) with 10 µL of RNPs and 10 µL of linearized plasmid (200 ng/µL). This 140 µL mix will be enough to transform the gRNA in 3 independent electroporations (40 µL each). Let the suspension sit for 10 min on ice. Prepare a 24-well plate with 600 µL of liquid TAP medium in each well. Next, wash the inside of a 2 mm-gap electroporation cuvette with TAP from one of the wells, using a sterile Pasteur pipette with thin and long tip. Completely remove the excess medium from the cuvette, and load 40 µL of the mix. Make sure there are no air bubbles and the volume is evenly distributed at the bottom of the cuvette. Load the cuvette in the electroporation chamber of the NEPA21 (NEPAGENE). Measure impedance: the value should be between 0.2 and 0.4 KΩ. Setup electroporation conditions as shown in Table 3. Electroporate. With the help of the pipette, transfer the 40 µL containing the electroporated cells into a sterile 1.5 mL tube. The same cuvette can be used to perform electroporation of the other 2 replicates (2 x 40 µL) from the same mix.
Note 4.3.1. It is important that the volume of 40 µL is exact.
Note 4.3.2. The electroporator needs to be setup in a sterile hood to keep conditions sterile during transformation.
Note 4.3.3. In case of using a different electroporator see Troubleshooting (f).
Note 4.3.4. We recommend including a control consisting of heat-shocked cells with linearized plasmid, but not RNPs (which should give colonies on a selection plate), and a control consisting of heat-shocked cells only (which should not render any colonies on the selection plate). These controls are only needed once for each strain and plasmid employed.
Note 4.3.5. The use of the 24-well plate is recommended given that the capacity of the wells (600 µL) is a convenient volume for all the described procedures. Combining the necessary washes, control and triplicates, one 24-well plate is sufficient for 5 transformation mixes (each in triplicate, therefore a total of 15 transformations plus 2 controls if using one strain and marker plasmid). Each gRNA transformation (triplicates) can use the same cuvette.

4.4 16 ºC incubation. Incubate tubes containing the electroporated cells at 16 ºC for 1 h (as indicated by Picariello et al. [12]).

4.5 Recovery: Transfer the 40 µL electroporated cells into the 600 µL TAP-filled 24-well plate (do not employ wells used for cuvette washes of Step 4.3). Seal the plate with parafilm and incubate cells at 24 ºC and gentle shaking (150 rpm), under constant light (50 µmol m^{-2} s^{-1}) overnight. If the mutation might confer photosensitivity (i.e. *psy1* mutants), wrap the plate in aluminum foil and perform recovery in the dark.

4.6 Plating. Gently plate the recovered electroporated cells (640 µL from one well) onto TAP-agar + paromomycin plates with the help of a sterile Drigalski spreader. Air dry plates for 1 h. Seal plates with parafilm, incubate plates upside down at 24ºC in continuous light (50 µmol m^{-2} s^{-1}) or in the dark if the mutation might confer photosensitivity. Colonies should appear after 2-4 weeks depending on the strain and light conditions. Using the impedance range of this protocol, 5-20 colonies should appear on each plate.

Note 4.6. In our experience for PSY1, the % of mutants was higher when impedance values were low (i.e. above 0.5 KΩ we did not generate any mutant, whereas with low values -below 0.35 KΩ- very few colonies were obtained but many contained mutations).

Table 3
Components of the electroporation mix and NEPA21 electroporator settings. These settings might require optimization depending on the electroporator and strain employed (see Troubleshooting (f)).

Electroporation

Reagent		*in vitro* test
Treated Chlamy cells	2 10^8 cells mL^{-1}	120 µL
RNPs	3.125 µM	10 µL
Linearized plasmid	200 ng $µL^{-1}$	10 µL
TOTAL	-	140 µL

NEPA21 Settings

Pulse	Voltage	Pulse Length	Interval	Nº of pulses	Decay Rate	Polarity
Poring Pulse	300 V	8 ms	50 ms	1	40 %	+
Transfer Pulse	20 V	50 ms	50 ms	5	40 %	+/-

Cell-wall containing CC-124 strain (Chlamydomonas Resource Center) was employed to generate *psy1* mutants. Transformation was performed using a NEPA21 electroporator (NEPAGENE): the settings displayed in Table 3 will likely work for most cell-wall containing strains, but cell-wall less strains require different electroporation settings (Kelterborn et al. [11]). Also, other electroporators have been shown to be successful for transformation using pre-assembled CRISPR-Cas9 RNPs [4,12].

Assembly of the CRISPR-Cas9 machinery

Under sterile conditions:

- Resuspend and aliquot crRNA and tracrRNA. Resuspend lyophilized crRNA and tracrRNA in IDTE pH 7.5 (1X TE Solution) (IDT) at 40 µM. Prepare single use aliquots in sterile 0.2 mL tubes and store at -80 ºC, as several cycles of freezing and thawing have been shown to decrease efficiency of mutant generation [12].
- Prepare gRNAs. Perform the reaction indicated in Table 4. Less concentration is used for *in vitro* tests.
  Note gRNAs. Although gRNAs can be ordered already assembled, we have always purchased gRNAs separately and assembled them ourselves as indicated.

Table 4
Assembly of gRNAs. Depending on the use of RNPs (*in vitro* / transformation) different amounts of the indicated reagents are required. Final concentration of gRNA is indicated at the bottom for both *in vitro* test (iv) and transformation (T).

gRNA assembly

Reagent		*in vitro* test	Transformation
crRNA	40 µM	1.05 µL	1.5 µL
tracrRNA	40 µM	1.05 µL	1.5 µL
DUPLEX Buffer	-	3.9 µL	3 µL
TOTAL	7 µM (iv) / 10 µM (T)	6 µL	6 µL

***Reaction condition**: 95 ºC for 2 min, ramp 95-to-20 ºC at 0.1 ºC s^{-1}*

- Prepare RNPs. Dilute (if necessary) SpCas9 (IDT) at 11 µM in DUPLEX Buffer. Perform the reaction indicated in Table 5 (Transformation).
  Note RNPs. The volume of Buffer O used highly affects impedance values (due to its BSA content): the higher the amount of this buffer the lower the impedance values.

Table 5
Assembly of RNPs. Depending on the use of RNPs (*in vitro* / transformation) different amounts of the indicated reagents are required. Final concentration of RNPs is indicated at the bottom for both *in vitro* test (iv) and transformation (T).

RNP assembly

Reagent		*in vitro* test	Transformation
gRNA	7 µM (iv) / 10 µL (T)	2 µL	4.4 µL
Cas9	11 µM	1 µL	3 µL
DUPLEX Buffer	-	1 µL	1.4 µL
Buffer O	10X	-	2.2 µL
TOTAL	2.75 µM (iv) / 3.125 µM (T)	4 µL	11 µL

***Reaction condition**: 37 ºC for 15 min, keep at 4 ºC*

Important. If CRISPR reagents are purchased from a different company it might be preferrable to use CRISPR buffers specified by the manufacturer (all buffers can be replaced except Buffer O, which can also be homemade prepared following manufacturers specifications). In this case, keep concentrations of CRISPR components as indicated in these tables.

Step 5: Screening for large-insertion and short-indel mutants

Time of execution. Colonies will appear 2-4 weeks after electroporation (depending on the strain used and light conditions). Screening takes approximately two days.

5.1 Isolate colonies and extract gDNA. Wait until colonies reach 3-4 mm of diameter (2-4 weeks depending on the strain and light conditions). For large colonies, pick colonies with a sterile toothpick: transfer a small amount to a fresh TAP-agar plate and use the rest to perform a crude gDNA extract as explained in 2.1. For smaller colonies even after 4 weeks, streak on a fresh TAP-agar plate and once grown take a small amount following instructions in 2.1.
Note 5.1. This procedure can be optimized to obtain crude gDNA from a high number of colonies at the same time, by performing the extractions in a 96-well plate as explained in Kelterborn et al. [11].

5.2 Screening for long insertions and short indels. For each colony, perform two PCRs as indicated in Step 2: a PCR to detect large insertions using primers SLfw+SLrv, and a second PCR to detect indels using primers SIDfw+SIDrv. Run PCRs on a 2% agarose gel. If no mutations are present in the target gene, both PCR reactions will yield a band of wild-type (wt) size; if a large insertion is present at the target site, PCR with SL primers yield a band of higher size; in the case of a small indel, PCR with SL primers will yield a band with the same size as the wt, but PCR with SID primers will not show amplification.
Note 5.2. If the insertion is large or if it involves rearrangement of the site for primer annealing, it is possible that none of the 2 PCRs yield a band. In this situation, PCR conditions and/or primer sequence will need to be adjusted. We also recommend running a control with a primer pair to amplify in a different region to control for the quality of the DNA extract.

5.3 Isolate colonies. Pick the original colony carrying a detected mutation and streak onto a fresh plate to obtain isolated colonies. Repeat SL PCR on a few isolated colonies to confirm analysis. This step controls for heterogeneity in the original colony and ensures singling of the mutant of interest.

5.4 Sequence of mutants. Perform a PCR with SL primers of a singled mutant colony in 40 µL total volume following the concentrations indicated in Step 2. Run 5 µL of this reaction on an agarose gel to confirm presence of the expected amplicon. Perform a PCR clean-up with the rest of the reaction, elute in the appropriate volume and sequence using the same SL primers.
Note 5.4. Sequencing of the obtained amplicon may fail using SL primers. This can be solved by cloning the amplicon into a TOPO type vector (Thermo Fisher) and using a vector primer for sequencing.

Fig. 5 shows colonies obtained after targeting *PSY1*. A number of successful *psy1* mutants could be detected by the pale green coloration of the colonies (Fig. 5A). PCR for these colonies using the SL and SID primer combinations detected both large insertion as well as indel mutants (Fig. 5B,C). The sequenced insertional mutant feature incorporation of a fragment of the marker plasmid through non-homologous end joining. Indel mutant sequencing revealed a mutant carrying 1 base insertion, and a mutant carrying a 11-base pair deletion, both at the Cas9 cutting site (Fig. 5C).

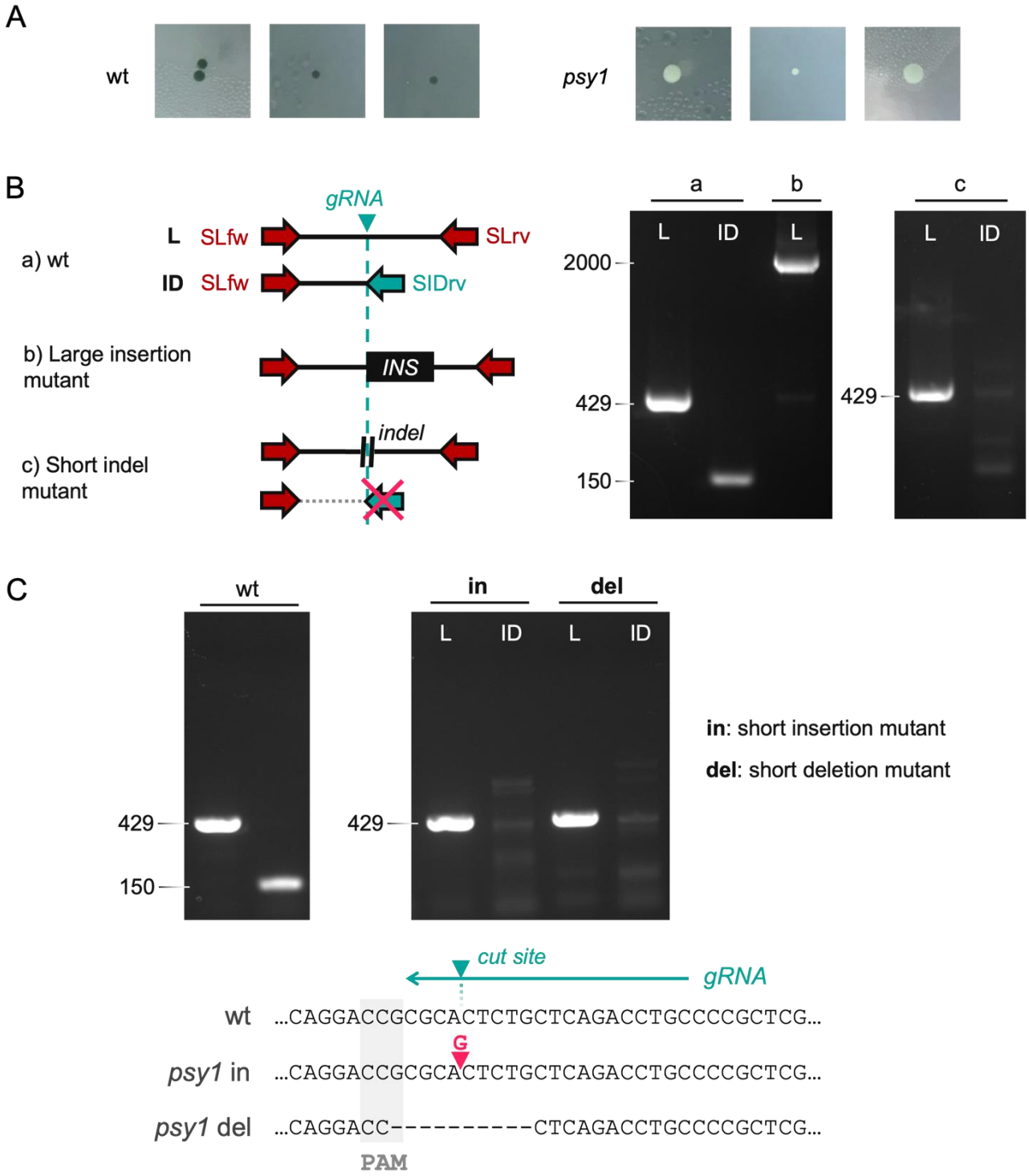

Fig. 5. A. Screening of *psy1* mutants by phenotype: *psy1* mutants exhibit pale green coloration. B. Screening of *psy1* mutants by genotype was carried out using primers to detect large insertions (SLfw+SLrv, giving L band) and short indels (SLfw+SIDrv, giving ID band). Screening by genotype resulted in three possible scenarios: a) wt colonies displayed both L and ID bands with the length expected in the absence of mutations at the cut site; b) large insertion mutants displayed L bands with much higher length; c) short indel mutants displayed the same L band with the same size as the wt, but didn't display the ID band. C. Screening and sequencing of *psy1* mutants from the latter scenario, one with a short insertion (in) and one with a short deletion (del). Uncropped electrophoresis gel images including the DNA ladder are provided in Supplemental Fig. 3.

Protocol validation

This protocol was employed to successfully generate *psy1* knockout mutants carrying large insertions or small indels. Importantly, this could be achieved in just 5 weeks from CRISPR design to the sequencing of the isolated mutants, using tools and reagents which are commercially available. Compared to other recent CRISPR methods for Chlamydomonas, our protocol is easy and quick to implement as it does not require specific procedures such as cloning or homemade production of CRISPR reagents (Table 6).

Here, we used *PSY1* due to the characteristic pale color of *psy1* mutant colonies (Fig. 5A). Initial screening with SL primers revealed that some *psy1* mutants did not carry large insertions and therefore were instrumental in setting up the strategy to screen for small indel mutants, a valuable feature of our protocol. Our designed indel primers do not allow amplification by PCR in the presence of modifications at the Cas9 target site, that result not only from large insertions but also from the presence of short indels (Fig. 5B). Remarkably, we found this strategy to be able to detect modifications at the target site as small as an insertion of a single nucleotide (Fig. 5C).

We have used this protocol to generate and identify mutants for *GOI*s other than *PSY1* that did not feature a visible phenotype. At the impedance range indicated (0.2-0.4 KΩ) we usually obtained a small number of colonies (<50), and gDNA extraction and screening PCRs were performed one-by-one. For larger number of colonies, the procedure can be performed in 96-well plates as described by

Table 6

Comparison of recent CRISPR protocols developed for Chlamydomonas. All protocols (ours included) share three common steps: 1) *in vitro* assembly of RNPs, 2) transformation by electroporation and 3) mutant selection.

[1] Mutation efficiency refers to the percentage of mutant colonies out of all the screened colonies (resistance-selected). *"Not applicable"*, when screened colonies were selected based on phenotype and numbers compared to total colonies are not provided; "*Not specified*", when efficiency is not discussed in original publication.

[2] Requirement of specific procedures in the protocol such as time-consuming cloning or homemade production of CRISPR reagents.

"PCR screen on 96-well plates": gDNA extraction + PCR screening of multiple selected colonies is performed individually. *"Pooled colony PCR screen"*: gDNA extraction + PCR screening of multiple combined colonies. "*qPCR*": quantitative PCR.

Previous protocols	Genome editing strategy	Screening method	Mutation efficiency[1]	Genes tested	Specific procedures required[2]
Kelterborn et al. 2022	HR of a custom cassette (NHEJ fallback)	PCR screen on 96-well plates	*Not specified*	*SNRK2.2*	- Synthesis and purification of SpCas9
Picariello et al. 2020	HR of a resistance marker cassette (NHEJ fallback)	PCR screen on 96-well plates	- Total (including NHEJ): 30-93% - Double gene targets: 3-15%	*IFT81, FAP70, MOT17, CDPK13, CEP131, IFT43*	- Cloning of resistance marker cassette - Autolysin preparation
Angstenberger et al. 2020	HR of a resistance marker cassette (NHEJ fallback)	PCR screen of phenotype-positive colonies	- Total (including NHEJ): 13.8-14.3% - HR: 30-40% of mutant colonies	*FTSY*	- Cloning of resistance marker cassette - Synthesis and purification of recombinant Cas9 - *in vitro* transcription of gRNAs
Dhokane et al. 2020	NHEJ and HR of a resistance marker cassette	PCR screen of phenotype-positive colonies	*Not applicable*	*MAA7*	- *in vitro* transcription of gRNAs - (For HR: cloning of resistance marker cassette)
Ferenczi et al. 2024	SSTR (NHEJ fallback)	PCR screen of phenotype-positive colonies	*Not applicable*	*FKB12, FTSY, SRP43*	- Synthesis and purification of Cas9 and/or Cas12a
Chen et al. 2023	Custom gene editing by HR	Pooled colony PCR screen	- Precise gene editing: 1.4-16% depending on the gene and editing strategy	*CrKU80, FTSY, VIPP1, IFT46, CrTET1, FLA3, FLA10, MAA7*	- Cloning of custom donor DNA - Synthesis and purification of SpCas9 - *in vitro* transcription of gRNAs
Nievergelt et al. 2024	Custom gene editing by HR	qPCR screen on 96-well plates	- Overall editing frequency: 65-90% - Precise gene editing: 20%	*IFT46*	- Cloning of custom donor DNA - Autolysin preparation
This protocol	NHEJ	PCR screen (large insertions and short indels detection)	- Total: 7-60% depending on the gene - Short indels: **15-50%** of mutants depending on the gene	*PSY1* (other *GOI* discussed)	**NO**

Kelterborn et al. [11] to reduce protocol times. In addition, although our protocol requires PCR analysis of single colonies to detect small indels, a pooled-PCR screening strategy might be implemented in Chlamydomonas based on the protocol described by Angelopoulou et al. in mouse cell cultures [21] based on PCR-induced mutagenesis-restriction fragment polymorphism (PIM-RFLP).
The overall efficiency of mutant generation for *PSY1* shown here (number of positive mutants vs total number of colonies) was 34% and 60% in two separate transformation runs (11 out 32 colonies, and 9 out of 15 colonies). In accordance to other reports, efficiency can highly vary among targeted genes and gRNA sequences. Indeed, we experienced a variety of efficiencies when targeting other genes using this same protocol (ranging 7-60%, comparable to other recent CRISPR protocols, see Table 6) and *PSY1* was our highest efficiency gene. Frequency of indel mutants ranged between 13-50% of all detected mutants.
In summary, our protocol provides a quick to implement and easy method for the generation of CRISPR-Cas9 knockout mutants in Chlamydomonas, including a strategy to identify short indels at the Cas9 target site and thus increasing mutant detection efficiency.

Troubleshooting

a) No PCR amplification or unspecific bands when using SL primers
Perform a gradient PCR to evaluate alternative annealing temperatures (T_m). DMSO amount can also be increased (up to 20% of final PCR reaction volume). When performing gDNA extractions, test different amounts of starting material and/or replace 10 mM EDTA pH 8 with alternative buffers as indicated by Kelterborn et al. [11], or Dhokane et al. [15]. If none of these adjustments work, design a new primer pair combination.

b) No PCR amplification or unspecific bands when using SIDrv primer
Follow the recommendations indicated in a). If none of these adjustments work, redesign both gRNA and indel primers. Remember to successfully complete Steps 1 and 2 before purchasing CRISPR-Cas9 reagents.

c) PCR amplification when using SIDrv primer*
Perform a gradient PCR to evaluate alternative annealing temperatures (T_m). If amplification is still observed, redesign gRNA and indel primers. Remember to successfully complete Steps 1 and 2 before purchasing CRISPR-Cas9 reagents.

d) We use a different DNA polymerase for PCR reactions
Several DNA polymerases and PCR kits have been successful for performing PCRs in Chlamydomonas, as reported by other CRISPR protocols [10-14]. When performing PCRs in this species for the first time, or in case of failed PCRs using a different DNA polymerase, we recommend to employ the PCR reagents and the proportions we indicate in this protocol.

e) Impedance values are not in the range of 0.2-0.4 KΩ
If impedance values are above this range, slightly increase the amount of Buffer O when preparing RNPs, or increase the amount of RNPs during the electroporation step. Impedance values up to 0.5 KΩ might be used, but above 0.5 KΩ we were not able to generate any mutant.
If impedance values are below the indicated range, decrease the amount of Buffer O and/or purify the linearized resistance-carrying plasmid after enzymatic digestion. Also, abnormally low levels of impedance can be an indication of cell lysis which can critically affect the generation of mutant colonies; check cells are in good health when harvesting them for electroporation and, if necessary, adjust growth conditions.

Typically, the higher the impedance values the more colonies obtained, but with decreased mutant generation efficiency. Values can also be adjusted by slightly changing the volume of electroporation mix inside the cuvette (2-3 µL at most) as indicated by Kelterborn et al. [11]: higher electroporation volumes decrease impedance values, and vice versa.

f) We have a different electroporator which does not measure the impedance value

Perform an electroporation trial by electroporating with treated cells and the linearized resistance-carrying plasmid. Test the effect of adding 10 µL of DUPLEX Buffer (or the employed CRISPR Buffer) to the electroporation mix with increasing amounts of Buffer O to setup the conditions to get 10-20 colonies/plate. Additional indications on the use of alternative electroporators can be found in Shin et al. [4], Picariello et al. [12] or Chen et al. [13] to mention a few.

g) No colonies obtained after electroporation

Check that cells are in good health before starting the transformation step. Make sure impedance values are within the range indicated in e). Perform an electroporation control using heat-shocked treated cells and the resistance-carrying plasmid, which should give much higher impedance values (>0.7 KΩ), due to the absence of the BSA-containing Buffer O. In this test, values <0.7 KΩ might be indicative of cell lysis, and/or that the linearized resistance-carrying plasmid needs to be purified after enzymatic digestion, then follow recommendations indicated in e). Much higher impedance values (>1.2 KΩ) do not represent an issue in these tests if the impedance is in the correct range in the presence of RNPs.

h) Transformed colonies are obtained but no mutants are detected.

Make sure to perform the *in vitro* cleavage test to test functionality of the Cas9 and the gRNA. Check impedance values are in the indicated range and cells are in good health before starting the transformation step. The time of transformation during the day cycle can also impact CRISPR efficiency. As described by Angstenberger et al. [10], 4h after the switch from dark to light would be the best option, given that cells are in G1 phase and NHEJ is the dominant DNA repairing mechanism. In addition, the accessibility of the locus to be edited might also have an impact, and editing might be more favorable in the time window when your *GOI* is expressed (can be checked in Strenkert et al. [22]). If none of these recommendations work, design new gRNAs.

i) Contamination on the selection plates

Make sure all components are sterile and manipulation of reagents is performed in strict sterile conditions. Check that the strain and cell culture do not carry any contamination. Make sure that the linearized resistance-carrying plasmid is heated at 80 ºC before transformation. The electroporation cell should be cleaned with 70% ethanol before its use and opened in sterile conditions. When re-utilizing electroporation cuvettes, clean them with ethanol and UV-sterilized them before using. If it is still a problem, ampicillin against bacteria (100-500 µg/mL) or cefotoxine against fungi (100 µg/mL) can be added to the media and the plates [11].

Limitations

Our protocol features the following limitations:

- **Random insertion of the resistance cassette in the genome**. To assign mutant phenotypes to the loss-of-function of a particular *GOI*, we recommend generating multiple mutants and/or complementing the mutant.
- **Variable efficiency of gene editing.** Mutant generation efficiency for different *loci* and/or gRNAs might vary, although a high gene editing efficiency is possible using this protocol as exemplified here for *PSY1*.
- **No high-throughput screening for indels.** High-throughput screening methods (pooling colonies) can be used to screen for large insertion mutants. Detection of small indels by PCR as described in this protocol need to be performed on single colonies.

Acknowledgements

We are grateful to Peter Hegemann for providing training and resources. This work was supported by grants PGC2018-099987-B-I00 and PID2021-122288NB-I00 to E.M., funded by MICIU/AEI /10.13039/501100011033/ and by "ERDF A way of making Europe", and from the CERCA Programme/Generalitat de Catalunya (Project References 2017SGR-718 and 2021SGR-792 to E.M.). We acknowledge financial support from the Spanish Ministry of Economy and Competitiveness, through the 'Severo Ochoa Programme for Centres of Excellence in R&D' CEX2019-000902-S funded by MCIN/AEI/10.13039/501100011033. M.A.DS. was supported by the predoctoral program AGAUR-FI ajuts (2020 FI_B_00343) of the Secretariat of Universities and Research of the Department of Research and Universities of the Generalitat of Catalonia and the European Social Plus Fund, C. S.-R. was supported by a FPI predoctoral fellowship PRE2019-089488 funded by MICIU/AEI /10.13039/501100011033 and by "ESF Investing in your future", and A.R-S received postdoctoral funding from the programs Juan de la Cierva Incorporación (Ministerio de Ciencia, Innovación y Universidades; IJC2018-035773) and Beatriu de Pinós (AGAUR & Marie Sklowdowska-Curie Actions; 2018 BP 0032).

Declaration of competing interest

The authors declare that they have no known competing financial interests or personal relationships that could have appeared to influence the work reported in this paper.

Supplementary materials

Supplementary material (Supplementary Figures 1-3) associated with this article can be found in the online version of the article.

References

[1] N.T. Tran, R. Kaldenhoff, Achievements and challenges of genetic engineering of the model green alga *Chlamydomonas reinhardtii*, Algal Res. 50 (2020) 101986.

[2] W. Jiang, H. Zhou, H. Bi, M. Fromm., B. Yang, D.P. Weeks, Demonstration of CRISPR/Cas9/sgRNA-mediated targeted gene modification in Arabidopsis, tobacco, sorghum and rice, Nucleic Acids Res. 41 (20) (2013) e188.

[3] M. Jinek, K. Chylinski, I. Fonfara, M. Hauer, J.A. Doudna, E. Charpentier, A Programmable Dual-RNA–Guided DNA Endonuclease in Adaptive Bacterial Immunity, Science 337 (6096) (2012) 816-821.

[4] S.-.E. Shin, J.-.M. Lim, H.G. Koh, E.K. Kim, N.K. Kang, S. Jeon, S. Kwon, W.-.S. Shin, B. Lee, K. Hwangbo, J. Kim, S.H. Ye, J.-.Y. Yun, H. Seo, H.-.M. Oh, K.-.J. Kim, J.-.S. Kim, W.-.J. Jeong, Y.K. Chang, B.-.R. Jeong, CRISPR/Cas9-induced knockout and knock-in mutations in *Chlamydomonas reinhardtii*, Sci. Rep. 6 (2016) 27810.

[5] K. Baek, D.H. Kim, J. Jeong, S.J. Sim, A. Melis, J.-.S. Kim, E. Jin, S. Bae, DNA-free two-gene knockout in *Chlamydomonas reinhardtii* via CRISPR-Cas9 ribonucleoproteins, Sci. Rep. 6 (2016) 30620.

[6] A. Greiner, S. Kelterborn, H. Evers, G. Kreimer, I. Sizova, P. Hegemann, Targeting of Photoreceptor Genes in *Chlamydomonas reinhardtii* via Zinc-Finger Nucleases and CRISPR/Cas9, Plant Cell 29 (10) (2017) 2498–2518.

[7] A. Ferenczi, D.E. Pyott, A. Xipnitou, A. Molnar, Efficient targeted DNA editing and replacement in *Chlamydomonas reinhardtii* using Cpf1 ribonucleoproteins and single-stranded DNA, Proc. Natl. Acad. Sci. U S A 114 (51) (2017) 13567-13572.

[8] S. Akella, X. Ma, R. Bacova, Z.P. Harmer, M. Kolackova, X. Wen, D.A. Wright, M.H. Spalding, D.P. Weeks, H. Cerutti, Co-targeting strategy for precise, scarless gene editing with CRISPR/Cas9 and donor ssODNs in Chlamydomonas, Plant Physiol. 187 (4) (2021) 2637-2655.

[9] A. Ferenczi, M. Fellbaum, Y.P. Chew, C. Kidner, A. Molnar, Comparison of CRISPR/Cas9 and Cas12a for gene editing in *Chlamydomonas reinhardtii*, Algal Res. 84 (2024) 103796.

[10] M. Angstenberger, F. de Signori, V. Vecchi, L. Dall'Osto, R. Bassi, Cell Synchronization Enhances Nuclear Transformation and Genome Editing via Cas9 Enabling Homologous Recombination in *Chlamydomonas reinhardtii*, ACS Synth. Biol. 9 (10) (2020) 2840-2850.

[11] S. Kelterborn, F. Boehning, I. Sizova, O. Baidukova, H. Evers, P. Hegemann, Gene Editing in Green Alga *Chlamydomonas reinhardtii* via CRISPR-Cas9 Ribonucleoproteins, Methods Mol. Biol. 2379 (2022) 45-65.

[12] T. Picariello, Y. Hou, T. Kubo, N.A. McNeill, H. Yanagisawa, T. Oda, G.B. Witman, TIM, a targeted insertional mutagenesis method utilizing CRISPR/Cas9 in *Chlamydomonas reinhardtii*, PLoS One 15 (5) (2020) e0232594.

[13] H. Chen, Q.-.L. Yang, J.-.X. Xu, X. Deng, Y.-.J. Zhang, T. Liu, M.G. Rots, G.-.L. Xu, K.-.Y. Huang, Efficient methods for multiple types of precise gene-editing in *Chlamydomonas*, Plant J. 115 (3) (2023) 846–865.

[14] A.P. Nievergelt, D.R. Diener, A. Bogdanova, T. Brown, G. Pigino, Protocol for precision editing of endogenous Chlamydomonas reinhardtii genes with CRISPR-Cas, STAR Protoc. 5 (1) (2024) 102774.

[15] D. Dhokane, B. Bhadra, S. Dasgupta, CRISPR based targeted genome editing of *Chlamydomonas reinhardtii* using programmed Cas9-gRNA ribonucleoprotein, Mol Biol Rep. 47 (11) (2020) 8747-8755.

[16] S.S. McCarthy, M.C. Kobayashi, K.K. Niyogi, White Mutants of Chlamydomonas reinhardtii Are Defective in Phytoene Synthase, Genetics 168 (3) (2004) 1249–1257.

[17] H. Liu, Y. Ding, Y. Zhou, W. Jin, K. Xie, L.-.L. Chen, CRISPR-P 2.0: An Improved CRISPR-Cas9 Tool for Genome Editing in Plants, Mol. Plant 10 (3) (2017) 530-532.

[18] J. Ye, G. Coulouris, I. Zaretskaya, I. Cutcutache, S. Rozen, T.L. Madden, Primer-BLAST: a tool to design target-specific primers for polymerase chain reaction, BMC Bioinformatics 13 (2012) 134.

[19] W.A. Kibbe, OligoCalc: an online oligonucleotide properties calculator, Nucleic Acids Res. 35 (2007) W43-W46.

[20] M. Cao, Y. Fu, Y. Guo, J. Pan, *Chlamydomonas* (Chlorophyceae) colony PCR, Protoplasma 235 (1-4) (2009) 107-110.

[21] L. Angelopoulou, E. Stylianopoulou, K. Tegopoulos, I. Farmakioti, M. Grigoriou, G. Skavdis, A PCR-Induced Mutagenesis-Restriction Fragment Length Polymorphism Method for the Detection of CRISPR-Induced Indels, CRISPR J. 6 (6) (2023) 514-526.

[22] D. Strenkert, S. Schmollinger, S.D. Gallaher, P.A. Salomé, S.O. Purvine, C.D. Nicora, T. Mettler-Altmann, E. Soubeyrand, A.P.M. Weber, M.S. Lipton, G.J. Basset, S.S. Merchant, Multiomics resolution of molecular events during a day in the life of Chlamydomonas, Proc. Natl. Acad. Sci. U S A 116 (6) (2019) 2374–2383.

Graphical Abstract

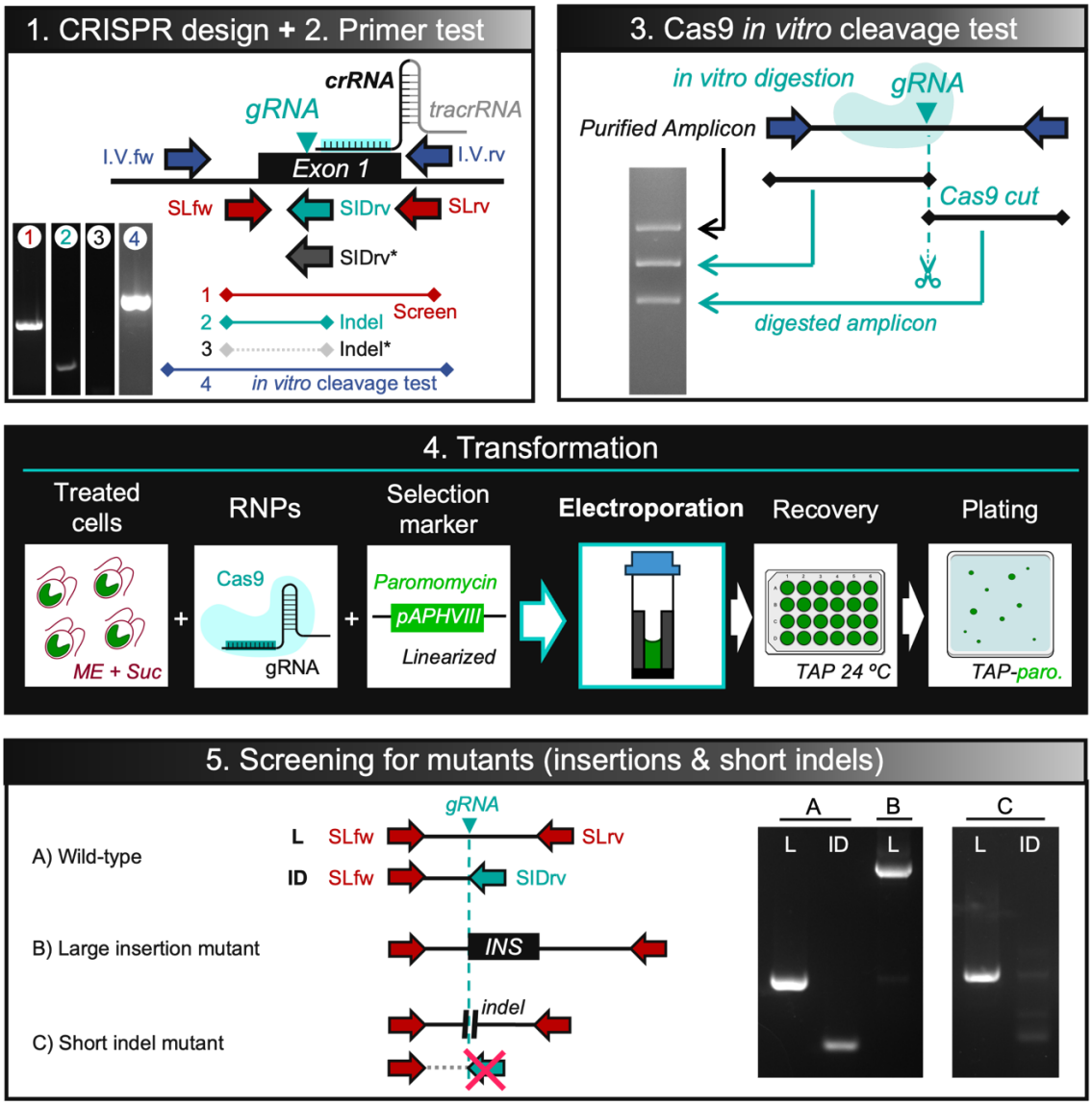

GENERAL DISCUSSION

Light is one of the most informative and variable environmental cues for photosynthetic organisms. Its fluctuations in intensity, spectral composition, direction, and duration require regulatory mechanisms that allow cells to adjust their physiology accordingly. Land plants such as *Arabidopsis thaliana* sense and respond to these cues through a well-characterized set of photoreceptors, including phytochromes, cryptochromes, phototropins, and UVR8, which predominantly regulate developmental and stress-related pathways via integrated transcriptional networks (Kami et al., 2010; Legris et al., 2016).

Like land plants, unicellular algae such as *Chlamydomonas reinhardtii* are regularly exposed to changing light conditions and have evolved mechanisms to detect and respond to them. In *C. reinhardtii*, light signals are processed through a variety of photoreceptors that regulate metabolism, movement, and photoprotection. These include retinal-based channelrhodopsins (ChR1, ChR2) involved in phototaxis (Nagel et al., 2002), a plant-like cryptochrome (aCRY), and several predicted blue-light receptors whose roles are still not fully understood (Beel et al., 2012).

However, one major class of photoreceptors is missing: Chlamydomonas lacks canonical phytochromes, red/far-red sensors found in land plants and some algae. This differs from the prasinophyte *Micromonas pusilla*, an early-diverging green alga that has retained a full-length phytochrome with both a photosensory module and a functional histidine kinase domain (Duanmu et al., 2014). Phylogenetic analyses suggest that phytochromes were present in the common ancestor of prasinophytes, chlorophytes, and streptophytes, and were lost independently in several lineages, including Chlamydomonas (Duanmu et al., 2014). This loss might be related to the presence or expansion of other light-sensing pathways. In line with this, we found two histidine kinases in Chlamydomonas, HIK1 and HIK2, that contain LOV (Light, Oxygen, or Voltage) domains, blue-light sensing modules found in many organisms, which contribute to its broader repertoire of photoreceptors.

Both proteins feature canonical domains of two-component signaling systems (TCS), extensively present in algae and prokaryotes but notably reduced or redirected toward hormonal signaling roles in terrestrial plants.

In land plants, including *Arabidopsis*, histidine kinases are primarily involved in hormonal signaling, mediating cytokinin pathways crucial for developmental processes like cell division and differentiation (Hwang, Sheen, & Müller, 2012). By contrast, Chlamydomonas HIK1 and HIK2 proteins possess cysteinyl-flavin adduct-forming domains characteristic of blue-light sensors. Indeed, our findings specifically implicate HIK1 in modulating NPQ induction under blue LL intensity, suggesting a role in photoprotective responses and

highlighting how TCS-like systems in Chlamydomonas effectively couple rapid environmental sensing with flexible physiological adjustments.

Dynamic environments further promote rapid and reversible photoprotective mechanisms such as NPQ. In our experiments, NPQ dynamics were strongly influenced by photoperiod length, underscoring the importance of daylength as a regulatory cue. Photoperiod also impacted other physiological traits, including pigment composition and photosynthetic efficiency. Notably, wild-type strains displayed divergent responses, indicating substantial natural variation in light acclimation strategies even among laboratory-maintained lineages. This phenotypic diversity likely arises from differences in regulatory networks and may reflect distinct environmental origins or selection pressures experienced during laboratory propagation. These findings underscore the ecological relevance of studying multiple genotypes, rather than relying on a single reference strain, to fully understand light response diversity in Chlamydomonas.

This contrasts with the situation in *Arabidopsis thaliana* and highlights a key issue in Chlamydomonas research: the lack of a standardized wild-type reference. Instead, most studies rely on a few commonly used strains, CC-124, CC-125, CC-503 (CLiP), among others, each with distinct mutations and mating types. While this complicates direct comparisons, it also provides valuable insights into strain-specific regulatory diversity.

Indeed, photoprotective strategies identified in Chlamydomonas, including adjustments in NPQ and pigment composition, are conserved across diverse algae groups. Diatoms employ Lhcx proteins for similar photoprotection functions as LHCSR in Chlamydomonas (Bailleul et al., 2010; Barnett et al., 2020), while macroalgae such as *Ulva* and *Porphyra* adjust chloroplast positioning and pigment accumulation to cope with dynamic light conditions (Franklin et al., 2002; Gao et al., 2018). These parallels emphasize both the broad ecological relevance and evolutionary flexibility in algal photoprotective mechanisms.

Moreover, considering current climate change scenarios, it is increasingly relevant to understand how alterations in irradiance might influence the selection and efficacy of photoprotective strategies (Beardall & Raven, 2013; Falkowski & Raven, 2007). Fluctuations in light intensity, both in amplitude and periodicity, can profoundly affect photosynthetic performance and induce oxidative stress, particularly in planktonic algae exposed to high-light surface layers. Rising UV-B levels and changes in PAR (photosynthetically active radiation) can increase photoinhibition, thereby intensifying the selective advantage of lineages capable of mounting efficient photoprotective responses, such as non-photochemical quenching (NPQ) (Beardall & Raven, 2013).

Environmental changes may thus shift selective pressures, potentially favouring genotypes with enhanced capacity to regulate excitation energy dissipation, pigment accumulation, or photoreceptor-mediated acclimation. These responses are not only plastic but also genetically encoded, as shown by comparative genomic analyses. For example, the genome of *Chlamydomonas reinhardtii* encodes multiple LHCSR and PSBS proteins, underscoring the importance of photoprotection in dynamic light environments (Merchant et al., 2007). Similarly, the diatom *Thalassiosira pseudonana* exhibits an expanded repertoire of light-responsive and carbon-fixation genes, suggesting an evolutionary adaptation to fluctuating irradiance in marine ecosystems (Armbrust et al., 2004).

Aquatic photosynthetic organisms have evolved under constantly changing conditions, and their functional diversity reflects a long history of adaptation to light gradients. Expanding comparative studies beyond model green algae to include diatoms, red algae, and other ecologically relevant lineages will be essential to fully understand the evolutionary trajectories and constraints shaping the diversity of photoprotective strategies observed today. (Falkowski & Raven 2007).

Advancements in Chlamydomonas genetics, including the CLiP mutant library (Li et al., 2019), refined genome annotations, and CRISPR/Cas9 methodologies, promise a more systematic and precise exploration of these adaptive responses. Nevertheless, challenges remain, particularly regarding transformation efficiency and off-target genome editing effects.

Altogether, our findings highlight the value of Chlamydomonas as a model for understanding how unicellular phototrophs sense and adapt to dynamic light environments. Framing these responses in ecological and evolutionary terms reveals how diverse algal strategies, such as rapid NPQ activation and blue-light perception via TCS-like systems, support resilience in fluctuating environments, particularly under the increasing light variability expected with climate-driven changes in aquatic ecosystems.

GENERAL CONCLUSIONS

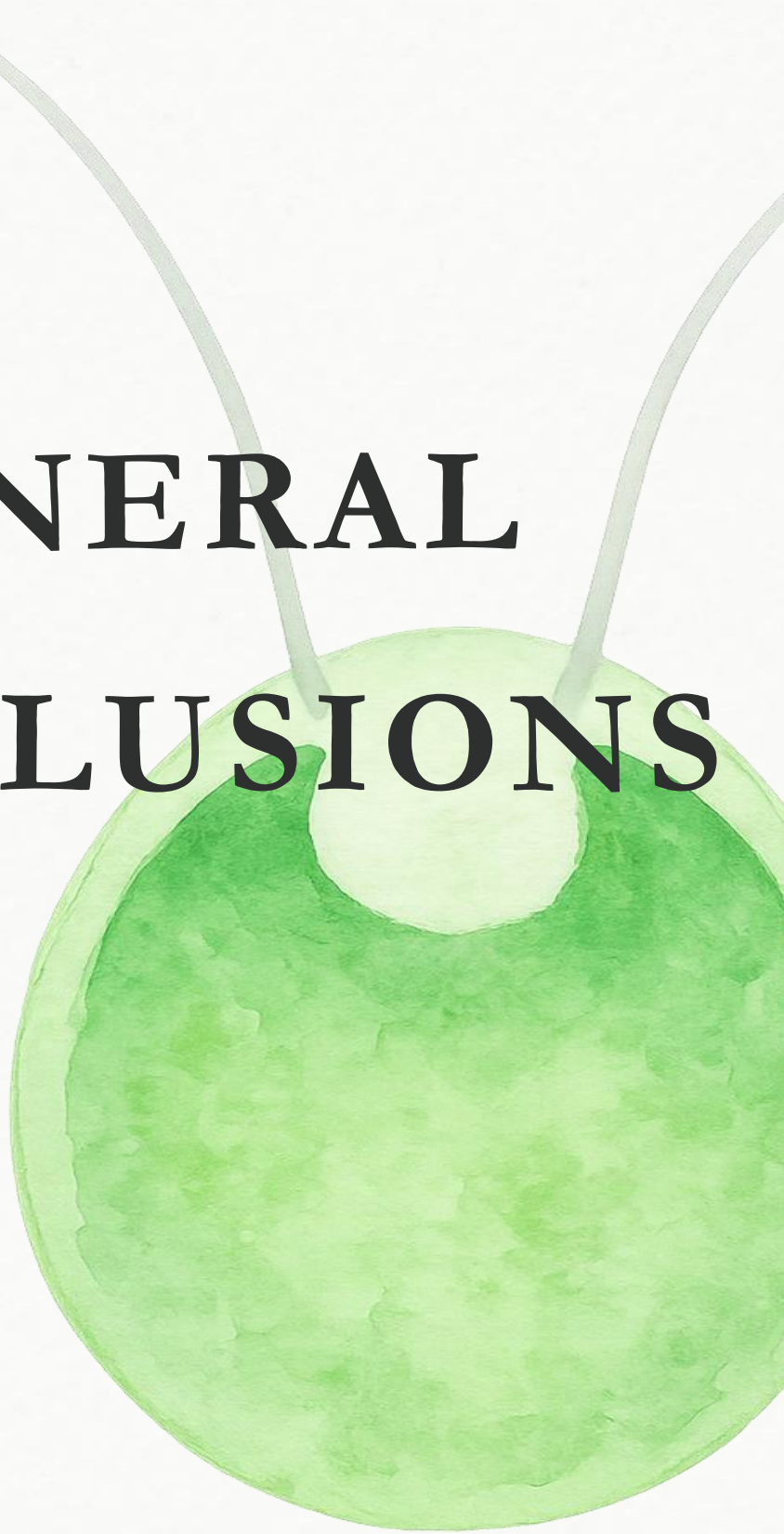

Chapter 2- "Shaped by light: Photoperiod and Intensity Responses in Chlamydomonas Strains"

1. **Photoperiod dominates over light intensity** in shaping growth, cell size, and pigment composition. Longer days promote higher growth rates but smaller cells, while short photoperiods maintain physiological stability and healthier morphology at expenses of growth, especially under HL.
2. **Photosynthetic responses are photoperiod-dependent:** LL supports stable PSII performance across light regimes. Under HL conditions, shorter photoperiods enhance photosynthetic efficiency and NPQ, while prolonged exposure induces stress symptoms.
3. **Pigment regulation reflects light and photoperiod interplay:** chlorophyll accumulates in short LL photoperiods; carotenoids remain stable in LL but degrade in long HL exposure. Antenna size adjustments (Chl a/b ratio) are shaped by photoperiod rather than intensity, and strain-specific differences are observed.
4. **Strain-specific trade-offs emerge:** CLiP combines strong photoprotection with sustained growth, CC-124 favors proliferation at the expense of PSII efficiency, and other strains occupy intermediate strategies.

Chapter 3- "Unravelling the role of the novel Chlamydomonas photoreceptors HIK1 and HIK2"

HIK1

1. **HIK1 seems to be a novel LOV-domain histidine kinase** that modulates photoprotection under blue light.
2. The ***hik1 442* mutant shows enhanced NPQ under blue LL and altered qE gene expression** (*LHCSR1/3, PSBS*), suggesting misregulation of photoprotection resembling HL stress.
3. These results indicate that **HIK1 normally suppresses qE activation under non-stress conditions,** potentially placing it as a new component of blue light signaling

pathways. However, complementation assays and generation of different HIK1 mutant lines will be required to confirm this.

HIK2

1. The **HL-sensitive phenotype of *hik2 149* is inconsistent** and was not reproduced in other *HIK2*-disrupted lines, suggesting that loss of *HIK2* function is not responsible for the phenotype observed.

2. The **PAS domain truncation in *hik2 149* remains a candidate mechanism** and testing whether the truncated transcript or protein (if originated) is expressed and functional will be crucial to determine if it interferes with stress or light signaling.

3. Despite uncertainties, **HIK2's domain architecture suggests a role in environmental signal transduction**, possibly linked to light, redox, or circadian regulation.

4. **Future work should combine validation of other independent lines, complementation, and interaction studies** (including *hik1hik2* double mutants) to clarify whether HIK2 contributes to photoreceptor pathways or stress integration in Chlamydomonas.

Chapter 4- "A quick and optimized CRISPR-Cas9 protocol to obtain insertional and small indel mutants in *Chlamydomonas reinhardtii*"

1. A **fast and accessible CRISPR-Cas9 workflow for Chlamydomonas** has been optimized, enabling efficient knockout generation without specialized equipment.

2. The PCR-**based screening strategy detects both large insertions and small indels**, including single-based changes, providing a reliable way to identify edits.

3. The protocol achieves editing **efficiencies up to 60%,** with variation across target loci and sgRNAs, and can deliver confirmed mutants within five weeks.

4. **This approach is particularly suitable for small-scale functional studies**, offering a practical tool for labs without high-throughput capabilities.

REFERENCES

Aihara, Y., Iwaki, T., & Nakaoka, Y. (2019). Algal photoprotection is regulated by the E3 ligase CUL4-DDB1DET1. *Nature Plants*, 5(9), 1054–1062.

Akella, S., Ma, X., Bacova, R., Harmer, Z. P., Kolackova, M., Wen, X., & Puchta, H. (2021). Co-targeting strategy for precise, scarless gene editing with CRISPR/Cas9 and donor ssODNs in *Chlamydomonas*. *Plant Physiology*, 187(4), 2637–2655.

Allorent, G., & Petroutsos, D. (2017). Photoreceptor-dependent regulation of photoprotection. *Current Opinion in Plant Biology*, 37, 102–108.

Allorent, G., Tokutsu, R., Roach, T., Peers, G., Cardol, P., Girard-Bascou, J., Seigneurin-Berny, D., Petroutsos, D., Kuntz, M., Breyton, C., Franck, F., Wollman, F.-A., Niyogi, K. K., Krieger-Liszkay, A., Minagawa, J., & Finazzi, G. (2013). A dual strategy to cope with high light in *Chlamydomonas reinhardtii*. *The Plant Cell*, 25(2), 545–557.

Allorent, G., Tokutsu, R., Roach, T., Peers, G., Cardol, P., Girard-Bascou, J., ... & Finazzi, G. (2016). UV-B photoreceptor-mediated protection of the photosynthetic machinery in *Chlamydomonas reinhardtii*. *PNAS*, 113(51), 14864–14869.

Alvarez, A. F., Barba-Ostria, C., Silva-Jiménez, H., & Georgellis, D. (2016). Organization and mode of action of two-component system signaling circuits from the various kingdoms of life. *Environmental Microbiology, 18*(10), 3210–3226.

Appleby, J. L., Parkinson, J. S., & Bourret, R. B. (1996). Signal transduction via the multi-step phosphorelay: Not necessarily a road less traveled. *Cell, 86*(6), 845–848.

Armbrust, E. V., Berges, J. A., Bowler, C., Green, B. R., Martinez, D., Putnam, N. H., ... & Rokhsar, D. S. (2004). The genome of the diatom *Thalassiosira pseudonana*: Ecology, evolution, and metabolism. *Science, 306*(5693), 79–86.

Asada, K. (2006). Production and scavenging of reactive oxygen species in chloroplasts and their functions. *Plant Physiology, 141*(2), 391–396.

Baek, K., Kim, D. H., Jeong, J., Sim, S. J., Melis, A., Kim, J. S., Jin, E., & Bae, S. (2016). DNA-free two-gene knockout in *Chlamydomonas reinhardtii* via CRISPR/Cas9 ribonucleoproteins. *Scientific Reports, 6*, 30620.

Bailleul, B., Rogato, A., de Martino, A., Coesel, S., Cardol, P., Bowler, C., Falciatore, A., & Finazzi, G. (2010). An atypical member of the light-harvesting complex stress-related protein family modulates diatom responses to light. Proceedings of the National Academy of Sciences, 107(42), 18214–18219.

Ballottari, M., Truong, T. B., De Re, E., Erickson, E., Stella, G. R., Fleming, G. R., Bassi, R., & Niyogi, K. K. (2016). Identification of pH-sensing sites in the light harvesting complex stress-related 3 protein essential for triggering non-photochemical quenching in *Chlamydomonas reinhardtii*. *Journal of Biological Chemistry, 291*(14), 7334–7346.

Barnett, A., Buck, J. M., Lepetit, B., Lavaud, J., & Kroth, P. G. (2020). Identification of sequence motifs in Lhcx proteins that confer qE-based photoprotection in the diatom Phaeodactylum tricornutum. The Plant Journal, 103(2), 472–482.

Baroli, I., & Melis, A. (1998). Photoinhibitory damage is modulated by the rate of photosynthesis and by the photosystem II light-harvesting chlorophyll antenna size. *Planta, 205*(2), 288–296.

Beardall, J., & Raven, J. A. (2013). Limits to photoprotection and adaptation in phytoplankton in a changing environment. *Philosophical Transactions of the Royal Society B: Biological Sciences, 368*(1622), 20120419.

Becker, B., Holtgrefe, S., Jung, S., Wunrau, C., Kandlbinder, A., Baier, M., Dietz, K.-J., Backhausen, J. E., & Scheibe, R. (2006). Influence of the photoperiod on redox regulation and stress responses in *Arabidopsis thaliana* L. (Heynh.) plants under long- and short-day conditions. *Planta, 224*(2), 380–393.

Beel, B., Prager, K., Spexard, M., Sasso, S., Weiss, D., Müller, N., Heinnickel, M., Dewez, D., Ikoma, D., Grossman, A. R., Kottke, T., & Mittag, M. (2012). A flavin binding cryptochrome photoreceptor responds to both blue and red light in *Chlamydomonas reinhardtii*. *The Plant Cell, 24*(7), 2992–3008.

Berntsson, O., Diensthuber, R. P., Panman, M. R., Björling, A., Gustavsson, E., Hoernke, M., Hughes, A. J., Henry, L., Niebling, S., Takala, H., Ihalainen, J. A., Newby, G., Kerruth, S., Heberle, J., Liebi, M., Menzel, A., Henning, R., Kosheleva, I., Möglich, A., & Westenhoff, S. (2017). Sequential conformational transitions and α-helical supercoiling regulate a sensor histidine kinase. *Nature Communications, 8*, Article 284.

Berthold, P., Tsunoda, S. P., Ernst, O. P., Mages, W., Gradmann, D., & Hegemann, P. (2008). Channelrhodopsin-1 initiates phototaxis and photophobic responses in *Chlamydomonas* by immediate light-induced depolarization. *The Plant Cell, 20*(6), 1665–1677.

Bonente, G., Ballottari, M., Truong, T. B., Morosinotto, T., Ahn, T. K., Fleming, G. R., Niyogi, K. K., & Bassi, R. (2011). Analysis of LhcSR3, a protein essential for feedback de-excitation in the green alga *Chlamydomonas reinhardtii*. *PLOS Biology, 9*(1), e1000577.

Bonente, G., Pippa, S., Castellano, S., Bassi, R., & Ballottari, M. (2012). Acclimation of *Chlamydomonas reinhardtii* to different growth irradiances. *Journal of Biological Chemistry*, *287*(8), 5833–5847.

Boyden, E. S., Zhang, F., Bamberg, E., Nagel, G., & Deisseroth, K. (2005). Millisecond-timescale, genetically targeted optical control of neural activity. *Nature Neuroscience, 8*(9), 1263–1268.

Boynton, J. E., Gillham, N. W., Harris, E. H., Hosler, J. P., Johnson, A. M., Jones, A. R., Randolph-Anderson, B. L., Robertson, D., Klein, T. M., Shark, K. B., & Sanford, J. C. (1988). Chloroplast transformation in *Chlamydomonas* with high velocity microprojectiles. Science, 240(4858), 1534–1538.

Cazzaniga, S., Dall'Osto, L., Szaub, J., Scibilia, L., Ballottari, M., Purton, S., & Bassi, R. (2014). Domestication of the green alga *Chlorella sorokiniana*: reduction of antenna size improves light-use efficiency in a photobioreactor. *Biotechnology for Biofuels*, 7, 157.

Chen, J., Chen, Y., He, W., Liang, H., Hong, T., Li, T., & Du, H. (2024). Transcriptome analysis reveals the molecular mechanism of differences in growth between photoautotrophy and heterotrophy in *Chlamydomonas reinhardtii*. *Frontiers in Plant Science, 15*, 1407915.

Christie, J. M., Reymond, P., Powell, G. K., Bernasconi, P., Raibekas, A. A., Liscum, E., & Briggs, W. R. (1998). *Arabidopsis* NPH1: A flavoprotein with the properties of a photoreceptor for phototropism. *Science, 282*(5394), 1698–1701.

Christie, J. M. (2007). Phototropin blue-light receptors. *Annual Review of Plant Biology, 58*, 21–45.

Christie, J. M., Blackwood, L., Petersen, J., & Sullivan, S. (2015). Plant flavoprotein photoreceptors. *Plant and Cell Physiology, 56*(3), 401–413.

Cole, D. G., Diener, D. R., Himelblau, A. L., Beech, P. L., Fuster, J. C., & Rosenbaum, J. L. (1998). *Chlamydomonas* kinesin-II–dependent intraflagellar transport (IFT): IFT particles contain proteins required for ciliary assembly in *Caenorhabditis elegans* sensory neurons. *The Journal of Cell Biology, 141*(4), 993–1008.

Craig, R. J., Gallaher, S. D., Glaesener, A. G., Pellegrini, M., & Merchant, S. S. (2023). The *Chlamydomonas* Genome Project, version 6: Reference assemblies for mating-type plus and minus strains reveal extensive structural mutation in the laboratory. *The Plant Cell, 35*(2), 644–661.

Cronmiller, E., Toor, D., Shao, N. C., Kariyawasam, T., Wang, M. H., & Lee, J.-H. (2019). Cell wall integrity signaling regulates cell wall-related gene expression in *Chlamydomonas reinhardtii*. *Scientific Reports, 9*, 12204.

Cross, F. R., & Umen, J. G. (2015). The Chlamydomonas cell cycle. *The Plant Journal, 82*(3), 370–392.

Cvetić, T., Sabovljević, A., Bogdanović, J., & Sabovljević, M. (2009). Effects of day length on photosynthetic pigments and antioxidative metabolism of in vitro cultured moss *Atrichum undulatum* (Hedw.) P. Beauv. (Bryophyta). *Botanica Serbica, 33*(1), 85–92.

de Carpentier, F., Lemaire, S. D., & Danon, A. (2019). When unity is strength: The strategies used by *Chlamydomonas* to survive environmental stresses. *Cells, 8*(11), 1307.

Dent, R. M., Haglund, C. M., Chin, B. L., Kobayashi, M. C., & Niyogi, K. K. (2005). Functional genomics of eukaryotic photosynthesis using insertional mutagenesis of *Chlamydomonas reinhardtii*. *Plant Physiology, 137*(2), 545–556.

Dent, R. M., Sharifi, M. N., Malnoë, A., Haglund, C., Calderon, R. H., Wakao, S., & Niyogi, K. K. (2015). Large-scale insertional mutagenesis of *Chlamydomonas* supports phylogenomic functional prediction of photosynthetic genes and analysis of classical acetate-requiring mutants. *The Plant Journal, 82*(2), 337–351.

Djouani-Tahri, E. B., Christie, J. M., Sanchez-Ferandin, S., Bouget, F.-Y., & Corellou, F. (2011). A eukaryotic LOV-histidine kinase with circadian clock function in the picoalga *Ostreococcus*. *The Plant Journal, 65*(4), 578–588.

Drop, B., Webber-Birungi, M., Yadav, S. K. N., Filipowicz-Szymanska, A., Fusetti, F., Boekema, E. J., & Croce, R. (2014). Light-harvesting complex II (LHCII) and its supramolecular organization in *Chlamydomonas reinhardtii*. *Biochimica et Biophysica Acta (BBA) - Bioenergetics, 1837*(1), 63–72.

Duanmu, D., Bachy, C., Sudek, S., Wong, C.-H., Jiménez, V., Rockwell, N. C., Martin, S. S., Ngan, C. Y., Reistetter, E. N., van Baren, M. J., Price, D. C., Wei, C.-L., Reyes-Prieto, A., Lagarias, J. C., & Worden, A. Z. (2014). Marine algae and land plants share conserved phytochrome signaling systems. *Proceedings of the National Academy of Sciences of the United States of America, 111*(44), 15827–15832.

Dupuis, S., & Merchant, S. S. (2023). *Chlamydomonas reinhardtii*: a model for photosynthesis and so much more. *Nature Methods, 20*(10), 1441–1442.

Engel, B. D., Schaffer, M., Kuhn Cuellar, L., Villa, E., Plitzko, J. M., & Baumeister, W. (2015). Native architecture of the *Chlamydomonas* chloroplast revealed by in situ cryo-electron tomography. *eLife, 4*, e04889.

Erickson, E., Wakao, S., & Niyogi, K. K. (2015). Light stress and photoprotection in *Chlamydomonas reinhardtii*. *The Plant Journal*, 82(3), 449–465.

Falkowski, P. G., & Raven, J. A. (2007).*Aquatic photosynthesis* (2nd ed.). Princeton University Press.

Fan, M., Li, M., Liu, Z., Cao, P., Pan, X., Zhang, H., Zhao, X., Zhang, J., & Chang, W. (2015). Crystal structures of the PsbS protein essential for photoprotection in plants. *Nature Structural & Molecular Biology, 22*(9), 729–735.

Ferenczi, A., Pyott, D. E., Xipnitou, A., & Molnar, A. (2017). Efficient targeted DNA editing and replacement in *Chlamydomonas reinhardtii* using Cpf1 ribonucleoproteins and single-stranded DNA. *Proceedings of the National Academy of Sciences*, 114(51), 13567–13572.

Flowers, J. M., Hazzouri, K. M., Pham, G. M., Rosas, U., Bahmani, T., Khraiwesh, B., Nelson, D. R., Jijakli, K., Abdrabu, R., Harris, E. H., Lefebvre, P. A., Hom, E. F. Y., Salehi-Ashtiani, K., & Purugganan, M. D. (2015). Whole-genome resequencing reveals extensive natural variation in the model green alga *Chlamydomonas reinhardtii*. *The Plant Cell, 27*(9), 2353–2369.

Franklin, L. A., Levavasseur, G., Osmond, C. B., Henley, W. J., & Ramus, J. (2002). Two components of UV-B photoinhibition of photosynthesis in Ulva rotundata. Journal of Phycology, 38(5), 826–834.

Franz, S., Ignatz, E., Wenzel, S., Zielosko, H., Putu, E. P. G. N., Maestre-Reyna, M., Tsai, M.-D., Yamamoto, J., Mittag, M., & Essen, L.-O. (2018). Structure of the bifunctional cryptochrome aCRY from *Chlamydomonas reinhardtii*. *Nucleic Acids Research, 46*(15), 8010–8022.

Friedland, N., Negi, S., Vinogradova-Shah, T., Wu, G., Ma, L., Flynn, S., Kumssa, T., Lee, C.-H., & Sayre, R. T. (2019). Fine-tuning the photosynthetic light harvesting apparatus for improved photosynthetic efficiency and biomass yield. *Scientific Reports, 9*, 13028.

Gabilly, S. T., Yamano, T., Fukuda, Y., Fukuzawa, H., & Minagawa, J. (2019). Regulation of photoprotection gene expression in *Chlamydomonas* by a putative E3 ubiquitin ligase complex and a homolog of CONSTANS. *Proceedings of the National Academy of Sciences, 116*(4), 1755–1760.

Gallaher, S. D., Fitz-Gibbon, S. T., Glaesener, A. G., Pellegrini, M., & Merchant, S. S. (2015). *Chlamydomonas* genome resource for laboratory strains reveals a mosaic of sequence variation, identifies true strain histories, and enables strain-specific studies. *The Plant Cell, 27*(9), 2335–2352.

Galperin, M. Y. (2010). Diversity of structure and function of response regulator output domains. *Current Opinion in Microbiology, 13*(2), 150–159.

Gao, K., Xu, J., Gao, G., Li, Y., Hutchins, D. A., Huang, B., Wang, L., Zheng, Y., Jin, P., Cai, X., Häder, D.-P., & Helbling, E. W. (2018). Solar UV radiation drives CO_2 fixation in marine phytoplankton: A double-edged sword. Global Change Biology, 24(1), 303–313.

Goodstein, D. M., Shu, S., Howson, R., Neupane, R., Hayes, R. D., Fazo, J., ... & Rokhsar, D. S. (2012). Phytozome: A comparative platform for green plant genomics. *Nucleic Acids Research*, 40(D1), D1178–D1186.

Grechanik, V. I., Bol'shakov, M. A., & Tsygankov, A. A. (2022). Hydrogen production by CO_2-deprived photoautotrophic *Chlamydomonas reinhardtii* cultures. *Biochemistry (Moscow), 87*(10), 1098–1108.

Greiner, A., Kelterborn, S., Evers, H., Kreimer, G., Sizova, I., & Hegemann, P. (2017). Targeting of photoreceptor genes in *Chlamydomonas reinhardtii* via zinc-finger nucleases and CRISPR/Cas9. *The Plant Cell, 29*(10), 2498–2518.

Harris, E. H. (1989). The *Chlamydomonas* Sourcebook: Cell architecture and division. Academic Press.

Harris, E. H. (2001). *Chlamydomonas* as a model organism. *Annual Review of Plant Physiology and Plant Molecular Biology, 52*, 363–406.

Harris, E. H. (2009). *The Chlamydomonas Sourcebook:* Introduction to *Chlamydomonas* and Its Laboratory Use (Vol. 1, 2ª ed.). Academic Press.

Heldt, F. S., Tyson, J. J., Cross, F. R., & Novák, B. (2020). A single light-responsive sizer can control multiple-fission cycles in *Chlamydomonas reinhardtii*. *Current Biology*, *30*(4), 634–644.e7.

Hegemann, P. (2008). Algal sensory photoreceptors. *Annual Review of Plant Biology, 59*, 167–189.

Heijde, M., & Ulm, R. (2012). UV-B photoreceptor-mediated signaling in plants. *Trends in Plant Science, 17*(4), 230–237.

Heifetz, P. B., Förster, B., Osmond, C. B., Giles, L. J., & Boynton, J. E. (2000). Effects of acetate on facultative autotrophy in *Chlamydomonas reinhardtii* assessed by photosynthetic measurements and stable isotope analyses. *Plant Physiology, 122*(4), 1439–1446.

Hemker, F., Ammelburger, N., & Jahns, P. (2024). Intervening dark periods negatively affect the photosynthetic performance of Chlamydomonas reinhardtii during growth under fluctuating high light. Plant, Cell & Environment. Advance online publication.

Herrou, J., & Crosson, S. (2011). Function, structure, and mechanism in bacterial photosensory LOV proteins. *Nature Reviews Microbiology, 9*(10), 713–723.

Holland, E. M., Harz, H., Uhl, R., & Hegemann, P. (1997). Control of phobic behavioral responses by rhodopsin-induced photocurrents in *Chlamydomonas*. *Biophysical Journal, 73*(1), 1395–1401.

Huang, K., & Beck, C. F. (2003). Phototropin is the blue-light receptor that controls multiple steps in the sexual life cycle of the green alga *Chlamydomonas reinhardtii*. *Proceedings of the National Academy of Sciences of the United States of America, 100*(10), 6269–6274.

Huang, K., Kunkel, T., & Beck, C. F. (2004). Blue-light-regulated genes in *Chlamydomonas reinhardtii:* Identification of phototropin-related genes and analysis of their expression patterns. *Plant Molecular Biology, 55*(5), 673–684.

Hérivaux, A., Lamacchia, M., Papon, N., & Dussert, C. (2016). Major sensing proteins in pathogenic fungi: The hybrid histidine kinase family. *PLoS Pathogens, 12*(7), e1005683.

Hwang, I., Sheen, J., & Müller, B. (2012). Cytokinin signaling networks. *Annual Review of Plant Biology, 63*, 353–380.

Imaizumi, T., Schultz, T. F., Harmon, F. G., Ho, L. A., & Kay, S. A. (2005). FKF1 F-box protein mediates cyclic degradation of a repressor of CONSTANS in Arabidopsis. Science, 309(5732), 293–297.

Iwai, M., Kato, N., Minagawa, J., & Satoh, K. (2007). Functional architecture of photosystem I–light-harvesting complex I supercomplexes from *Chlamydomonas reinhardtii*: Protein composition and interactions. *Journal of Biological Chemistry, 282*(50), 36877–36887.

Jiang, W., Brueggeman, A. J., Horken, K. M., Plucinak, T. M., & Weeks, D. P. (2014). Successful transient expression of Cas9 and single guide RNA genes in *Chlamydomonas reinhardtii*. *Eukaryotic Cell*, 13(11), 1465–1469.

Johnson, X., & Alric, J. (2013). Central carbon metabolism and electron transport in *Chlamydomonas reinhardtii*: Metabolic constraints for carbon partitioning between oil and starch. *Eukaryotic Cell, 12*(6), 776–793.

Kami, C., Lorrain, S., Hornitschek, P., & Fankhauser, C. (2010). Light-regulated plant growth and development. *Current Topics in Developmental Biology, 91*, 29–66.

Kamrani, Y. Y., Matsuo, T., Mittag, M., & Minagawa, J. (2018). *ROC75* is an attenuator for the circadian clock that controls *LHCSR3* expression in *Chlamydomonas reinhardtii*. *Plant and Cell Physiology, 59*(12), 2602–2607.

Kindle, K. L. (1990). High-frequency nuclear transformation of *Chlamydomonas reinhardtii*. *Proceedings of the National Academy of Sciences*, 87(3), 1228–1232.

Kirst H, Garcia-Sedan JG, Zurbriggen A et al (2012) Truncated photosystem chlorophyll antenna size in the green microalga *Chlamydomonas reinhardtii* upon deletion of the TLA3-CpSRP43 gene. Plant Physiol 160:2251–2260.

Kottke, T., Oldemeyer, S., Wenzel, S., Zou, Y., & Mittag, M. (2017). Cryptochrome photoreceptors in green algae: Unexpected versatility of mechanisms and functions. *Journal of Plant Physiology, 217*, 4–14.

Koufopanou, V. (1994). The evolution of soma in the Volvocales. *The American Naturalist, 143*(5), 907–931.

Kröger, P., & Hegemann, P. (1994). Photophobic responses and phototaxis in *Chlamydomonas* are triggered by a single rhodopsin photoreceptor. *FEBS Letters*, 341(1), 5–9.

Kropat, J., Hong-Hermesdorf, A., Casero, D., Ent, P., Castruita, M., Pellegrini, M., Merchant, S. S., & Malasarn, D. (2011). *A revised mineral nutrient supplement increases biomass and growth rate in Chlamydomonas reinhardtii. The Plant Journal, 66*(5), 770–780.

Li, X., Zhang, R., Patena, W., Gang, S. S., Blum, S. R., Ivanova, N., ... & Jonikas, M. C. (2016). An indexed, mapped mutant library enables reverse genetics studies of biological processes in *Chlamydomonas reinhardtii*. *The Plant Cell*, 28(2), 367–387.

Li, X., Patena, W., Fauser, F., Jinkerson, R. E., Saroussi, S., Meyer, M. T., ... & Jonikas, M. C. (2019). A genome-wide algal mutant library and functional screen identifies genes required for eukaryotic photosynthesis. *Nature Genetics*, 51(4), 627–635.

Lichtenthaler, H. K., & Buschmann, C. (2001). Chlorophylls and carotenoids: Measurement and characterization by UV–VIS spectroscopy. In R. E. Wrolstad et al. (Eds.), *Current Protocols in Food Analytical Chemistry* (Unit F4.3.1–F4.3.8). John Wiley & Sons.

Lee, J.-H., Waffenschmidt, S., Small, L., & Goodenough, U. (2007). Between-species analysis of short-repeat modules in cell wall and sex-related hydroxyproline-rich glycoproteins of *Chlamydomonas*. *Plant Physiology*, 144, 1813–1826.

Legris, M., Klose, C., Burgie, E. S., Rojas, C. C., Neme, M., Hiltbrunner, A., Wigge, P. A., & Schäfer, E. (2016). Phytochrome B integrates light and temperature signals in *Arabidopsis*. *Science, 354*(6314), 897–900.

Lemeille, S., Turkina, M. V., Vener, A. V., & Rochaix, J.-D. (2010). Stt7-dependent phosphorylation during state transitions in the green alga *Chlamydomonas reinhardtii*. *Molecular & Cellular Proteomics, 9*(6), 1281–1295.

Lohr, M. (2023). Carotenoids in *Chlamydomonas*. In *Carotenoids: Biosynthetic and Biofunctional Approaches* (pp. 123–145). Elsevier.

Lu, D., Zhang, Y., Zhang, A., & Lu, C. (2022). Non-photochemical quenching: From light perception to photoprotective gene expression. *International Journal of Molecular Sciences, 23*(2), 687.

Luck, M., Mathes, T., Bruun, S., Fudim, R., Hagedorn, R., Nguyen, T. M., Kateriya, S., & Hegemann, P. (2012). A photochromic histidine kinase rhodopsin (HKR1) in *Chlamydomonas reinhardtii*. *Journal of Biological Chemistry*, 287(51), 43502–43509.

Mackinder, L. C. M., Meyer, M. T., Mettler-Altmann, T., Chen, V. K., Mitchell, M. C., Caspari, O., ... & Jonikas, M. C. (2016). A repeat protein links Rubisco to form the eukaryotic carbon-concentrating organelle. *Proceedings of the National Academy of Sciences*, 113(21), 5958–5963.

Marshall, W. F. (2024). *Chlamydomonas* as a model system to study cilia and flagella using genetics, biochemistry, and microscopy. *Frontiers in Cell and Developmental Biology, 12*, 1412641.

Matsuo, T., & Ishiura, M. (2011). *Chlamydomonas reinhardtii* as a new model system for studying the molecular basis of the circadian clock. *FEBS Letters, 585*(10), 1495–1502.

Matsuoka, D., & Tokutomi, S. (2005). Blue light-regulated molecular switch of Ser/Thr kinase in phototropin. *Proceedings of the National Academy of Sciences, 102*(37), 13337–13342.

Merchant, S. S., Prochnik, S. E., Vallon, O., Harris, E. H., Karpowicz, S. J., Witman, G. B., ... & Rokhsar, D. S. (2007). The *Chlamydomonas* genome reveals the evolution of key animal and plant functions. *Science, 318*(5848), 245–250.

Michelet, L., Zaffagnini, M., Morisse, S., Sparla, F., Pérez-Pérez, M. E., Francia, F., ... & Lemaire, S. D. (2013). *Redox regulation of the Calvin–Benson cycle: Something old, something new*. *Frontiers in Plant Science*, 4, 470.

Miller, D. H., Mellman, I. S., Lamport, D. T., & Miller, M. (1974). The chemical composition of the cell wall of *Chlamydomonas gymnogama* and the concept of a plant cell wall protein. *Journal of Cell Biology*, 63, 420–429.

Minagawa, J. (2009). State transitions—the molecular remodeling of photosynthetic supercomplexes that controls energy flow in the chloroplast. *Biochimica et Biophysica Acta (BBA) - Bioenergetics, 1807*(8), 897–905.

Minagawa, J., & Takahashi, Y. (2004). Structure, function and assembly of Photosystem II and its light-harvesting proteins. *Photosynthesis Research,*82(3):241-63.

Minagawa, J., & Tokutsu, R. (2015). Dynamic regulation of photosynthesis in *Chlamydomonas reinhardtii*. *The Plant Journal*, 82(3), 413–428.

Möglich, A., Ayers, R. A., & Moffat, K. (2009). Structure and signaling mechanism of Per-ARNT-Sim domains. *Protein Science*, 17(10), 1282–1294.

Möglich, A. (2019). Signal transduction in photoreceptor histidine kinases. *Protein Science*, 28(11), 1923–1946.

Morgan, A. D., Ness, R. W., Keightley, P. D., & Colegrave, N. (2014). Spontaneous mutation accumulation in multiple strains of the green alga *Chlamydomonas reinhardtii*. *Evolution*, 68(9), 2589–2602

Müller, N., Wenzel, S., Zou, Y., Künzel, S., Sasso, S., Weiß, D., Prager, K., Grossman, A. R., Kottke, T., & Mittag, M. (2017). A plant cryptochrome controls key features of the *Chlamydomonas* circadian clock and its life cycle. *Plant Physiology, 174*(1), 185–201.

Murchie, E. H., & Lawson, T. (2013). Chlorophyll fluorescence analysis: A guide to good practice and understanding some new applications. *Journal of Experimental Botany, 64*(13), 3983–3998.

Nagel, G., Szellas, T., Huhn, W., Kateriya, S., Adeishvili, N., Berthold, P., Ollig, D., Hegemann, P., & Bamberg, E. (2002). Channelrhodopsin-1: A light-gated proton channel in green algae. *Science, 296*(5577), 2395–2398.

Nakasone, Y., Ohshima, M., Okajima, K., Tokutomi, S., & Terazima, M. (2018). Photoreaction dynamics of LOV1 and LOV2 of phototropin from *Chlamydomonas reinhardtii*. *The Journal of Physical Chemistry B, 123*(51), 10939–10950.

Nawrocki, W. J., Tourasse, N. J., Taly, A., Rappaport, F., & Wollman, F.-A. (2019). The plastid terminal oxidase: its elusive function points to multiple contributions to plastid physiology. Annual Review of Plant Biology, 70, 403–427.

Nawrocki, W. J., Liu, X., & Croce, R. (2020). *Chlamydomonas reinhardtii* exhibits de facto constitutive NPQ capacity in physiologically relevant conditions. *Plant Physiology, 182*(1), 472–479.

Negi, S., Perrine, Z., Friedland, N., Kumar, A., Tokutsu, R., Minagawa, J., Berg, H., Barry, A. N., Govindjee, G., & Sayre, R. (2020). Light regulation of light-harvesting antenna size substantially enhances photosynthetic efficiency and biomass yield in green algae. *The Plant Journal*, *103*(2), 584–603.

Neupert, J., Karcher, D., & Bock, R. (2009). Generation of *Chlamydomonas* strains that efficiently express nuclear transgenes. *The Plant Journal, 57*(6), 1140–1150.

Ngan, C. Y., Wong, C.-H., Choi, C., Yoshinaga, Y., Louie, K., Jia, J., Chen, C., Bowen, B., Cheng, H., Leonelli, L., Kuo, R., Baran, R., García-Cerdán, J. G., Pratap, A., Wang, M., Lim, J., Tice, H., Daum, C., Xu, J., Northen, T., Visel, A., Bristow, J., Niyogi, K. K., & Wei, C.-L. (2015). Lineage-specific chromatin signatures reveal a regulator of lipid metabolism in microalgae. *Nature Plants*, 1, 15107.

Nishimura, Y. (2010). Uniparental inheritance of cpDNA and the genetic control of sexual differentiation in *Chlamydomonas reinhardtii*. *Journal of Plant Research*, 123(2), 149–162. https://doi.org/10.1007/s10265-009-0292-y.

Niyogi, K. K., Grossman, A. R., & Björkman, O. (1998). *Arabidopsis* mutants define a central role for the xanthophyll cycle in the regulation of photosynthetic energy conversion. *The Plant Cell*, *10*(7), 1121–1134.

Oldemeyer, S., Franz, S., Wenzel, S., Essen, L. O., Mittag, M., & Kottke, T. (2016). Essential role of an unusually long-lived tyrosyl radical in the response to red light of the animal-like cryptochrome aCRY. *Journal of Biological Chemistry*, 291(27), 14062–14071.

Osakabe, Y., Yamaguchi-Shinozaki, K., Shinozaki, K., & Tran, L. S. P. (2013). Sensing the environment: Key roles of membrane-localized kinases in plant perception and response to abiotic stress. *Journal of Experimental Botany*, 64(2), 445–458. https://doi.org/10.1093/jxb/ers354.

Papon, N., & Stock, A. M. (2019). What do archaeal and eukaryotic histidine kinases sense? *F1000Research*, 8, F1000 Faculty Rev-2145.

Peers, G., Truong, T. B., Ostendorf, E., Busch, A., Elrad, D., Grossman, A. R., Hippler, M., & Niyogi, K. K. (2009). An ancient light-harvesting protein is critical for the regulation of algal photosynthesis. *Nature, 462*(7272), 518–521.

Perozeni, F., Beghini, G., Cazzaniga, S., et al. (2020). Chlamydomonas reinhardtii LHCSR1 and LHCSR3 proteins involved in photoprotective non-photochemical quenching have different quenching efficiency and different carotenoid affinity. Scientific Reports, 10, 21957.

Petroutsos, D., Busch, A., Janssen, I., Trompelt, K., Bergner, S. V., Weinl, S., Holtkamp, M., Karst, U., Kudla, J., & Hippler, M. (2011). The chloroplast calcium sensor CAS is required for photoacclimation in *Chlamydomonas reinhardtii*. *The Plant Cell, 23*(8), 2950–2963.

Petroutsos, D., Tokutsu, R., Maruyama, S., Flori, S., Greiner, A., Magneschi, L., Cusant, L., Kottke, T., Mittag, M., Hegemann, P., Finazzi, G., & Minagawa, J. (2016). A blue-light photoreceptor mediates the feedback regulation of photosynthesis. *Nature,* 537(7621), 563–566.

Petroutsos, D. (2017). Photoreceptor-dependent regulation of photoprotection. *Current Opinion in Plant Biology, 37*, 102–108.

Picariello, T., Hou, Y., Kubo, T., McNeill, N. A., Yanagisawa, H.-a., Oda, T., & Witman, G. B. (2020). TIM, a targeted insertional mutagenesis method utilizing CRISPR/Cas9 in *Chlamydomonas reinhardtii*. *PLOS ONE*, 15(5), e0232594.

Redekop, P., Sanz-Luque, E., Yuan, Y., & Grossman, A. R. (2022). Transcriptional regulation of photoprotection in dark-to-light transition—More than just a matter of excess light energy. *Science Advances, 8*(23), eabn1837.

Rochaix, J.-D. (2011). Regulation of photosynthetic electron transport. *Biochimica et Biophysica Acta (BBA) - Bioenergetics, 1807*(3), 375–383.

Rochaix, J.-D. (2014). *Regulation and* dynamics of the light-harvesting system. Annual *Review of* Plant Biology, 65(1), 287–309.

Romero-Campero, F. J., Pérez-Hurtado, I., Lucas-Reina, E., Romero, J. M., & Valverde, F. (2016). ChlamyNET: A *Chlamydomonas* gene co-expression network reveals global properties of the transcriptome and the early setup of key co-expression patterns in the green lineage. *BMC Genomics*, 17, 227.

Rredhi, A., Petersen, J., Schubert, M., Li, W., Oldemeyer, S., Westermann, M., Wagner, V., Kottke, T., & Mittag, M. (2021). DASH cryptochrome 1, a UV-A receptor, balances the photosynthetic machinery of *Chlamydomonas reinhardtii*. *New Phytologist, 232*(2), 610–624.

Ruiz-Sola, M. Á., Flori, S., Yuan, Y., Villain, G., Sanz-Luque, E., Redekop, P., Tokutsu, R., Küken, A., Tsichla, A., Kepesidis, G., Allorent, G., Arend, M., Iacono, F., Finazzi, G., Hippler, M., Nikoloski, Z., Minagawa, J., Grossman, A. R., & Petroutsos, D. (2023). Light-

independent regulation of algal photoprotection by CO_2 availability. *Nature Communications, 14*, Article 1977.

Salomé, P. A., & Merchant, S. S. (2019). A series of fortunate events: Introducing *Chlamydomonas* as a reference organism. *The Plant Cell*, 31(8), 1682–1707.

Sasso, S., Stibor, H., Mittag, M., & Grossman, A. R. (2018). From molecular manipulation of domesticated *Chlamydomonas reinhardtii* to survival in nature. *eLife*, *7*, e39233.

Serrano-Bueno, G., Romero-Campero, F. J., Lucas-Reina, E., Romero, J. M., & Valverde, F. (2017). Evolution of daily gene co-expression patterns from algae to plants. *Frontiers in Plant Science, 8*, 1217.

Shin, S. E., Lim, J. M., Koh, H. G., Kim, E. K., Kang, N. K., Jeon, S., ... & Jeong, B. R. (2016). CRISPR/Cas9-induced knockout and knock-in mutations in *Chlamydomonas reinhardtii*. *Scientific Reports*, 6, 27810.

Shin, W.-S., Lee, B., Jeong, B.-R., Chang, Y. K., & Kwon, J.-H. (2016). Truncated light-harvesting chlorophyll antenna size in *Chlorella vulgaris* improves biomass productivity. *Journal of Applied Phycology*, *28*, 3193–3202.

Shimogawara, K., Fujiwara, S., Grossman, A., & Usuda, H. (1998). High-efficiency transformation of *Chlamydomonas reinhardtii* by electroporation. *Genetics*, 148(4), 1821–1828.

Siaut, M., Cuiné, S., Cagnon, C., Fessler, B., Nguyen, M., Carrier, P., Beyly, A., Beisson, F., Triantaphylidès, C., Li-Beisson, Y., & Peltier, G. (2011). Oil accumulation in the model green alga *Chlamydomonas reinhardtii*: Characterization, variability between common laboratory strains, and relationship with starch reserves. *BMC Biotechnology, 11*, Article 7.

Sizova, I., Greiner, A., Awasthi, M., Kateriya, S., & Hegemann, P. (2013). Nuclear gene targeting in *Chlamydomonas* using engineered zinc-finger nucleases. *The Plant Journal*, 73(5), 873–882.

Somers, D. E., Schultz, T. F., Milnamow, M., & Kay, S. A. (2000). ZEITLUPE encodes a novel clock-associated PAS protein from Arabidopsis. Cell, 101(3), 319–329.

Sorokina, O., Corellou, F., Dauvillée, D., Sorokin, A., Goryanin, I., Ball, S., Bouget, F.-Y., & Millar, A. J. (2011). Microarray data can predict diurnal changes of starch content in the picoalga *Ostreococcus*. *BMC Systems Biology, 5*, 36.

Spudich, J. L., & Sager, R. (1980). Regulation of the *Chlamydomonas reinhardtii* cell cycle by light and dark. *Journal of Cell Biology*, *85*(1), 136–145.

Strenkert, D., Schmollinger, S., Gallaher, S. D., Salomé, P. A., Purvine, S. O., Nicora, C. D., Mettler-Altmann, T., Soubeyrand, E., Weber, A. P. M., Lipton, M. S., Basset, G. J., & Merchant, S. S. (2019). Multiomics resolution of molecular events during a day in the life of *Chlamydomonas*. *Proceedings of the National Academy of Sciences of the United States of America, 116*(6), 2374–2383.

Teramoto, H., Ono, T., & Minagawa, J. (2001). Identification of Lhcb gene family encoding the light-harvesting chlorophyll-a/b proteins of Photosystem II in *Chlamydomonas reinhardtii*. *Plant and Cell Physiology, 42*(8), 849–856.

Tilbrook, K., Dubois, M., Crocco, C. D., Yin, R., Chappuis, R., Allorent, G., Schmid-Siegert, E., Goldschmidt-Clermont, M., & Ulm, R. (2016). UV-B perception and acclimation in *Chlamydomonas reinhardtii*. *The Plant Cell, 28*(4), 966–983.

Trippens, J., Greiner, A., Schellwat, J., Neukam, M., Rottmann, T., Lu, Y., Kateriya, S., Hegemann, P., & Kreimer, G. (2012). Phototropin influence on eyespot development and regulation of phototactic behavior in *Chlamydomonas reinhardtii*. *The Plant Cell, 24*(11), 4687–4702.

Ueki, N., Ide, T., Mochiji, S., Kobayashi, Y., Tokutsu, R., Minagawa, J., & Wakabayashi, K. (2016). Eyespot-dependent determination of the phototactic sign in *Chlamydomonas reinhardtii*. *Proceedings of the National Academy of Sciences of the United States of America, 113*(19), 5299–5304.

Ünlü, C., Drop, B., Croce, R., & van Amerongen, H. (2014). State transitions in *Chlamydomonas reinhardtii* strongly modulate the functional size of photosystem II but not of photosystem I. *Proceedings of the National Academy of Sciences, 111*(9), 3460–3465.

Virtanen, O., Khorobrykh, S., & Tyystjärvi, E. (2021). Acclimation of Chlamydomonas reinhardtii to extremely strong light. Photosynthesis Research, 147, 91–106.

Vreede, J., van der Horst, M. A., Hellingwerf, K. J., Crielaard, W., & van Aalten, D. M. F. (2003). PAS domains: Common structure and common flexibility. *Journal of Biological Chemistry, 278*(20), 18434–18439.

Xu, Y., Ibrahim, I. M., & Harvey, P. J. (2016). The influence of photoperiod and light intensity on the growth and photosynthesis of *Dunaliella salina* (Chlorophyta) CCAP 19/30. Plant Physiology and Biochemistry, 104, 305–315.

Yamasaki, T., Miyasaka, H., & Ohama, T. (2008). Unstable RNAi effects through epigenetic silencing of an inverted repeat transgene in *Chlamydomonas reinhardtii*. *Genetics*, 180(4), 1927–1944.

Wang, Q., & Lin, C. (2020). Mechanisms of cryptochrome-mediated photoresponses in plants. *Annual Review of Plant Biology, 71*, 103–129.

Warren, C. R. (2008). Rapid measurement of chlorophylls with a microplate reader. *Journal of Plant Nutrition, 31*(7), 1321–1332.

SUPPLEMENTARY INFORMATION

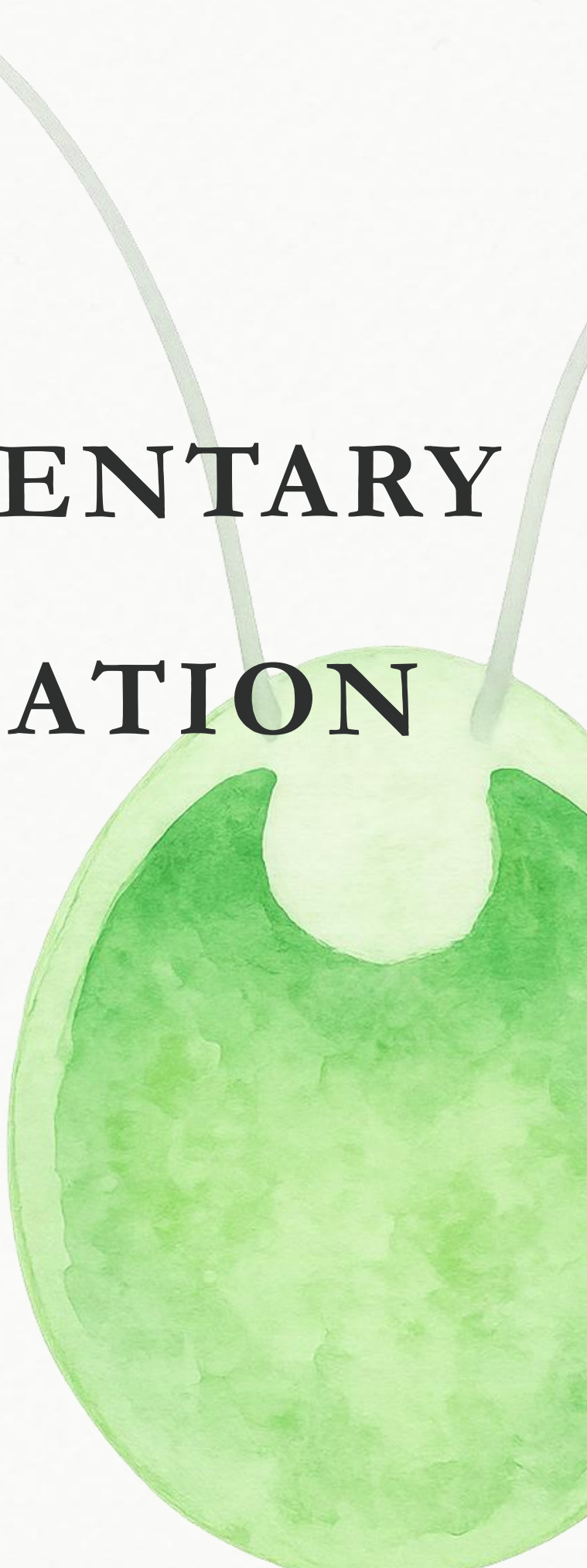

Supplementary information 1: Media preparation

1.1 Trace Elements Recipe

Make preliminary concentrated stock solutions in Part A first, and, where indicated, use these to make the individual stock solutions in Part B listed below. Only solutions in Part B are added directly to media.

A. Preliminary concentrated stock solutions

Pre-1. EDTA-Na_2 concentrate (**S10**) with	125 mM	13.959 g in ~ 250 ml, titrate to pH 8.0 trace element grade KOH (~1.7 g), and bring up to a volume of 300 ml
Pre-2. $(NH_4)_6Mo_7O_{24}$	concentrate (**S104**) bring up to a volume of 250 mL	285 µM $(NH_4)_6Mo_7O_{24}·4H_2O$: 0.088 g,
Pre-3. Na_2SeO_3 concentrate (**Lab**) a volume of 250 mL	1 mM	Na_2SeO_3: 0.043 g, bring up to

B. Individual Stock Solutions for medium (1000×)

Bring each stock solution up to 250 mL in water. Use 1 mL of each individual stock solution in 1 L medium.

Stock Solution	Concentration in stock	Composition
1. EDTA-Na_2	25 mM	EDTA-Na_2: 50 mL of 125 mM EDTA-Na_2 concentrate (Pre-1) from Step A
2. $(NH_4)_6Mo_7O_{24}$	28.5 µM*	$(NH_4)_6Mo_7O_{24}·4H_2O$: 25 mL of 285 µM $(NH_4)_6Mo_7O_{24}$ concentrate (Pre-2) from Step A
3. Na_2SeO_3	0.1 mM	Na_2SeO_3: 25 mL of 1 mM Na_2SeO_3 concentrate (Pre-3) from Step A

4. Zn·EDTA 2.5 mM $ZnSO_4 \cdot 7H_2O$ (**S87**): 0.18 g

2.75 mM EDTA-Na_2: 5.5 mL of 125 mM EDTA-Na_2 concentrate (Pre-1) from Step A

5. Mn·EDTA 6 mM $MnCl_2 \cdot 4H_2O$ (**Lab**): 0.297 g

6 mM EDTA-Na_2: 12 mL of 125 mM EDTA-Na_2 concentrate (Pre-1) from Step A

6. Fe·EDTA 20 mM $FeCl_3 \cdot 6H_2O$ (**Lab**): 1.35 g

22 mM EDTA-Na_2: 2.05 g

22 mM Na_2CO_3 (sodium carbonate) (**S24**): 0.58 g

(Combine EDTA-Na_2 with sodium carbonate in water and mix. Add $FeCl_3 \cdot 6H_2O$ after the first two components dissolve. Do Not Use Pre-1.)

(*) cover the bottle with aluminum folder

7. Cu·EDTA 2 mM $CuCl_2 \cdot 2H_2O$ (**Lab**): 0.085 g

2 mM EDTA-Na_2: 4 mL of 125 mM EDTA-Na_2 concentrate (Pre-1) from Step A

Notes:

*The final [Mo] in the 1× medium is 0.2 µM

Total [EDTA] in 1× medium: (25 + 2.75 + 6 + 22 + 2) = 57.75 µM

1.2 TAP (Tris-Acetate-Phosphate) recipe

A) First prepare:

Filner's Beijerincks Solution (FBS) 40x, 1L

16g NH_4Cl

2 g $CaCl_2x2H_2O$

4 g $MgSO_4x7H_2O$

Dissolve separately the $CaCl_2$ from the $MgSo_4$ + NH_4Cl

Autoclave and store at room temperature

Phosphate buffer 1M pH 7.0

Mix the required amount of already prepared 1M solutions:

250 mL K_2HPO_4 1M

~170 mL KH_2PO_4 1M (up to pH 7.0)

Autoclave and store at room temperature

B) For 1L of TAP prepare:

2.42 g Tris base

25 mL FBS 40x

1 mL phosphate buffer 1M pH 7.0

1 mL (each) Trace Salt solutions

Water until 1L

Set up pH at 7.0 with glacial acetic acid (~1mL per liter)

Autoclave and store at room temperature

Optional: 15 g agar for plates (1.5% final concentration)

1.3 HSM (Sueoka High-Salt) media

A) First prepare:

<u>HSM Filner's Beijerincks Solution (H-FBS) 40x, 1L</u>

100g NH_4Cl (CRAG S68)

2 g $CaCl_2x2H_2O$ (CRAG S126)

4 g $MgSO_4x7H_2O$ (CRAG S7)

Dissolve separately the $CaCl_2$ from the $MgSo_4$ + NH_4Cl

Autoclave and store at room temperature

<u>Phosphate buffer 1M pH 7.0</u>

Mix the required amount of already prepared 1M solutions:

250 mL K_2HPO_4 1M

~170 mL KH_2PO_4 1M (up to pH 7.0)

Autoclave and store at room temperature

B) For 1L of THSM prepare:

5 mL H-FBS 40x

13.6 mL phosphate buffer 1M pH 7.0

1 mL (each) Trace Salt solutions

Water until 1L

Autoclave and store at room temperature

Optional: 15 g agar for plates (1.5% final concentration)

Supplementary information 2: Tables

	Light regime	Strain	Fv/Fm (mean ± SD)	Statistical Grouping[1]
LL	SD	CLiP	0,38 ± 0,01	a
		4a+	0,40 ± 0,02	a
		CC-124	0,40 ± 0,02	a
		CC-125	0,38 ± 0,01	a
	12/12	CLiP	0,44 ± 0,03	a
		4a+	0,35 ± 0,07	a
		CC-124	0,39 ± 0,02	a
		CC-125	0,33 ± 0,07	a
	LD	CLiP	0,41 ± 0,03	a
		4a+	0,33 ± 0,06	a
		CC-124	0,31 ± 0,09	a
		CC-125	0,36 ± 0,02	a
	CL	CLiP	0,19 ± 0,17	a
		4a+	0,33 ± 0,16	a
		CC-124	0,33 ± 0,05	a
		CC-125	0,30 ± 0,06	a

	Light regime	Strain	Fv/Fm (mean ± SD)	Statistical Grouping[1]
HL	SD	CLiP	0,34 ± 0,03	a
		4a+	0,30 ± 0,04	a
		CC-124	0,35 ± 0,09	a
		CC-125	0,33 ± 0,03	a
	12/12	CLiP	0,39 ± 0,04	a
		4a+	0,30 ± 0,06	a
		CC-124	0,36 ± 0,06	a
		CC-125	0,31 ± 0,03	a
	LD	CLiP	0,19 ± 0,11	a
		4a+	0,24 ± 0,09	a
		CC-124	0,31 ± 0,03	a
		CC-125	0,19 ± 0,03	a
	CL	CLiP	0,09 ± 0,08	**a**
		4a+	0,02 ± 0,03	**ab**
		CC-124	0,00 ± 0,00	**b**
		CC-125	0,00 ± 0,01	**b**

Supplementary Table 1. Photosynthetic efficiency (Fv/Fm ratio) of *Chlamydomonas reinhardtii* strains under LL and HL conditions across different light regimes. Table on the right is for LL (Low Light) conditions; the one on the left for HL (High Ligh). Mean values ± standard deviation (SD) are shown. Different lowercase letters indicate statistically significant differences between strains within each individual light regime: SD (short day), 12/12 (12 h light/12 h dark), LD (long day), and CL (continuous light) ($p < 0.05$, one-way ANOVA followed by Tukey's post hoc test). LL: 50µmol photons/m²/s; HL: 250µmol photons/m²/s.

	Light regime	Strain	Chlorophylls (µg/mL) / cell number * 10^6 (mean ± SD)	Statistical Grouping[1]
LL	SD	CLiP	7,73 ± 0,43	a
		4a+	6,49 ± 0,38	a
		CC-124	6,58 ± 0,60	a
		CC-125	6,92 ± 0,54	a
	12/12	CLiP	8,94 ± 1,89	**a**
		4a+	5,83 ± 0,22	**ab**
		CC-124	6,02 ± 0,40	**ab**
		CC-125	4,73 ± 0,67	**b**
	LD	CLiP	4,52 ± 0,84	a
		4a+	4,37 ± 0,70	a
		CC-124	3,77 ± 0,56	a
		CC-125	3,67 ± 0,61	a
	CL	CLiP	5,91 ± 0,94	a
		4a+	5,41 ± 0,33	a
		CC-124	4,48 ± 0,05	a
		CC-125	5,63 ± 0,13	a

	Light regime	Strain	Chlorophylls (µg/mL) / cell number * 10^6 (mean ± SD)	Statistical Grouping[1]
HL	SD	CLiP	9,52 ± 1,81	**a**
		4a+	5,35 ± 1,20	**b**
		CC-124	5,91 ± 1,25	**b**
		CC-125	5,73 ± 0,32	**b**
	12/12	CLiP	7,33 ± 2,71	a
		4a+	5,34 ± 2,15	a
		CC-124	5,29 ± 1,43	a
		CC-125	6,89 ± 1,26	a
	LD	CLiP	2,55 ± 0,29	**b**
		4a+	4,83 ± 1,42	**a**
		CC-124	2,09 ± 0,56	**b**
		CC-125	2,78 ± 0,45	**b**
	CL	CLiP	1,97 ± 0,51	a
		4a+	1,93 ± 0,65	a
		CC-124	1,11 ± 0,19	a
		CC-125	1,90 ± 0,60	a

Supplementary Table 2. Total chlorophyll content of *Chlamydomonas reinhardtii* strains under LL and HL conditions across different light regimes. Chlorophylls expressed as (µg/mL)/ cell number * 10^6. Table on the right is for LL (Low Light) conditions; the one on the left for HL (High Ligh). Mean values ± standard deviation (SD) are shown. Different lowercase letters indicate statistically significant differences between strains within each individual light regime: SD (short day), 12/12 (12 h light/12 h dark), LD (long day), and

CL (continuous light) ($p < 0.05$, one-way ANOVA followed by Tukey's post hoc test). LL: 50µmol photons/m²/s; HL: 250µmol photons/m²/s.

	Light regime	Strain	Carotenoids (µg/mL) / cell number * 10^6 (mean ± SD)	Statistical Grouping[1]
LL	SD	CLiP	0,70 ± 0,06	**b**
		4a+	0,82 ± 0,12	**ab**
		CC-124	1,02 ± 0,09	**a**
		CC-125	0,86 ± 0,05	**ab**
	12/12	CLiP	0,94 ± 0,21	**a**
		4a+	0,74 ± 0,03	**ab**
		CC-124	0,84 ± 0,06	**ab**
		CC-125	0,58 ± 0,09	**b**
	LD	CLiP	0,81 ± 0,14	a
		4a+	0,82 ± 0,23	a
		CC-124	0,78 ± 0,18	a
		CC-125	0,64 ± 0,08	a
	CL	CLiP	0,66 ± 0,06	a
		4a+	0,77 ± 0,03	a
		CC-124	0,62 ± 0,01	a
		CC-125	0,81 ± 0,05	a

	Light regime	Strain	Carotenoids (µg/mL) / cell number * 10^6 (mean ± SD)	Statistical Grouping[1]
HL	SD	CLiP	1,18 ± 0,22	a
		4a+	0,85 ± 0,21	a
		CC-124	0,96 ± 0,26	a
		CC-125	0,89 ± 0,10	a
	12/12	CLiP	1,14 ± 0,39	a
		4a+	0,88 ± 0,34	a
		CC-124	0,97 ± 0,33	a
		CC-125	1,18 ± 0,25	a
	LD	CLiP	0,38 ± 0,07	**b**
		4a+	0,80 ± 0,18	**a**
		CC-124	0,40 ± 0,10	**b**
		CC-125	0,57 ± 0,07	**ab**
	CL	CLiP	0,33 ± 0,11	a
		4a+	0,42 ± 0,11	a
		CC-124	0,22 ± 0,06	a
		CC-125	0,42 ± 0,18	a

Supplementary Table 3. Total carotenoid content of *Chlamydomonas reinhardtii* strains under LL and HL conditions across different light regimes. Carotenoids expressed as (µg/mL)/ cell number * 10^6. Table on the right is for LL (Low Light) conditions; the one on the left for HL (High Ligh). Mean values ± standard deviation (SD) are shown. Different lowercase letters indicate statistically significant differences between strains within each individual light regime: SD (short day), 12/12 (12 h light/12 h dark), LD (long day), and CL (continuous light) ($p < 0.05$, one-way ANOVA followed by Tukey's post hoc test). LL: 50µmol photons/m²/s; HL: 250µmol photons/m²/s.